UNIVERSITY OF LEEDS

Predictability and variability of East African rainfall seasons

by

DEAN PHILIP WALKER

Submitted in accordance with the requirements for the degree of Doctor of Philosophy

The University of Leeds

School of Earth and Environment

November 2020

ii

Declaration of authorship

The candidate confirms that the work submitted is their own, except where work which has formed part of jointly authored publications has been included. The contribution of the candidate and the other authors to this work has been explicitly indicated below. The candidate confirms that appropriate credit has been given within the thesis where reference has been made to the work of others.

The publication Walker et al., 2019, *Skill of dynamical and GHACOF consensus seasonal forecasts of East African rainfall, Climate Dynamics* 53(7), p4911-4935, doi: `https://doi.org/10.1007/s00382-019-04835-9`, jointly authored with Cathryn E. Birch, John H. Marsham, Adam A. Scaife, Richard J. Graham and Zewdu T. Segele, is included as Chapter 2 of the thesis. The candidate performed all data analysis, produced all figures and wrote the text. Birch, Marsham and Scaife supervised the direction of the work, Graham and Segele provided information on the methodology of the GHACOF consensus forecasts. All co-authors contributed to interpretation of results and provided comments on the text.

The publication Walker et al., 2020, *Common mechanism for inter-annual and decadal variability in the East African long rains, Geophysical Research Letters* 47 (22), doi: `https://doi.org/10.1029/2020GL089182`, jointly authored with John H. Marsham, Cathryn E. Birch, Adam A. Scaife and Declan L. Finney, is included as Chapter 3 of the thesis. The candidate performed all data analysis, produced all figures and wrote the text. Birch, Marsham, and Scaife supervised the direction of the work, Finney provided code for analysis of the MJO phase. All co-authors contributed to interpretation of results and provided comments on the text.

The work in Chapter 4, Walker et al., *Skilful dynamical seasonal predictions of the East African long rains with a mid-latitude driver*, jointly authored with

John H. Marsham, Adam A. Scaife and Cathryn E. Birch, has been prepared for submission to *Geophysical Research Letters*. The candidate performed all data analysis, produced all figures and wrote the text. Marsham, Scaife, and Birch supervised the direction of the work. All co-authors contributed to interpretation of results and provided comments on the text.

Acknowledgements

I would firstly like to thank my supervisors, Cathryn Birch, John Marsham, and Adam Scaife for all their support, guidance, and encouragement they gave me throughout. Their eternal optimism and belief in me kept me going in the moments where I doubted myself. Thanks also to the Dynamics group in ICAS for making me feel welcome from the start, and for providing a great research environment.

I would like to thank Richard Graham, Michael Vellinga, Andrew Colman, and Dave Rowell at the Met Office for their helpful discussions and ideas. I would also like to thank ICPAC, and in particular Zewdu Segele, who invited me to attend the GHACOF meeting in August 2018.

Thanks also go to Fairbairn office 2.10 (Anya, Ben, and Beth) and also to the East Africa posse (Beth and Declan), and all of Priestley office 11.06, for the fun times and helpful discussions. I would also like to thank Craig Poku for all the evenings of wine, endless baked goods, and occasionally scientific chats, and Lucy Recchia for all the tea breaks, much needed distractions, more baked goods and wine, and for keeping me active and on my toes. Thanks also to Laura, for helping keep me sane during the final few months!

Thanks goes to all of my family and friends for their endless support from the very beginning, always encouraging me and believing I can achieve anything, and for putting up with me!

Finally, I would like to dedicate this thesis to my Dad, and to my Grandad Keith and Nan Jean.

Abstract

Droughts and flooding over East Africa produce large scale humanitarian disasters such as famine. The recent 2010-11 drought led to an estimated 250,000 deaths in the region, whilst flooding also causes deaths, population displacement, and damage to infrastructure. A better understanding of East African rainfall variability, leading to improved seasonal forecasts, could drastically reduce the impact of these events.

The most widely used operational seasonal forecast in the region is the consensus based Greater Horn of Africa Climate Outlook Forum (GHACOF) forecast, produced using a combination of dynamical and statistical model forecasts alongside local knowledge. In this thesis, for the first time, East African rainfall forecasts from GHACOF are compared directly to dynamical seasonal forecasts from the UK Met Office Unified Model, and both are evaluated against observations. Both forecasts appear to show good skill at forecasting the short rains (October-December), whilst poor skill in forecasting the long rains (March-May) is found.

The drivers of variability in the long rains are studied, linking the long rains to zonal winds over the Congo basin on both inter-annual and decadal timescales, with westerly anomalies leading to more rainfall over East Africa. A source of variability in these zonal winds is found to be the North Atlantic Oscillation (NAO). A Rossby wave response in the mid-latitudes to pressure changes during NAO events propagates equatorward, eventually reaching the Congo basin. The Met Office seasonal forecast model is able to represent both the connection between zonal winds over the Congo and rainfall, as well as the NAO Rossby wave mechanism, in its ensemble members. However, the NAO amplitude in the ensemble mean is too small, and so the teleconnection linking the NAO and the long rains in the ensemble mean is hidden by noise, but these results offer hope for future skilful dynamical predictions of the long rains.

Contents

3. **Common mechanism for inter-annual and decadal variability in the East African long rains**   **101**

List of Figures

xvi

List of Tables

xx

Abbreviations

AHL Arabian heat low

AMIP Atmospheric Model Intercomparison Project

AUC area under the curve

BS Brier score

BSS Brier skill score

C3S Copernicus Climate Change Service

CFSv2 Climate Forecast System version 2

CICE Los Alamos Sea-Ice Model

CMIP Coupled Model Intercomparison Project

CMIP3 Coupled Model Intercomparison Project version 3

CMIP5 Coupled Model Intercomparison Project version 5

CPT Climate Predictability Tool

DFID Department for International Development

DJF December January February

DMI dipole mode index

ECMWF European Centre for Medium-range Weather Forecasts

ENSO El Niño-Southern Oscillation

EOF empirical orthogonal function

ERA-Interim ECMWF interim reanalysis

FAO Food and Agriculture Organisation

FAR false alarm rate

FEWS NET Famine Early Warning System Network

ForPAc Towards Forecast-based Preparedness Action

FSNAU Food Security and Nutritional Analysis Unit

GCRF Global Challenges Research Fund

GDP gross domestic product

GeoCOF Geospatial Climate Outlook Forecasting Tool

GFDRR Global Facility for Disaster Reduction and Recovery

GHA Greater Horn of Africa

GHACOF Greater Horn of Africa Climate Outlook Forum

GLOBE Global Land One-kilometer Base Elevation

GloSea Global Seasonal Forecast System

GloSea5 Global Seasonal Forecast System version 5

GPC Global Producing Centre

GPCP Global Precipitation Climatology Project

HadGEM3 Hadley Centre Global Environmental Model version 3

HadISST Hadley Centre Sea Ice and Sea Surface Temperature

HR hit rate

HSS Heidke skill score

ICPAC IGAD Climate Prediction and Applications Centre

IGAD Intergovernmental Authority on Development

IMD Indian Meteorological Department

IMF International Monetary Fund

IOD Indian Ocean Dipole

IOZM Indian Ocean Zonal Mode

IPCC Intergovernmental Panel on Climate Change

ITCZ Intertropical Convergence Zone

JJA June July August

JULES Joint UK Land Environment Simulator

MAM March April May

MERRA-2 Modern Era Retrospective Analysis for Resarch and Applications version 2

MetUM Met Office Unified Model

MJO Madden-Julian Oscillation

MLR multiple linear regression

MSE moist static energy

NAO North Atlantic Oscillation

NASA National Aeronautics and Space Administration

NCAR National Center for Atmospheric Research

NCEP National Centers for Envrionmental Protection

NE northeast

NEMO Nucleus for European Modelling of the Ocean

NMME North American Multi Model Ensemble

NOAA National Oceanic and Atmospheric Administration

NWP numerical weather prediction

OCHA Office for the Coordination of Humanitarian Affairs

OND October November December

PC proportion correct

PDO Pacific Decadal Oscillation

QBO Quasi-Biennial Oscillation

RCM regional climate model

RCOF Regional Climate Outlook Forum

RH relative humidity

RMM Real-time Multivariate MJO

ROC relative operating characteristic

ROCS relative operating characteristic score

ROCSS relative operating characteristic skill score

SE southeast

SETIO southeastern tropical Indian Ocean

SH specific humidity

SHEAR Science for Humanitarian Emergencies and Resilience

SHL Saharan heat low

SLP sea level pressure

SOI Southern Oscillation Index

SON September October November

SST sea surface temperature

SVSLRF standard verification system for long range forecasts

SWIFT Science for Weather Information and Forecasting Techniques

TRMM Tropical Rainfall Measuring Mission

UN United Nations

W2-SIP WISER Support to ICPAC Project

WISER Weather and Climate Information Services for Africa

WMO World Meteorological Organization

WRF Weather Research and Forecasting

WTIO western tropical Indian Ocean

Z700 geopotential height at 700hPa

Chapter 1.

Introduction

1.1. Motivation

East Africa is a region highly vulnerable to severe weather, climate change, and climate variability. From the arid lowlands near the Indian Ocean coast, to the steep highlands further inland, as well as several large lakes, the large contrasts in geography over relatively short distances provides a challenge to forecasting on all time scales. The East Africa region (shown in Figure 1.1a) consists of a number of developing countries, with the region having one of the most rapid population growths on the entire planet. This means that the impact of weather and climate extremes can often be exacerbated by socio-economic and political factors, and also that the region is particularly vulnerable due to a relative lack of technology and infrastructure. Many countries within the East African region have been identified by the International Monetary Fund (IMF) World Economic Outlook Database (International Monetary Fund 2020) as having some of the fastest real gross domestic product (GDP) growth rates in the world; 4 out of the top 10 fastest GDP growth rates in the world in 2018 were located in East Africa (World Bank 2020). However, they are also some of the countries with highest proportion of GDP coming from the agricultural sector (CIA World Factbook 2020), for example, in 2017, in Kenya 34.5% of GDP was from the agricultural sector, compared to a world average of 6.4%, whilst in Somalia in 2013, 60.2% of GDP comprised of agriculture. This renders the economies of these countries particularly susceptible to extreme events.

Of the severe weather and climate events, the Global Facility for Disaster Reduction and Recovery (GFDRR) has identified that droughts and floods are the most damaging natural disasters in the region (GFDRR 2020). For example the 2011 drought, caused by the failure of two consecutive rainfall seasons, resulted in widespread famine. It is
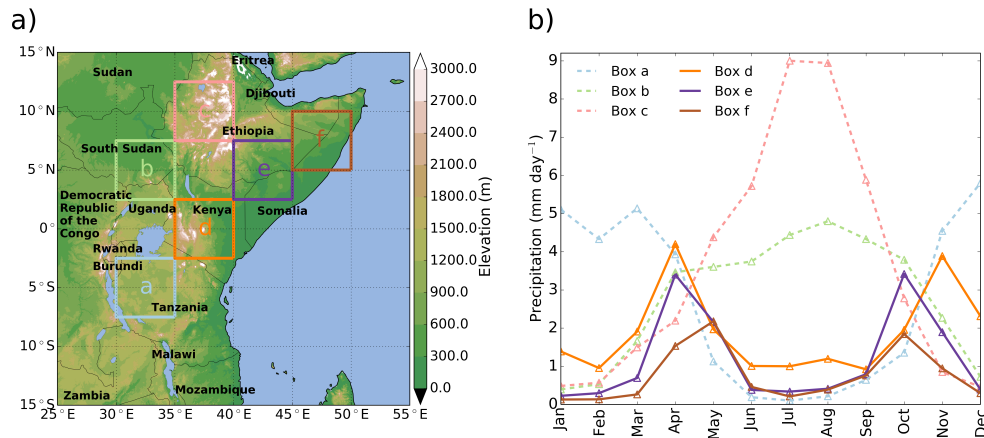
Figure 1.1.: a) Map showing geographic features and topography of East Africa. Elevation data come from the Global Land One-kilometer Base Elevation (GLOBE) project database (Hastings and Dunbar 1999). b) Annual cycle of rainfall over different regions of East Africa, with colours matching up to the boxes in a. Dashed lines show unimodal rainfall cycles, whilst solid lines show bimodal rainfall cycles with long rains and short rains seasons. Rainfall data is taken from the Tropical Rainfall Measuring Mission (TRMM; Huffman et al. 2007).

estimated that there were over 250,000 deaths as a result of lack of food availability caused by the drought, with Somalia in particular experiencing widespread famine (FAO and FEWS NET 2013). This crisis was also exacerbated by political factors, such as the prevention of aid reaching the local population by militant groups that controlled affected regions. Meanwhile, during the long rains (March-May) in 2018, heavy rainfall caused widespread flooding (Kilavi et al. 2018). In Kenya 186 lives were lost and 300,000 people were displaced (UN Office for the Coordination of Humanitarian Affairs (OCHA) 2018). Further, drought and flood events can occur in quick succession (Nicholson 2016b), for example much of East Africa having experienced widespread droughts in 2017 before the flooding in 2018.

Due to the seasonal nature of rainfall in the region, these events can be driven by the seasonal timescale, meaning that seasonal forecasts can be an invaluable tool for mitigating and preventing humanitarian disasters related to the events. Seasonal forecasts have been used to reduce the potential impact of natural disasters, or to take advantage of favourable conditions for crop growth to provide an economic boost to the region. For example, in 2009, after forecasts issued by the Greater Horn of Africa Climate Outlook Forum (GHACOF) predicted normal to above normal rainfall, the Kenya Red Cross distributed seeds to 70,000 Kenyan farmers, resulting in a bumper harvest (Graham et al. 2012). However, use of seasonal forecasts can still be improved.

A briefing paper by Oxfam and Save the Children (2012) looking at the 2010-11 famine revealed that despite accurate predictions of below normal rainfall for the 2010 short rains (October-December), that led to Kenya Red Cross issuing appeals in early 2011 (Graham et al. 2012), and FEWS NET warning of a crisis in the case of the failure of the long rains, little response was taken until near the end of the long rains season in May 2011, by which time the famine was well underway. A similar pattern was also noted for the Kenyan drought of 2005-06 (Oxfam and Save the Children 2012).

Meanwhile, tropical regions have been identified by the Intergovernmental Panel on Climate Change (IPCC 2018) as likely to experience some of the most disproportionate consequences of anthropogenic climate change, with East Africa being one area likely to first feel the impacts. In fact, several recent climate events have been identified as having been caused or exacerbated by anthropogenic climate change. For example Lott et al. (2013) performed event attribution on the rainfall seasons preceding the 2011 drought, finding that human influence increased the probability of the long rains being as dry as in 2011, although there was no evidence of human influence on the 2010 short rains. Meanwhile Uhe et al. (2018) identified that the likelihood of the La Niña event of 2016 that led to Kenyan drought was increased due to human-induced climate change. Under climate change, it is widely expected that throughout the tropics rainfall will become less frequent but more intense (Seneviratne et al. 2012). This will have negative impacts, such as increased stress on agriculture, increased frequency of flooding and landslides, more people displaced from their homes, and damage to transport links and infrastructure. As well as increased water stress, rising sea levels also threaten many in coastal areas.

East Africa is also currently facing a long term decline in its main rainfall season, the long rains (e.g. Funk et al. 2005, 2008, Lyon and Dewitt 2012), which contrasts with wetter conditions predicted by many climate projections (e.g. Shongwe et al. 2011, Anyah and Qiu 2012). This has been termed the East African Climate Paradox (Rowell et al. 2015), and this uncertainty poses problems for long-term planning and adaptation to climate change as it is unclear whether to expect wetter or drier conditions in the future, as well as undermining user confidence in the climate projections.

All of these factors mean that reliable, accurate, seasonal forecasts, underpinned by knowledge and understanding of the mechanisms influencing variability of rainfall on this timescale, are critical for the well-being and development of the region. Understanding of longer term variability of seasonal rainfall, particularly under climate change, is also essential for the long term planning needed to mitigate large-scale dis-

asters. Seasonal forecasting is key for planning, however, it remains a huge challenge with little forecasting ability for many regions and seasons. This thesis looks to make progress in improving the current state of understanding to improve seasonal forecasting for East Africa.

1.2. East Africa

1.2.1. Climatology of East Africa

1.2.1.a. Annual cycles of rainfall

East Africa is located within the tropics and so experiences seasonal rainfall cycles as a result of the motion of the Intertropical Convergence Zone (ITCZ). The ITCZ is a band of enhanced convection, driven by trade winds from the southern and northern hemispheres converging, leading to upwards motion. The water vapour in the air forced upwards condenses, forming clouds. This upward motion is part of the Hadley Cell, a circulation that involves low level air moving towards the equator and rising through the troposphere, before travelling away from the equator. It then descends at approximately 25° north or south. This descending branch of the Hadley Cell leads to many of the major deserts being located at approximately these latitudes, including the Sahara and Arabian deserts in the northern hemisphere (Webster 2020).

The ITCZ moves meridionally throughout the year, following the region of most intense heating from the sun. It passes over the equator twice per year, leading to two distinct rainfall seasons in equatorial regions, whilst further north and south close to the limits of movement of the ITCZ, there is a singular rainfall season per year. In the equatorial East Africa region (Kenya, northern Tanzania, southern/ coastal Somalia, southern Ethiopia, eastern Uganda), the ITCZ passes over twice per year, giving two rainfall seasons. These are commonly referred to as the long rains (also known as Gu in Somalia, Belg in Ethiopia or Masika in Tanzania) and the short rains (Deyr in Somalia, Vuli in Tanzania). The short rains season occurs roughly from October to December (OND), whilst the long rains occur from March to May (MAM), seen in boxes d, e, and f in Figure 1.1. Further north and south are unimodal wet seasons; in southern Tanzania the Tanzania unimodal rains, occurring approximately from November through to April (Figure 1.1 box a) in South Sudan the South Sudan rains from April to October (Figure 1.1 box b), and over the Ethiopian highlands the Kiremt rains, occurring from June to
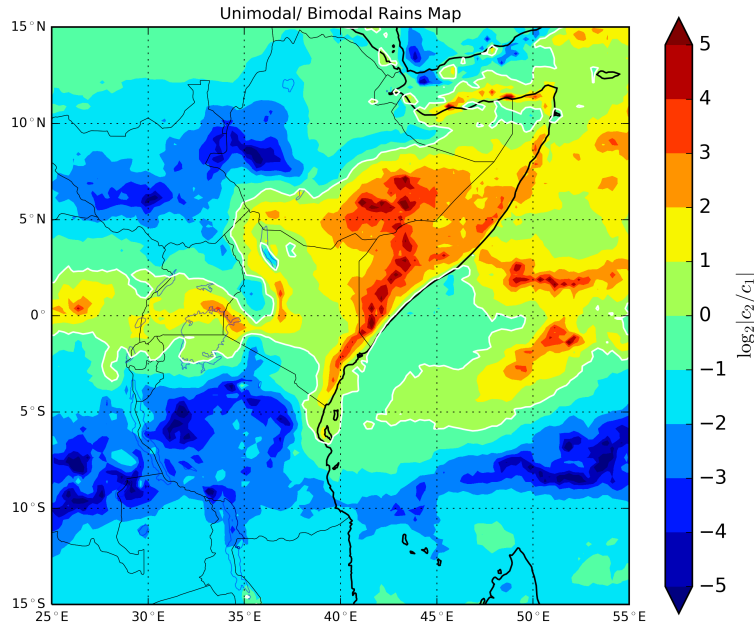
Figure 1.2.: Bimodal and unimodal rainfall regions calculated by considering the dominant Fourier harmonic of the rainfall cycle, with c_2 and c_1 the amplitude coefficients of the semi-annual and annual harmonics respectively. Values of $\log_2 |c_2/c_1| > 0$ (colours) have two rainfall seasons per year, whilst $\log_2 |c_2/c_1| < 0$ have one rainfall season per year. The 0 line is shown as a white contour. Figure adapted from Yang et al. (2015a) FIG. 3. Rainfall data used to calculate the harmonics is taken from TRMM.

September (Figure 1.1 box c). Figure 1.2, adapted from FIG. 3 of Yang et al. (2015a), uses Fourier harmonics of the precipitation annual cycle to determine where unimodal or bimodal peaks in rainfall occur. The semi-annual, c_2, and annual, c_1, harmonics are calculated, then the ratio of semi-annual to annual, c_2/c_1, is found. The base-2 logarithm, $\log_2 |c_2/c_1|$, is then taken. Areas where this is positive (or $c_2 > c_1$) suggest the area experiences two rainfall seasons, whilst areas where this is negative (or $c_2 < c_1$) have one rainfall season per year. This method does however exclude the possibility of capturing regions with more than two rainfall peaks per year, and Seregina et al. (2019), using a method of determining onset and cessation of rainfall seasons, showed that there were small areas within the East Africa region that undergo three rainfall seasons per year.

1.2.1.b. Topography

A map of the topography of East Africa is seen in Figure 1.1a. The dominant features of the region are related to the Great Rift Valley. Two main mountain ranges, the Ethiopian highlands (located at 15°N to 5°N, 35°E to 43°E), in central Ethiopia, and the East African highlands (located at 3°N to 5°S, 28°E to 37°E), covering western Kenya, northern Tanzania, Uganda, Rwanda and Burundi, have a large influence on the weather experienced within the region.

There are also several large lakes within the region, together referred to as the Rift Valley Lakes. Of these the most significant is Lake Victoria, in the centre of the East African highlands. Lake Victoria is the second largest freshwater lake in the world by surface area, at approximately 68,800km^2 (Bengtsson et al. 2012), and a great number of the East African population (approximately 40 million, African Great Lakes Information Platform 2020) reside upon its shores, whilst the lake itself provides a livelihood for many, including approximately 200,000 fishermen. The lake is large enough to have a great influence on the weather in the region immediately surrounding it, with much recent research focused on understanding and predicting storms that form over the lake (e.g. Chamberlain et al. 2014, Williams et al. 2015, Woodhams et al. 2018, 2019). These storms, and associated impact on the surface water conditions claim approximately 5,000 lives per year (Atieno et al. 2017), and so being able to predict and give warnings of these storms is of great importance. The majority of water within Lake Victoria is provided by rainfall (Piper et al. 1986), whilst the lake outflows into the River Nile. Due to this, the water level of Lake Victoria is highly sensitive to rainfall totals. For example after record-breaking rainfall in 1961, the level of the lake jumped by over a metre (Kite 1981, 1982), the largest jump on record, as well as the highest recorded level of the lake. As the lake outflows into the Nile, the lake level is important in providing water downstream, where many depend upon it as a water source. Aside from Lake Victoria, several other lakes of note include Lake Malawi, Lake Tanganyika, and Lake Turkana. Furthermore, the topography influences the climatology of the low level circulation in the region.

1.2.1.c. Circulation features

Within the lower troposphere over East Africa there is a distinct annual cycle within the circulation. Figure 1.3 shows monthly climatologies of winds at 850hPa. One of the key features at 850hPa is a jet over the southern Indian Ocean, flowing in to East

Africa from the south east, before curving towards India in a southeasterly direction. This is known as the Somali Jet, and was first observed by Findlater (1966, 1969, 1977). This jet occurs from approximately May to October, at which point it breaks down, and the northern part of the jet reverses direction by December, travelling from over India towards East Africa. The second reversal then occurs approximately in March. As noted by Okoola (1999a), East Africa therefore lies under two monsoon systems, the northeast (NE) and southeast (SE), the NE occurring during southern hemisphere summer, and the SE during northern hemisphere summer. The twice annual reversals of the Somali Jet coincide with the short and long rains seasons respectively. The transition between the two monsoons lead to weak convergence over East Africa, with air masses moving equatorward from both hemispheres, moving onshore and forced to ascend by coastal friction and topography (Nicholson 1996).

A smaller scale, low-level jet that occurs throughout the year is also present in Figure 1.3, located in northwest Kenya. This jet forms in the valley between the East African highlands and the Ethiopian highlands, known as the Turkana channel. This jet is called the Turkana jet and was first observed by Kinuthia and Asnani (1982) and Kinuthia (1992). The jet travels in a southeasterly direction through the Turkana channel. The jet has been found to be responsible for the arid climate within the northwestern Kenya, southwestern Ethiopia, and southern Somalia region, with strongly divergent flow over this region at low levels as the wind enters the Turkana channel (Nicholson 2016a).

The upper and lower tropospheric zonal winds across the equator form the Walker circulation (Bjerknes 1969), a series of closed circulation cells analogous to the Hadley Cells oriented zonally around the equator. This leads to regions of low level convergence/ divergence, with the reverse at upper level, and upward/ downward motion, impacting on the levels of convection seen in these regions. In the climatology, East Africa is frequently considered to be under a descending branch of the Walker circulation. The Walker circulation is formed due to the pressure gradient force: there is a high-pressure region over the eastern Pacific Ocean, near the coast of South America, with a low-pressure region over Indonesia. This leads to low level easterly winds across the Pacific Ocean. These easterly winds impact the ocean, causing upwelling of cool water off the coast of South America. In contrast, low level westerly winds are present across the Indian Ocean, drawing moisture away from East Africa. The combination of circulation features over East Africa lead to the region experiencing divergence or weak convergence throughout the year, contributing to the arid climate observed within the region (Lyon 2014).
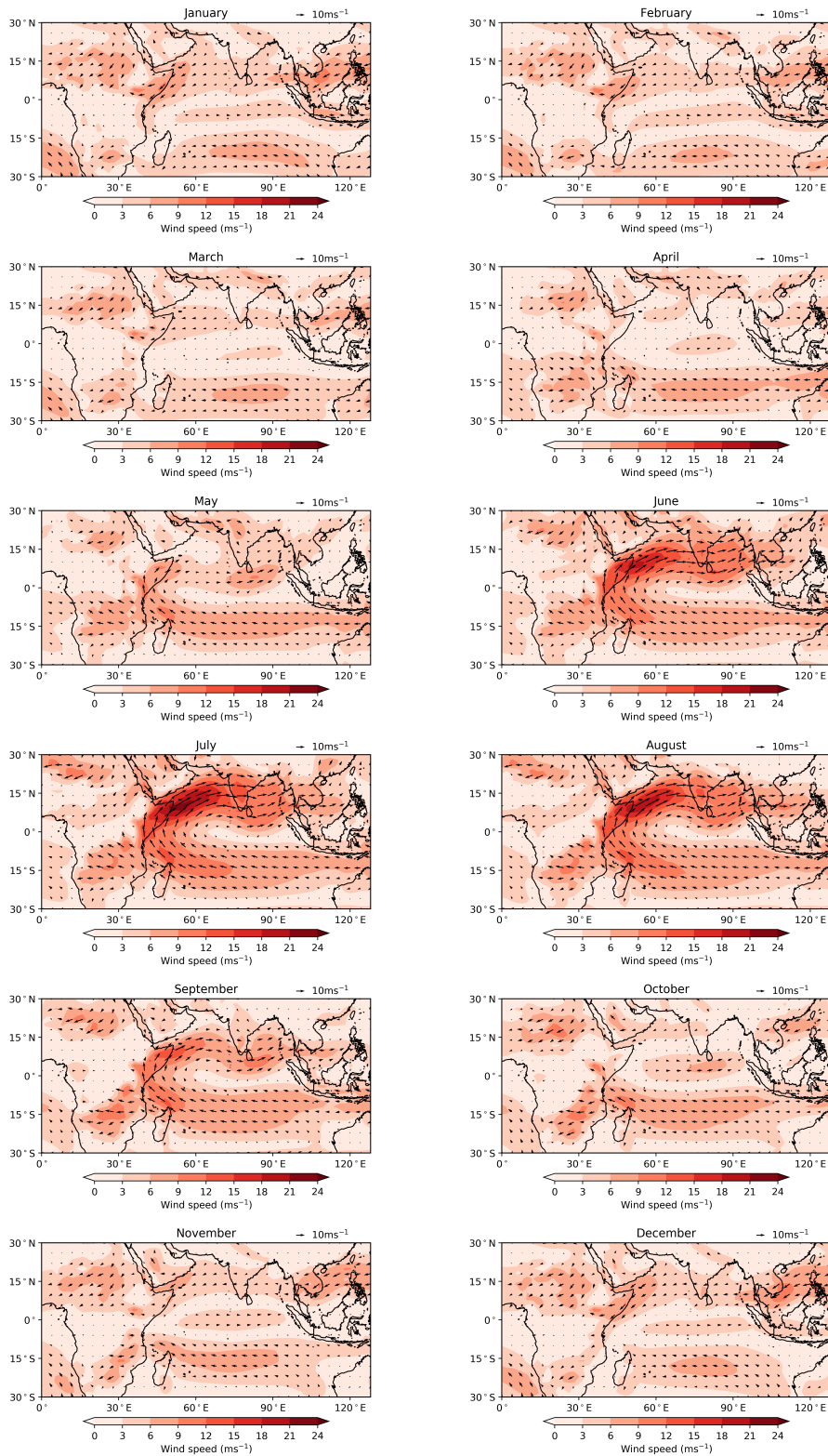
Figure 1.3.: Monthly climatology of 850hPa winds (vectors) and wind speeds (colours). Wind data are taken from the European Centre for Medium-range Weather Forecasts (ECMWF) interim reanalysis (ERA-Interim; Dee et al. 2011).
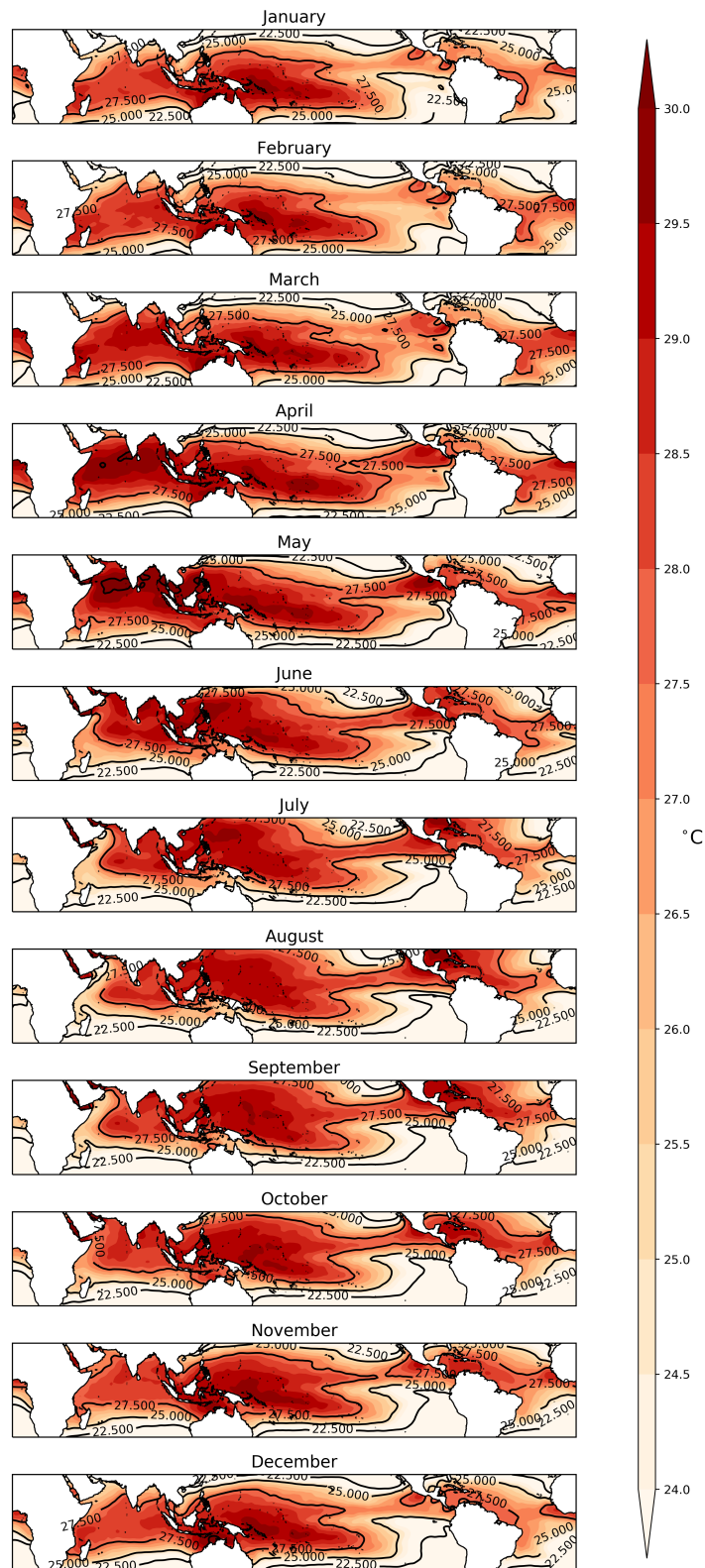
Figure 1.4.: Monthly sea surface temperature (SST) climatology in the tropics. SST data taken from the Hadley Centre Sea Ice and Sea Surface Temperature (HadISST) dataset (Rayner et al. 2003).

1.2.2. Climate and rainfall characteristics

Much of East Africa is classified as being either arid or semi-arid under the Köppen-Geiger climate classification (Köppen 1900, 1936, Peel et al. 2007). This is notable as East Africa is equatorially located, and the majority of the rest of the land mass around the equator is categorised as tropical. Several explanations have been proposed for the aridity. As discussed above, there is generally divergent large-scale flow over East Africa (Lyon 2014), preventing the formation of deep convection, whilst Nicholson (1996) suggested that the orography also played a role, as it controls features of the circulation. Nicholson (1996) suggested that the chain of mountains within the East African and Ethiopian highlands effectively redirect the low level jet, leading it to run approximately parallel with the coastline, minimising the flux of moisture into the region. The frictional contrast between the shore and water also induces subsidence (Bryson and Kuhn 1961). The chain of mountains also effectively blocks moist, unstable air from the Congo airmass from entering into East Africa (Okoola 1999a,b). Nicholson (1996) also suggests that the NE and SE monsoons are associated with thermally stable, dry air, and that moist air streams are relatively shallow. Also likely to play a role are the relatively low sea surface temperatures (SSTs) off the coast of Somalia, as shown in Figure 1.4, in comparison to other tropical SSTs, further reducing rainfall amounts.

An alternative, thermodynamic explanation to East Africa's aridity was proposed by Yang et al. (2015a), describing a ventilation mechanism. The annual cycle of rainfall over the region is dominated by the moist static energy (MSE): the atmosphere over East Africa is found to be convectively stable due to the import of low MSE near-surface air from over the Indian Ocean, from the winter hemisphere, whilst the rainfall seasons occur during rises in the local SSTs (seen in Figure 1.4), causing the import of less stable air. The ventilation (import of low MSE air) depresses local convection and precipitation, leading to the dry climate.

1.2.3. Interannual variability of rainfall: short rains season

The short rains season, occurring from October to December, is the rainfall season with the largest interannual variability (Hastenrath et al. 1993, Camberlin and Okoola 2003), and correspondingly correlates well with the annual rainfall total of the region despite contributing less rainfall than the long rains (Nicholson 1996, Camberlin and Wairoto 1997).
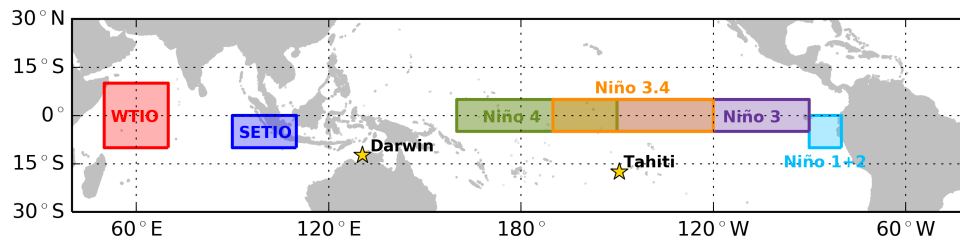
Figure 1.5.: Locations of indices used to measure El Niño-Southern Oscillation and the two poles of the Indian Ocean Dipole; western tropical Indian Ocean (WTIO) and southeastern tropical Indian Ocean (SETIO).

1.2.3.a. El Niño-Southern Oscillation

The largest source of interannual variability in the tropics is El Niño-Southern Oscillation (ENSO; Rasmusson and Carpenter 1982). A coupled atmosphere-ocean mode of variability, El Niño refers to the oceanic part, which consists of a warming off the Pacific coast of equatorial Peru in boreal winter. The Southern Oscillation is the atmospheric part, a periodic oscillation in the pressure gradient between the western and eastern Pacific Ocean.

The Southern Oscillation was first observed in the 1920s (Walker 1928, Walker and Bliss 1932), during research into how the pressure over the Pacific Ocean influenced the Indian Monsoon. Walker (1925, 1928) noticed that the pressure "seesawed" between the western Pacific Ocean close to the Indian Ocean, and the eastern Pacific Ocean. Specifically, the most common index for the Southern Oscillation, the Southern Oscillation Index (SOI; Chen 1982) considers the pressure difference between weather stations at Darwin, Australia, and on the island of Tahiti (locations shown on Figure 1.5). A negative (positive) SOI value implies higher (lower) than usual pressure over Darwin and lower (higher) than usual pressure over Tahiti.

Meanwhile, the oceanic part of ENSO was first observed as warming of the waters off the Pacific coast of South America every few years, negatively impacting fishing. It was observed to occur in boreal winter, or around Christmas, leading to the name "El Niño", meaning the boy child. An inverse event, with cooler waters off the Pacific coast was also observed to occur, and is called "La Niña", meaning the girl child. In particular, the SST anomaly of several regions of the Pacific Ocean have since been determined to monitor and define the occurrence of ENSO events. Four Niño regions were originally defined (labelled Niño 1+2, Niño3, and Niño 4 shown on Figure 1.5) throughout the Pacific Ocean, reflecting the life cycle of an El Niño event, based on

ship tracks studied by Rasmusson and Carpenter (1982), starting off the coast of Peru and moving westwards into the central equatorial Pacific. Later, Barnston et al. (1997) identified and defined the Niño3.4 region, lying halfway between the Niño3 and Niño4 regions, as being the most appropriate measure of strength of ENSO. This covers a region of the Pacific Ocean from (170°W to 120°W, 5°S to 5°N).

It was later found by Bjerknes (1966, 1969) that El Niño and the Southern Oscillation were a coupled system, with a negative SOI coinciding with El Niño, and positive SOI coinciding with La Niña. A more complete picture of the physical processes of ENSO is as follows. Under normal conditions, low level trade winds travel in an easterly direction across the equatorial Pacific Ocean, pushing warm water westwards, causing cool upwelling off the coast of Peru. Under the surface exists a thermocline, the location of the maximum vertical gradient in temperature. In usual conditions, due to the cool upwelling, the thermocline is shallow in the east, and deep in the west. A reduction in the pressure gradient across the Pacific Ocean, with higher pressure further west, slackens the low level winds. This reduces the cool upwelling off the coast of South America, reducing the gradient of the thermocline, and leading to an increase in SSTs off the coast of South America. The warmer SST then leads to a lower atmospheric pressure directly above the ocean here, partly due to increased convection caused by the warmer SSTs, further reducing the pressure gradient. This leads to a positive feedback loop (known as a Bjerknes feedback), whereby the anomalies sustain and enhance each other. Wyrtki (1975) further proposed that El Niño events are actually a response to excessively strong easterly trade winds. These strengthen the westward current, causing an east to west gradient in sea level by pushing water to the western Pacific. When the wind stress relaxes, the sea level gradient then causes the warm surface water to move eastwards, leading to the El Niño event. Figure 1.6 shows a composite of typical SST and low level winds during an El Niño and La Niña.

Whilst El Niño was originally observed around Christmas, it has since been found that the direction of the El Niño/ La Niña event will begin to develop in boreal summer from around June onwards, peak near the beginning of winter, and decay late into winter, usually January to February (Webster 2020). In very strong cases, the event can persist into boreal spring (March to May). The blue line in Figure 1.7 shows the standard deviation of the Niño3.4 index throughout the year, with a clear rise into boreal summer, and decay from boreal winter into spring. The minimum in variance of the Niño3.4 index occurs during the boreal spring, and this is generally considered the transitional period for events. It has also been found that predictability of ENSO is limited by this spring transitional period (Webster and Yang 1992), this is commonly
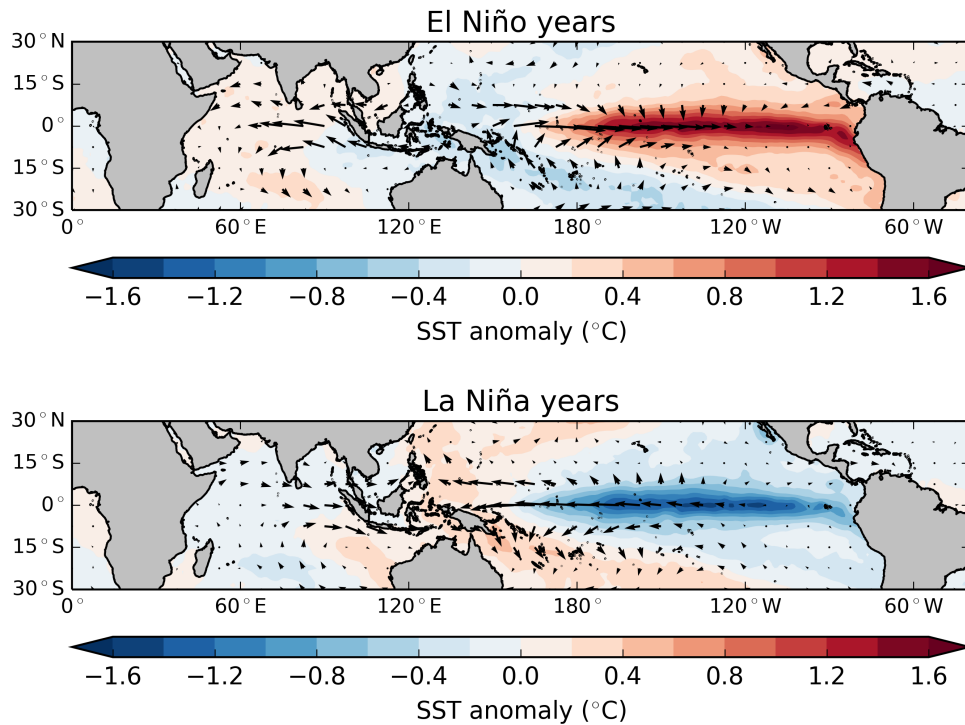
Figure 1.6.: Composite plot of seasonal mean SST (colours) and 925hPa wind (arrows) anomalies during September to December of El Niño and La Niña years. SST data are from HadISST (Rayner et al. 2003), and winds are from ERA-Interim (Dee et al. 2011). The years used were selected by taking seasonal mean anomalies of the Niño 3.4 index greater than 1 or less than -1 for El Niño and La Niña respectively.

referred to as the spring predictability barrier (Torrence and Webster 1998). It means that forecasts that rely on the predictability and time persistence of ENSO cannot pass over this time of the year, ie forecasts for the peak of ENSO (in the winter) in a certain year, cannot be made earlier than approximately May. This can be seen in Figure 1.7, where the persistence of the Niño 3.4 region is low during spring months even at short lead times. It is found that ENSO is quasi-periodic, with a period of roughly 3 to 7 years (Trenberth 1997). It has also since been determined that the impacts on weather of this mode of climate variability are seen around the globe (Rasmusson and Carpenter 1982), e.g. India (Bhalme et al. 1983), Australia (McBride and Nicholls 1983), New Zealand (Gordon 1986), South America (Aceituno 1988), and the Sahel (Folland et al. 1986).

ENSO has been found to have strong links to interannual variability of East African rainfall, particularly the short rains season. El Niño events lead to increased seasonal rainfall totals, whilst La Niña events cause decreased seasonal rainfall (Nicholson and
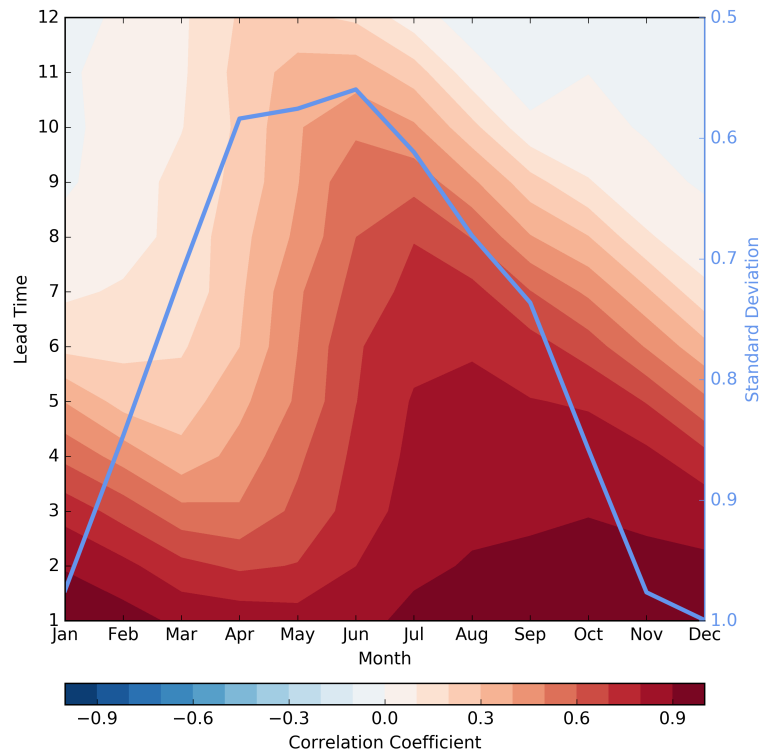
Figure 1.7.: Persistence of the Niño 3.4 region, by month and lead time, measured by calculating the correlation coefficient between the SST of each month and the following 11 months for lead times 1 to 12 (colours). A high correlation coefficient indicates high persistence between months. Blue line shows standard deviation of Niño 3.4 region over each month, with inverted y-axis. SST data taken from HadISST (Rayner et al. 2003).

Selato 2000). Early evidence of this was found by Rodhe and Virji (1976) and Ogallo (1979), who identified periodicities in the short rains interannual variability that were similar to those of ENSO. Rodhe and Virji (1976) suggested that determining the physical processes responsible for the periodicities could be used to estimate years with rainfall above or below certain limits, an early suggestion that forecasting on a seasonal timescale may be possible. Ogallo (1988), based on this study, found that across many rain gauges in East Africa there existed a significant zero-lag correlation between the monthly SOI and the monthly rainfall total for the months coinciding with the short rains, finding correlation values up to around 0.6 over the period 1923-1984, whilst also noting that there also existed significant lagged correlations between monthly SOI and rainfall during the short rains, extending as far back as July. Several studies since have investigated and confirmed this relationship (e.g. Ogallo 1989, Hutchinson 1992, Nicholson and Kim 1997, Indeje et al. 2000, Camberlin et al. 2001).

Ogallo (1988) noted, however, that some extreme wet and dry episodes during the short rains were not related to the Southern Oscillation, whilst Rodhe and Virji (1976) also observed other periodicities than the one connected to ENSO, in particular, one with a period of approximately 2 years.

1.2.3.b. Indian Ocean Dipole

Another, more recently discovered, mode of variability exists in the Indian Ocean. This is most often termed the Indian Ocean Dipole (IOD), or in some cases the Indian Ocean Zonal Mode (IOZM). It was first observed by Saji et al. (1999) and Webster et al. (1999). Saji et al. (1999) identified a pattern of variability with above normal SSTs in the western Indian Ocean off the coast of East Africa alongside below normal SSTs in the eastern Indian Ocean around Indonesia, alongside wind and rainfall anomalies. In particular, Saji et al. (1999) demonstrated a very strong link between surface equatorial zonal winds across the Indian Ocean basin, and an index defined as the difference in SST anomaly between the western tropical Indian Ocean (50°E to 70°E, 10°S to 10°N; WTIO) and the south-eastern tropical Indian Ocean (90°E to 110°E, 10°S to 0°; SETIO), both shown on Figure 1.5. This index is referred to as the dipole mode index (DMI). Several other studies since have investigated and confirmed this relationship (e.g. Black et al. 2003, Owiti et al. 2008, Ummenhofer et al. 2009). Figure 1.8 shows composites of typical SST and wind anomalies during IOD events.

Later work identified the mechanism through which the IOD influences rainfall. By comparing events, Black et al. (2003) identified that the rainfall anomalies over East Africa during the short rains are driven by the easterly wind anomalies, weakening the climatological westerly flow that transports moisture away from the African continent. This also leads to reduced rainfall over the central and eastern Indian Ocean. Black et al. (2003) also suggested that this time of year is most susceptible to changes in SST gradient as climatologically the west to east gradient is at its minimum, meaning small changes can reverse the direction of the gradient and have large impacts on the circulation. This mechanism also lines up well with the observation of Saji et al. (1999) that the low level zonal wind strength is strongly tied to the rainfall, which was also confirmed by Hastenrath (2007). Ummenhofer et al. (2009) found that in simulations, the western pole of the IOD is more important in controlling rainfall during the East African short rains.

These mechanisms are consistent with that observed by Hastenrath et al. (1993) prior
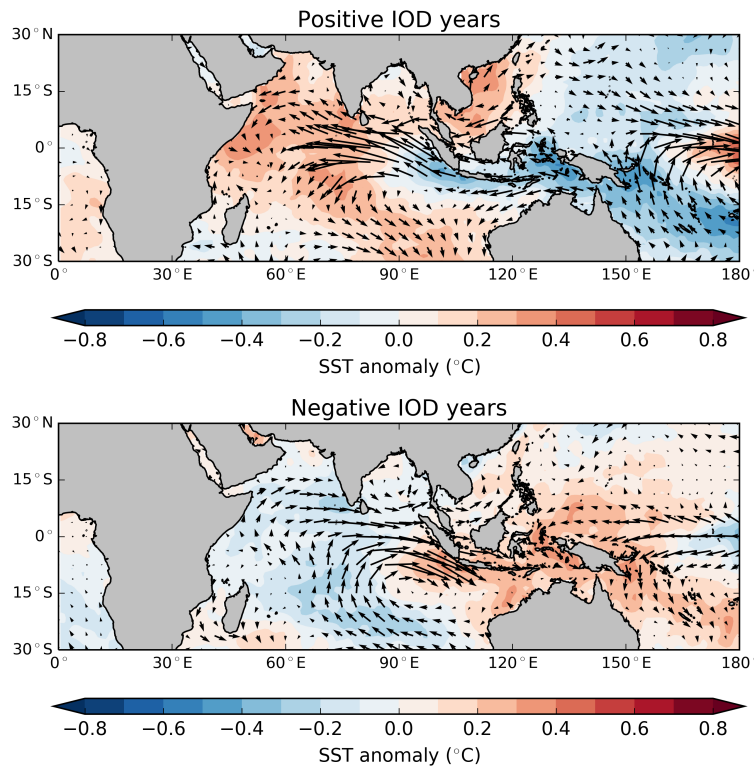
Figure 1.8.: Composite plot of seasonal mean SST (colours) and 925hPa wind (arrows) anomalies during September to December of positive and negative IOD years. SST data are from HadISST (Rayner et al. 2003), and winds are from ERA-Interim (Dee et al. 2011). The years used were selected by taking seasonal mean anomalies of the dipole mode index (DMI) greater than 0.5 or less than 0.5 for positive and negative IOD events respectively.

to the discovery of the IOD. They proposed a link with ENSO; in the case of a high SOI (equivalent to La Niña), there is high pressure over the western Indian Ocean, and low pressure over the eastern Indian Ocean, causing cool waters off the coast of East Africa, and strong westerlies across the Indian Ocean. This produces a positive feedback loop leading to increased divergence over East Africa. Hastenrath (2000) found the opposite occurs when the zonal circulation is weak. This mechanism is related to the Walker circulation cell over the Indian Ocean, and the alterations are analogous to that of ENSO in the Pacific Ocean, with a Bjerknes-like upwelling in the eastern Indian Ocean.

1.2.3.c. Independence of IOD and ENSO

Both IOD and ENSO influence weather patterns through changes in the Walker circulation. They occur at a similar time of year, and often the positive and negative phases of IOD and ENSO occur simultaneously. This has led many authors to question whether the IOD is indeed an independent mode of variability or whether it is an extension of ENSO (Marchant et al. 2007, Meyers et al. 2007). Work prior to the identification of the IOD attributed changes over the Indian Ocean basin to ENSO (Hastenrath et al. 1993).

Black et al. (2003) stated that IOD should not be viewed in isolation from ENSO, and suggested that strong ENSO forcing sets up the IOD event that then impacts East African rainfall. However, Saji et al. (1999) and Saji and Yamagata (2003) suggest that IOD is indeed an independent mode of variability, as demonstrated by the fact that there are years where a strong IOD occurs and impacts East African rainfall, in absence of an ENSO event. The key example of this is the year 1961 (Saji et al. 1999), which saw record-breaking rainfall, and a strong positive IOD, whilst ENSO conditions were neutral. Yamagata et al. (2004) suggested that only approximately one third of IOD events are associated with ENSO. Yamagata et al. (2004) and Behera et al. (2005) produced composites of the short rains in years where IOD was positive but ENSO neutral, and years where IOD was neutral but ENSO positive. From this it was seen that IOD acting alone produced excess rainfall over East Africa. However, when ENSO acted alone, no significant change in the short rains was observed. Bahaga et al. (2015) and Wenhaji Ndomeni et al. (2018) also found similar results, and demonstrated that both IOD and ENSO acting together produced a strong response in the rainfall. Yamagata et al. (2004) and Behera et al. (2005) also showed that correlations between ENSO and the short rains disappeared when the influence of IOD is removed, whilst in the opposite case, correlations between IOD and the short rains were still strong after the influence of ENSO is removed.

1.2.3.d. Nonstationarity in teleconnections

Whilst the mechanisms behind both the IOD and ENSO's ability to control rainfall over East Africa are relatively well understood, which means they are fairly reliable tools for seasonal forecasting, several authors have proposed that the relationship between the short rains and these teleconnections could be nonstationary over longer timescales. This could present complications in using them for forecasting. For example, it has

been suggested that the IOD control on the short rains has increased in strength in recent decades (e.g. Clark et al. 2003, Manatsa et al. 2012, Manatsa and Behera 2013, Nicholson 2015). There is also evidence of climate shifts, and low frequency oscillations in strength of teleconnections.

However, there are issues with these studies. Firstly, both IOD and ENSO undergo fluctuations in their activity on longer timescales: it is likely that if fewer strong ENSO or IOD events occur in a certain time period, then the typical measures of strength of relation used in these studies (such as correlation) between these and rainfall will appear to weaken. This does not necessarily mean that how an individual IOD or ENSO event impacts East African rainfall has changed. These measures also fail to account for other processes that may be impacting rainfall totals, that also have their own fluctuations in activity. Additionally, several papers report abrupt changes in correlation values when applying a sliding window technique onto time series of data, however, these are likely to occur naturally when an outlying year in the data enters into the window. For example in Manatsa and Behera (2013), an abrupt change is reported in the year 1961, however, this is simply adding an outlying point into the data: the year 1961 is one of the wettest years on record, lying several standard deviations above the mean. This causes a jump change in the correlation, but this change is mostly reversed when the outlying point exits the window 30 years later. It is also unsurprising that these studies report lower correlations when there are few active events in a period, as it is only when the conditions in these climate phenomena shift away from normal conditions that they have a control on the weather: in years where for example IOD or ENSO conditions are near normal, there will still be variability in the short rains due to other factors, but the signal coming from IOD/ENSO would be relatively smaller than usual, and so the correlation between IOD/ENSO and rainfall would naturally be lower in these cases.

Despite these issues, longer term variability in teleconnections should not be ignored, as they could be indicative of changes in lower frequency modes of variability, but care should be taken in the methods used to determine such changes.

1.2.4. Interannual variability of rainfall: long rains season

The long rains, although generally considered less variable, and more consistent than the short rains, still contain substantial year to year variability in total rainfall amounts. This has wide impacts as the main crop-growing season, so being able to predict this variability is of great importance. Whilst the short rains season has been found to

be linked to global scale modes of variability such as ENSO and IOD, little evidence for this has been found for the long rains (e.g. Ogallo 1988, Camberlin and Wairoto 1997, Pohl and Camberlin 2006b). This is partly linked to the time of year at which the long rains occurs; during the transition period for ENSO, where the inter-annual variance in the SSTs in this region of the Pacific is lowest (Torrence and Webster 1998). Hastenrath et al. (1993) also demonstrated that in boreal spring surface pressure is low across the Indian Ocean, ruling out the mechanism of the IOD and ENSO altering the Walker circulation. Hastenrath et al. (2011) assigned the lack of a zonal circulation cell over the Indian Ocean in boreal spring to winter cooling.

Several of the phenomena discussed in this section are also relevant for the short rains season, however their influences are small compared to the previously discussed tele-connections of ENSO and IOD.

1.2.4.a. Madden-Julian Oscillation

The Madden-Julian Oscillation (MJO) is an eastward propagating oscillation in the tropical atmosphere, first observed and described by Madden and Julian (1971, 1972, 1994). Madden and Julian (1971) observed an opposing oscillation in zonal wind anomalies in the lower and upper troposphere (around 850hPa and 150hPa respectively). Madden and Julian (1972) further noted that a disturbance in the surface pressure followed the zonal wind anomalies, and suggested that the MJO is linked to a concurrently observed area of enhanced large-scale convection driven by low level convergence, followed by an area of suppressed convection. This can be seen in the rainfall composites in Figure 1.9, resembling a shift of the Walker circulation.

Wheeler and Hendon (2004) proposed a system for describing the activity and location of the MJO. It uses a system of 8 phases, which determine the location, and an amplitude for determining how active the event is. These are derived using empirical orthogonal functions (EOFs). The two leading modes are referred to as Real-time Multivariate MJO series 1 and 2, or RMM1 and RMM2. Using the values of these in a polar coordinate system, an amplitude and phase can be determined, where the amplitude is the distance from 0 ($\sqrt{(\text{RMM1})^2 + (\text{RMM2})^2}$), and the phase related to the angle. These are visualised in a Wheeler-Hendon diagram, as seen in Figure 1.10. The angles are labelled as phases from 1 to 8, with phase 1 meaning that the enhanced convection is over Africa, and the phases move eastwards around the equator, for example phases 2 and 3 mean the centre of enhanced convection is over the Indian Ocean. The MJO
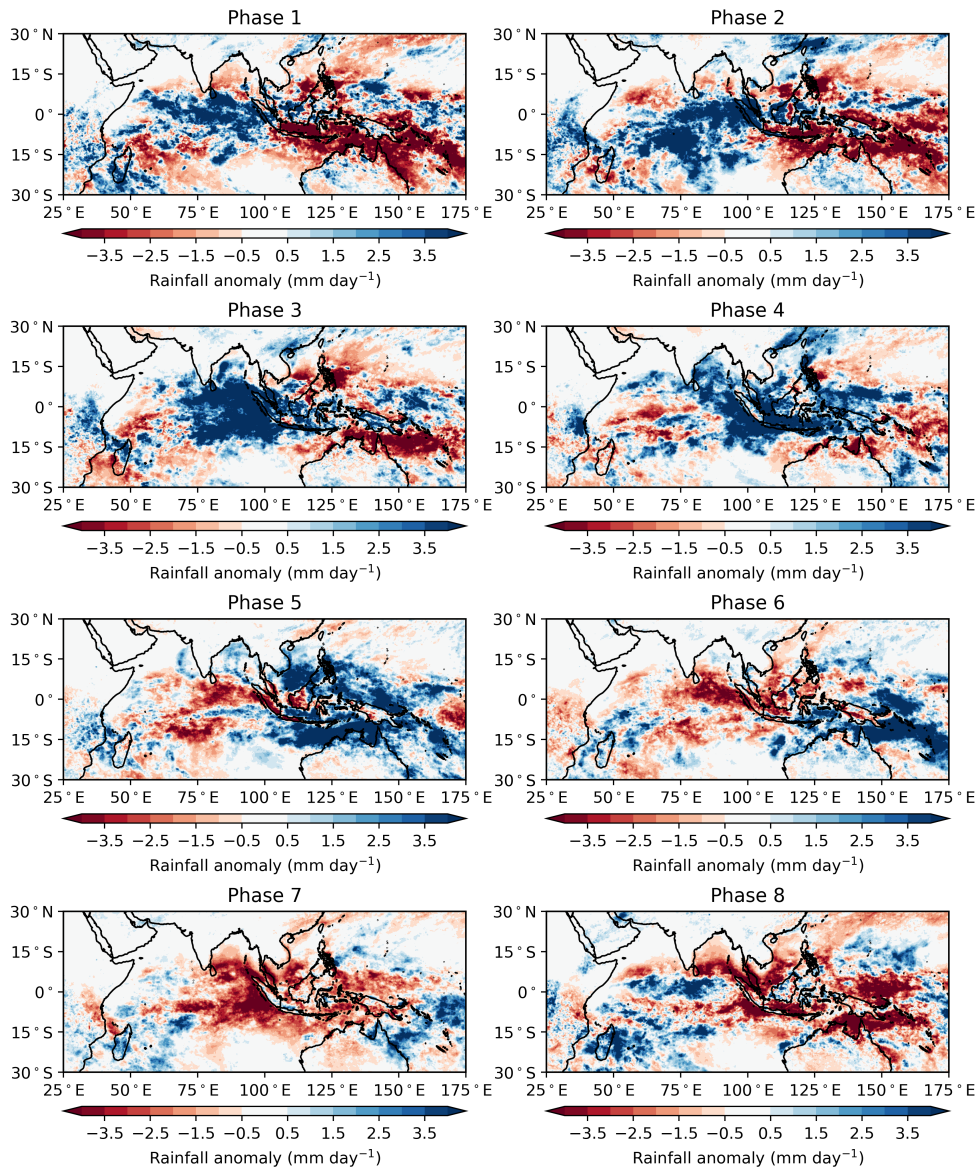
Figure 1.9.: Composite maps of rainfall anomaly compared to climatology, over 1998-2018, by MJO phase. Rainfall data is from TRMM (Huffman et al. 2007), MJO data is taken from Bureau of Meteorology (2020).
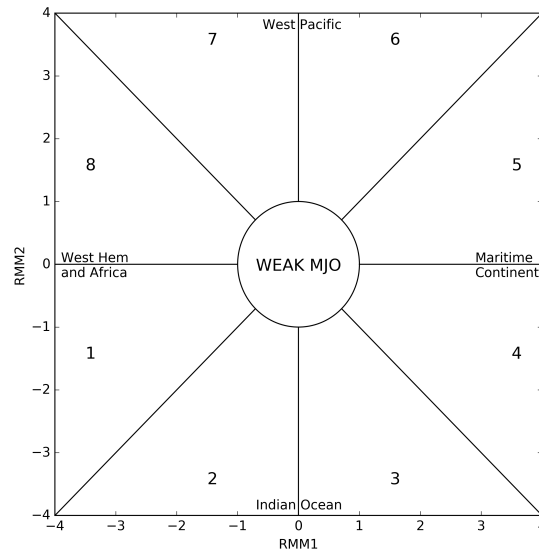
Figure 1.10.: An example of the Wheeler-Hendon diagram (Wheeler and Hendon 2004). The MJO amplitude is the square root of the distance from the centre. Amplitude less than 1 is considered as a weak/ inactive MJO, marked by the centre circle with radius of 1. The MJO phases and corresponding locations are labelled within the sections.

is considered active if the amplitude is greater than 1 (marked by the inner circle).

The MJO is the primary source of intraseasonal variability within the tropics (Madden and Julian 1994). Pohl and Camberlin (2006a) studied the intraseasonal influence of the MJO on East African rainfall during both rainfall seasons. They found that intraseasonal wet events in East Africa occur alongside large-scale anomalies in zonal circulation patterns around the equator. The wet events were found to preferentially occur during certain phases of the MJO. A west/ east split in the behaviour was also noted. Phases 1 to 3 of the RMM indices lead to wet spells over the western highlands region of East Africa, with dry spells observed over the coastal region. Inversely, phases 5 to 7 corresponded to dry spells over the western highlands with wet spells over the coast. This can be seen in Figure 1.9. Over the highlands the wet spells during these phases were linked to deep convection, caused by low-level westerly anomalies, whilst MJO induced wet spells over the coastal region were linked to suppressed convection over East Africa and the western Indian Ocean. However, Pohl and Camberlin (2006a) suggested that during these phases the suppressed convection induces increased moisture advection from over the Indian Ocean. Berhane and Zaitchik (2014) also found that the MJO affected wet and dry spells within both rainfall seasons, with results generally consistent with the previous studies, however, they found different results dependent on which month was being considered. They suggested a variety of different

ways the MJO influences rainfall, including through modulating the Somali Jet early and late in the rainfall seasons, as well as those suggested previously. Hogan et al. (2015) investigated the MJO in the Met Office Unified Model (MetUM; Walters et al. 2011). They found in agreement with previous studies that in observations phases 2-4 lead to increased rainfall over the highlands with suppression over the coast, and the inverse occurs during phases 6-8. They also found that the MetUM could replicate these patterns with up to 5 days lead time.

Further to this, studies have been performed examining the inter-annual impact of the MJO on the long rains season. Pohl and Camberlin (2006b) found that the MJO amplitude alone, regardless of the phase of the MJO, can explain up to 44% of the variance in seasonal totals of the long rains. They also found that higher MJO amplitude leads to an early onset of the long rains, although, as demonstrated by Camberlin et al. (2009), the onset date of the season and total rainfall are strongly correlated, and could account for this. More recently Vellinga and Milton (2018) also demonstrated the link between MJO amplitude and the long rains, and proposed an explanation for this. Intuitively, one would expect that in a season with higher MJO amplitude, on average, for the phases conducive to rain to be cancelled out by those that suppress rain. However, Vellinga and Milton (2018) demonstrated that the anomalous ascent or descent caused by active MJO of their respective phases, is asymmetric. Anomalous ascending motion has a larger impact on the absolute total rainfall experienced than anomalous descending motion. This is partially due to the fact that rainfall amounts cannot sink below 0, so the relationship between rainfall amounts and MJO amplitude is not linear.

1.2.4.b. Quasi-Biennial Oscillation

Another source of inter-annual variability is the Quasi-Biennial Oscillation (QBO). This is a highly periodic change in stratospheric winds (approximately between 10 and 70hPa) from westerlies to easterlies, with a period of approximately 26-28 months, first observed by Ebdon (1960) and Reed et al. (1961). The transition in wind direction propagates downwards, meaning that the wind direction in the upper (10hPa) and lower (70hPa) levels are regularly out of phase (Baldwin et al. 2001). The QBO has a teleconnection to the North Atlantic Oscillation (NAO), which is of importance for seasonal predictability within the extra-tropics (Scaife et al. 2014). A common measure of the QBO, and often referred to as the QBO-index, is the zonally averaged zonal winds over the equator at pressure levels around 50hPa.

Few studies have considered how the QBO influences East African rainfall, however, a study by Indeje and Semazzi (2000) demonstrated remarkably high correlations between a the QBO-index at 30hPa and the long rains, including at up to 3 seasons ahead of the rainfall season. A mechanism, however, is not clear, and the correlations were not cross-validated. The long rains do appear to fluctuate with an approximately 2 year period, however, given, the phasing of the QBO depends on the height considered, selecting the correct height that happens to be in phase with the long rains may lead to an inflated correlation. More recently Vellinga and Milton (2018) utilised a QBO-index when constructing a multiple linear regression equation for producing forecasts of the long rains, suggesting that it may modify the large-scale subsidence over East Africa, however, they noted that the QBO alone provides only a small amount of the predictive information. Recent studies have, however, demonstrated that the QBO may play a role in modulating the MJO (Yoo and Son 2016, Son et al. 2017 , Klotzbach et al. 2019), although this is currently understood to mainly occur during boreal winter (December to February).

1.2.4.c. Congo airmass and zonal winds

To the west of East Africa lies the Congo basin, containing the second largest rainforest in the world after the Amazon. In the lower troposphere above the rainforest sits the so-called Congo airmass. This is an airmass with a very high moisture content, as shown by considering relative humidity (RH) as in Figure 1.11, taken from Finney et al. (2019). Its position adjacent to East Africa means that incursions of the airmass could provide more moisture to enhance rainfall amounts. An early study by Nakamura (1968) suggested that the western highlands region of East Africa in particular experiences abundant rainfall when westerly winds were present. It was noted that when westerly winds were observed the relative humidity within the lower troposphere was much greater. However, Nakamura (1968) also noted that westerlies are observed most often during the summer, and least often during the peak months of the two rainfall seasons (November and April). Okoola (1999b) notes that stronger than average easterly winds over East Africa coincide with dry spells, whilst Okoola (1999a) found that during the long rains alternating westerly and easterly patterns were observed, with westerlies leading to wet spells. However, they also noted that the frequency of westerly winds were likely reduced due to the orography of the western side of East Africa. Pohl and Camberlin (2006b,a) and Berhane and Zaitchik (2014) noted that phases of the MJO coinciding with enhanced rainfall over East Africa also produce a westerly wind anomaly to the west.
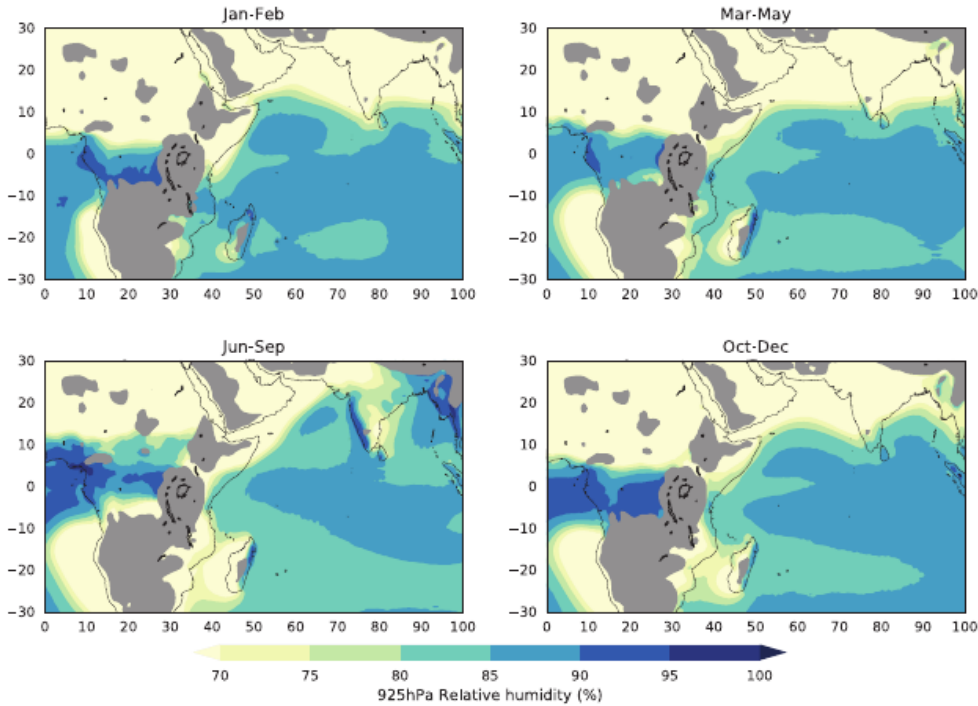
Figure 1.11.: Maps of 925hPa relative humidity over Africa and the Indian Ocean, for the seasons January-February, March-May, June-September and October-December (colours). Grey shading shows regions where seasonal mean surface pressure is less than 925hPa. Taken from Finney et al. (2019) Figure 4.

A comprehensive study of the Congo airmass and its influence on East African rainfall was performed by Finney et al. (2019), motivated by the excessively wet long rains of 2018 (Kilavi et al. 2018). It was first demonstrated that wet spells in the 2018 long rains coincided with westerly incursions from the Congo airmass. Finney et al. (2019) then corroborated some of the results initially found by Nakamura (1968). By considering westerly events to be a westerly column integrated moisture flux, it was found that westerly days were linked to more abundant rainfall, although they were least frequent during the two rainfall seasons. It was noted, however, that westerly days were more frequent during the long rains than the short rains, highlighting their potential importance for the long rains season. Further, Finney et al. (2019) demonstrated a strong correlation between the number of westerly days in a long rains season and the rainfall total for the season. It was proposed that on westerly days, moisture from the Congo airmass was imported over East Africa, increasing the specific humidity (SH) on these days, supplying additional moisture to enhance rainfall, demonstrated in Figure 1.12, taken from Finney et al. (2019). Further, it was suggested that days with weaker easterlies than usual also lay between easterly and westerly days in terms of its response, suggesting that the overall strength of the wind profile matters, rather than simply the overall direction.

Finally, it was suggested that the MJO may play a role in driving the westerly winds. As noted before, the MJO in phases 2-4 leads to enhanced rainfall over East Africa (e.g. Pohl and Camberlin 2006a), however, this is when the convective core of the MJO is over the Indian Ocean rather than Africa, suggesting the rainfall enhancement is not a direct effect of the MJO. It is likely that the observed westerlies are part of the Matsuno-Gill response (Matsuno 1966, Gill 1980. Finney et al. (2019) also linked the MJO to an increase in tropical cyclones, and noted that during the 2018 long rains season several tropical cyclones occurred in the Indian Ocean to the east of Madagascar, and were found to drive the westerly winds over East Africa that led to abundant rainfall. Meanwhile in 2019, a tropical cyclone that tracked into the Mozambique channel, to the west of Madagascar, caused a delay in the 2019 long rains, again due to its effect on the large-scale flow over Africa.
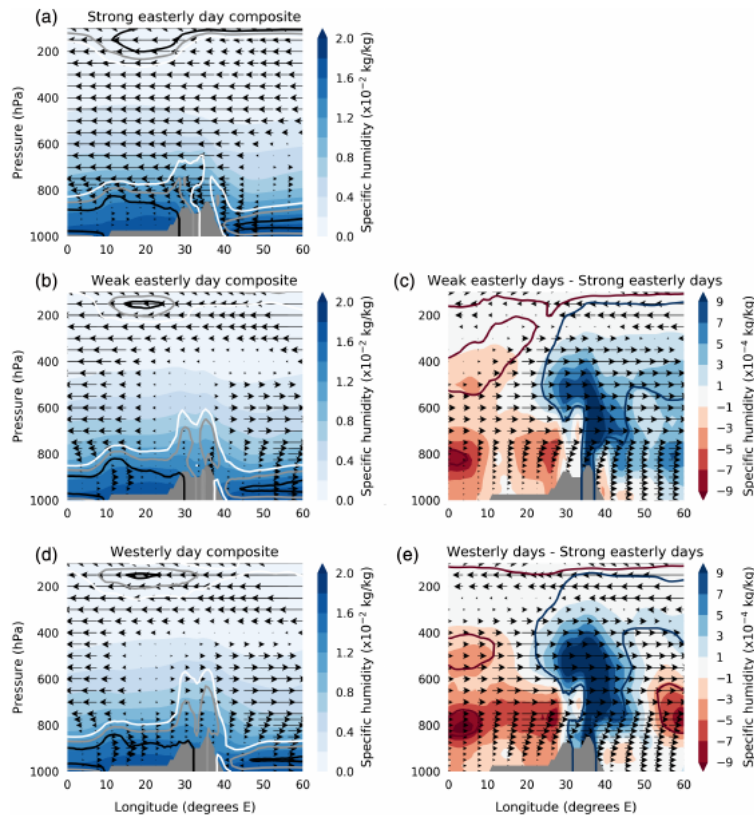
Figure 1.12.: Pressure-longitude cross-section composites of specific humidity (colours), relative humidity (contours; black, grey, and white mark 85%, 80%, and 75% RH respectively), and zonal wind (arrows), for a) easterly days, b) weak easterly days, c) weak easterly minus easterly days d) westerly days, e) westerly minus easterly days. Grey shading shows regions where seasonal mean surface pressure is less than 925hPa. Taken from Finney et al. (2019) Figure 5.

1.2.5. Recent and future trends in rainfall

1.2.5.a. Observed trends

A recent topic, as longer observational datasets are generated than were previously available, is long term trends in seasonal rainfall totals. One of the most striking recent trends is that of the long rains. Many authors (e.g. Funk et al. 2005, 2008, Lyon and Dewitt 2012, Viste et al. 2013, Liebmann et al. 2014, Hoell and Funk 2014, Nicholson 2016b, Ongoma and Chen 2017) have identified a declining trend in the observed long rains rainfall totals, from approximately the 1980s. Tierney et al. (2015), from studying tree rings, suggest that the observed drying trend is unusual within the context of the last 2,000 years, implying links to anthropogenic climate change. It has also recently been identified by Wainwright et al. (2019) that it is possible that the long rains rainfall totals may have begun to recover, from approximately 2011 onwards.

Several authors have sought explanations for the observed long rains drying trend, with much focus being on the Pacific and Indian Oceans, the Indo-Pacific region, and linking the two. Funk et al. (2008) suggested that a warming Indian Ocean is influencing East Africa by setting up a Walker cell-like circulation anomaly. Meanwhile Williams and Funk (2011) suggest that the rapid warming of the Indian Ocean has extended the tropical warm pool, producing a westward extension of the ascending branch of the Walker circulation, suppressing convection over East Africa. Lyon and Dewitt (2012), Lyon et al. (2014), and Lyon (2014) identified the decline as an abrupt change from approximately 1999 onwards, linked to the Pacific Decadal Oscillation (PDO; Mantua et al. 1997). Yang et al. (2014) meanwhile suggests that the SST anomaly pattern is La Niña like. Hoell and Funk (2014) identified Indo-Pacific SSTs as the main driver, suggesting that warming over the Indo-Pacific region as well as decadal variability are the causes of more frequent drought. Liebmann et al. (2014), by using simulations, identified an increased zonal gradient in SST between Indonesia and the central Pacific Ocean. Funk and Hoell (2015) furthered this by using EOF analysis to identify a western Pacific "V" pattern, with the point of the "V" over the Maritime continent, and the two legs stretching northeast and southeast into the Pacific Ocean. Funk and Hoell (2015) suggested this was driven by radiative forcing and not natural variability. Wainwright et al. (2019) meanwhile find that the long rains decline is down to a reduction in the length of the season rather than a change in intensity of rainfall.

A secondary argument related to the long rains decline is the question of the relative contribution of natural decadal variability versus anthropogenic climate change. Sev-

eral authors argued for natural variability (e.g. Lyon and Dewitt 2012, Lyon et al. 2014, Lyon 2014, Yang et al. 2014, Bahaga et al. 2019), whilst others suggest human factors (e.g. Funk et al. 2008, Williams and Funk 2011, Funk and Hoell 2015, Tierney et al. 2015), or a combination of the two (Hoell and Funk 2014). Hoell et al. (2017) tried to reconcile the two main theories: human induced climate change causing warming of Indo-Pacific region SSTs, and natural change due to ENSO-like Pacific decadal variability, warming the western Pacific whilst cooling the central Pacific. By comparing simulations both with and without human influences, they suggest that its likely the interplay of global warming and decadal variability together could enhance drying trends relative to natural variability alone. However, they note that these are speculative results, and so the ultimate cause of the decline is uncertain.

Meanwhile, less work has considered trends in the short rains season, however, Liebmann et al. (2014), Rowell et al. (2015), and Tierney et al. (2015) also identified an increasing trend in rainfall in this season. This was linked to western Indian Ocean warming (Liebmann et al. 2014), and a weakening of the Walker circulation (Tierney et al. 2015).

1.2.5.b. Future climate projections

Shongwe et al. (2011), Otieno and Anyah (2013), Kent et al. (2015), and Ongoma et al. (2018) all looked at East African rainfall in the Coupled Model Intercomparison Project version 5 (CMIP5; Taylor et al. 2012). Shongwe et al. (2011) found a positive shift across both rainfall seasons, indicating increase in mean precipitation and high intensity rainfall, and less severe droughts. Ongoma et al. (2018) showed that both rainfall seasons are projected to increase, but the short rains moreso than the long rains, whilst Otieno and Anyah (2013) and Kent et al. (2015) note a high uncertainty in the projections, particularly over the long rains. Anyah and Qiu (2012) reported similar results in the Coupled Model Intercomparison Project version 3 (CMIP3; Meehl et al. 2007). Yang et al. (2014) demonstrated that the CMIP5 historical experiments fail to capture the observed downward trend in the long rains rainfall, meanwhile, the CMIP5 Atmospheric Model Intercomparison Project (AMIP) experiment models using SSTs forced by observations do capture the observed decline in rainfall over the 1979 to near present period.

Several studies have also used regional climate models (RCMs) to investigate future climate projections. Vizy and Cook (2012) suggest that the number of wet days over

East Africa is projected to decrease, primarily during the long rains, whilst Cook and Vizy (2013) found that the long rains are reduced, related to an increase in rainfall over the Congo basin, whilst the length of the short rains increases. Endris et al. (2018) found that the long rains are projected to have a stronger ENSO teleconnection in the future, although also see a decrease in rainfall during this season. Overall, there exists a large uncertainty in the future direction of long rains rainfall totals.

1.2.5.c. The East African climate paradox

The fact that the long rains is observed to be drying, whilst coupled model projections suggest that the long rains will experience more rainfall in the future has attracted much attention. This is commonly termed the East African climate paradox (Rowell et al. 2015). It leads to uncertainty over the future of East Africa, and questions the reliability of climate models. Such contradictory information makes it much more difficult for decision makers to take actions, as it is unclear whether preparations should be made with the expectation that the long rains season will keep getting drier, with the implication of more frequent drought and food insecurity, or whether to trust the projections and prepare for a wetter future, which may lead to more efficient crop growth, but also comes with risks such as increased flooding.

Rowell et al. (2015) proposed several hypotheses to reconcile this issue. The first is that the observed trend is due to poor quality observations, however they discount this. A second is simply that the projection cannot be trusted. Other proposed hypotheses include: the past or future trends are linked to natural variability, a balance between competing anthropogenic forces is changing (e.g. aerosol versus carbon emissions), or the balance between mechanisms that determine the response to anthropogenic forcing is changing. Several other authors also highlight the fact that coupled climate models fail to correctly capture the annual cycle of rainfall over East Africa; having a wetter short rains season than long rains (e.g. Yang et al. 2014, Tierney et al. 2015, Yang et al. 2015b), and suggest therefore that caution should be used when considering these projections.

1.3. Seasonal forecasting

This section provides a brief overview of the history of seasonal forecasting. Extensive in-depth literature exists on this topic through the following book: Troccoli et al. (2008);

and several review papers (Palmer and Anderson 1994, Troccoli 2010, and Doblas-Reyes et al. 2013).

1.3.1. Early methods of seasonal forecasting

The first attempts at seasonal forecasting can be traced back to the Indian Meteorological Department (IMD). In the 1870s, following drought related famines, studies were undertaken to try to predict the Indian Monsoon, through surface pressure data from countries around the Indian Ocean (Troccoli 2010). Through these studies it was identified that droughts in India often aligned with droughts in Australia, the first observation of a teleconnection. Blanford (1884), in a study linking snow over the Himalayas and drought in India, identified that during a famine in India that took place over 1876-77, an extensive region of abnormally high pressure was present. It has since been found that this was connected to a particularly strong El Niño event. Further work by Walker (1925, 1928), and Walker and Bliss (1932) identified links between seasonal variations in centres of action of pressure oscillations, and found in particular a link between the Southern Oscillation and the Indian Monsoon rainfall amounts. Walker and Bliss (1932) developed forecasts for the Indian monsoon using regression models.

Following the dawn of aviation, from approximately the 1930s, a major shift of focus to advancing forecasting on short timescales was made, leading to a stagnation in progress on developing seasonal forecasts. Attention turned back towards seasonal forecasting upon the identification of the coupling between El Niño and the Southern Oscillation (Bjerknes 1966, 1969). In particular Charney and Shukla (1981) realised that tropical predictability is related to surface boundary conditions such as SSTs and demonstrated the potential for predictability on timescales of months, with a focus on the Indian Monsoon.

1.3.2. Statistical predictions

Shortly after the study by Charney and Shukla (1981), a very strong El Niño took place, during 1982-83, the effects of which, alongside lack of early warning (Kirtman and Pirani 2008), brought the phenomenon into widespread media attention for the first time (Caviedes 1984). It was also noted that many of the widespread global impacts could be matched to similar impacts of previous El Niño events. The combination of new understanding and newfound interest prompted the true dawn of seasonal forecasting

in the form of statistical models.

Several early models were based primarily on measures of ENSO, using techniques such as linear regression. For example Gray (1984) used ENSO and the QBO to predict Caribbean hurricane activity, and Farmer (1988) for the East African short rains used the SOI. Folland et al. (1991) also used Atlantic and Indian Ocean anomalies to predict Sahel rainfall, whilst Nicholls (1989) used both the Pacific and Indian Ocean for predictions of Australian winter rainfall. Statistical forecasts are still regularly used operationally today, alongside dynamical model forecasts, although in many cases have since increased in complexity (Doblas-Reyes et al. 2013).

The general principle behind statistical prediction is to identify a set of predictors: climate variables that are monitored and observed (for example SSTs or indices of climate modes such as ENSO), that are known to have a relation to the predictand, i.e. the thing to be predicted, often seasonal rainfall total. Past observations of the predictors and predictand are then used to develop an equation or model linking the two. The most simple, common method used for this is a linear regression model. To make a forecast for an upcoming season the observed values of the predictors are then placed into the model to give a prediction of the predictand. The most simple methods may use only predictors for which the physical mechanism linking them to the predictand are understood, such as using a metric for the IOD for predicting the short rains in East Africa. However, more complex statistical tools can systematically search for linkages between predictors and the predictand, such as checking global SST data for connections to be used in the model.

The risk with using predictors without a physical basis is that the tools may find correlations that occur by chance throughout the past observational data, and may not actually improve predictions, but improve the closeness of fit of the model over the past. This can lead to inflated estimates of the skill of the statistical model, known as model overfitting. To avoid, or minimise this, past observational data can be split into training and test data. Some portion of the past observations are used to generate the model, these are the training data. The rest of the past observations are then fed into the model, to test how well it predicts past observations of the predictand over a set of observations that have not been used to generate it. These are the test data. This method gives a much better estimate of how well the model performs, as the model is not tested on information already used to define the model.

An advantage of using statistical forecasts is that in places where processes driving predictability are well understood a relatively useful forecast can be made with little

computational expense in comparison to using a dynamical model. New knowledge and understanding can also be quickly applied to statistical models.

1.3.3. Dynamical seasonal forecast models

In the late 1980s and 1990s research began on filling the gap between the numerical weather prediction (NWP) models used operationally for forecasting weather on timescales of a few days, and the long term climate models (Palmer and Anderson 1994). Initial focus of these dynamical models was to predict ENSO events (Doblas-Reyes et al. 2013), the first of these to successfully forecast the onset of an ENSO event was Cane et al. (1986). Progress was then made towards forecasting the global atmosphere using the Pacific Ocean only (Ji, M. and Kumar, A. and Leetmaa, A. 1994, Kirtman et al. 1997) before a first global coupled model forecasting precipitation was developed in the late 1990s (Stockdale et al. 1998). Since this time, many of the Global Producing Centres (GPCs) around the world have formulated and produce operational dynamical seasonal forecast models.

The majority of modern dynamical seasonal forecast systems are run as coupled ocean-atmosphere models. A more detailed description of the structure of a dynamical seasonal forecast model will be given in Section 1.5.1, describing the dynamical model used for the work within the thesis.

Dynamical seasonal forecast models attempt to forecast the conditions of the climate system months ahead by using initial conditions from observations around the Earth to computationally solve equations describing the evolution of the Earth's climate system. They perform this by splitting the ocean and atmosphere up into grids, and solving these equations at each grid point. Consequently, dynamical models are computationally very expensive to run. There are several causes of errors common within these models. Three major ones are: 1) uncertainty in the observations used to initialise the models. Due to the nonlinear form of the equations this can lead to large errors, and drastically different results from small changes in the observations (Troccoli et al. 2008). 2) The finite resolution of models. Due to limits on computational power, each grid cell can be of the scale of 100km, and there are many processes that occur on scales smaller than this. 3) The tendency of models to drift away from reality. Models also display biases, some of which are common amongst models, such as the double ITCZ problem (e.g. Doblas-Reyes et al. 2013, Li and Xie 2014, Richter et al. 2016).

These errors could render dynamical forecasts as unusable, however, methods have

been developed to tackle or reduce the impact on forecasting ability caused by these problems. 1) An ensemble of models is run for each forecast, with a range of starting conditions to capture some of the uncertainty in the observations and give a range of probable outcomes. 2) Some of the key subgrid processes are parameterised, such as convection (Troccoli et al. 2008). Additionally, with increased computational power, models can be run with increasingly high resolution. 3) To tackle model biases, a set of hindcasts is created for the model. These are forecasts using the same model, but run over historical periods. This allows for a comparison of the model behaviour against observations, and means that a model climatology is built. Forecasts can then be based upon the difference from the model climatology rather than the observed climatology e.g. if a model rainfall forecast has a wet bias in a certain location then by comparing to observations a wetter than average season will be forecast too frequently, and often incorrectly. However, if the forecast is compared against the model climatology for this location, the bias can be removed, and it can be determined whether the forecast is wetter or drier than usual. There are, however, other biases in addition to shifts from mean (e.g. distributions with incorrect standard deviation or shape), which can also be corrected for after the model is run (Troccoli et al. 2008).

Despite these errors, and the fact that statistical models can offer reasonably good skill for predicting a field of interest with much less computational power, dynamical models offer a wealth of additional information beyond simply the value of interest. For example, a full spatial and temporal picture of global atmospheric conditions over the period of interest, estimates of uncertainty, and the ability to study how certain prevailing conditions may be causing changes in the field of interest (Troccoli 2010).

1.4. Seasonal prediction methods for East Africa

1.4.1. Statistical models

1.4.1.a. Short rains season

The earliest attempts at forecasting seasonal rainfall totals over East Africa involved using simplistic statistical models. Farmer (1988), furthering the work from Behrend (1987), and Ogallo (1988) who observed lagged correlations between the SOI and East African rainfall, used the SOI averaged over the meteorological seasons, defined as December to February (DJF), March to May (MAM), June to August (JJA) and Septem-

ber to November (SON), to forecast the short rains rainfall anomalies over the Kenyan coast region over the period 1901-1984. The method used was a simple linear regression with the SOI with the lag of interest as the predictor and rainfall totals as the predictand. It was found that whilst simultaneous correlation between rainfall and SOI was the highest, there is a strong persistence in the SOI from the summer to the autumn (JJA against SON) with a correlation between the two of 0.74, allowing for a strong correlation between SOI at one season lag and short rains rainfall (0.51). By splitting the period into two sub-periods (1901-42 and 1943-84) and generating a linear regression based on the JJA SOI data from the first sub-period to predict East African rainfall, a realistic expectation of the skill of a seasonal forecast using this method can be estimated. Splitting the observations into a training set and a test set in this way avoids the potential problem of overfitting a model. This method yielded correlations up to 0.6 with the observations, implying the potential for being able to operationally forecast rainfall totals during the short rains using only the SOI as a predictor.

A more complex statistical model for forecasting of the East African short rains was developed by Mutai et al. (1998). They demonstrated that July to September SSTs contain relationships to short rains seasonal rainfall totals. They used EOFs to find SST patterns in the Pacific (related to ENSO), the Indian Ocean (detecting the IOD before its formal definition), and also in the Atlantic Ocean. Two types of statistical model were tested, multiple linear regression (MLR) and linear discriminant analysis. For the MLR, the SST data was split into two periods 1945-1966 and 1967-1988, with one used as a training period and the other a testing period, then repeating with the periods switched, to avoid model overfitting. With the 1967-1988 test period a correlation of 0.78 with the entire region was found, whilst with the periods reversed a lower correlation of 0.56 was obtained. It was also found that forecast correlations at individual locations were substantially lower than the correlation of the entire region.

Philippon et al. (2002) also developed a statistical model for the short rains. They looked to develop the work of Mutai et al. (1998), and included atmospheric variables as well as SSTs. Focusing on a region covering Kenya and Uganda, they produced a similar MLR model, achieving a correlation of 0.8, using a cross-validation method over the period 1968-1997. Their model used indices representing Indian monsoon dynamics that are linked to the SSTs in the western Indian Ocean, 200hPa meridional winds over Southern Africa which are linked to SST anomalies in the Atlantic Ocean, and a principal component representing the Walker cell over the western Indian Ocean.

Several more recent studies have further investigated the idea of utilising atmospheric

variables as well as SSTs, or used more complex approaches. These studies have mostly focused on trying to predict the long rains season, and so are discussed in the next section, although some have considered both the short and long rains (Nicholson 2014, Chen and Georgakakos 2015). Nicholson (2017) notes that forecasts using atmospheric variables can outperform those using purely SST based predictors, in both seasons.

1.4.1.b. Long rains season

Forecasting over the long rains season has been less well pursued, partially due to the lack of historical links to major modes of SST variability allowing for predictions to be made. However, motivated by the increase in recent droughts over East Africa, Funk et al. (2014) considered the western Pacific Ocean gradient in the long rains found to be partially responsible for the decline in the East African long rains (Williams and Funk 2011). They constructed a regression using SSTs from January over this western Pacific region, finding that it explained approximately 50% of the variance of the first principle component of rainfall over East Africa. Funk et al. (2014), however, notes that this is only a recently emerging trend and so caution must be taken when such a forecast is used. Chen and Georgakakos (2015) developed a method to detect dipoles in SST anomalies in the global SST field to rainfall in East African regions divided into $5° \times 5°$ boxes, over 1980-2011. Significant dipoles are used to develop linear regression models, with the number of dipoles used determined by minimising the mean absolute error of the forecast, although is generally around 20. Cross-validation is used, and highly overlapping dipoles are removed from selection, to try and reduce overestimation of skill. High skill is found in predicting most regions across East Africa for both seasons. In particular high skill is found for the long rains, with correlations up to 0.72 with the observations, in some cases with up to 11 months lead time. Dipoles identified in the short rains largely coincide with the IOD regions, whilst for the long rains poles are found in the southwest Indian Ocean, southern Atlantic, and the Arabian Sea. A concern for this study is that despite the precautions, these forecasts may be overestimating the level of real skill to be expected. Mechanisms linking the identified poles in the long rains are not clear, although SSTs over the Arabian Sea have been highlighted as a possible control on long rains rainfall in other studies (Vellinga and Milton 2018, Wainwright et al. 2019).

As discussed in the previous section, the idea that atmospheric variables may be used to produce statistical forecasts renewed some efforts to predict the long rains. Nicholson (2014) developed multiple linear regression models to forecast both the short and long

rains using both atmospheric fields and SSTs as predictors. For the long rains, predictors from January and February were used, with correlations up to 0.76 for February, but dropping to 0.63 when cross-validation was used. The predictors included zonal and meridional wind boxes from north Africa, off the south coast of South Africa, the northern tip of Madagascar, as well as SSTs in the Indian and Pacific Oceans. For the short rains, sea level pressure (SLP) fields were also used, finding correlations of up to 0.8 with observations. Again, linkages between these selected fields and rainfall are not always clear and so may still demonstrate inflated skill levels. Nicholson (2015) furthered this study by splitting the long rains into individual months (March, April, May) and found that this generally increased prediction scores.

Vellinga and Milton (2018) developed a multiple linear regression model for the long rains over March and April using three predictors: The MJO amplitude over February and March, the 30hPa QBO index from the preceding September to November, and SSTs from the northwest Indian Ocean. The regression was tested over a number of observation and reanalysis datasets, with fairly consistent results, with correlations up to 0.77. Vellinga and Milton (2018) suggests that all three predictors affect the long rains through changes to the large-scale subsidence over East Africa.

1.4.2. Dynamical model capability

1.4.2.a. Short rains season

A small number of authors have previously assessed the capabilities of certain dynamical models, that at the time of their assessment were cutting-edge, at predicting seasonal rainfall over East Africa. The ENSEMBLES project multimodel ensemble seasonal forecasts demonstrated good skill over East Africa during the short rains due to covariance with the Pacific and Indian Oceans (Batté and Déqué 2011). Meanwhile Dutra et al. (2013) showed that the European Centre for Medium-range Weather Forecasts (ECMWF) System 3 and 4 seasonal forecasts also achieved high anomaly correlation coefficients with 3 months lead time. Bahaga et al. (2016) investigated the ability of a multimodel ensemble constructed from North American and Asian seasonal forecast models. He found that the multimodel ensemble performed reasonably well in forecasting the short rains, but was outperformed by several individual models. However selecting only skilful models led to much better results for the multimodel ensemble. It was also demonstrated that these models skilfully predicted the IOD, and the multimodel ensemble captured the teleconnection between the IOD and the short rains

well.

1.4.2.b. Long rains season

In contrast to the short rains season, where dynamical models have demonstrated useful prediction skill even at coarse resolutions, dynamical models have had a difficult time in predicting variability in seasonal rainfall within the long rains. As discussed in previous sections, this is largely down to a lack of any known connection to large-scale sources of seasonal predictability such as ENSO (Ogallo 1988, Camberlin and Wairoto 1997). The studies of previous generations of dynamical models such as the ENSEMBLES project (Batté and Déqué 2011), and ECMWF System 3 and 4 (Dutra et al. 2013, Mwangi et al. 2014) have little skill in predicting the long rains, although Dutra et al. (2013) demonstrated that System 4 displayed some limited skill for forecasts initialised in March.

Despite not being able to directly predict precipitation, there is still some promise for being able to use dynamical models for forecasting over the long rains. For example, the models still possess skill in predicting tropical SSTs, which, given the emerging relationship with Niño3.4 and relationship with the Pacific gradient displayed by Funk et al. (2014), could then be used to produce hybrid models, using forecast SSTs to statistically predict rainfall as demonstrated by Shukla et al. (2014).

1.4.3. Greater Horn of Africa Climate Outlook Forum (GHACOF) forecasts

An initiative led by the World Meteorological Organization (WMO) in the late 1990s produced a method of generating and disseminating seasonal forecasts, known as Regional Climate Outlook Forums (RCOFs), in several regions around the world, which have since expanded to cover most of the globe (Ogallo et al. 2008, World Meteorological Organization 2020). One of the first of its kind was the Greater Horn of Africa Climate Outlook Forum (GHACOF), which began producing forecasts in 1998. GHACOF is organised by the Intergovernmental Authority on Development (IGAD) Climate Prediction and Applications Centre (ICPAC).

GHACOF events takes place 3 times per year, preceding the long rains, short rains, and summer rainfall season. The format has changed several times throughout the years, however, the event generally takes place in two stages. Firstly a pre-COF workshop,

where forecasters representing each country attend to generate the forecast, and to receive training. The second stage is the forum itself. The seasonal forecast is presented to users from around the region. Representatives from a wide variety of industries attend, including health, agriculture, water resource management and disaster risk management. The forum also includes breakout sessions encouraging users to consider plans based on the forecast, and allows users to interact with regional forecasters and climate experts from around the world.

The forecast is described as a consensus forecast. To construct the forecast, a wide variety of sources are used, including statistical models, dynamical forecasts from various WMO Global Producing Centres (GPCs), seasonal Weather Research and Forecasting (WRF; Skamarock et al. 2008) model runs performed by ICPAC themselves, and analogue years of similar conditions. Forecasters then use these various sources of information to generate a single forecast based on their own knowledge, giving the consensus aspect. The forecast is then presented as a map split into zones, for each zone probabilities are issued for the likelihood of total rainfall being within tercile categories (above normal, near normal, below normal) compared to the climatological rainfall total. An example of a GHACOF forecast is shown in Figure 2.1.

1.5. Methods

1.5.1. Met Office Global Seasonal Forecast System Version 5 (GloSea5)

The primary dynamical seasonal forecast model used in this work is the UK Met Office Global Seasonal Forecast System Version 5 (GloSea5, or GloSea, MacLachlan et al. 2015). GloSea5 is a global coupled ocean-atmosphere model. The core of GloSea5 is the Hadley Centre Global Environmental Model version 3 (HadGEM3; Hewitt et al. 2011). It consists of an atmospheric component (MetUM Global Atmosphere 3.0), land surface component (Joint UK Land Environment Simulator (JULES) Global Land 3.0; Best et al. 2011), ocean component (Nucleus for European Modelling of the Ocean (NEMO) Global Ocean 3.0; Madec 2016), and sea-ice component (The Los Alamos Sea-Ice Model (CICE) Global Sea-Ice 3.0; Hunke and Lipscomb 2010). The atmospheric horizontal resolution is $0.833° \times 0.556°$ with 85 vertical levels. The oceanic horizontal resolution is $0.25° \times 0.25°$ with 75 vertical levels.

The forecast system comprises of two parts, the forecast, and a set of hindcasts. The

model is run for 210 days from initialisation. The forecast is run as an ensemble, with 2 members initialised each day, and members from the past 3 weeks used for the forecast, generating an ensemble of 42 members.

The hindcast is run for the purpose of bias correcting and assessing the skill of the model, and has been used for Chapters 2 and 4 of this thesis. For the results in Chapter 2, 3 members were initialised on 4 fixed days per month (1st, 9th, 17th, 25th) and covered 23 years (1993-2015). For the results in Chapter 4, following an upgrade to GloSea5, 7 hindcast members were initialised on each of the 4 fixed days, giving an ensemble of 28 members in a month, and covered 24 years (1993-2016). Ensemble members initialised on the same date differ by using a stochastic physics scheme to perturb the initial conditions (Bowler et al. 2009), to capture some of the uncertainty within the observations. These later hindcasts are made available through the Copernicus Climate Change Service (C3S) Climate Data Store (C3S 2020).

1.5.2. Forecast verification techniques

The main purpose of a forecast is to provide information to a user to help them make a decision. However, not all forecasts are useful, and a forecast should not be used without some understanding of how well it performs. For example, if a forecast is no better than guesswork, then there is no advantage to using the information from it in order to make a decision.

There are a wide array of methods for verifying seasonal forecasts. Presented in this section are those used within Chapters 2 to 4 of this thesis. These are by no means an exhaustive list of verification measures, however, they provide a good overview of how well the seasonal forecast performs, and provide complementary information to each other, giving information of different aspects of the seasonal forecast performance, without too much redundancy, or generating lists of repetitive numbers that provide little extra information. The methods chosen here were also chosen due to their use in the WMO Standard Verification System for Long Range Forecasts (SVSLRF; Mason 2013). Wilks (2011) provides information on all the verification methods discussed in this section and many more besides. In particular, some methods for evaluating probabilistic forecasts are presented in this section.

Evaluating probabilistic forecasts is more complex than evaluating the performance of a yes or no forecast, also known as a deterministic forecast. For example, consider a forecast predicting whether it will rain today or not. If the forecast says yes, and it

		Observed		
		Above	Below	
Forecast	Above	a	b	$a + b$
	Below	c	d	$c + d$
		$a + c$	$b + d$	$n = a + b + c + d$

Table 1.1.: Example 2×2 contingency table for above or below mean rainfall, a, b, c, d represent the number of times each observation-forecast category pairing occurs, n is the total number of observations and forecasts.

subsequently rains, we can say the forecast has done well. However, if a probabilistic forecast predicts a 40% chance of rain on a certain day, and it subsequently rains on that day, has the forecast done well or poorly? To get around this, probabilistic forecasts are not considered individually, but are considered over a large sample of forecasts. In this way, it is possible to determine to what extent a probabilistic forecast provides useful information, which can help in understanding what decision to make based upon its predictions.

Whilst it may intuitively seem that a deterministic forecast is better and easier to use than a probabilistic forecast, a deterministic answer fails to capture the inherent uncertainty in forecasting a complex system such as the atmosphere. No forecast is perfect, as the atmosphere is simply too complex and chaotic to perfectly predict its evolution. Therefore, there are often times when even the most skilful deterministic forecast will be wrong, whilst a probabilistic forecast gives an idea of the confidence that an event might happen, and represents the fact that even in cases where there is a high confidence of the event occurring, there is still the probability that it does not.

1.5.2.a. Contingency tables

A contingency table shows the joint distribution of forecasts and observations by counting the number of events in each category (Wilks 2011). An example of a 2×2 contingency table is seen in Table 1.1, for above or below mean rainfall. The 4 cells in the table have different meanings. Taking above normal rainfall as the "event": a is a "hit", a correctly forecast event; b is a "false alarm", a forecast event that did not occur; c is a "miss", an event that occurred but was not forecast; d is a "correct negative", a non-event that was correctly forecast not to occur. Each forecast in the set to be evaluated is placed into one of the cells in the table based on the prediction and subsequent observation.

There are a large number of statistics that can be calculated from these tables, giving useful information about the forecasts. Those to be used in this work will be introduced. The proportion correct (PC; Finley 1884) is given by:

$$PC = \frac{a+d}{n} \tag{1.1}$$

which is simply the proportion of forecasts that were in the same category as the observations. A perfect score is 1, suggesting all forecasts were in the correct category. However this score can be misleading if an event or non-event is a very likely outcome. For example in the forecasting of tornadoes by Finley (1884), never forecasting a tornado to occur results in a very high PC as it is a rare occurrence.

The hit rate is given by:

$$H = \frac{a}{a+c} \tag{1.2}$$

which is the fraction of above events that occurred that were correctly forecast. This can also be calculated for below events. A perfect score is 1, implying that all above events were correctly forecast.

The false alarm rate is given by:

$$F = \frac{b}{b+d} \tag{1.3}$$

which is the fraction of non-events that were incorrectly forecast as events. A perfect score would be 0, suggesting that an above event forecast was never given for an observed below event.

A common skill score used for contingency tables is the Heidke skill score (HSS; Heidke 1926). This is given by:

$$HSS = \frac{2(ad - bc)}{(a+c)(c+d) + (a+b)(b+d)}. \tag{1.4}$$

This score measures the ratio between the fraction of correct forecasts minus the fraction of correct forecasts obtained by chance, and, the fraction of correct forecasts obtained by a perfect forecast minus the fraction of correct forecasts obtained by chance. A perfect score is 1, whilst a score of 0 suggests that the forecast is no better than a biased random prediction.

For multi-category forecasts, contingency tables can be extended to any size, for example Table 1.2 shows a 3×3 contingency table for a 3 category rainfall forecast. Many

	Observed			
	Above	Near	Below	
Forecast Above	a	b	c	$a+b+c$
Near	d	e	f	$d+e+f$
Below	g	h	i	$g+h+i$
	$a+d+g$	$b+e+h$	$c+f+i$	n

Table 1.2.: Example 3×3 contingency table for 3 categories of rainfall, a to i represent the number of times each observation-forecast category pairing occurs, n is the total number of observations and forecasts.

of the statistics for 2×2 tables can be adapted for larger tables. For example the proportion correct is given by:

$$PC = \frac{a+e+i}{n}. \qquad (1.5)$$

The hit rate and false alarm rate can be found for each category separately by forming a 2×2 contingency table for that category, collapsing the 2 other categories into a single non-event category.

For a $k \times k$ contingency table the Heidke skill score can be generalised to:

$$HSS = \frac{\sum_{i=1}^{k} p_{ii} - \sum_{i=1}^{k} \left(\sum_{j=1}^{k} p_{ij} \right) \left(\sum_{j=1}^{k} p_{ji} \right)}{1 - \sum_{i=1}^{k} \left(\sum_{j=1}^{k} p_{ij} \right) \left(\sum_{j=1}^{k} p_{ji} \right)}, \qquad (1.6)$$

where p_{ij} is the probability of the i'th row and j'th column of the contingency table. This can be rewritten as:

$$HSS = \frac{PC - E}{1 - E}, \qquad (1.7)$$

where E is the expected proportion correct for a random forecast. E is calculated by taking the sum of the probability of a forecast of event i multiplied by the probability of observing event i, for each i.

1.5.2.b. Relative operating characteristic (ROC) curves

Relative operating characteristic (ROC) diagrams have been used in meteorology since their first use by Mason (1982), however, the origins of the diagram come from signal

detection theory, and is commonly used in medicine (Green and Swets 1988). They are often used to determine a decision threshold for action, and show the hit rate against false alarm rate for a number of decision thresholds.

To construct a ROC curve, first a set of decision thresholds must be decided. These are a set of probability values at which, when a forecast predicts a greater likelihood of the event occurring than the threshold value, the forecast is treated as predicting the event. For example if a threshold for acting upon an above normal rainfall is 40%, and the forecast predicts a 50% chance of above normal rainfall, then this is treated as the forecast predicting the event to occur. For evaluating ensemble forecasts, where the probability of an event is determined by the number of ensemble members forecasting the event, these thresholds will be decided based upon ensemble size. If there are many more thresholds than ensemble members then multiple thresholds will have the same hit rate and false alarm rates. Meanwhile if too few are used then the resolution of the ROC curve will be low, and estimates of the ROC score will be inaccurate.

By considering each threshold in turn, the probabilistic forecasts can be split into forecasting an event or not, and therefore a 2×2 contingency table for the set of forecasts can be made for each decision threshold. For each decision threshold, the hit rate and false alarm rate can be calculated from the contingency table. The set of hit rates and false alarm rates are then plotted against each other, with hit rate on the y-axis and false alarm rate on the x-axis, as shown in Figure 1.13a. The curve is then made by joining these points. When the decision threshold is low (e.g. 10%) then a large number events are forecasts are classified as forecasting the event. This leads to a high hit rate but correspondingly a high false alarm rate. Similarly a high decision threshold (e.g. 90%) means that only the most confident forecasts will be classified as forecasting the event, leading to a low hit rate, but also a low false alarm rate. By definition thresholds of 0% mean the event is always forecast, leading to a hit rate and false alarm rate of 1, whilst a threshold of greater than 100% means the event is never forecast, leading to a hit rate and false alarm rate of 0, forcing the ROC curve to be connected to the lower left and upper right corners of the diagram.

From the ROC curve, the ROC score (ROCS) can be calculated. This is simply the area under the curve (AUC). This ranges from 0 to 1. A diagonal line from (0,0) to (1,1) is drawn on the ROC diagram. This marks the line of no skill, when the hit rate and false alarm rate are equal. From this a ROC score of 0.5 then defines a forecast with no skill compared to a random forecast. A ROC score of greater than 0.5 means the forecast has positive skill, and less than 0.5 means the forecast has negative skill.
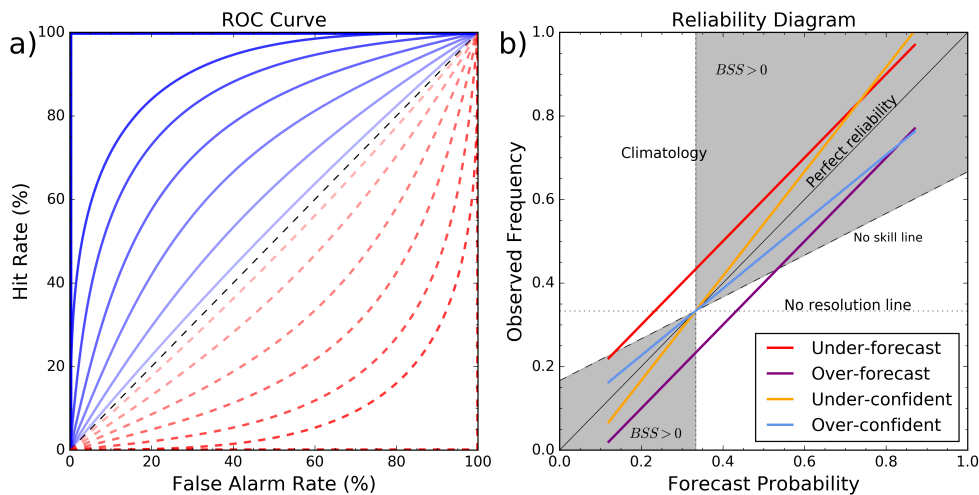
Figure 1.13.: a) Example of a ROC diagram. Example ROC curves are plotted with blue lines showing positive skill, and red lines showing negative skill, with darker lines increasingly high levels of positive and negative skill. b) Example of a reliability diagram. The shaded region indicates forecasts that would positively contribute to the Brier skill score of the forecast. Example lines are plotted showing characteristics of forecasts with over-confidence (blue), under-confidence (orange), over-forecasting (purple), under-forecasting (red).

A ROC score of 1 is a perfect forecast, and a good forecast should stretch as close to the top left corner of the diagram as possible. The ROC score can be converted to a traditional skill score metric (ranging from -1 to 1), known as the ROC skill score (ROCSS) by the simple equation ROCSS= 2ROCS−1.

For multiple category events (for example forecasts split into 3 equally likely categories, or terciles, of above normal, near normal, below normal) an individual ROC curve is made for each category: the probability of forecasting an event is the same as a 2 category (yes or no) forecast, whilst the probability of not forecasting an event is the sum of the probabilities of forecasting any of the other categories.

1.5.2.c. Reliability diagrams

Reliability diagrams, introduced by Hartmann et al. (2002), are graphs displaying the observed frequency of an event as a function of the forecast probability of the event. It is a desirable attribute of a probabilistic forecast that if the predicted likelihood of an event is issued, this matches up to the same observed likelihood. This is regularly not the case meaning that the forecast probability of an event may need to be calibrated

to obtain the true probability of the event occurring. To understand these biases in probability, a reliability diagram is used.

To formulate this, a number of probability bins are defined. Each bin contains all forecasts where the probability of the event occurring lies within the bin. For example a forecast predicting a 35% chance of an event would be placed in the bin containing forecasts between 30 and 40%. Contingency tables are made for each bin, by comparing that set of forecasts against their relevant observations, and the hit rates of each bin are then calculated. As the forecasts are separated by their predicted probability for an event, the hit rate in this case tells us the observed frequency of an event, given a forecast of a certain probability. The hit rate is then plotted on the y-axis against the centre of the probability bins on the x-axis.

A forecast with perfect reliability would have a forecast probability equal to the observed frequency. To represent this, a horizontal line is drawn from (0,0) to (1,1) on the diagram. Horizontal and vertical lines representing the climatological frequency of the event are also added. In the case of tercile category forecasts this will be 1/3, or for forecasts of above or below a median, this would be 1/2. The vertical line represents a climatology forecast: for example if a forecast of climatology was used in the case of terciles, the forecast probability would always be 1/3 regardless of the observed frequency. Meanwhile the horizontal line represents a forecast with no resolution. This means that regardless of the forecast that was issued, the observed outcome was equally likely and the forecast provides no additional information. Finally, a line bisecting the perfect resolution and no resolution lines is drawn. This bisecting line marks the line of no skill. The area between the climatology and no skill lines is shaded. Points that lie within the shaded area contribute positively to the Brier skill score (introduced in Section 1.5.2.d) of the forecast, whilst lines outside contribute negatively. These lines are labelled on an example reliability diagram in Figure 1.13b.

Several common terms are used when describing forecasts based on reliability diagrams (Mason 2013). These are over-confidence, under-confidence, over-forecasting, and under-forecasting. Examples of each are provided in coloured lines on Figure 1.13b.

Over-confidence means that the forecast overestimates the likelihood of events more common than climatological frequency occurring, and underestimates the likelihood of events less common than climatological frequency occurring. On the reliability diagram this appears as a line with a gradient less than 1. This can be seen as the blue line in Figure 1.13b. Conversely, under-confidence means that the forecast underestimates the

likelihood of events more common than climatological frequency occurring, and overestimates the likelihood of events less common than climatological frequency occurring. On the reliability diagram this appears as a line with a gradient greater than 1. This can be seen as the orange line in Figure 1.13b.

Over-forecasting means that the forecast consistently predicts an event to occur more often than is observed. On the reliability diagram this appears as a line that on average sits below the diagonal line. this can be seen as the purple line in Figure 1.13b. Conversely, under-forecasting means that the forecast consistently predicts an event to occur less often than is observed. On the reliability diagram this appears as a line that on average sits above the diagonal line. this can be seen as the red line in Figure 1.13b.

If a forecast displays any of these features it is desirable to calibrate the forecast, or to use this information when making a decision: for example if an over-confident forecast suggests an event is likely to occur, some caution may be needed as the actual probability of occurrence will be on average lower than the forecast probability suggests, and this should be factored into the decision making process.

1.5.2.d. Brier skill score

The Brier score, (BS), is a scalar accuracy measure of probabilistic forecasts (Wilks 2011). It is the mean squared error of the set of forecasts, if the observation $o = 1$ if the event occurs, and $o = 0$ otherwise. For a binary event with n forecast instances, the Brier score can be calculated as

$$BS = \frac{1}{n} \sum_{i=1}^{n} (f_i - o_i)^2,$$

(1.8)

where f_i and o_i are the i'th forecast and observation respectively. As the Brier score is analogous to mean squared error, a perfect forecast would have a value of $BS = 0$ indicating zero error, whilst the worst possible score is $BS = 1$.

The Brier score can also be extended to multi-category forecasts, as in the original definition given by Brier (1950):

$$BS = \frac{1}{n} \sum_{j=1}^{r} \sum_{i=1}^{n} (f_{ij} - o_{ij})^2,$$

(1.9)

where r is the number of categories for the forecast, and f_{ij} and o_{ij} are the i'th forecast

and observation respectively, for the j'th forecast category. In the event of a 2 category forecast, this formulation generates a score exactly twice that of Equation 1.8, and so Equation 1.8 is sometimes referred to as the half-Brier score.

Alternatively for multi-category forecasts, Equation 1.8 can be calculated for each category separately, treating each forecast category as a binary event. This provides separate Brier score for each forecast category. In this case, the sum of the Brier scores of every category will produce the the Brier score found from using Equation 1.9.

The Brier score can be used to calculate a skill score known as the Brier skill score (BSS). This follows a conventional skill-score equation, giving:

$$BSS = 1 - \frac{BS}{BS_{ref}}, \tag{1.10}$$

where BS is the Brier score for the set of forecasts, and BS_{ref} is the Brier score for a set of reference forecasts, often climatological relative frequencies. As a skill score, the BSS has a range from -1 to 1. A perfect forecast would achieve a score of $BSS = 1$, whilst a forecast with no skill relative to the reference forecasts would achieve $BSS = 0$.

1.5.3. Other statistical techniques

A brief description of other statistical techniques used within this work is presented in this section.

1.5.3.a. Pearson's correlation coefficient

The Pearson correlation coefficient (Pearson 1920), r, or Pearson product-moment correlation is a measure of the linear correlation between two variables. It is defined by:

$$r = \frac{\sum_{i=1}^{n} (x_i - \bar{x})(y_i - \bar{y})}{\sqrt{\sum_{i=1}^{n} (x_i - \bar{x})^2} \sqrt{\sum_{i=1}^{n} (y_i - \bar{y})^2}}, \tag{1.11}$$

where r is the Pearson correlation coefficient, x_i, y_i are the i'th value of the two variables, n is the number of values in each variable and $\bar{x}, \bar{y}$ are the mean values of the two variables. This value ranges from 1 to -1, with 1 being a perfect positive correlation, -1 a perfect negative correlation, and 0 implying no correlation between the two variables.

To test the statistical significance of a correlation a p-value can be calculated. If this

value is less than a pre-determined value for α (regularly $\alpha = 0.05$, or significant at 5% level), then the correlation is considered statistically significant and not a product of random chance. The p-value is the two-tailed probability of finding a random variable $T \geq t$ using Student's t-distribution, where t is defined by:

$$t = r\sqrt{\frac{n-2}{1-r^2}} \qquad (1.12)$$

and r and n are the Pearson's correlation coefficient and the sample size respectively. This process is known as a two-tailed Student's t-test.

The correlation coefficient can be used to compare observational and model data with each other, or themselves. A high correlation suggests that the two sets of data are similar, and can be interpreted as a model representing well the variation that occurs in observations, with the square of the correlation coefficient indicating the proportion of variability described by the relation. However, there are limitations to the correlation coefficient, for example if two sets of data agree on the shape of a data set, but have different absolute values, the correlation coefficient does not decrease. It can also be skewed by outlying points; a large discrepancy in one point can have a large effect on the value of the coefficient.

1.5.3.b. Partial correlation

The partial correlation (Yule 1907, Lawrence 1976) is a measure of the relation between two variables, with the effect of another controlling variable removed. This can be used in cases where the relation between two variables is desired, but a third variable also correlates with both. The partial correlation removes the effects of the third variable. The equation for the partial correlation of variables 1 and 2, with the influence of variable 3 removed, denoted $r_{12,3}$, is as follows

$$r_{12,3} = \frac{r_{12} - r_{13}r_{23}}{\sqrt{(1-r_{13}^2)(1-r_{23}^2)}}, \qquad (1.13)$$

where r_{ij} is the Pearson's correlation coefficient between variables i and j. Analogous to the original correlation coefficient, the partial correlation has a value between -1 and 1, with, the value of 1 being a perfect positive correlation, -1 a perfect negative correlation, and 0 implying no correlation between the two variables after the influence of the third is removed. The partial correlation can be extended to any number of variables (Yule 1907).

1.5.3.c. Composite analysis

Composite analysis is a technique used to understand the structure or properties of a weather or climate event of interest, for example understanding global impacts of El Niño. To produce a composite, a large set of observations is required, and from this set of observations a climatology, or the average conditions, is determined. For the El Niño example this might be the mean global SST field over boreal winter. From this set of observations, only those in which the event of interest occurs is then selected, and the average conditions of this subset of data are then also determined. The difference between the mean of the subset of data and the climatology (in this example SSTs for El Niño occurrences minus the SST climatology) then produces an average of the anomalies present during the event of interest. This is known as a composite, and can determine features that are common to a certain event. In the example of El Niño a pattern of positive SST anomalies in the eastern equatorial Pacific Ocean will stand out.

Further complexity can be added to composite analyses, for example rather than subtracting the climatological values from the event of interest, a separate event of interest, or the inverse of the event of interest, can be subtracted. For example SST conditions for El Niño events minus SST conditions for La Niña events.

1.5.3.d. Linear regression analysis

Linear regression analysis is the process of modelling the relationship between one dependent variable, and a set of independent variables. The most simple linear regression uses a single independent variable, and is known as simple linear regresssion.

For a simple linear regression, for a set of (x,y) points, where y is the dependent variable and x the independent, the aim is to find a line of the form

$$y = \alpha + \beta x, \tag{1.14}$$

where α and β are constants to be determined, that minimises the sum of the squares of the vertical distances between the points and the line (a least-squares fit). A common measure of the goodness-of-fit of the regression is the coefficient of determination, R^2. This is the proportion of variation of the independent variable that is described by the regression. The square root of the coefficient of determination is the Pearson correlation coefficient, r.

The simple linear regression can be generalised for multiple independent variables, but keeping a single dependent variable. This is known as a multiple linear regression (MLR). The aim is then to find, for a set of n independent variables, a line of the form

$$y = \beta_0 + \beta_1 x_1 + \beta_2 x_2 + ... + \beta_n x_n, \tag{1.15}$$

where x_i is the i'th independent variable, and β_i are a set of $n + 1$ constants to be determined, known as regression parameters, again using a least-squares fit. The statistical robustness of the regression model can be tested by determining whether the set of regression parameters are significantly different from zero, using an F-test (Draper and Smith 1998).

1.6. Thesis aims and summary

A great deal of past work has focused on understanding and forecasting rainfall on seasonal timescales over East Africa. Forecasts of East African rainfall are regularly made, but the most common operational forecast, GHACOF, has not been evaluated for some time. A result of the previous work has been the notable success in the discovery of the close relation between the short rains and the large-scale modes of variability of El Niño-Southern Oscillation and the Indian Ocean Dipole, which lead to capability in producing skilful forecasts of this season. However, the situation for the long rains is considerably less ideal. Understanding of the long rains is relatively poor, and predictability for this season remains difficult, although there has been some recent promising progress, primarily through its relation to the Madden-Julian Oscillation. Meanwhile the long term decline of total rainfall amounts over East Africa during the long rains and conflicting climate model projections of a wetter future are still not completely understood and undermine attempts at long term planning.

This thesis aims to provide improvements to the current state of seasonal forecasting for the East Africa region, and develop understanding of predictability and variability within East Africa's rainfall seasons on inter-annual and longer term timescales, taking a logical three step approach. First, the current state of forecasts in the region is evaluated with strengths and weaknesses identified. The thesis will then look to improve current understanding of variability in the long rains season. It will then build on this improved understanding to try to identify potential new sources of predictability that could be used to improve seasonal forecasts for the long rains.

The main objectives of the PhD are:

- Investigate the skill of a cutting edge dynamical seasonal forecast model in predicting seasonal rainfall over East Africa

    – How does the skill vary between the two rainfall seasons?

    – How does the skill compare between the dynamical model and the most widely distributed operational consensus forecast in the region?

    – Does the skill vary with factors such as the initial conditions of large-scale drivers and lead time?

    – Does the model display any biases, and what are the origins of these?

- Investigate processes controlling the long rains seasonal rainfall totals

    – Are there large-scale atmospheric factors that are connected to the long rains seasonal rainfall, and what is the apparent physical mechanism connecting them?

    – On what timescales do these processes act, such as seasonal or decadal?

    – Could these processes explain the observed long rains drying trend?

- Investigate whether processes controlling the long rains are captured in the dynamical model, and whether there is potential for future predictability of these

    – Does the dynamical model realistically capture the observed relationship between processes controlling the long rains and rainfall?

    – Are these linked to any known predictable large-scale modes of variability?

    – Is there the potential for future skilful predictions of the long rains if specific improvements are made to the dynamical model or post-processing?

Chapter 2 presents an evaluation of the skill of the UK Met Office dynamical seasonal forecast system, GloSea5, in forecasting the long and short rains over East Africa, and compares it to the GHACOF consensus forecasts. This is the first work comparing the widely used operational forecasts of GHACOF to a dynamical model. The chapter aims to find where each forecast performs well, or could be improved, identifying conditions where forecasts are more likely to be correct, as well as identifying model biases that

could hinder the forecasts, and understanding their origins. This chapter provides information for both forecast generators and users that will aid use of the forecasts in their current state, and provides suggestions for improvements to the forecasts.

Chapter 3 presents an investigation into the atmospheric conditions that lead to above and below normal seasonal rainfall during the long rains. The aim of the chapter is to improve understanding of what causes variability in the long rains both on seasonal timescales and on longer decadal timescales, by considering variability in neighbouring circulation features that are likely to directly impact the rainfall. It identifies zonal winds over the nearby Congo region as key, and demonstrates that this influences rainfall on both the seasonal and decadal timescale. This improved understanding could help forecasters to produce better forecasts of the rainfall on seasonal timescales, and provides further information on factors driving the recent drying observed during the long rains, which could also provide an alternative viewpoint for the possible future of the long rains, and the East African climate paradox.

Chapter 4 presents the potential ability of GloSea5 to better forecast the long rains if improvements to key rainfall drivers, which the model is known to already have some level of skill in forecasting, were made. The aim of the chapter is to determine whether GloSea5 captures the physical processes driving variability in the long rains in observations, and deduce whether more skilful forecasts of the long rains could be made using dynamical models if key drivers were better predicted. The chapter also provides a potential direction for future work in improving seasonal forecasts for model developers, through consideration of the signal-to-noise paradox.

The results of Chapters 2-4 will be summarised, synthesised, and placed into wider context in Chapter 5. Recommendations for future work based on these conclusions will also be made.

References

Aceituno, P. (1988). On the functioning of the Southern Oscillation in the South American sector. Part I: surface climate. *Monthly Weather Review*, 116(3):505–524.

African Great Lakes Information Platform (2020). Lake Victoria. Available at: `https://www.africangreatlakesinform.org/page/lake-victoria`. Last accessed: 23 September 2020.

Anyah, R. O. and Qiu, W. (2012). Characteristic 20th and 21st century precipitation and temperature patterns and changes over the Greater Horn of Africa. *International Journal of Climatology*, 32(3):347–363.

Atieno, A. J., Onyango, W. P., Joyce, O., Onyisi, A. J., and Omondi, O. M. (2017). Relationship Between Technological Hazards And Fishermen Vulnerability In Lake Victoria, Kenya. *IOSR Journal of Humanities and Social Science*, 22(1):18–31.

Bahaga, T. K., Fink, A. H., and Knippertz, P. (2019). Revisiting interannual to decadal teleconnections influencing seasonal rainfall in the Greater Horn of Africa during the 20th century. *International Journal of Climatology*, 39(5):2765–2785.

Bahaga, T. K., Kucharski, F., Tsidu, G. M., and Yang, H. (2016). Assessment of prediction and predictability of short rains over equatorial East Africa using a multi-model ensemble. *Theoretical and Applied Climatology*, 123(3-4):637–649.

Bahaga, T. K., Mengistu Tsidu, G., Kucharski, F., and Diro, G. T. (2015). Potential predictability of the sea-surface temperature forced equatorial east african short rains interannual variability in the 20th century. *Quarterly Journal of the Royal Meteorological Society*, 141(686):16–26.

Baldwin, M. P., Gray, L. J., Dunkerton, T. J., Hamilton, K., Haynes, P. H., Randel, W. J., Holton, J. R., Alexander, M. J., Hirota, I., Horinouchi, T., Jones, D. B. A., Kinnersley, J. S., Marquardt, C., Sato, K., and Takahashi, M. (2001). The Quasi-Biennial Oscillation. *Reviews of Geophysics*, 39(2):179–229.

Barnston, A. G., Chelliah, M., and Goldenberg, S. B. (1997). Documentation of a highly ENSO-related SST region in the equatorial pacific: Research note. *Atmosphere - Ocean*, 35(3):367–383.

Batté, L. and Déqué, M. (2011). Seasonal predictions of precipitation over Africa using

coupled ocean-atmosphere general circulation models: Skill of the ENSEMBLES project multimodel ensemble forecasts. *Tellus, Series A: Dynamic Meteorology and Oceanography*, 63A(2):283–299.

Behera, S. K., Luo, J. J., Masson, S., Delecluse, P., Gualdi, S., Navarra, A., and Yamagata, T. (2005). Paramount impact of the Indian ocean dipole on the East African short rains: A CGCM study. *Journal of Climate*, 18(21):4514–4530.

Behrend, H. (1987). Teleconnections of rainfall anomalies and of the Southern Oscillation over the entire tropics and their seasonal dependence. *Tellus A*, 39 A(2):138–151.

Bengtsson, L., Herschy, R. W., and Fairbridge, R. W., editors (2012). *Encyclopedia of Lakes and Reservoirs*. Springer, London.

Berhane, F. and Zaitchik, B. (2014). Modulation of daily precipitation over East Africa by the Madden-Julian oscillation. *Journal of Climate*, 27(15):6016–6034.

Best, M. J., Pryor, M., Clark, D. B., Rooney, G. G., Essery, R. L. H., Ménard, C. B., Edwards, J. M., Hendry, M. A., Porson, A., Gedney, N., Mercado, L. M., Sitch, S., Blyth, E., Boucher, O., Cox, P. M., Grimmond, C. S. B., and Harding, R. J. (2011). The Joint UK Land Environment Simulator (JULES), model description – Part 1: Energy and water fluxes. *Geoscientific Model Development*, 4(3):677–699.

Bhalme, H. N., Mooley, D. A., and Jadhav, S. K. (1983). Fluctuation in the drought/flood area over India and relationships with the Southern Oscillation. *Monthly Weather Review*, 111(1):86–94.

Bjerknes, J. (1966). A possible response of the atmospheric Hadley circulation to equatorial anomalies of ocean temperature. *Tellus*, 18(4):820–829.

Bjerknes, J. (1969). Atmospheric teleconnections from the equatorial Pacific. *Monthly Weather Review*, 97(3):163–172.

Black, E., Slingo, J., and Sperber, K. R. (2003). An observational study of the relationship between excessively strong short rains in coastal East Africa and Indian Ocean SST. *Monthly Weather Review*, 131(1):74–94.

Blanford, H. F. (1884). On the connexion of the Himalaya snowfall with dry winds and seasons of drought in India. *Proceedings of the Royal Society of London*, 37(232-234):3–22.

Bowler, N. E., Arribas, A., Beare, S. E., Mylne, K. R., and Shutts, G. J. (2009). The local ETKF and SKEB: Upgrades to the MOGREPS short-range ensemble prediction system. *Quarterly Journal of the Royal Meteorological Society*, 135:767–776.

Brier, G. W. (1950). Verification of forecasts expressed in terms of probability. *Monthly Weather Review*, 78(1):1–3.

Bryson, R. A. and Kuhn, P. M. (1961). Stress — Differential Induced Divergence with Application to Littoral Precipitation. *Erdkunde*, 15:287–294.

Bureau of Meteorology (2020). Madden-Julian Oscillation. Available at: `http://www.bom.gov.au/climate/mjo/`. Last accessed: 08 October 2020.

C3S (2020). Climate Data Store. Available at: `https://cds.climate.copernicus.eu/#!/home`. Last accessed: 02 October 2020.

Camberlin, P., Janicot, S., and Poccard, I. (2001). Seasonality and atmospheric dynamics of the teleconnection between African rainfall and tropical sea-surface temperature: Atlantic vs. ENSO. *International Journal of Climatology*, 21(8):973–1005.

Camberlin, P., Moron, V., Okoola, R., Philippon, N., and Gitau, W. (2009). Components of rainy seasons' variability in Equatorial East Africa: Onset, cessation, rainfall frequency and intensity. *Theoretical and Applied Climatology*, 98(3-4):237–249.

Camberlin, P. and Okoola, R. E. (2003). The onset and cessation of the " long rains " in eastern Africa and their interannual variability. *Theoretical and Applied Climatology*, 54(1-2):43–54.

Camberlin, P. and Wairoto, J. G. (1997). Intraseasonal wind anomalies related to wet and dry spells during the "long" and "short" rainy seasons in Kenya. *Theoretical and Applied Climatology*, 58(1-2):57–69.

Cane, M. A., Zebiak, S. E., and Dolan, S. C. (1986). Experimental forecasts of the El Nino. *Nature*, 321:827–832.

Caviedes, C. N. (1984). El Nino 1982-83. *Geographical Review*, 74(3):267–290.

Chamberlain, J. M., Bain, C. L., Boyd, D. F. A., McCourt, K., Butcher, T., and Palmer, S. (2014). Forecasting storms over Lake Victoria using a high resolution model. *Meteorological Applications*, 21(2):419–430.

Charney, J. G. and Shukla, J. (1981). Predictability of monsoons. In Lighthill, J. and Pearce, R. P., editors, *Monsoon Dynamics*, pages 99–110. Cambridge University Press, Cambridge, UK.

Chen, C. J. and Georgakakos, A. P. (2015). Seasonal prediction of East African rainfall. *International Journal of Climatology*, 35(10):2698–2723.

Chen, W. Y. (1982). Assessment of Southern Oscillation Sea-Level Pressure Indices. *Monthly Weather Review*, 110(7):800–807.

CIA World Factbook (2020). Gross Domestic Product (GDP) composition by sector of origin. Available at: `https://www.cia.gov/library/publications/resources/the-world-factbook/fields/214.html`. Last accessed: 17 September 2020.

Clark, C. O., Webster, P. J., and Cole, J. E. (2003). Interdecadal variability of the relationship between the Indian Ocean zonal mode and East African coastal rainfall anomalies. *Journal of Climate*, 16(3):548–554.

Cook, K. H. and Vizy, E. K. (2013). Projected changes in east african rainy seasons. *Journal of Climate*, 26(16):5931–5948.

Dee, D. P., Uppala, S. M., Simmons, A. J., Berrisford, P., Poli, P., Kobayashi, S., Andrae, U., Balmaseda, M. A., Balsamo, G., Bauer, P., Bechtold, P., Beljaars, A. C., van de Berg, L., Bidlot, J., Bormann, N., Delsol, C., Dragani, R., Fuentes, M., Geer, A. J., Haimberger, L., Healy, S. B., Hersbach, H., Hólm, E. V., Isaksen, L., Kållberg, P., Köhler, M., Matricardi, M., Mcnally, A. P., Monge-Sanz, B. M., Morcrette, J. J., Park, B. K., Peubey, C., de Rosnay, P., Tavolato, C., Thépaut, J. N., and Vitart, F. (2011). The ERA-Interim reanalysis: configuration and performance of the data assimilation system. *Quarterly Journal of the Royal Meteorological Society*, 137(656):553–597.

Doblas-Reyes, F. J., García-Serrano, J., Lienert, F., Biescas, A. P., and Rodrigues, L. R. (2013). Seasonal climate predictability and forecasting: status and prospects. *Wiley Interdisciplinary Reviews: Climate Change*, 4(4):245–268.

Draper, N. and Smith, H. (1998). *Applied Regression Analysis*. John Wiley and Sons Ltd.

Dutra, E., Magnusson, L., Wetterhall, F., Cloke, H. L., Balsamo, G., Boussetta, S., and Pappenberger, F. (2013). The 2010-2011 drought in the Horn of Africa in

ECMWF reanalysis and seasonal forecast products. *International Journal of Climatology*, 33(7):1720–1729.

Ebdon, R. A. (1960). Notes on the wind flow at 50 mb in tropical and sub-tropical regions in January 1957 and January 1958. *Quarterly Journal of the Royal Meteorological Society*, 86(370):540–542.

Endris, H. S., Lennard, C., Hewitson, B., Dosio, A., Nikulin, G., and Artan, G. A. (2018). Future changes in rainfall associated with ENSO, IOD and changes in the mean state over Eastern Africa. *Climate Dynamics*, 0(0):1–25.

FAO and FEWS NET (2013). Mortality among populations of southern and central Somalia affected by severe food insecurity and famine during 2010-2012. Available at: `https://reliefweb.int/report/somalia/mortality-among-populations-southern-and-central-somalia-affected-severe-food`. Last accessed: 22 September 2020.

Farmer, G. (1988). Seasonal forecasting of the Kenya coast short rains, 1901-84. *Journal of Climatology*, 8(5):489–497.

Findlater, J. (1966). Cross-equatorial jet streams at low-levels over Kenya. *Meteor. Mag.*, 95:353–364.

Findlater, J. (1969). A major low level air current near the Indian ocean during the nothern ummer. *Meteorological Science*, 95(404):362–380.

Findlater, J. (1977). Observational aspects of the low-level cross-equatorial jet stream of the western Indian Ocean. *Pure and Applied Geophysics PAGEOPH*, 115(5-6):1251–1262.

Finley, J. P. (1884). Tornado Predictions. *Science*, IV(80):126–127.

Finney, D. L., Marsham, J. H., Walker, D. P., Birch, C. E., Woodhams, B. J., Jackson, L. S., and Hardy, S. (2019). The effect of westerlies on East African rainfall and the associated role of tropical cyclones and the Madden-Julian Oscillation. *Quarterly Journal of the Royal Meteorological Society*.

Folland, C., Owen, J., Ward, M. N., and Colman, A. (1991). Prediction of seasonal rainfall in the sahel region using empirical and dynamical methods. *Journal of Forecasting*, 10(1-2):21–56.

Folland, C. K., Palmer, T. N., and Parker, D. E. (1986). Sahel rainfall and worldwide sea temperatures, 1901-1985. *Nature*, 320:602–607.

Funk, C. C., Dettinger, M. D., Michaelsen, J. C., Verdin, J. P., Brown, M. E., Barlow, M., and Hoell, A. (2008). Warming of the Indian Ocean threatens eastern and southern African food security but could be mitigated by agricultural development. *Proceedings of the National Academy of Sciences*, 105(32):11081–11086.

Funk, C. C. and Hoell, A. (2015). The leading mode of observed and CMIP5 ENSO-residual sea surface temperatures and associated changes in indo-pacific climate. *Journal of Climate*, 28(11):4309–4329.

Funk, C. C., Hoell, A., Shukla, S., Bladé, I., Liebmann, B., Roberts, J. B., Robertson, F. R., and Husak, G. (2014). Predicting East African spring droughts using Pacific and Indian Ocean sea surface temperature indices. *Hydrology and Earth System Sciences*, 18(12):4965–4978.

Funk, C. C., Senay, G., Asfaw, A., and Verdin, J. (2005). Recent drought tendencies in Ethiopia and equatorial-subtropical eastern Africa. *FEWS NET Special Report*.

GFDRR (2020). Disaster Risk Country Profiles. Available at: `https://www.gfdrr.org/en/disaster-risk-country-profiles`. Last accessed: 22 September 2020.

Gill, A. E. (1980). Some simple solutions for heat-induced tropical circulation. *Quarterly Journal of the Royal Meteorological Society*, 106(449):447–462.

Gordon, N. (1986). The Southern Oscillation and New Zealand weather. *Monthly Weather Review*, 114(2):371–387.

Graham, R., Colman, A., Vellinga, M., and Wallace, E. (2012). Use of dynamical seasonal forecasts in the consensus outlooks of African Regional Climate Outlook Forums (RCOFs). *ECMWF Seminar on Seasonal Prediction*, (September):3–7.

Gray, W. M. (1984). Atlantic seasonal hurricane frequency. Part I: El Niño and 30 mb quasi-biennial oscillation influences. *Monthly Weather Review*, 112(9):1649–1668.

Green, D. M. and Swets, J. A. (1988). *Signal detection theory and psychophysics*. John Wiley and Sons Inc., New York.

Hartmann, H. C., Pagano, T. C., Sorooshian, S., and Bales, R. (2002). Confidence builders: Evaluating seasonal climate forecasts from user perspectives. *Bulletin of*

the American Meteorological Society, 83(5):683–698.

Hastenrath, S. (2000). Zonal circulations over the equatorial Indian Ocean. *Journal of Climate*, 13(15):2746–2756.

Hastenrath, S. (2007). Circulation mechanisms of climate anomalies in East Africa and the equatorial Indian Ocean. *Dynamics of Atmospheres and Oceans*, 43(1-2):25–35.

Hastenrath, S., Nicklis, A., and Greischar, L. (1993). Atmospheric-hydrospheric mechanisms of climate anomalies in the western equatorial Indian Ocean. *Journal of Geophysical Research*, 98(C11):20219–20235.

Hastenrath, S., Polzin, D., and Mutai, C. (2011). Circulation mechanisms of Kenya rainfall anomalies. *Journal of Climate*, 24(2):404–412.

Hastings, D. A. and Dunbar, P. K. (1999). Global Land One-km Base Elevation(GLOBE) Digital Elevation Model, Version 1.0. Technical report, National Oceanic and Atmospheric Administration, National Geophysical Data Center.

Heidke, P. (1926). Berechnung Des Erfolges Und Der Güte Der Windstärkevorhersagen Im Sturmwarnungsdienst. *Geografiska Annaler*, 8(4):301–349.

Hewitt, H. T., Copsey, D., Culverwell, I. D., Harris, C. M., Hill, R. S., Keen, A. B., McLaren, A. J., and Hunke, E. C. (2011). Design and implementation of the infrastructure of HadGEM3: The next-generation Met Office climate modelling system. *Geoscientific Model Development*, 4(2):223–253.

Hoell, A. and Funk, C. C. (2014). Indo-Pacific sea surface temperature influences on failed consecutive rainy seasons over eastern Africa. *Climate Dynamics*, 43(5-6):1645–1660.

Hoell, A., Hoerling, M., Eischeid, J., Quan, X. W., and Liebmann, B. (2017). Reconciling theories for human and natural attribution of recent East Africa drying. *Journal of Climate*, 30(6):1939–1957.

Hogan, E., Shelly, A., and Xavier, P. (2015). The observed and modelled influence of the Madden–Julian Oscillation on East African rainfall. *Meteorological Applications*, 22(3):459–469.

Huffman, G. J., Bolvin, D. T., Nelkin, E. J., Wolff, D. B., Adler, R. F., Gu, G., Hong, Y., Bowman, K. P., and Stocker, E. F. (2007). The TRMM Multisatellite Precip-

itation Analysis (TMPA): Quasi-Global, Multiyear, Combined-Sensor Precipitation Estimates at Fine Scales. *Journal of Hydrometeorology*, 8(1):38–55.

Hunke, E. C. and Lipscomb, W. H. (2010). CICE : the Los Alamos Sea Ice Model Documentation and Software User's Manual Version 4.1. Technical report.

Hutchinson, P. (1992). The Southern Oscillation and prediction of "Der" season rainfall in Somalia. *Journal of Climate*, 5(5):525–531.

Indeje, M. and Semazzi, F. H. (2000). Relationships between QBO in the lower equatorial stratospheric zonal winds and East African seasonal rainfall. *Meteorology and Atmospheric Physics*, 73(3-4):227–244.

Indeje, M., Semazzi, F. H., and Ogallo, L. J. (2000). ENSO signals in East African rainfall seasons. *International Journal of Climatology*, 20(1):19–46.

International Monetary Fund (2020). Real Gross Domestic Product (GDP) growth. Available at: `https://www.imf.org/external/datamapper/NGDP_RPCH@WEO/OEMDC/ADVEC/WEOWORLD`. Last accessed: 17 September 2020.

IPCC (2018). Summary for Policymakers. In Masson-Delmotte, V., Zhai, P., Pörtner, H. O., Roberts, D., Skea, J., Shukla, P. R., Pirani, A., Moufouma-Okia, W., Péan, C., Pidcock, R., Connors, S., Matthews, J. B. R., Chen, Y., Zhou, X., Gomis, M. I., Lonnoy, E., Maycock, T., Tignor, M., and Waterfield, T., editors, *Global Warming of 1.5°C. An IPCC Special Report on the impacts of global warming of 1.5°C above pre-industrial levels and related global greenhouse gas emission pathways, in the context of strengthening the global response to the threat of climate change,*, pages 1–32. World Meteorological Organization, Geneva, Switzerland.

Ji, M. and Kumar, A. and Leetmaa, A. (1994). A multiseason climate forecast system at the National Meteorological Center. *Bulletin - American Meteorological Society*, 75(4):569–577.

Kent, C., Chadwick, R., and Rowell, D. P. (2015). Understanding uncertainties in future projections of seasonal tropical precipitation. *Journal of Climate*, 28(11):4390–4413.

Kilavi, M., MacLeod, D., Ambani, M., Robbins, J., Dankers, R., Graham, R., Helen, T., Salih, A. A., and Todd, M. C. (2018). Extreme rainfall and flooding over central Kenya including Nairobi city during the long-rains season 2018: Causes, predictability, and potential for early warning and actions. *Atmosphere*, 9(12).

Kinuthia, J. H. (1992). Horizontal and Vertical Structure of the Lake Turkana Jet. *Journal of Applied Meteorology*, 31(11):1248–1274.

Kinuthia, J. H. and Asnani, G. C. (1982). A Newly Found Jet in North Kenya (Turkana Channel). *Mon. Weather Rev.*, 110(11):1722–1728.

Kirtman, B. and Pirani, A. (2008). WCRP Position Paper on Seasonal Prediction. Report from the First WCRP Seasonal Prediction Workshop. Technical report.

Kirtman, B. P., Shukla, J., Huang, B., Zhu, Z., and Schneider, E. K. (1997). Multiseasonal predictions with a coupled tropical ocean-global atmosphere system. *Monthly Weather Review*, 125(5):789–808.

Kite, G. W. (1981). Recent changes in level of Lake Victoria. *Hydrological Sciences Journal*, 26(3):233–243.

Kite, G. W. (1982). Analysis of Lake Victoria levels. *Hydrological Sciences Journal*, 27(2):99–110.

Klotzbach, P., Abhik, S., Hendon, H. H., Bell, M., Lucas, C., G. Marshall, A., and Oliver, E. C. (2019). On the emerging relationship between the stratospheric Quasi-Biennial oscillation and the Madden-Julian oscillation. *Scientific Reports*, 9(1):1–9.

Köppen, W. (1900). Versuch einer Klassifikation der Klimate, vorzugsweise nach ihren Beziehungen zur Pflanzenwelt. *Geogr. Zeitschrift*, 6(11):657–679.

Köppen, W. (1936). Das Geographische System der Klimate. In Köppen, W. and Geiger, G. C., editors, *Handbuch der Klimatologie*.

Lawrence, A. J. (1976). On conditional and partial correlation. *The American Statistician*, 30(3):146–149.

Li, G. and Xie, S. P. (2014). Tropical biases in CMIP5 multimodel ensemble: the excessive equatorial pacific cold tongue and double ITCZ problems. *Journal of Climate*, 27(4):1765–1780.

Liebmann, B., Hoerling, M. P., Funk, C. C., Bladé, I., Dole, R. M., Allured, D., Quan, X., Pegion, P., and Eischeid, J. K. (2014). Understanding recent eastern Horn of Africa rainfall variability and change. *Journal of Climate*, 27(23):8630–8645.

Lott, F. C., Christidis, N., and Stott, P. A. (2013). Can the 2011 East African drought

be attributed to human-induced climate change? *Geophysical Research Letters*, 40(6):1177–1181.

Lyon, B. (2014). Seasonal drought in the Greater Horn of Africa and its recent increase during the March-May long rains. *Journal of Climate*, 27(21):7953–7975.

Lyon, B., Barnston, A. G., and DeWitt, D. G. (2014). Tropical pacific forcing of a 1998-1999 climate shift: Observational analysis and climate model results for the boreal spring season. *Climate Dynamics*, 43(3-4):893–909.

Lyon, B. and Dewitt, D. G. (2012). A recent and abrupt decline in the East African long rains. *Geophysical Research Letters*, 39(2):L02702.

MacLachlan, C., Arribas, A., Peterson, K. A., Maidens, A., Fereday, D., Scaife, A. A., Gordon, M., Vellinga, M., Williams, A., Comer, R. E., Camp, J., Xavier, P., and Madec, G. (2015). Global Seasonal forecast system version 5 (GloSea5): a high-resolution seasonal forecast system. *Quarterly Journal of the Royal Meteorological Society*, 141(689):1072–1084.

Madden, R. A. and Julian, P. R. (1971). Detection of a 40-50 day oscillation in the zonal wind in the tropical Pacific. *Journal of the Atmospheric Sciences*, 28(5):702–708.

Madden, R. A. and Julian, P. R. (1972). Description of global-scale circulation cells in the tropics with a 40-50 day period. *Journal of the Atmospheric Sciences*, 29(6):1109–1123.

Madden, R. A. and Julian, P. R. (1994). Observations of the 40-50-Day Tropical Oscillation—A Review. *Monthly Weather Review*, 122(5):814–837.

Madec, G. (2016). NEMO ocean engine, Note du Pôle de modélisation. Technical report.

Manatsa, D. and Behera, S. K. (2013). On the epochal strengthening in the relationship between rainfall of East Africa and IOD. *Journal of Climate*, 26(15):5655–5673.

Manatsa, D., Chipindu, B., and Behera, S. K. (2012). Shifts in IOD and their impacts on association with East Africa rainfall. *Theoretical and Applied Climatology*, 110(1-2):115–128.

Mantua, N. J., Hare, S. R., Zhang, Y., Wallace, J. M., and Francis, R. C. (1997). A Pacific Interdecadal Climate Oscillation with Impacts on Salmon Production. *Bulletin*

of the American Meteorological Society, 78(6):1069–1079.

Marchant, R., Mumbi, C., Behera, S., and Yamagata, T. (2007). The Indian Ocean dipole - The unsung driver of climatic variability in East Africa. *African Journal of Ecology*, 45(1):4–16.

Mason, I. (1982). *A model for assessment of weather forecasts*, volume 30.

Mason, S. J. (2013). Guidance on verification of operational seasonal climate forecasts. In *World Meteorological Organisation, Commision for Climatology XIV Technical Report*.

Matsuno, T. (1966). Quasi-geostrophic motions in the equatorial area. *Journal of the Meteorological Society of Japan. Ser. II*, 44(1):25–43.

McBride, J. L. and Nicholls, N. (1983). Seasonal relationships between Australian rainfall and the Southern Oscillation. *Monthly Weather Review*, 111(10):1998–2004.

Meehl, G. A., Covey, C., Delworth, T., Latif, M., Mcavaney, B., Mitchell, J. F. B., Stouffer, R. J., and Karl, E. T. (2007). The WCRP CMIP3 Multimodel: A new era in climate change research. *American Meteorological Society*, (September):1383–1394.

Meyers, G., McIntosh, P., Pigot, L., and Pook, M. (2007). The years of El Niño, La Niña and interactions with the tropical Indian Ocean. *Journal of Climate*, 20(13):2872–2880.

Mutai, C. C., Ward, M. N., and Colman, A. W. (1998). Towards the prediction of the East Africa short rains based on sea-surface temperature-atmosphere coupling. *International Journal of Climatology*, 18(9):975–997.

Mwangi, E., Wetterhall, F., Dutra, E., Di Giuseppe, F., and Pappenberger, F. (2014). Forecasting droughts in East Africa. *Hydrology and Earth System Sciences*, 18(2):611–620.

Nakamura, K. (1968). Equatorial westerlies over East Africa and their climatological significance. *Geographical Review of Japan*, 41(6):359–373.

Nicholls, N. (1989). Sea surface temperatures and Australian winter rainfall. *Journal of Climate*, 2(9):965–973.

Nicholson, S. (1996). A review of climate dynamics and climate variability in Eastern

Africa. In *The limnology, climatology and paleoclimatology of the East African lakes*, pages 25–56. CRC Press.

Nicholson, S. (2016a). The Turkana low-level jet: Mean climatology and association with regional aridity. *International Journal of Climatology*, 36(6):2598–2614.

Nicholson, S. E. (2014). The predictability of rainfall over the Greater Horn of Africa. Part I: Prediction of seasonal rainfall. *Journal of Hydrometeorology*, 15(3):1011–1027.

Nicholson, S. E. (2015). The predictability of rainfall over the Greater Horn of Africa. Part II: Prediction of monthly rainfall during the long rains. *Journal of Hydrometeorology*, 16(5):2001–2012.

Nicholson, S. E. (2016b). An analysis of recent rainfall conditions in eastern Africa. *International Journal of Climatology*, 36(1):526–532.

Nicholson, S. E. (2017). Climate and climatic variability of rainfall over eastern Africa. *Reviews of Geophysics*, 55(3):590–635.

Nicholson, S. E. and Kim, J. (1997). The relationship of the El Niño Southern Oscillation to African rainfall. *International Journal of Climatology*, 17(2):117–135.

Nicholson, S. E. and Selato, J. C. (2000). The influence of La Nina on African rainfall. *International Journal of Climatology*, 20(14):1761–1776.

Ogallo, L. (1979). Rainfall variability in Africa. *Monthly Weather Review*, 107(9):1133–1139.

Ogallo, L., Bessemoulin, P., Ceron, J.-P., Mason, S., and Connor, S. (2008). Adapting to climate variability and change: the Climate Outlook Forum process. *WMO Bulletin*, 57(2):93–102.

Ogallo, L. J. (1988). Relationships between seasonal rainfall in East Africa and the Southern Oscillation. *Journal of Climatology*, 8(1):31–43.

Ogallo, L. J. (1989). The spatial and temporal patterns of the East African seasonal rainfall derived from principal component analysis. *International Journal of Climatology*, 9(2):145–167.

Okoola, R. E. (1999a). A diagnostic study of the eastern Africa monsoon circulation during the northern hemisphere spring season. *International Journal of Climatology*,

19(2):143–168.

Okoola, R. E. (1999b). Midtropospheric Circulation Patterns Associated with Extreme Dry and Wet Episodes over Equatorial Eastern Africa during the Northern Hemisphere Spring. *Journal of Applied Meteorology*, 38(8):1161–1169.

Ongoma, V. and Chen, H. (2017). Temporal and spatial variability of temperature and precipitation over East Africa from 1951 to 2010. *Meteorology and Atmospheric Physics*, 129(2):131–144.

Ongoma, V., Chen, H., and Gao, C. (2018). Projected changes in mean rainfall and temperature over East Africa based on CMIP5 models. *International Journal of Climatology*, 38:1375–1392.

Otieno, V. O. and Anyah, R. O. (2013). CMIP5 simulated climate conditions of the Greater Horn of Africa (GHA). Part II: Projected climate. *Climate Dynamics*, 41(7-8):2099–2113.

Owiti, Z., Ogallo, L. A., and Mutemi, J. (2008). Linkages between the Indian Ocean Dipole and east African seasonal rainfall anomalies. *Journal of Kenya Meteorological Society*, 2(1):3 –17.

Oxfam and Save the Children (2012). A Dangerous Delay: The cost of late response to early warnings in the 2011 drought in the Horn of Africa. Technical report.

Palmer, T. N. and Anderson, D. L. T. (1994). The prospects for seasonal forecasting- a review paper. *Quarterly Journal of the Royal Meteorological Society*, 120(518):755–793.

Pearson, K. (1920). Notes on the history of Correlation. *Biometrika*, 13(1):25–45.

Peel, M. C., Finlayson, B. L., and Mcmahon, T. A. (2007). Updated world map of the Köppen-Geiger climate classification. *Hydrology and Earth System Sciences Discussions*, 11(5):1633–1644.

Philippon, N., Camberlin, P., and Fauchereau, N. (2002). Empirical predictability study of October-December East African rainfall. *Quarterly Journal of the Royal Meteorological Society*, 128(585 PART A):2239–2256.

Piper, B. S., Plinston, D. T., and Sutcliffe, J. V. (1986). The water balance of Lake Victoria. *Hydrological Sciences Journal*, 31(1):25–37.

Pohl, B. and Camberlin, P. (2006a). Influence of the Madden-Julian Oscillation on East African rainfall. I: Intraseasonal variability and regional dependency. *Quarterly Journal of the Royal Meteorological Society*, 132(621):2521–2539.

Pohl, B. and Camberlin, P. (2006b). Influence of the Madden-Julian Oscillation on East African rainfall. II: March-May season extremes and interannual variability. *Quarterly Journal of the Royal Meteorological Society*, 132(621):2541–2558.

Rasmusson, E. M. and Carpenter, T. H. (1982). Variations in Tropical Sea Surface Temperature and Surface Wind Fields Associated with the Southern Oscillation/El Niño. *Monthly Weather Review*, 110(5):354–384.

Rayner, N. A., Paker, D. E., Horton, E. B., Folland, C. K., Alexander, L. V., Rowell, D. P., Kent, E. C., and Kaplan, A. (2003). Global analyses of sea surface temperature, sea ice, and night marine air temperature since the late nineteenth century. *Journal of Geophysical Research*, 108(D14):4407.

Reed, R. J., Campbell, W. J., Rasmussen, L. A., and Rogers, D. G. (1961). Evidence of a downward-propagating, annual wind reversal in the equatorial stratosphere. *Journal of Geophysical Research*, 66(3):813–818.

Richter, I., Chang, P., Doi, T., Kataoka, T., Nagura, M., Oettli, P., de Szoeke, S., Tozuka, T., and Xu, Z. (2016). An overview of coupled GCM biases in the tropics. In *Indo-Pacific Climate Variability and Predictability*, pages 213–263.

Rodhe, H. and Virji, H. (1976). Trends and periodicities in East African rainfall data. *Monthly Weather Review*, 104(3):307–315.

Rowell, D. P., Booth, B. B., Nicholson, S. E., and Good, P. (2015). Reconciling past and future rainfall trends over East Africa. *Journal of Climate*, 28(24):9768–9788.

Saji, N. H., Goswami, B. N., Vinayachandran, P. N., and Yamagata, T. (1999). A dipole mode in the tropical Indian ocean. *Nature*, 401(6751):360–363.

Saji, N. H. and Yamagata, T. (2003). Possible impacts of Indian Ocean Dipole mode events on global climate. *Climate Research*, 25(2):151–169.

Scaife, A. A., Arribas, A., Blockey, E., Brookshaw, A., Clark, R. T., Dunstone, N., Eade, R., Fereday, D., Folland, C. K., Gordon, M., Hermanson, L., Knight, J. R., Lea, D. J., MacLachlan, C., Maidens, A., Martin, M., Peterson, A. K., Smith, D., Vellinga, M., Wallace, E., Waters, J., and Williams, A. (2014). Skillful long range

prediction of European and North American winters. *Geophysical Research Letters*, 5(7):2514–2519.

Seneviratne, S. I., Nicholls, N., Easterling, D., Goodess, C. M., Kanae, S., Kossin, J., Luo, Y., Marengo, J., Mc Innes, K., Rahimi, M., Reichstein, M., Sorteberg, A., Vera, C., and Zhang, X. (2012). Changes in climate extremes and their impacts on the natural physical environment. In Field, C. B., Barros, V., Stocker, T. F., Qin, D., Dokken, D. J., Ebi, K. L., Mastrandrea, M. D., Mach, K. J., Plattner, G. K., Allen, S. K., Tignor, M., and Midgley, P. M., editors, *Managing the Risks of Extreme Events and Disasters to Advance Climate Change Adaptation: Special Report of the Intergovernmental Panel on Climate Change*, pages 109–230. Cambridge University Press, Cambridge, UK and New York, NY, USA.

Seregina, L. S., Fink, A. H., van der Linden, R., Elagib, N. A., and Pinto, J. G. (2019). A new and flexible rainy season definition: Validation for the Greater Horn of Africa and application to rainfall trends. *International Journal of Climatology*, 39(2):989–1012.

Shongwe, M. E., van Oldenborgh, G. J., van den Hurk, B., and van Aalst, M. (2011). Projected changes in mean and extreme precipitation in Africa under global warming. Part II: East Africa. *Journal of Climate*, 24(14):3718–3733.

Shukla, S., Funk, C. C., and Hoell, A. (2014). Using constructed analogs to improve the skill of National Multi-Model Ensemble March-April-May precipitation forecasts in equatorial East Africa. *Environmental Research Letters*, 9(9):094009.

Skamarock, W. C., Klemp, Joseph, B., Dudhia, J., Gill, D. O., Barker, D. M., Duda, M. G., Xiang-Yu, H., Wang, W., and Powers, J. G. (2008). A description of the advanced research WRF version 3. *NCAR/TN-475+STR*, pages 1–113.

Son, S. W., Lim, Y., Yoo, C., Hendon, H. H., and Kim, J. (2017). Stratospheric control of the Madden-Julian Oscillation. *Journal of Climate*, 30(6):1909–1922.

Stockdale, T. N., Anderson, D. L. T., Alves, J. O. S., and Balmaseda, M. a. (1998). Global seasonal rainfall forecasts using a coupled ocean-atmosphere model. *Nature*, 392(6674):370–373.

Taylor, K. E., Stouffer, R. J., and Meehl, G. A. (2012). An overview of CMIP5 and the experiment design. *Bulletin of the American Meteorological Society*, 93(4):485–498.

Tierney, J. E., Ummenhofer, C. C., and DeMenocal, P. B. (2015). Past and future rainfall in the Horn of Africa. *Science Advances*, 1(9):e1500682.

Torrence, C. and Webster, P. J. (1998). The annual cycle of persistence in the El Niño/Southern Oscillation. *Quarterly Journal of the Royal Meteorological Society*, 124(550):1985–2004.

Trenberth, K. E. (1997). The Definition of El Niño. *Bulletin of the American Meteorological Society*, 78:2771–2777.

Troccoli, A. (2010). Seasonal climate forecasting. *Meteorological Applications*, 17(3):251–268.

Troccoli, A., Harrison, M., Anderson, D. L. T., and Mason, S. J., editors (2008). *Seasonal Climate: Forecasting and Managing Risk, NATO Science Series*. Springer Academic Publishers, Dordrecht, Netherlands.

Uhe, P., Philip, S., Kew, S., Shah, K., Kimutai, J., Mwangi, E., van Oldenborgh, G. J., Singh, R., Arrighi, J., Jjemba, E., Cullen, H., and Otto, F. (2018). Attributing drivers of the 2016 Kenyan drought. *International Journal of Climatology*, 38:e554–e568.

Ummenhofer, C. C., Gupta, A. S., England, M. H., and Reason, C. J. C. (2009). Contributions of Indian Ocean sea surface temperatures to enhanced East African rainfall. *Journal of Climate*, 22(4):993–1013.

UN Office for the Coordination of Humanitarian Affairs (OCHA) (2018). Floods in Kenya June 2018. Available at: `https://reliefweb.int/report/kenya/ocha-flash-update-6-floods-kenya-7-june-2018`. Last accessed: 22 September 2020.

Vellinga, M. and Milton, S. (2018). Drivers of interannual variability of the East African 'Long Rains'. *Quarterly Journal of the Royal Meteorological Society*.

Viste, E., Korecha, D., and Sorteberg, A. (2013). Recent drought and precipitation tendencies in Ethiopia. *Theoretical and Applied Climatology*, 112(3-4):535–551.

Vizy, E. K. and Cook, K. H. (2012). Mid-twenty-first-century changes in extreme events over northern and tropical Africa. *Journal of Climate*, 25(17):5748–5767.

Wainwright, C. M., Marsham, J. H., Keane, R. J., Rowell, D. P., Finney, D. L., Black, E., and Allan, R. P. (2019). 'Eastern African Paradox' rainfall decline due to shorter

not less intense Long Rains. *npj Climate and Atmospheric Science*, 2(1):1–9.

Walker, G. (1928). World weather. *Nature*, 121(3053):713–716.

Walker, G. T. (1925). Correlation in seasonal variations of weather—a further study of world weather. *Monthly Weather Review*, 53(6):252–254.

Walker, G. T. and Bliss, E. W. (1932). World Weather V - NAO. *Memoirs of the Royal Meteorological Society*, IV(36):54–84.

Walters, D. N., Best, M. J., Bushell, A. C., Copsey, D., Edwards, J. M., Falloon, P. D., Harris, C. M., Lock, A. P., Manners, J. C., Morcrette, C. J., Roberts, M. J., Stratton, R. A., Webster, S., Wilkinson, J. M., Willett, M. R., Boutle, I. A., Earnshaw, P. D., Hill, P. G., MacLachlan, C., Martin, G. M., Moufouma-Okia, W., Palmer, M. D., Petch, J. C., Rooney, G. G., Scaife, A. A., and Williams, K. D. (2011). The Met Office Unified Model Global Atmosphere 3.0/3.1 and JULES Global Land 3.0/3.1 configurations. *Geoscientific Model Development*, 4(4):919–941.

Webster, P. J. (2020). *Dynamics of the Tropical Atmosphere and Oceans*. John Wiley and Sons Inc., Hoboken, New Jersey, USA.

Webster, P. J., Moore, A. M., Loschnigg, J. P., and Leben, R. R. (1999). Coupled ocean-atmosphere dynamics in the Indian Ocean during 1997-98. *Nature*, 401(6751):356–360.

Webster, P. J. and Yang, S. (1992). Monsoon and ENSO:Selectively interactive systems. *Quart. J. Roy. Meteorol. Soc.*, 118(507):877–926.

Wenhaji Ndomeni, C., Cattani, E., Merino, A., and Levizzani, V. (2018). An observational study of the variability of East African rainfall with respect to sea surface temperature and soil moisture. *Quart. J. Roy. Meteor. Soc.*, pages 1–44.

Wheeler, M. C. and Hendon, H. H. (2004). An all-season real-time multivariate MJO Index: Development of an index for monitoring and prediction. *Monthly Weather Review*, 132(8):1917–1932.

Wilks, D. S. (2011). *Statistical Methods in the Atmospheric Sciences*. Elsevier, Oxford, 3rd edition.

Williams, A. P. and Funk, C. C. (2011). A westward extension of the warm pool leads to a westward extension of the Walker circulation, drying eastern Africa. *Climate*

Dynamics, 37(11-12):2417–2435.

Williams, K., Chamberlain, J., Buontempo, C., and Bain, C. (2015). Regional climate model performance in the Lake Victoria basin. *Climate Dynamics*, 44(5-6):1699–1713.

Woodhams, B. J., Birch, C. E., Marsham, J. H., Bain, C. L., Roberts, N. M., and Boyd, D. F. (2018). What is the added value of a convection-permitting model for forecasting extreme rainfall over tropical East Africa? *Monthly Weather Review*, 146(9):2757–2780.

Woodhams, B. J., Birch, C. E., Marsham, J. H., Lane, T. P., Bain, C. L., and Webster, S. (2019). Identifying key controls on storm formation over the lake Victoria basin. *Monthly Weather Review*, 147(9):3365–3390.

World Bank (2020). World Development Indicators. Available at: `https://databank.worldbank.org/source/world-development-indicators/preview/on`. Last accessed: 17 September 2020.

World Meteorological Organization (2020). Regional Climate Outlook Forums. Available at: `https://public.wmo.int/en/our-mandate/climate/regional-climate-outlook-products`. Last accessed: 04 October 2020.

Wyrtki, K. (1975). El Niño-the dynamic response of the equatorial Pacific Ocean to atmospheric forcing. *Journal of Physical Oceanography*, 5(4):572–584.

Yamagata, T., Behera, S. K., Luo, J.-J., Masson, S., Jury, M. R., and Rao, S. A. (2004). Coupled ocean-atmosphere variability in the tropical Indian Ocean. In *Earth's Climate*, pages 189–211.

Yang, W., Seager, R., Cane, M. A., and Lyon, B. (2014). The East African long rains in observations and models. *Journal of Climate*, 27(19):7185–7202.

Yang, W., Seager, R., Cane, M. A., and Lyon, B. (2015a). The annual cycle of East African precipitation. *Journal of Climate*, 28(6):2385–2404.

Yang, W., Seager, R., Cane, M. A., and Lyon, B. (2015b). The rainfall annual cycle bias over East Africa in CMIP5 coupled climate models. *Journal of Climate*, 28(24):9789–9802.

Yoo, C. and Son, S. W. (2016). Modulation of the boreal wintertime Madden-Julian os-

cillation by the stratospheric quasi-biennial oscillation. *Geophysical Research Letters*, 43(3):1392–1398.

Yule, G. U. (1907). On the theory of correlation for any number of variables, treated by a new system of notation. *Proceedings of the Royal Society of London. Series A, Containing Papers of a Mathematical and Physical Character*, 79(529):182–193.

Chapter 2.

Skill of dynamical and GHACOF consensus seasonal forecasts of East African rainfall

Skill of dynamical and GHACOF consensus seasonal forecasts of East African rainfall

Dean P. Walker[1] · Cathryn E. Birch[1] · John H. Marsham[1,2] · Adam A. Scaife[3,4] · Richard J. Graham[3] · Zewdu T. Segele[5]

Abstract

Seasonal forecasts of rainfall are considered the priority timescale by many users in the tropics. In East Africa, the primary operational seasonal forecast for the region is produced by the Greater Horn of Africa Climate Outlook Forum (GHACOF), and issued ahead of each rainfall season. This study evaluates and compares the GHACOF consensus forecasts with dynamical model forecasts from the UK Met Office GloSea5 seasonal prediction system for the two rainy seasons. GloSea demonstrates positive skill (r = 0.69) for the short rains at 1 month lead. In contrast, skill is low for the long rains due to lack of predictability of driving factors. For both seasons GHACOF forecasts show generally lower levels of skill than GloSea. Several systematic errors within the GHACOF forecasts are identified; the largest being the tendency to over-estimate the likelihood of near normal rainfall, with over 70% (80%) of forecasts giving this category the highest probability in the short (long) rains. In a more detailed evaluation of GloSea, a large wet bias, increasing with forecast lead time, is identified in the short rains. This bias is attributed to a developing cold SST bias in the eastern Indian Ocean, driving an easterly wind bias across the equatorial Indian Ocean. These biases affect the mean state moisture availability, and could act to reduce the ability of the dynamical model in predicting interannual variability, which may also be relevant to predictions from coupled models on longer timescales.

Keywords Seasonal climate forecasts · Consensus outlooks · East Africa · Precipitation · Probabilistic verification

1 Introduction

East Africa is a region that is highly vulnerable to rainfall variability, as consistent rainfall is vital for crops and livestock. Extreme events such as the 2010-11 year long drought have major effects on society, and flooding events can occur even in years of water scarcity, such as in 2018, when heavy boreal spring rains followed the severe drought conditions of late 2017 (http://fews.net/east-africa). Seasonal prediction

of these events, if skilful, can therefore provide users with information to mitigate or avoid humanitarian disasters.

Equatorial East Africa experiences two rainfall seasons per year, commonly termed the long rains, occurring from March to May (MAM), and the short rains, occurring from October to December (OND). The long rains have higher total rainfall (Camberlin and Wairoto 1997), and are more reliable, and so coincide with the main growing season (Camberlin and Philippon 2002), whilst the short rains have a much larger interannual variability (Hastenrath et al. 1993; Nicholson 1996). The two rainfall seasons lie within the seasonal reversals of the Somali Jet (Okoola 1999), are observed to be dynamically different (Camberlin and Wairoto 1997), and are classically attributed to the motion of the Intertropical Convergence Zone (e.g. Okoola 1998; Mutai and Ward 2000).

The correlation between the major modes of sea surface temperature (SST) variability and East African rainfall is different in the two rainfall seasons, and as such, the predictability of rainfall is different in the long and short rains (Camberlin and Philippon 2002). The short rains have been

✉ Dean P. Walker
  eedpw@leeds.ac.uk

[1] School of Earth and Environment, University of Leeds, Leeds, UK

[2] National Centre for Atmospheric Science, Leeds, UK

[3] Met Office Hadley Center, Exeter, UK

[4] College of Engineering, Mathematics and Physical Sciences, University of Exeter, Exeter, UK

[5] IGAD Climate Prediction and Applications Centre, Nairobi, Kenya

linked to variability within the Pacific Ocean, with Rodhe and Virji (1976) observing similar periodicities in East African rainfall variability to those observed for El Niño-Southern Oscillation (ENSO). Many studies since (e.g. Nicholson and Entekhabi 1986; Ogallo 1988; Nicholson 1996; Nicholson and Kim 1997; Indeje et al. 2000), have investigated the role and mechanism of ENSO in influencing East African rainfall, through its effect on the Walker Circulation. More recently, a mode of variability within the Indian Ocean, termed the Indian Ocean Dipole (IOD), has been linked to East African rainfall variability (Saji et al. 1999; Webster et al. 1999; Black et al. 2003; Marchant et al. 2007; Ummenhofer et al. 2009). The positive phase of the IOD is often found to occur simultaneously with El Niño, and as such, several authors have investigated the dependence of this mode on El Niño. The general consensus is that whilst El Niño modulates the IOD and is favourable for the evolution of an IOD event (Black et al. 2003), the IOD is an independent mode of variability from ENSO (Saji and Yamagata 2003; Yamagata et al. 2004; Behera et al. 2005; Bahaga et al. 2015). There are years where the IOD occurs under neutral ENSO conditions, such as in 1961 when a strong positive IOD event took place in absence of anomalies in the Pacific Ocean, causing heavy rains in East Africa (Saji et al. 1999).

A major source of moisture variability for East African rainfall during the short rains originates from the flow over the Indian Ocean (Hastenrath et al. 2011). These zonal winds are described as being part of a Walker circulation cell (Hastenrath et al. 1993; Hastenrath 2000). Areas of ascent and descent lie over Indonesia and East Africa respectively, with a mean state of near-surface westerlies and upper level easterlies over the Indian Ocean. Years with near-surface easterly anomalies coincide with upper level westerly anomalies, increased ascent over East Africa and higher rainfall (Hastenrath et al. 1993; Yamagata et al. 2004; Hastenrath 2007). These anomalies are driven by a positive IOD, which drives high near-surface pressure in the eastern Indian Ocean and low pressure in the west.

Meanwhile, predictability during the long rains is less well understood (Camberlin and Philippon 2002), with several studies demonstrating that the season is not strongly constrained by SST variability (e.g. Ogallo 1988; Liebmann et al. 2014). Nicholson (2014) suggested that this is likely to be because El Niño is in transition during this time of year, a phenomenon referred to as the spring predictability barrier (Torrence and Webster 1998). Several authors have suggested that atmospheric phenomena could control the interannual variability in this season (Philippon et al. 2002; Nicholson 2014, 2015), with Pohl and Camberlin (2006a, b) showing that the Madden-Julian Oscillation (MJO; Madden and Julian 1971, 1972) plays an important role, as well as Indeje and Semazzi (2000)

identifying a possible contribution from the Quasi-Biennial Oscillation (QBO; Ebdon 1960; Reed et al. 1961), although the underlying mechanism is not well described.

Real time forecasts of seasonal rainfall in East Africa have been made for several decades, with reasonable success over the short rains, initially based upon statistical methods linking SST variability and rainfall (e.g. Farmer 1988; Mutai et al. 1998). More recently, statistical forecasts of the long rains have also been produced. Nicholson (2014, 2015) used several variables including zonal and meridional wind fields at several pressure levels, as well as sea level pressure (SLP) values, to create models with strong correlations (up to 0.76) for February predictors, and also noted that using atmospheric fields improved statistical models of the short rains. Vellinga and Milton (2018) meanwhile created a multiple linear regression model for the long rains (defined in this study as March to April) using February to March MJO amplitude, QBO from September to November of the previous year, and an area of Indian Ocean SSTs close to the coast of Somalia in the Arabian Sea, finding a correlation with the first principal component of the long rains of 0.77, with the largest contribution generally coming from the MJO amplitude.

In recent years, dynamical models have advanced greatly, and have become increasingly used to produce seasonal forecasts. Batté and Déqué (2011) evaluated the ENSEMBLES project multi-model ensemble of seasonal forecasts over Africa, finding mixed results over East Africa, with the model performing better during the short rains than the long rains. Bahaga et al. (2016) also evaluated a multi-model ensemble with models sourced from North America and Asia over the short rains at 1 month lead. Models that could better forecast the Indian Ocean Dipole were found to have better skill, with the multi-model ensemble achieving a correlation of 0.44 between observed and forecast rainfall, increasing to 0.67 when using only the models that had significant skill when evaluated individually. Although Nicholson (2017) noted that statistical forecasts generally outperform dynamical forecasts in this region, the latter are constantly improving, with ever increasing resolution, and improved representation of physical processes. The skill of statistical models in producing real time forecasts is also often overestimated due to the method of their construction, with common mistakes being overfitting the model, and using too many predictors or unphysical predictors. They also often fail to consider the nonstationary relationship between rainfall and the predictors. Such nonstationary relationships of teleconnections to East African rainfall in particular have been highlighted by Clark et al. (2003), Bahaga et al. (2019). To best meet user needs, a combination of statistical and dynamical methods is often most appropriate (Doblas-Reyes et al. 2013).

Supported by the World Meteorological Organisation (WMO), consensus seasonal forecasts are produced by Regional Climate Outlook Forums (RCOFs) for many locations around the world (Ogallo et al. 2008). The Greater Horn of Africa Climate Outlook Forum (GHACOF), organised by the Intergovernmental Authority on Development (IGAD) Climate Prediction and Applications Centre (ICPAC), has been issuing seasonal consensus forecasts for East Africa since 1998. GHACOFs are held three times per year, in the lead up to the long and short rains, and the summer rainfall season. For the long rains, GHACOFs are typically held in mid February (lead time less than 1 month), whilst for the short rains, they are typically held late in August (lead time greater than 1 month). For the summer rainfall season, the GHACOF is typically held in the second half of May. The WMO has also fostered coordination among centres running operational dynamical seasonal forecast systems, so-called Global Producing Centres for Long-Range Forecasts (GPCs), with a specific objective to increase access and use of the model outputs in regional forecasting activities (Graham et al. 2011). Details of the GHACOF process will be presented in Sect. 2.3.

As well as producing the forecasts, RCOFs have been praised as an excellent opportunity for networking and information sharing between nations within the region, and within the different stakeholder groups (Ogallo et al. 2008; Mwangi et al. 2014). Success stories of GHACOF forecasts having positive impact on the region have been recorded, such as a bumper harvest in 2009, where, based upon information from the GHACOF forecast, Kenya Red Cross distributed extra seeds to farmers across Kenya, leading to enhanced stores of grain (Graham et al. 2012), and in 2002, where forecasts of below normal rainfall in Ethiopia were acted upon to relieve food insecurity (Patt et al. 2007; Hellmuth et al. 2007).

An evaluation of the GHACOF consensus forecasts was performed by Mason and Chidzambwa (2008) for 10 years of forecasts, as part of an RCOF review by the WMO. The forecasts were found to have positive skill but observed some notable biases that were also common to the West Africa and southern Africa RCOFS. In particular, forecast probabilities for the near average category were found to be systematically too high, indicating a tendency to "hedge" to average conditions. Current assessment of GHACOF includes an evaluation of each individual forecast's performance using a form of hit score (http://rcc.icpac.net/index.php/long-range-forecast/verification-products), and an analysis of the performance of the previous forecast at the following GHACOF event.

Comparisons between consensus and dynamical forecasts are few and far between. Mwangi et al. (2014) investigated whether European Centre for Medium-Range Weather Forecasts (ECMWF) seasonal forecasting system product

4 (SYS-4) can provide additional information, however, no statistical side-by-side comparison has been produced. Additionally, biases within dynamical models are well known, and regularly documented, such as in the Coupled Model Intercomparison Project Phase 5 (CMIP5; Taylor et al. 2012) and Phase 3 (CMIP3; Meehl et al. 2007) models (Yang et al. 2015; Li and Xie 2014; Richter et al. 2016), however, their origins, and their effects on the models ability to produce skilful forecasts is rarely considered. In operational models, mean state biases are linearly removed from the forecast models using hindcasts (Troccoli 2010). A recent study by Hirons and Turner (2018) demonstrated that biases in the CMIP5 models' mean states can drastically influence their ability to correctly represent the atmospheric response to anomalies from the mean state, whilst a study by Delsole and Shukla (2010) suggested that models whose mean state are most similar to the observations have a tendency to demonstrate higher skill.

As part of its GPC output the UK Met Office issues monthly-updating seasonal forecasts with global coverage and with a focus on RCOF regions including the Greater Horn of Africa using the dynamical forecast system: Global Seasonal Forecasting System Version 5 (GloSea5; MacLachlan et al. 2015). Skill maps to assist in use of the forecast are also published (https://www.metoffice.gov.uk/research/climate/seasonal-to-decadal/gpc-outlooks). In this paper a detailed assessment of the ability of GloSea in predicting the rainfall seasons over East Africa is presented and for the first time, a quantitative comparison of skill between forecasts from a dynamical model and the GHACOF consensus forecasts is made. This analysis goes beyond that of Mason and Chidzambwa (2008), by using a larger period of assessment, and considering the impact of the skill conditional on a remote driver of rainfall. A secondary objective is to investigate the sources of rainfall biases within GloSea, to understand whether these biases could have a negative effect on the model's prediction skill.

The structure of the rest of the paper will be as follows: Sect. 2 will introduce the data used for this study, and analysis methodologies. Section 3.1 will evaluate the climatology and interannual variability of GloSea. A statistical comparison of the forecast skill of GloSea and GHACOF forecasts will be presented in Sect. 3.2. Section 3.3 will consider the drivers of variability in the short rains, and their effects on skill within both GloSea and GHACOF, whilst Sect. 3.4 will discuss and investigate the origin of biases of rainfall within the short rains in GloSea. Section 4 summarises the key findings.

2 Data and methodology

2.1 Verification data

The observational rainfall data used in this study is Global Precipitation Climatology Project (GPCP) version 2.3 (Adler

et al. 2003), a monthly rainfall dataset from 1979 to present, that combines observations from rain gauges and several satellite datasets. This is gridded onto a $2.5° \times 2.5°$ resolution grid. This commonly used dataset covers the study period and region with both land and ocean rainfall estimates.

Sea surface temperature (SST) observations are obtained from the Hadley Centre Sea Ice and Sea Surface Temperature (HadISST) dataset (Rayner et al. 2003). HadISST provides monthly mean data at $1° \times 1°$ resolution. For comparison with wind climatologies, the European Centre for Medium-Range Weather Forecasts (ECMWF), interim reanalysis (ERA-Interim; Dee et al. 2011) is used. Mean sea level pressure data use the National Centers for Environmental Prediction-National Center for Atmospheric Research (NCEP-NCAR) reanalysis (Kalnay et al. 1996).

2.2 Seasonal forecast model

The forecast system used in this study is the UK Met Office Global Seasonal Forecast System 5 (GloSea5; MacLachlan et al. 2015). The core of GloSea5 is the Hadley Centre Global Environmental Model version 3 (HadGEM3; Hewitt et al. 2011), with atmosphere resolution $0.833° \times 0.556°$, with 85 atmospheric levels. The ocean resolution is $0.25° \times 0.25°$. The higher ocean resolution improves predictions of sea surface temperature anomalies in the Tropical Pacific, as tropical instability waves can be better resolved, and improves mid-latitude ocean biases (Scaife et al. 2011). The seasonal forecast model runs for 210 days from initialisation. An operational hindcast is produced in parallel and is used to bias correct the forecast. Further details of the GloSea5 system and the previous version (GloSea4) are discussed in MacLachlan et al. (2015) and Arribas et al. (2011) respectively.

This study makes use of operational hindcasts produced in parallel to the forecast, covering the period 1993–2015. Hindcasts are run 4 times per month (1st, 9th, 17th, 25th of each month) with three ensemble members initialised per start date. Members initialised on the same date differ by stochastic physics (Bowler et al. 2009). Three months preceding each rainfall season are used: December, January, February for the long rains, and July, August, September for the short rains, giving a total of 36 ensemble members available for each season. When gridpoint to gridpoint comparison with observational data is needed, GloSea is interpolated onto a $2.5° \times 2.5°$ resolution grid. The word forecast will be used from here on to refer to the GloSea hindcasts in the evaluation. This is because the evaluation treats the hindcasts as forecasts, and provides consistency when referring to both GloSea and GHACOF.

The full 36 members are used only in results investigating effects of ensemble size and lead time on model behaviour. For results investigating the forecast skill of the system,

and in comparison with the GHACOF forecasts, a smaller ensemble is used to represent a forecast initialised with 1 month lead time. To create this 1 month lead forecast, three start dates centred around the first of the month prior to the start of the season are used (25th January, 1st February, 9th February for the long rains, and 25th August, 1st September, 9th September for the short rains). As 3 ensemble members are initialised per start date this produces an ensemble of 9 members. The use of members from three different dates is to create a larger ensemble, representing the skill of the central date, as there is little difference in skill between hindcasts from neighbouring weeks, and any advantage gained from the shorter lead time members will be balanced out by the longer lead time members.

2.3 GHACOF forecasts and the GHACOF process

Currently, the GHACOF process is split into two parts: a pre-COF capacity building workshop with the purpose of both producing the consensus forecast and giving training to forecasters from the East Africa member states; and the GHACOF itself, where the forecast for the season is presented to the media and representatives from climate sensitive sectors such as agriculture, energy, water resources, and health, and gives an opportunity for representatives of these sectors to interact with forecasters from East Africa as well as climate experts from around the world.

To produce the GHACOF forecast, predictions from many sources are used. ICPAC produce a seasonal forecast using the weather and research forecast (WRF; Skamarock et al. 2008) model over the Greater Horn of Africa (GHA) region, covering 11 countries. The model is driven by the NCEP Climate Forecast System version 2 (CFSv2; Saha et al. 2014). This model has an horizontal resolution of 30km, with an ensemble of up to 15 members, many of which are initialized from different dates and, more recently, some members use different convective parameterization schemes for the same initial and boundary conditions. The model domain covers all of Africa and the adjoining water bodies, which incorporate the large-scale systems that drive the weather and climate of the region. In addition to rainfall and temperature, the dynamical forecast diagnostics available to the forecasters include the onset of the rainfall season, its cessation, intervening dry and wet spells, and duration of the season, for the entire GHA region.

Predictions from global dynamical seasonal forecast models from the North American Multi Model Ensemble (NMME; Kirtman et al. 2014) are considered, as well as dynamical forecasts from the UK Met Office, Metéo-France and ECMWF. These are looked at both in their raw form, with simple mean bias correction, linear regression, and also as calibrated forecasts using the Climate Predictability Tool (CPT; Mason and Tippett 2016). A statistical model

approach is also used, using the Geospatial Climate Outlook Forecasting Tool (GeoCOF; Magadzire et al. 2016) and CPT to produce multiple linear regression forecasts using predictors such as observed or GCM predicted SSTs and wind fields. Each country uses all of these data sources, as well as their own knowledge of their country's climate, to produce a subjective forecast for their country, dividing it into zones where the forecast falls into the same probability categories. ICPAC then collate the country level forecasts together onto a map. At this point, inconsistencies at country borders are considered, with forecasters from each country giving their justification for the forecast category they have used, to come to an agreement on how to solve these inconsistencies. The forecast is presented on a map of the region (Fig. 1), displaying the probability of the seasonal rainfall tercile categories, above normal (upper tercile category), near normal (centre tercile category), and below normal (lower tercile category), in zones delineated by regions where the forecasts were the same.

2.4 Gridding of GHACOF forecasts

The rainfall outlooks produced by the GHACOF were sourced from ICPAC (http://geoportal.icpac.net/), in the form of digital shapefiles containing the different forecast probability regions for each season, starting with the first GHACOF in 1998. These forecasts were then gridded using rasterization into a $2.5° \times 2.5°$ grid matching the GPCP verification data. In this way, the GHACOF forecasts can be evaluated in the same manner as a probabilistic dynamical model forecast, against a gridded comparison dataset. For direct comparison between GloSea and GHACOF the overlapping 18 year period of 1998 to 2015 is used. Regions where a climatological forecast was given due to the region being dry for that particular season were removed from the evaluation to avoid evaluating a forecast that by definition has zero skill in many of the metrics used.

2.5 Limitations of the probabilistic evaluation method

In converting the GHACOF consensus forecast into a gridded probabilistic forecast of the same format as a dynamical model forecast, and making comparison to a dynamical model, some considerations need to be made. Firstly, the GHACOF consensus forecasts, although issued in a probabilistic format, are not true probabilistic forecasts due to the subjectivity that is applied throughout their production meaning the probabilities given may not necessarily be the true probability. However, for the purposes of this study these numbers will be assumed to represent the true probability.
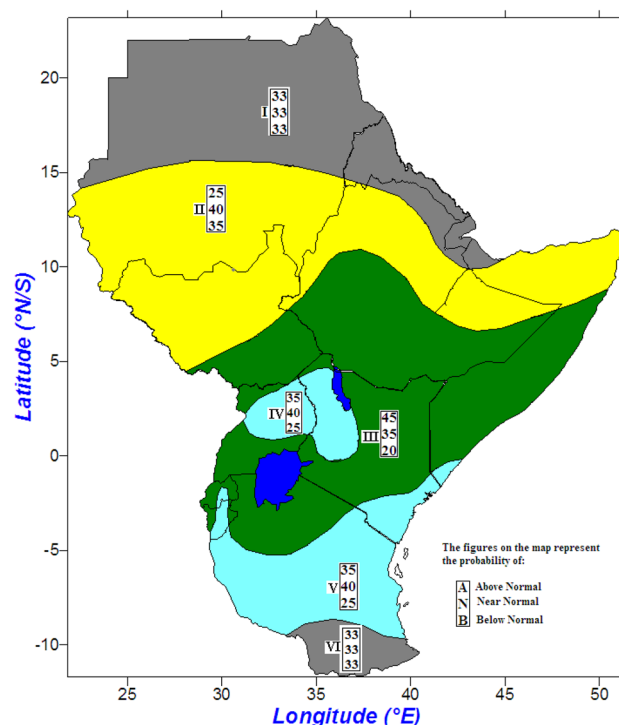

Fig. 1 Example GHACOF consensus seasonal forecast for rainfall for OND 2015. The different coloured regions represent regions with different forecast probabilities. The column of three numbers in each region gives the probability of the total rainfall amount for the season being within the upper, middle, and lower tercile with respect to climatology. Colours indicate regions where the issued forecast is the same. As described in the GHACOF statement: grey indicates the region is usually dry during this season, yellow indicates regions likely to receive near normal to below normal rainfall, green indicates regions likely to receive above normal to near normal rainfall, blue indicates regions likely to receive near normal to above normal rainfall

Another limitation is due to the resolution of the observation data to be used. Although $2.5° \times 2.5°$ observation data is the most commonly used for verification of seasonal forecasts (and hence why it is used in this study) this relatively low resolution can cause problems when converting the hand drawn lines of the consensus forecast into a grid, as several grid squares are likely to cover regions split between two or even more different forecast zones, and are simply treated as the zone which has the greatest area inside the grid square. This is not necessarily representative of the forecast issued for that location, however, the lines drawn within the forecast are themselves subjective.

Finally, there are limitations related to the timing of the forecasts. These forecasts are being treated as 1 month lead time forecasts, this is to represent the time when the forecast becomes available. Whilst this is a fair comparison for the long rains, which is often released at a less than 1 month lead time (ie later than 1st February) and utilises 1 month lead dynamical model predictions, this is less favourable for the

short rains forecast, which is released in late August (compared to 1st September for the 1 month lead forecast of the dynamical model). Although the availability of these forecasts is therefore often only a few days apart, the GHACOF process for the short rains utilises dynamical forecasts from August, or 2 month lead time. Consideration should also be given to the fact that older GHACOF forecasts of the short rains were issued for September to December rather than October to December, and that when issuing probabilities based on terciles, the terciles are based on the climatological normal period at the time of issue (currently 1981–2010), rather than the period used here (1998–2015: the period over which the analysis is performed).

In order to address these limitations, it must be stated that the presented analysis only represents an estimate of the true skill of the consensus forecasts. Similarly the analysis of the dynamical forecasts are only an estimate of the true forecast skill due to the differing sizes of ensembles and different availability of initialisation data between forecasts and hindcasts, and as such, statistical significance tests have not been applied to any identified differences in skill between the two forecasts. Finally, there is a level of uncertainty within the observed data used that must be taken into consideration when performing any comparison between models and observations.

Despite these limitations, the comparison between the two forecasts is an important aspect of this study, as it provides information of the ability the GHACOF forecast with respect to state of the art models, which can be used to judge the GHACOF forecasts against the predictability of the rainfall seasons that the forecasts are being issued for.

2.6 Statistical techniques

To construct the relative operating characteristic (ROC) curve (Mason 1982), thresholds of predicted probabilities for each tercile category (above, near, and below average) were selected at every 10% for GloSea due to ensemble size, and every 5% for GHACOF chosen due to the practice of issuing forecasts with probabilities rounded to the nearest 5% recommended by Mason (2013). For each threshold, if the forecast probability of a category is greater than the threshold value, it is classed as a forecast event, otherwise it is classed as a forecast non-event. The observation matching the forecast is then considered, to determine which category occurred. This produces for each threshold value a 2×2 contingency table, whereby a forecast event that occurred in observations is a hit, a forecast non-event where the event subsequently occurred in observations is a miss, a forecast event that did not occur in the observations is a false alarm, and a forecast non-event that did not occur in the observations is a correct negative. For each contingency table the hit rate (HR), defined as *hits/(hits + misses)* and false alarm rate (FAR), defined as *false alarms/ (false alarms + correct negatives)* can then be calculated. These values are plotted with hit rate on the y-axis, and false alarm rate on the x-axis, for each threshold value. The curve passing through the points is referred to as the ROC curve, and the area under the ROC curve is the ROC score, which can be any value between 0 and 1. A line of gradient 1 passing through the origin defines the line of no skill compared to a random forecast with a ROC score of 0.5. ROC scores greater than 0.5 are therefore considered to have positive predictive skill with respect to a random forecast. Threshold values of 0% (the event is always forecast) and greater than 100% (the event is never forecast) are used to fix the curves to (1,1) and (0,0), as these threshold values will always produce hit rates of 1 and 0, and false alarm rates of 1 and 0, respectively, regardless of the forecast being evaluated.

To construct the reliability diagram (Hartmann et al. 2002), forecasts are split into bins dependent on the forecast probability of an event. For each bin, the forecasts are matched up to their corresponding observations, and the observed frequency of the event occurring is calculated for each bin. The forecast probability is then plotted against the observed frequency for each bin. A perfectly reliable forecast would have a forecast probability equal to the observed frequency in all bins, leading to a diagonal line of gradient 1, shown on the diagrams. Horizontal and vertical lines are plotted through the climatological frequency of the event (in the case of terciles, 1/3). The horizontal line corresponds to no resolution (ie the outcome is the same regardless of what was forecast), whilst the vertical line is a forecast of climatology. Another line is added bisecting the diagonal and no resolution lines, marking the line of no skill. Forecast points that lie in the region between this line and the vertical line contribute positively to the Brier skill score of the forecast.

When analysing reliability diagrams, several terms are regularly used, with their definitions as follows: over/underconfidence, meaning the line has a gradient less/ greater than one, and over/under-forecasting, meaning that the line lies mostly below/ above the diagonal line, as defined in Mason (2013).

The Heidke Skill Score (HSS; Heidke 1926) is computed using the results from an $n \times n$ contingency table. HSS is defined as:

$$HSS = \frac{\sum_{i=1}^{n} p_{ii} - \sum_{i=1}^{n} \left(\sum_{j=1}^{n} p_{ij} \right) \left(\sum_{j=1}^{n} p_{ji} \right)}{1 - \sum_{i=1}^{n} \left(\sum_{j=1}^{n} p_{ij} \right) \left(\sum_{j=1}^{n} p_{ji} \right)} \quad (1)$$

where p_{ij} is the probability of the *i*'th row and *j*'th column of the contingency table. This can be rewritten as:

$$HSS = \frac{PC - E}{1 - E} \quad (2)$$

where *PC* is the proportion correct, or the sum of the values on the diagonal of the contingency table, and *E* is the expected proportion correct for a random forecast, found by taking the sum of the probability of a forecast of event *i* multiplied by the probability of observing event *i*, for each *i*. HSS is a standard skill score metric, with a minimum of −1, and a maximum of 1, with a score of 0 meaning the forecast is no better than a random chance forecast.

For further information on ROC curves, reliability diagrams, and skill scores or metrics used in this study, the reader is referred to Wilks (2006).

2.7 Time series indices

For time series of area averaged rainfall over East Africa, the land area within the region (12°N–10°S, 30°E–55°E) is used, and is also averaged over the 3 months of March, April, and May (MAM) referred to as the East African long rains, and the 3 months of October, November, and December (OND) for the East African short rains. To represent the state of ENSO, the Niño 3.4 index is used, with its usual definition of the average SST anomaly over the region (5°N–5°S, 170°W–120°W; Barnston et al. 1997). In particular, the time averaged Niño 3.4 index is used, with the anomaly being the average SST anomaly over OND with respect to the 1993-2015 climatological SST average over OND within this region. Similarly, two indices within the Indian Ocean are used. The Western Tropical Indian Ocean (WTIO) is the average SST anomaly over the region (10°N–10°S, 50°E–70°E) and the South Eastern Tropical Indian Ocean (SETIO) is the average SST anomaly over the region (0°N–10°S, 90°E–110°E), as defined by Saji et al. (1999), and calculated in the same manner as the Niño 3.4 index. Finally the Indian Ocean Dipole (IOD) index is calculated as the difference between the WTIO and SETIO indices, again as defined by Saji et al. (1999).

3 Results

3.1 East African climatology and interannual variability in GloSea

In this section, the performance of GloSea in forecasting the climatology and interannual variability is analysed over East Africa in both rainfall seasons. The rainfall and 850 hPa wind climatology of the short rains for GloSea and observations, with relative biases, is shown in Fig. 2. Large scale patterns in both rainfall and wind vectors are captured well by GloSea, however the dominant feature is a clear wet bias, approximately 40% over land areas over OND, with an approximately 35% bias over the land areas in the region (12°N–10°S, 30°E–55°E) to be used in later analysis, with greatest bias over the regions with greatest rainfall. This is followed by a dry bias during the dry season, evident in December when a spatially coherent dry bias is present north of the equator, but a wet bias remains to the south. Consistent with this, the change in wind direction in GloSea from a southerly to northerly flow appears to occur too early in the season, suggesting a possible mistiming in the progression of the ITCZ. The rainfall biases based on the distributions coincidingly show a larger bias in October and November than December.

In Fig. 3, the climatology for the long rains is shown. Large scale patterns are again captured well by GloSea, however in this season an overall dry bias over land is present. The reversal of the northerly flow appears to occur too late in the season, and whilst a dry bias is present over the land points in the region (12°N–10°S, 30°E–55°E) in March, it has changed to a slight wet bias by May. The net effect is that the rainfall bias in this season is of relatively small magnitude, as seen in Fig. 3d. A large wet bias persists over the Indian Ocean, although moves northwards throughout the season, following the peak in rainfall.

The wet bias in the short rains, coupled with a minor dry bias in the long rains leads to a pattern where the short rains in the model provide greater rainfall than the long rains. This same error in the annual cycle of rainfall over East Africa is present in other models, as has been documented in previous studies of the CMIP3 (Anyah and Qiu 2012) and CMIP5 (Yang et al. 2015) climate models. Wet biases are found in most tropical regions in many seasonal forecast systems (Scaife et al. 2018).

The key feature of interest within a seasonal rainfall forecast is the prediction of a rainfall anomaly over the season in comparison to climatology. Figure 4 shows the predicted rainfall anomaly for each year of the forecast period for both GloSea and observations for both rainfall seasons. During the short rains, a correlation skill of 0.69 is achieved. This result is insensitive to the exact definition of the region. The model predicts the sign of many of the extreme years correctly such as 1997 and 2006, however ensemble members do not reach the extreme values seen in observations. The ensemble mean has a standard deviation of 0.40 mm day^{-1}, and the observations have a standard deviation of 0.85 mm day^{-1}. Some lack of variance with respect to the observations is expected, as the ensemble mean represents the predictable part of the variance (Scaife and Smith 2018). However, the mean ensemble member standard deviation over all members and years is 0.55 mm day^{-1}, also lower than the observations. Ensemble members should have approximately the same variance on average as the observations, to represent a possible realisation of the observations. This lack of variance explains why the ensemble members struggle to forecast the extremity of the most extreme wet or dry years (e.g. 1997, 1998, 2005,
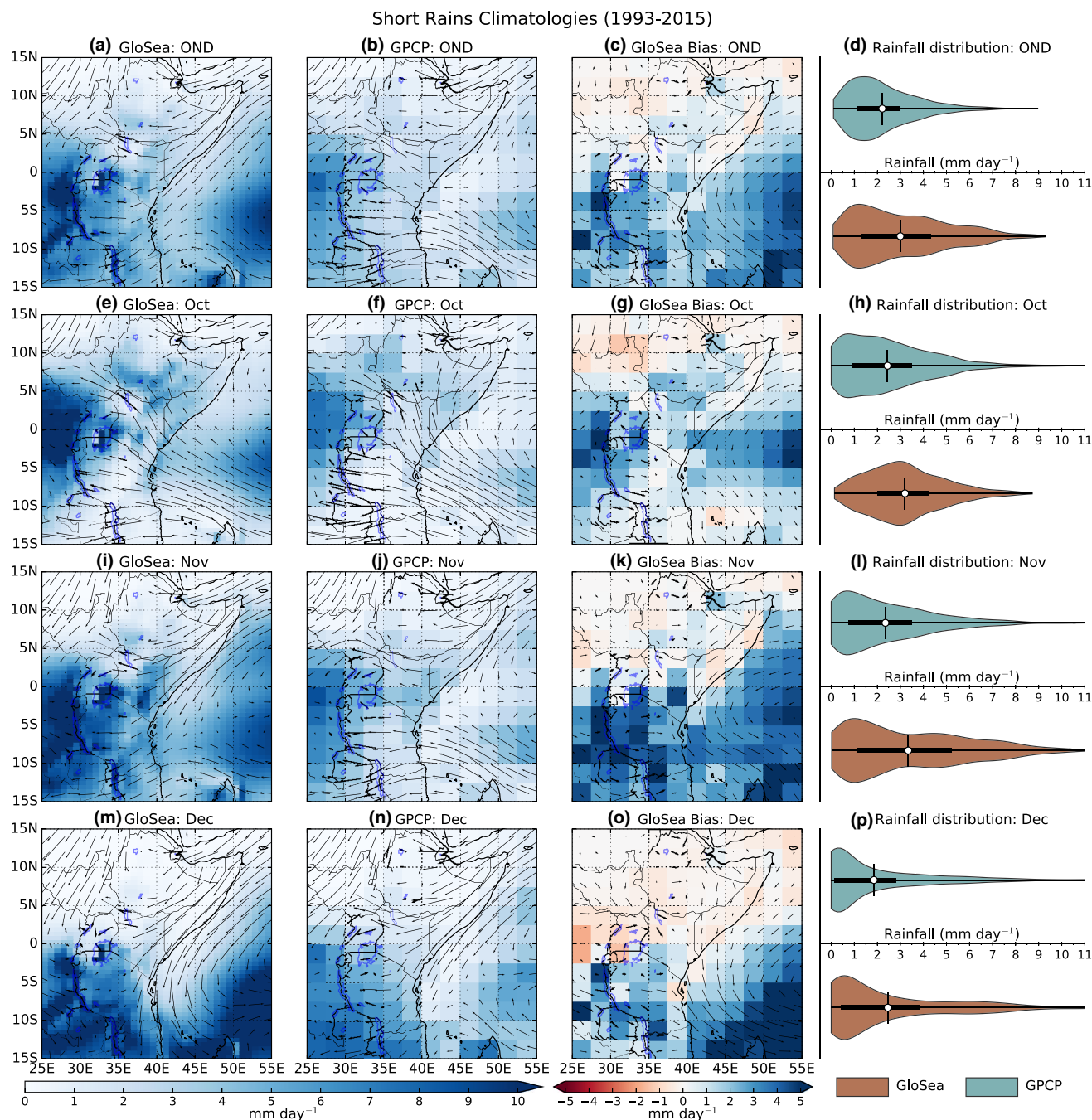
Fig. 2 East Africa rainfall (colours) and 850 hPa wind (vectors) climatology during the short rains for an ensemble mean of 36 members for GloSea (left), GPCP rainfall and ERA-Interim winds (second column), GloSea minus GPCP/ ERA-Interim (third column), and violin plots of rainfall distributions of GloSea and GPCP, with white dots representing the mean, the thick black line the interquartile range, and the shaded areas showing the distribution, for each land gridpoint within the region (12°N–10°S, 30°E–55°E), for each year (right). The rows show the climatologies for OND (**a–d**), then October (**e–h**), November (**i–l**), December (**m–p**), separately

2006). In a well calibrated forecast where each ensemble member represents a possible realization, the observations would be expected to appear as one of the extreme outer realisations in 2 out of 10 years (if treated as a 10th ensemble member then it would be expected to be the most wet 1 in 10 times, or most dry 1 in 10 times), so somewhere between

4 and 5 occurrences would be expected to happen over 23 years. This is considerably less than the 10 occurrences over the 23 years found here.

During the long rains, a correlation of 0.07 is achieved, this is insignificant at the 5% level and demonstrates that the model is unable to predict the long rains interannual
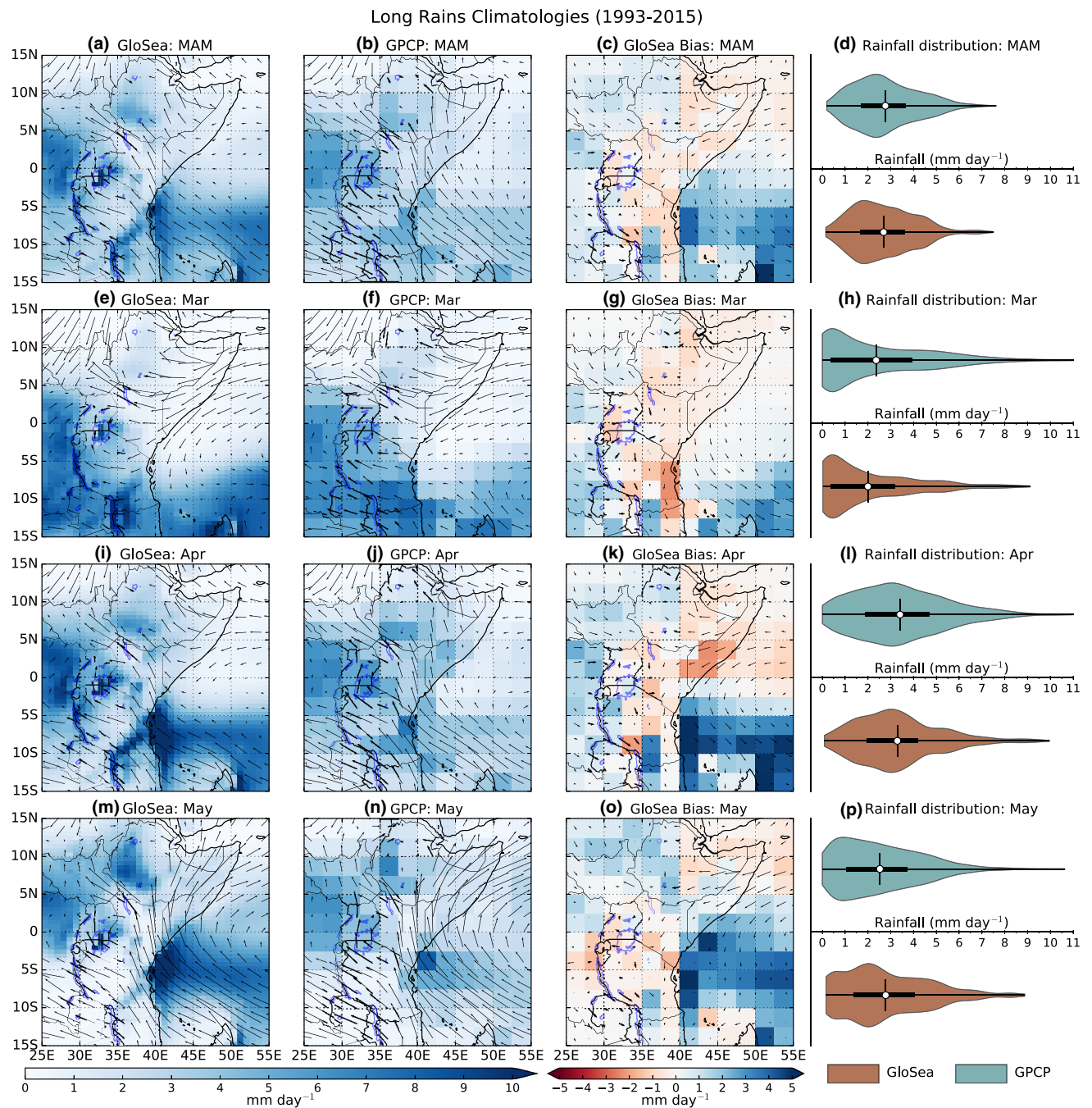
Long Rains Climatologies (1993-2015)

Fig. 3 As in Fig. 2, but for the long rains (MAM)

variability over land, consistent with previous results based on other models (e.g. Batté and Déqué 2011; Shukla et al. 2016). There is also an apparent failure of the model in capturing anomalies in the most extreme wet (e.g. 1996, 2013) and dry (e.g. 2000, 2009) years in this season. In all years the spread of the ensemble members exceeds the spread of the observations.

A common question within dynamical models is whether an increase in ensemble size could further improve the

forecast. To examine this, the correlation coefficient of the ensemble mean with the observations as a function of ensemble size is shown in Fig. 5. To create this, for each ensemble size, ensemble members are randomly sampled to build an ensemble of the correct size, then correlated with the observations. This is repeated 10,000 times, and the mean result is taken for each ensemble size. In the short rains the curves using both all 36 members available and the 12 member sub-samples demonstrate a curve approaching
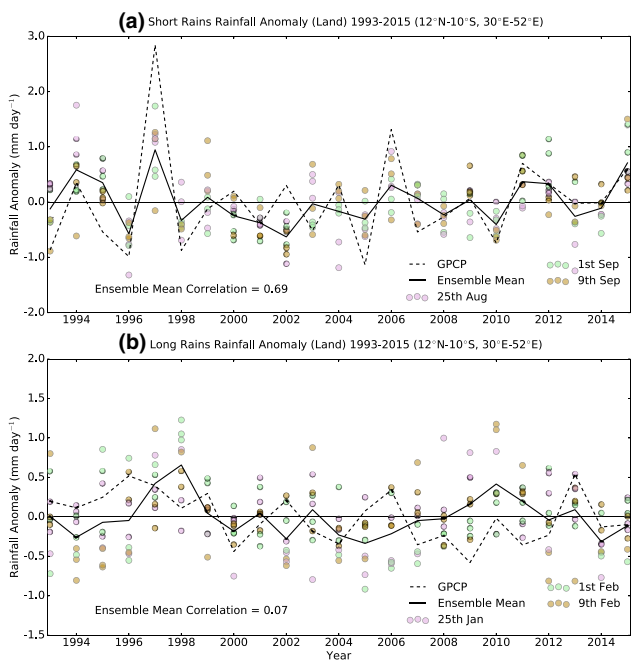
Fig. 4 Time series of rainfall anomaly from climatology for the short rains (**a**) and long rains (**b**), for 1 month lead time forecasts from Glo-Sea ensemble mean (solid line), ensemble members (dots, coloured by initialisation date), and GPCP (dashed line). Correlation coefficient between ensemble mean and GPCP shown at bottom of each panel
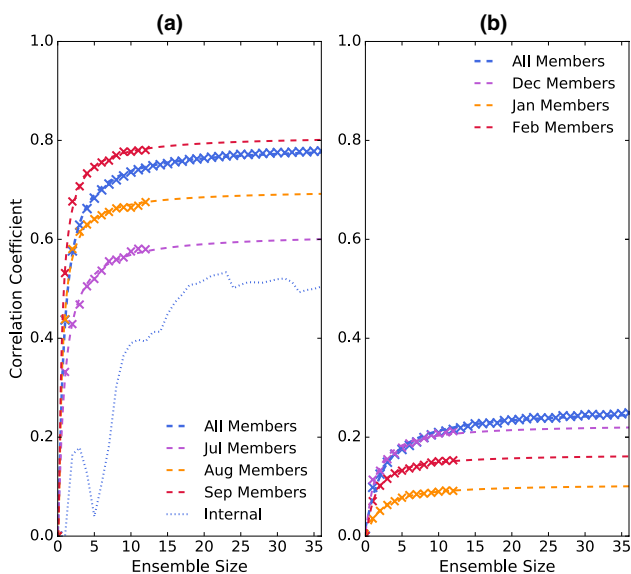

Fig. 5 Correlation skill of GloSea forecasts as a function of ensemble size for the short rains (**a**), and long rains (**b**), for randomised ensembles using all 36 members available (blue crosses) and each initialisation month consisting of 12 members (coloured crosses). Dashed lines show curve fitted to crosses of corresponding colour. Dotted line in **a** shows correlation of GloSea ensemble mean rainfall against a single removed ensemble member, demonstrating internal predictability

an asymptote, with the curves flattening between 10 and 15 ensemble members. The small increase from 12 to 36 members indicates that a further increase in ensemble size would provide limited additional benefit, given that the current operational forecasts use an ensemble size of 42. Also demonstrated here is a monotonic increase in skill with decreasing lead time. As well as studying potential improvements from increasing ensemble size, the potential skill; the ability of the model to predict itself (as in Kumar et al. 2014; Scaife et al. 2014), is also investigated. This is achieved by replacing the observations with a single member of the ensemble, and calculating the correlation between the ensemble mean of the rest of ensemble and the single member. This is repeated for each member in the ensemble, and the mean score is taken. It is also repeated for each ensemble size, leading to the dotted line in Fig. 5. The average correlation between a single member and the ensemble is shown to be consistently lower than the correlation between the ensemble and the observations, suggesting the model can better predict the observations than itself. This phenomenon has also been found elsewhere by Eade et al. (2014), and by Scaife and Smith (2018) who note its prevalence in the extratropical Atlantic, however this is one of few tropical examples of this behaviour as models generally overestimate the predictability of tropical rainfall.

The long rains similarly demonstrate the pattern that an increase in ensemble size would have limited benefits, although for the 36 member line there is an increase in skill with ensemble size. The asymptote value for an infinitely large ensemble in this case is 0.26. In the long rains, the correlation does not increase monotonically with decreasing lead time, as was observed in the short rains. This is likely due to the limited skill at any lead time.

3.2 Forecast skill in GloSea and GHACOF

In this section, a comparison is made between GloSea and GHACOF consensus forecasts. Both are regridded to $2.5° \times 2.5°$, and the period 1998–2015 is used. A discussion on this process and the limitations of the comparisons made in this section was given in Sects. 2.4 and 2.5. Figure 6 shows ROC curves and reliability diagrams for both forecasts during the short rains. Both forecasts demonstrate skill for the outer categories, with the above average rainfall category being highest. GloSea demonstrates some level of skill in predicting the middle category although lower than in the outer categories, as is often the case for categorical forecasts (van den Dool and Toth 1991), and generally achieves higher scores in all categories than GHACOF at one month lead. ROC scores of two month lead forecasts of GloSea were also calculated, finding values of 0.621 and 0.567 in the above and below normal categories respectively, remaining higher than the GHACOF forecast. In the GloSea

Fig. 6 Tercile category ROC curves (**a**, **b**) and reliability diagrams (**c**, **d**) for GloSea (left) and GHACOF (right), for the short rains. Upper tercile category shown in blue, lower tercile category in red, centre tercile category in black. ROC scores inset onto curves, labelled points on ROC curves correspond to threshold value used for each point. Dashed line in **a**, **b** refers to line of no ROC skill. Dashed line in **c**, **d** refers to line of zero Brier skill, horizontal dotted line shows line of no resolution, vertical dotted line represents climatological forecast. Points lying between climatological forecast and dashed line contribute positively to Brier skill score. Size of circles demonstrate relative frequency of occurrence of the probability being forecast
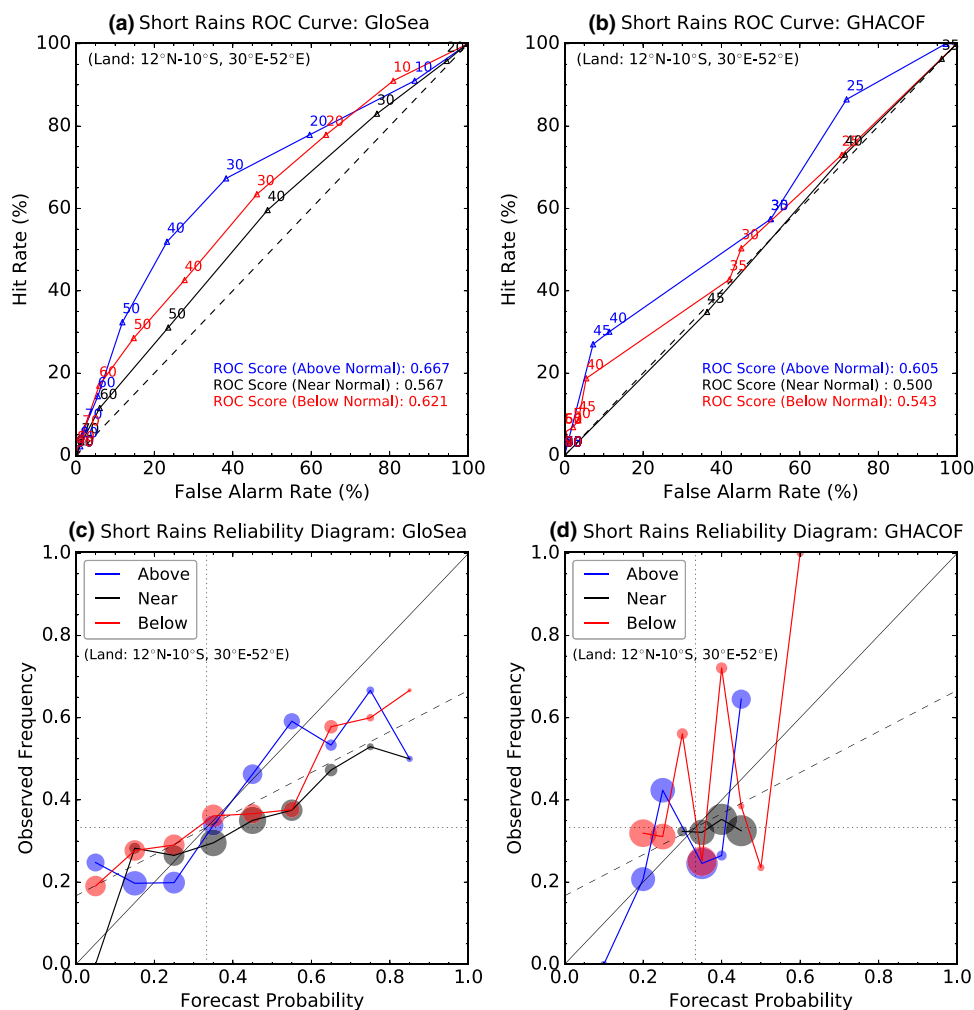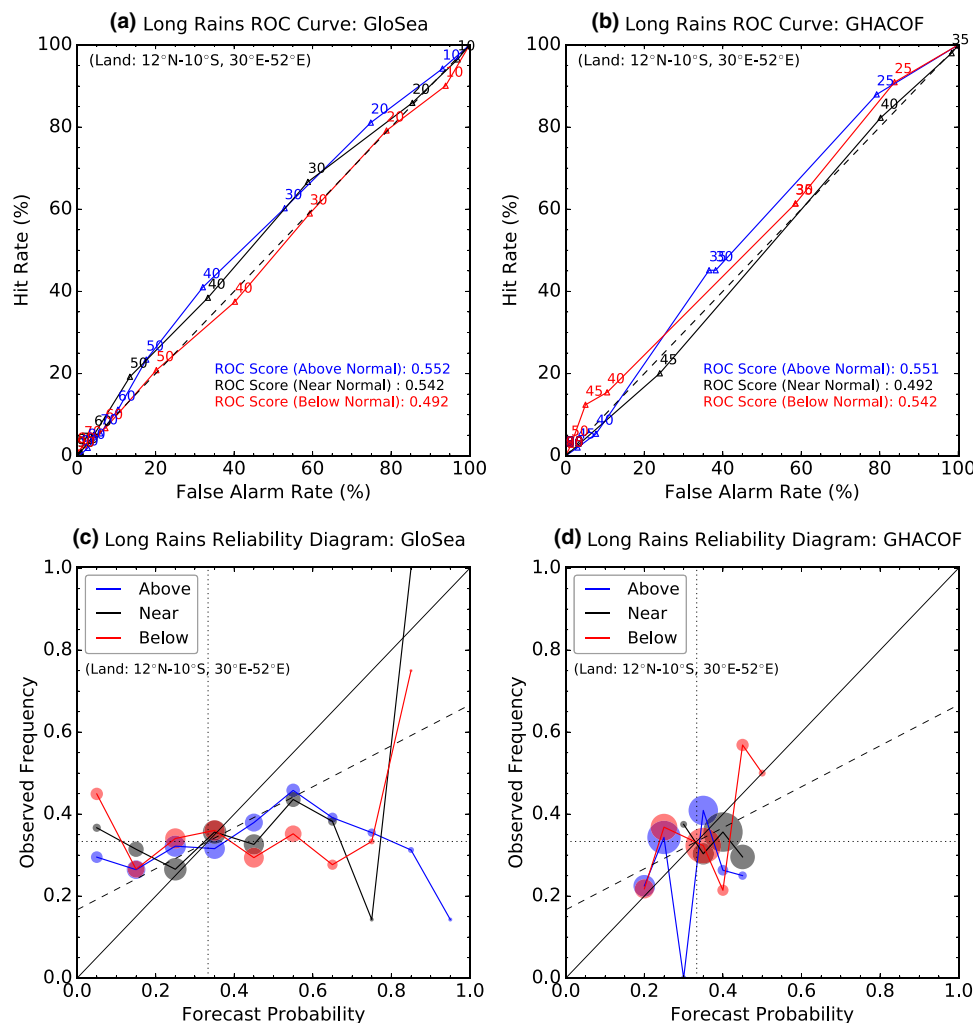

reliability diagam, there is clear evidence of forecast over-confidence in all three categories: a gradient less than 1. This means that for categories forecast with increased/decreased probability of occurrence with respect to climatology, the increase/decrease in probability is larger in magnitude than is observed. Meanwhile, the GHACOF reliability diagrams appear to show under-confidence in the outer categories, with a gradient greater than one, implying shifts in probability from climatology are on average too small.

Figure 7 shows the ROC curves and reliability diagrams for the long rains. Both GloSea and GHACOF display little skill during this season for any tercile, although ROC scores are generally greater than 0.5 by a marginal amount. The GloSea reliability diagram displays very little resolution for any category, the observed frequency being approximately the same regardless of the forecast probability. GHACOF appears to show slightly greater reliability for this season. Both of the reliability diagrams for GHACOF demonstrate a lack of forecasts landing within the 30% category. Forecasts of 30% for any category are rarely issued. This is related to the method of construction

of the probabilities. In general, 40% is often taken as the starting point for the probability of the near normal category, meaning that a probability of 30% for either outer category would then result in a forecast of equal probability for both outer categories. Situations in which forecasts for both outer categories are given equal probabilities are avoided, as they are seen by users as not being a useful forecast.

In Fig. 8, a spatial map of the ROC score for each category is shown for GloSea and GHACOF for the short rains. In the outer categories there is a coherent region of higher skill over Kenya, coastal Somalia, southeast Ethiopia and northeast Tanzania, as well as over the Indian Ocean. This region is apparent in both GloSea and GHACOF, and in both outer categories. These diagrams show highest skill in the regions where the heaviest rainfall is present. ROC scores for the long rains (Fig. 9) are lower than for the short rains for both GloSea and GHACOF for all categories, and less coherently distributed in GloSea. Kenya however appears to show some evidence of positive skill in the above tercile for GloSea, and both outer categories of GHACOF. The GloSea

Fig. 7 As in Fig. 6, but for the long rains

(a) Long Rains ROC Curve: GloSea

(b) Long Rains ROC Curve: GHACOF

(c) Long Rains Reliability Diagram: GloSea

(d) Long Rains Reliability Diagram: GHACOF

ROC maps demonstrate that positive skill is achieved over the Indian Ocean off the coast of East Africa in both outer categories.

Although it is not good practice to interpret the probability forecasts deterministically, it is still a widespread practice (Patt et al. 2007). To explore the performance of the forecasts interpreted in this way, the probabilistic forecasts were converted into deterministic categorical forecasts whereby the forecast is assigned as the category of the highest probability of occurrence. If an outer category and centre category are equal highest (for example a split of 40,40,20 for above, near, below categories respectively), then the higher outer category is assigned. If both outer categories are equal highest then the forecast is not included in this evaluation, this removes climatological forecasts, and bimodal forecasts. Table 1 presents a contingency table evaluation of deterministic forecasts generated in this way for both GloSea and GHACOF, and for both the long and short rains. The most striking difference between the GHACOF and GloSea forecasts are the large number of forecasts in which GHACOF

has the highest weighting assigned to the normal category, with 81% of forecasts being made for this category for the long rains, and 71% of forecasts being made for this category in the short rains. This is something common to the West African RCOF (Bliefernicht et al. 2018), and RCOFs elsewhere in Africa (Mason and Chidzambwa 2008). It is clear from the middle row of Table 1 that within GHACOF, as often occurs in categorical forecasts (van den Dool and Toth 1991), there is very low skill in forecasting this category: when the near normal category is forecast, observations are spread approximately equally across the three categories. The number of correct forecasts within this category falls at approximately one third (34% for both MAM and OND). GloSea has similarly equal spread across this category, although has a lower number of forecasts falling into it. Approximately 35% of near normal forecasts are correct for MAM, 40% for OND, and a total of 30% of forecasts are issued into the near normal category for MAM, and 38% for OND. This high level of hedging in GHACOF drastically lowers the hit rates for the outer tercile categories, as seen

Fig. 8 Maps of ROC score for GloSea (left) and GHACOF (right) for tercile categories of rainfall, upper tercile category (**a**, **b**), centre tercile category (**c**, **d**), lower tercile category (**e**, **f**), for the short rains
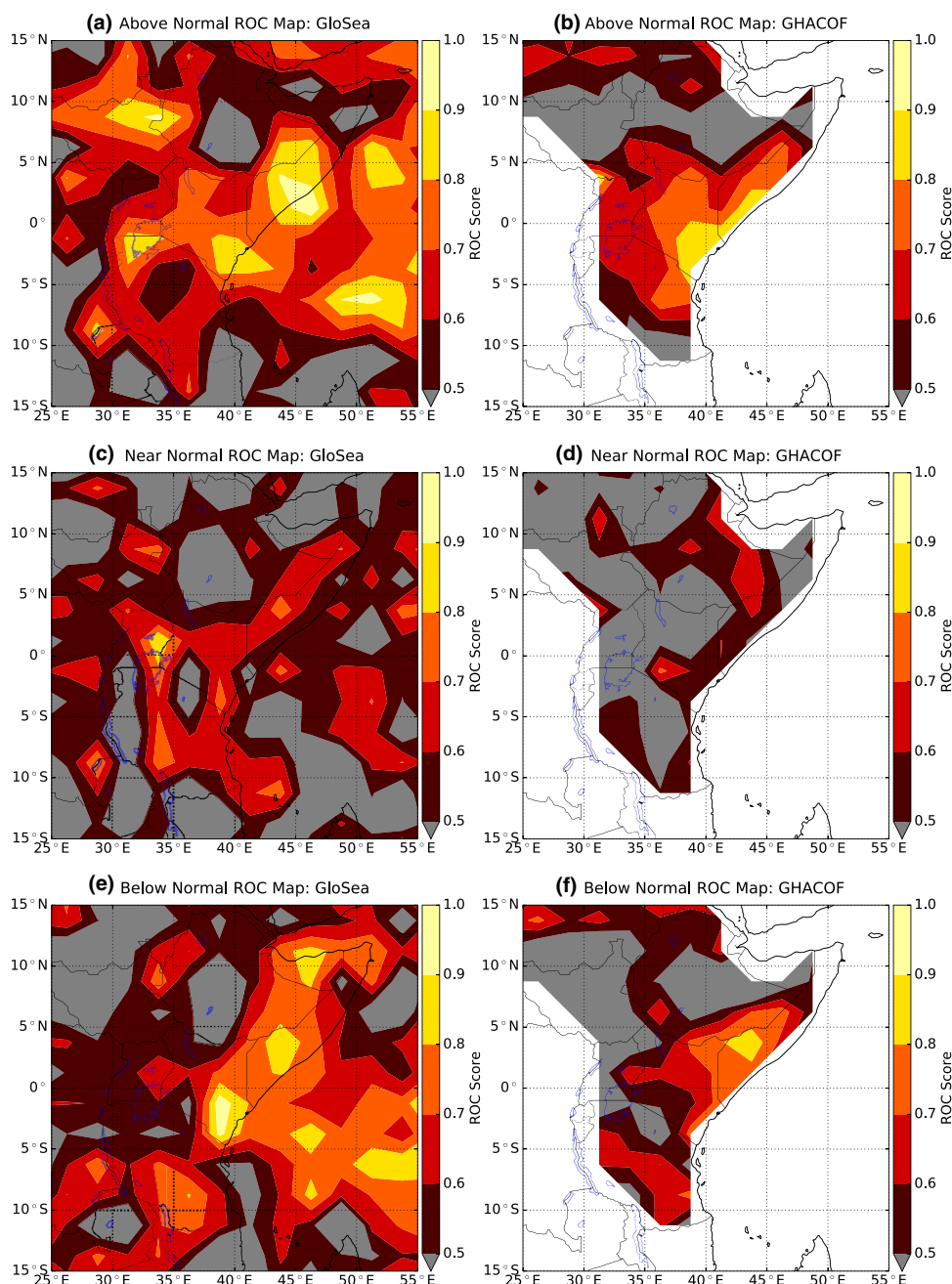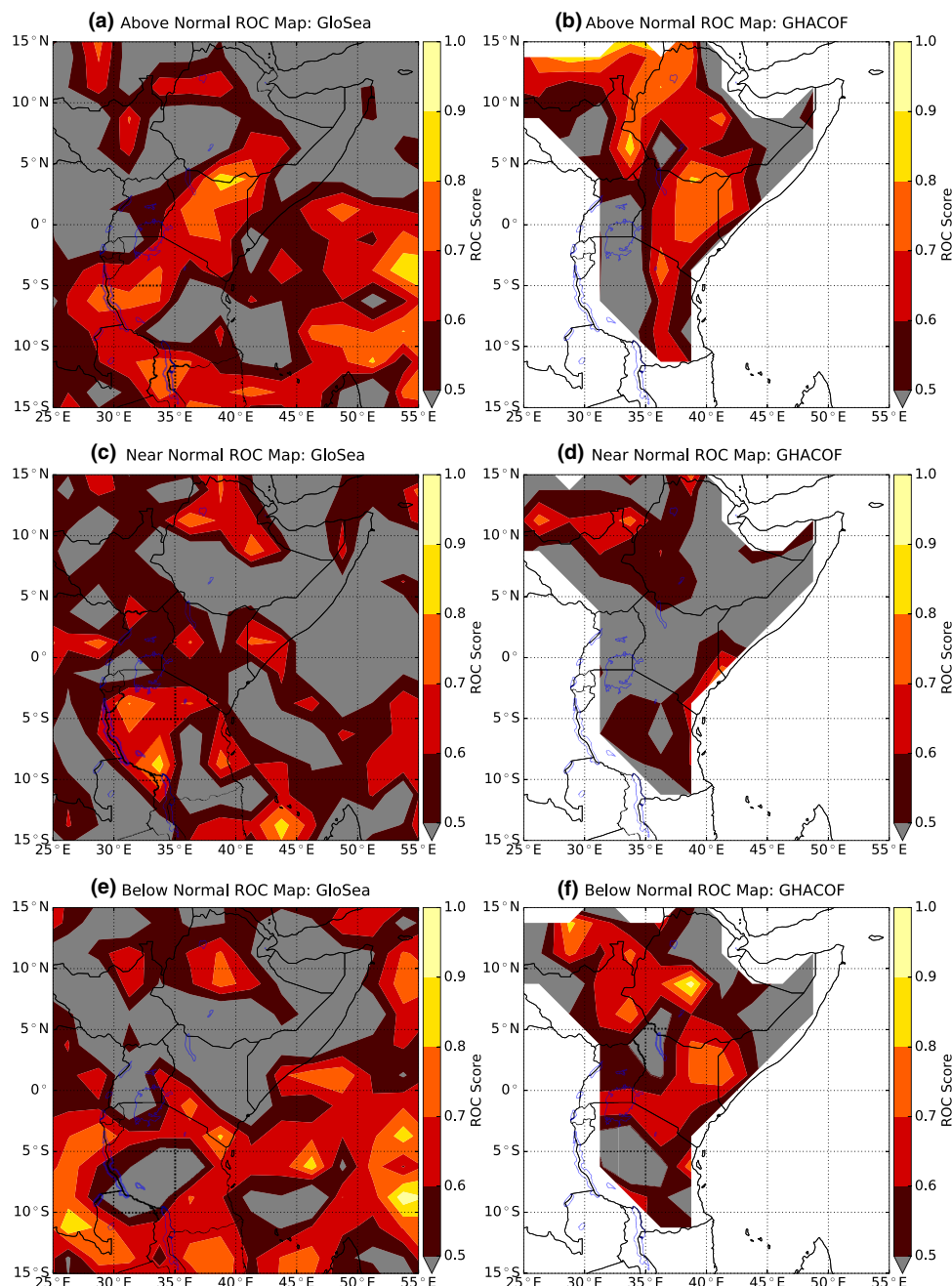

in Table 2, and thus the usefulness of the forecasts, and was identified by Mason and Chidzambwa (2008) as one of the key issues within RCOF forecasts.

Some favourable conclusions for GHACOF can however be drawn from this table. Table 2 shows that for all categories except for the above normal category in MAM, GHACOF has a higher hit rate than false alarm rate, a signal that there is positive skill coming from these forecasts. By looking at the Heidke Skill Score (HSS) for the forecasts, positive values are achieved in both seasons by both forecasts, however GloSea shows marginally higher scores in each season. It is likely that the GHACOF forecast has lower

scores in this measure due to the large number of forecasts that contained highest weighting into the centre category, which could have had higher weighting towards the correct outer category than incorrect, but is instead interpreted as a forecast for the near normal category. It is again clear from Table 2, the difference in skill for forecasting between the two seasons, with higher HSS and generally greater differences between the hit rates and false alarm rates in each category for the short rains than for the long rains.

By considering within GHACOF, the forecasts of the outer categories, it is clear from Table 1 that the forecasts are in fact capable of identifying years in which an above or

Fig. 9 As in Fig. 8, but for the long rains

(a) Above Normal ROC Map: GloSea

(b) Above Normal ROC Map: GHACOF

(c) Near Normal ROC Map: GloSea

(d) Near Normal ROC Map: GHACOF

(e) Below Normal ROC Map: GloSea

(f) Below Normal ROC Map: GHACOF

below average year is most likely, with many more forecasts for the correct outer category than incorrect outer category, with the exception of above normal forecasts of the long rains. These forecasts then have a property which, when considering the relative risks of an incorrect forecast compared to the return for a correct forecast, may be considered highly desirable; a low rate of forecasts with two category errors, much lower than is seen in GloSea.

Combining both GloSea and GHACOF also appears to display some complementary information. Whilst GloSea generally performs better over the previously displayed statistical measures, it appears that GloSea shows a lack of skill

in predicting below average rainfall in the long rains, whilst GHACOF performs best in this category, with a higher ROC score (Fig. 7), and positive scores from the contingency table (Table 2), with this skill appearing to originate from over Kenya (Fig. 9). This is possibly due to alternative sources of predictability utilised by the forecasters that are not currently represented in GloSea, but could be related to other factors. For example the higher skill in both forecasts observed over Kenya could be related to higher observed data quality in this region. This could be due to, for example, the less complex orography over the coastal area, as satellite estimates

Table 1 3×3 contingency table for GHACOF (top) and GloSea (bottom) for the long rains (left) and short rains (right), for tercile probability categories, A: above normal, N: near normal, B: below normal

MAM Forecast	Observed			OND Forecast	Observed		
	A	N	B		A	N	B
GHACOF				GHACOF			
A	16	22	24	A	91	56	20
N	251	246	228	N	197	220	227
B	32	31	46	B	8	25	57
GloSea				GloSea			
A	119	75	104	A	145	69	63
N	76	94	92	N	93	135	113
B	98	127	106	B	62	99	126

Table 2 Hit rates (HR), false alarm rates (FAR) separated by forecast category, and Heidke Skill Score (HSS) for both forecasts and both seasons

Season	Forecast	HR	FAR	HSS
OND	GHACOF			
	Above	0.31	0.13	
	Near	0.73	0.71	0.11
	Below	0.19	0.06	
	GloSea			
	Above	0.48	0.22	
	Near	0.45	0.34	0.17
	Below	0.42	0.27	
MAM	GHACOF			
	Above	0.05	0.08	
	Near	0.82	0.80	0.02
	Below	0.15	0.11	
	GloSea			
	Above	0.41	0.30	
	Near	0.32	0.28	0.04
	Below	0.35	0.38	

often struggle to estimate correctly rainfall rates over steeper orography (e.g. Cattani et al. 2016; Kimani et al. 2017).

3.3 Drivers of interannual rainfall variability in the short rains

Many previous studies have shown the relationship between the East African short rains and SST anomalies in the equatorial Pacific, and more recently, Indian Ocean, as discussed in Sect. 1, in particular highlighting the importance of the El Niño-Southern Oscillation and Indian Ocean Dipole. For a model of the short rains to be successful it needs to predict correctly both the evolution of these modes of variability in the oceans, and also produce the correct atmospheric response to the predicted SST anomalies. Figure 10 shows the correlations of rainfall over East Africa within each grid point to the Niño 3.4 and IOD indices for GloSea

and for observations. The spatial patterns of both indices correlations are well represented by GloSea; the model correctly represents the effect of these modes of variability on the rainfall, however some differences are noted. There is a sharp decrease in correlation running north to south through Kenya in the model in both indices, suggesting a sharp change in rainfall interannual variability here. This is not present in the observations (although some gradient does exist in the IOD map) and hints at a misplaced teleconnection, too far east in the model, as well as some possible incorrect orographic effects taking place in the model, as this north to south decrease runs down the eastern edge of the East African highlands. The region with the highest correlation to IOD in the model coincides with the region of highest skill.

Figure 11 shows the correlation of SST anomalies at each grid point with the East African short rains, in the

Fig. 10 Correlation of rainfall over East Africa during the short rains with Niño 3.4 (left), and IOD (right) over East Africa for GloSea mean correlation over individual members (**a**, **b**), and GPCP/ HadISST (**c**, **d**). Grey line shows 1000 m contour
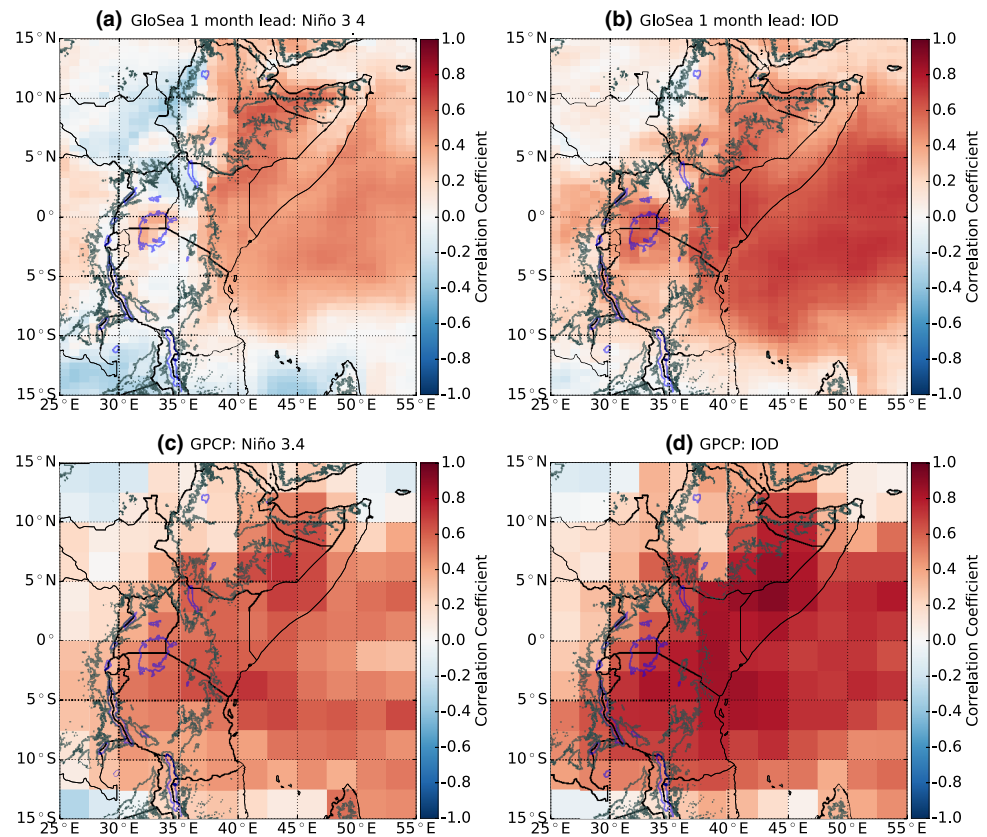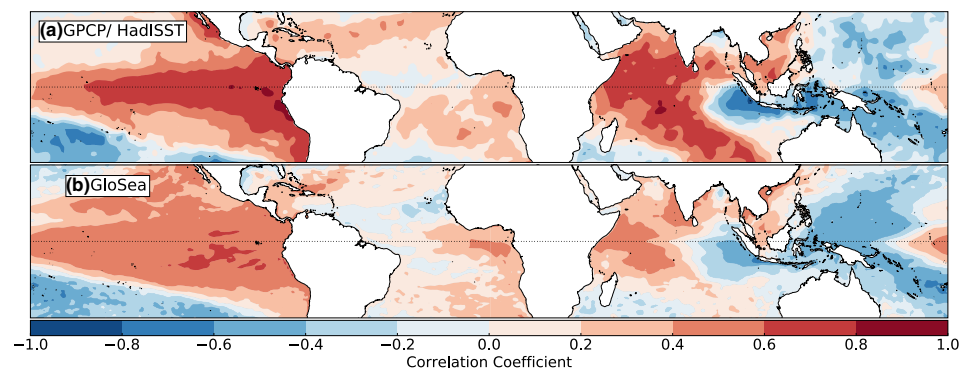

Fig. 11 Correlation of SST anomalies with East African short rains land based points within (12°N–10°S, 30°E–55°E), for GPCP/ HadISST (**a**) and GloSea mean correlation over individual members (**b**)

observations and in GloSea. In both panels the large scale pattern is clear, with the strongest, coherent correlations coming from the Pacific and Indian Oceans, representing the El Niño and IOD modes of variability. The correlations within GloSea are of a smaller magnitude than within the observations, suggesting that the coupling between the ocean and atmosphere may be too weak in the model. The positive correlation in the Pacific Ocean also stretches too far west, as does the negative correlation over the eastern Indian Ocean, matching with the rainfall response to ENSO noted by MacLachlan et al. (2015) within GloSea in December to February.

As well as capturing the correct teleconnections, the model also needs to capture the evolution of SSTs to be useful as a forecast model. To examine whether the model captures the evolution of SSTs, SST indices within the Indian and Pacific Oceans over OND were forecast with 1 month lead time. These were then compared with observations, and a 1 month persistence forecast was used as a reference forecast. This was done as high correlation scores are likely to occur even if the model doesn't correctly model the evolution of the SSTs, due to the slowly evolving nature of SSTs. If the forecast can beat the correlation of the persistence forecast this implies that some useful information can be obtained from the forecast. The persistence forecast uses
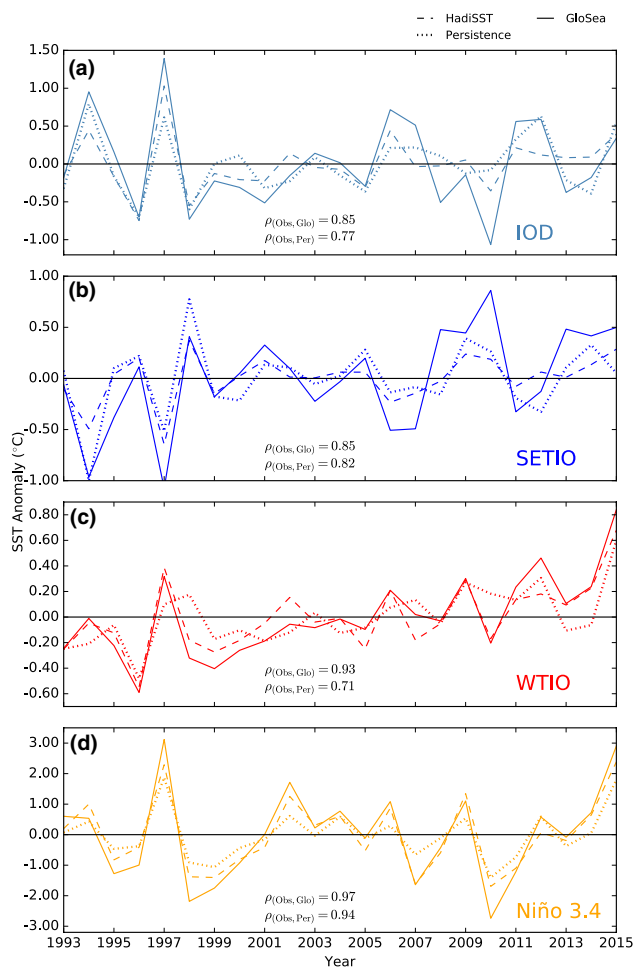
Fig. 12 Time series of OND values of SST indices; **a** IOD, **b** SETIO, **c** WTIO, **d** Niño 3.4. Solid lines show GloSea SST forecast anomalies, dotted line shows persisted SST anomalies from August, dashed lines show observed SST anomalies

the average SST anomalies over the entire month of August, whilst the forecast is that which would be used for the 1st September, for a direct comparison. These were then compared with the observed SST anomaly over OND, as shown in Fig. 12. GloSea consistently outperformed the persistence forecast in all indices, with the most promising results being over the western Indian Ocean (WTIO) where GloSea had a correlation of 0.93 with the observations, whilst the persistence forecast had a value 0.71. GloSea also captured well the observed warming trend in the ocean in this region. This improvement over a persistence forecast also meant a notably better forecast IOD than persistence, with a correlation score for GloSea of 0.85, whilst persistence achieved 0.77. The eastern Indian Ocean and Niño 3.4 region both showed marginal improvements in comparison to persistence. Whilst there is already improved prediction compared to persistence at 1 month lead time, at longer lead times, better performance of the dynamical model against persistence

is expected for the Niño 3.4 region (Graham et al. 2012). For IOD it is less clear whether this is the case, as Graham et al. (2012) found that the previous version, GloSea4, was outperformed by persistence at forecasting IOD at both short and longer lead times.

A common feature of all the SST indices within GloSea was a variance larger than the observations, as can be seen in Fig. 12. This is in contrast to lower than observed variability in rainfall, and further suggests that the coupling between SSTs and the short rains is too weak. This large variance was particularly noticeable in the SETIO index, where the standard deviation was more than double that of the observed. This region also achieved the lowest correlation score in GloSea (equal with the IOD, which is itself dependent on the SETIO forecast). Difficulty in forecasting SST evolution in this region has been highlighted previously by Lu et al. (2018).

As well as correctly predicting rainfall, GloSea has shown that it potentially can hold value over a purely statistical forecast of rainfall by skilful prediction of the evolution of SST anomalies in the Pacific and Indian Ocean. To confirm this, multiple linear regression models were built using indices from the Pacific and Indian Ocean. A regression model was built using observed SST indices over OND to predict OND rainfall within the observations. The regression value achieved by the model utilising IOD and Niño 3.4 was 0.90, and demonstrates the dominance that these two modes of variability have over the region, during this period. Bahaga et al. (2019) demonstrated however that the correlation between these modes can fluctuate on decadal timescales, with the period used here found to have a particularly high correlation.

Building a regression model from the persisted values of IOD and Niño 3.4 achieved a regression value of 0.77. This value is actually larger than the rainfall forecast from GloSea (at 0.69), and although the difference is not significant, demonstrates the strength of a statistical forecast in this region.

Since the persistence model value is lower than the regression model using the observed SSTs, correct predictions of SST evolution may give an improvement on the persistence model. To test this, a regression model was then built using GloSea forecast SST indices of IOD and Niño 3.4 for OND. This model achieved a regression value of 0.80, bettering the persistence forecast, although again the difference is not significant at this short lead time. The fact that the observed SST regression model achieved the same score regardless of whether the Niño 3.4 index was included, whilst in the persistence model it improved the model, leads to the hypothesis that the high correlation observed between El Niño and East African rainfall is primarily through modulation of the Indian Ocean, rather than independent influence, similar to the
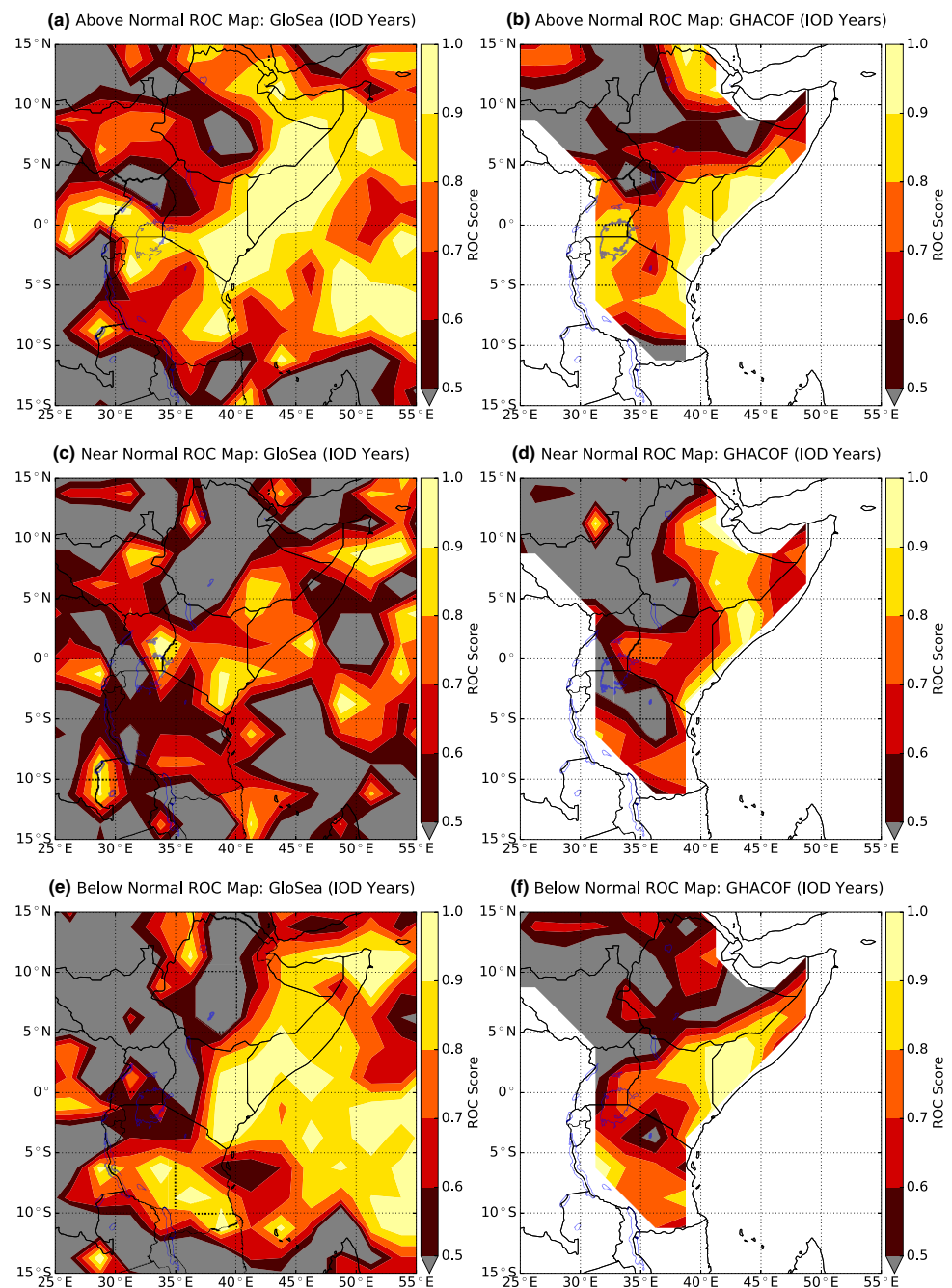
conclusions of Behera et al. (2005), Bahaga et al. (2015). To examine whether this is the case, the partial correlation of two variables (subscript 1, 2) with the influence of a third variable (subscript 3) removed (Yule 1907; Lawrence 1976), is calculated, defined as:

$$\rho_{12,3} = \frac{\rho_{12} - \rho_{13}\rho_{23}}{\sqrt{(1 - \rho_{13}^2)(1 - \rho_{23}^2)}} \tag{3}$$

where ρ_{ij} refers to the Pearson correlation coefficient of variables i and j. This value runs from -1 to 1 as in the

Pearson correlation coefficient. In particular the partial correlation of East African rainfall with the IOD with the influence of ENSO removed, $\rho_{ri,n}$, and the partial correlation of East African rainfall with ENSO with the influence of IOD removed, $\rho_{rn,i}$, are calculated, where the r, n, and i subscripts refer to the time series of East African rainfall, Niño 3.4, and IOD respectively. In the observations, a value of $\rho_{ri,n} = 0.82$ is found, suggesting that when the effect of ENSO is excluded, the IOD still maintains a strong relation to East African rainfall. Meanwhile a value of $\rho_{rn,i} = 0.02$ was found in the observations, suggesting that when the

Fig. 13 As in Fig. 8, but for years with a GloSea forecast active Indian Ocean Dipole event. Positive IOD years were identified as 1994, 1997, 2006, 2007, 2011, 2012. Negative IOD years were identified as 1996, 1998, 2001, 2008, 2010

effect of the IOD is excluded, ENSO has very little effect on East African rainfall, supporting the hypothesis above, also suggested by Behera et al. (2005), Bahaga et al. (2015). By performing the same calculations for GloSea's forecast SST indices against rainfall, we find values of 0.83 and − 0.06 for $\rho_{ri,n}$ and $\rho_{rn,i}$ respectively, suggesting GloSea does very well at capturing the relationship between the IOD, ENSO, and East African rainfall. From this, it could be suggested that when an ENSO event is forecast, if anomalies in the Indian Ocean remain small, then a response in East African rainfall should not necessarily be expected.

Given the strength of connection between SST anomalies and the short rains, and the ability of GloSea at predicting SST evolution, it should be expected that during years where an IOD or ENSO event is forecast, the capability of the model should increase (Frías et al. 2010; Pegion and Kumar 2013). To test this, both GloSea, and GHACOF forecasts were re-evaluated conditional on years where an IOD event (defined by an anomaly greater than 0.5°C) is forecast by the model. The model forecast IOD years are used rather than observed to demonstrate the skill based on making decisions using forecast SSTs. Figure 13 shows tercile category ROC maps (as in Fig. 8) for years where GloSea has forecast an IOD event, for both GloSea and GHACOF. In both forecasts the increase in skill is clear, with both having regions along coastal East Africa above 0.8 or 0.9, with this region coinciding well with the regions of highest skill and highest correlation with IOD shown in Figs. 8 and 10. Figure 14 shows the corresponding ROC curves, and reliability diagrams for this set of forecasts. Both GloSea and GHACOF show an increased ROC score, with the above normal category scoring highest in both. GloSea again generally outperforms GHACOF in this score.

The reliability diagram for GloSea demonstrates that during these years the forecast is highly reliable, with the outer categories lying consistently close to the perfect reliability line. Some evidence of under-forecasting is present in the below normal category, with the observed frequency consistently higher than the forecast probability. There is also a hint of under-confidence in the above normal category, with a gradient greater than 1 apparent for this line. During these years the centre tercile category appears to be over-forecast.

Fig. 14 As in Fig. 6, but for years with a GloSea forecast active Indian Ocean Dipole event. Positive IOD years were identified as 1994, 1997, 2006, 2007, 2011, 2012. Negative IOD years were identified as 1996, 1998, 2001, 2008, 2010
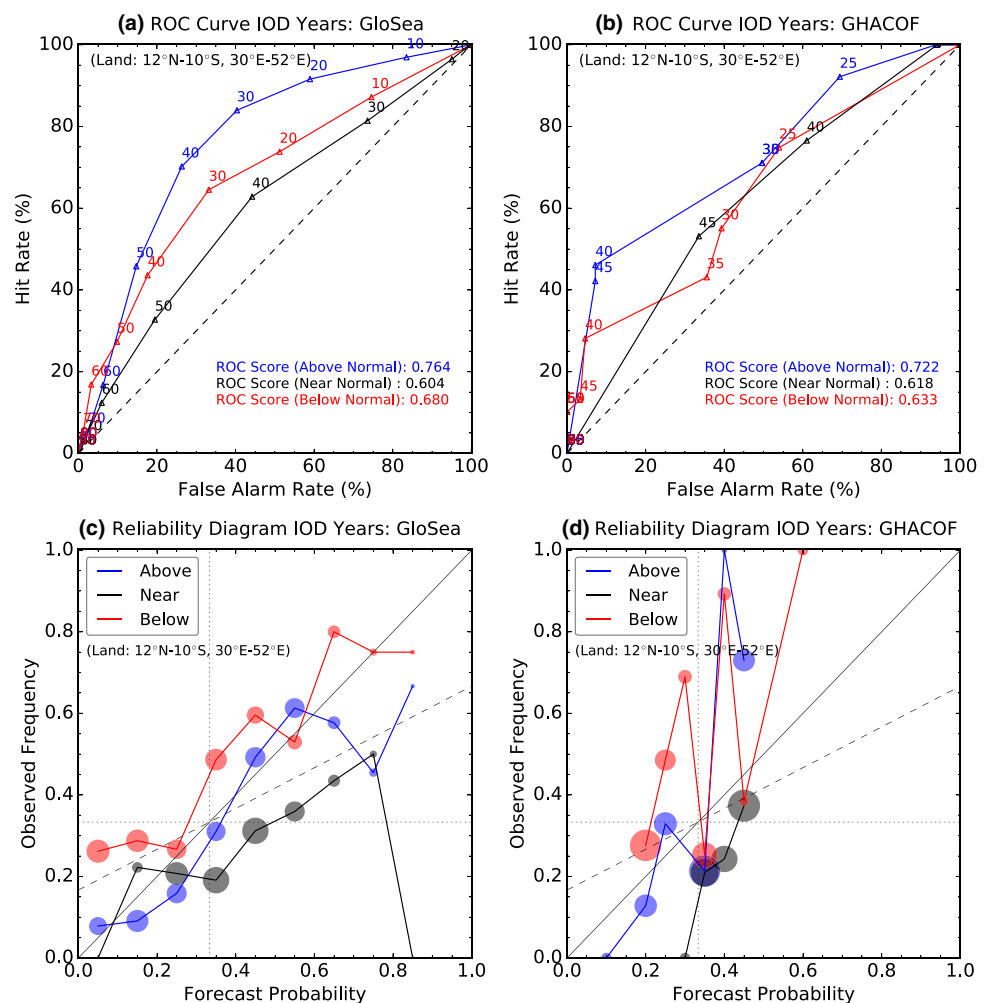
The reliability diagram for GHACOF, although noisy, demonstrates the under-confidence of forecasts during these years in the outer terciles, with a gradient greater than one apparent. This is more evident within the above average category. The below average category demonstrates both some under-confidence, and some under-forecasting, below average years have occurred with greater probability than were forecast.

Similar results were found for years with an active ENSO event (not shown), however, in many of the years where IOD is active, ENSO was also found to be active. Years where SST anomalies in both the Niño 3.4 and the IOD index were small were also investigated. GloSea demonstrated positive skill in the outer categories in these neutral years, with a ROC score for the above (below) normal category being 0.61 (0.54). GHACOF meanwhile shows less skill in the years where neutral conditions are forecast, with ROC score for the above (below) normal category being 0.52 (0.48).

3.4 Drivers of GloSea rainfall bias in the short rains

The large wet bias in GloSea over East Africa during the short rains was highlighted in Fig. 2. Whilst it is known that coupled dynamical models regularly have too much rainfall in the tropics (Li and Xie 2014; Scaife et al. 2018), this wet bias is large in size when compared to the rest of the tropics within GloSea. Although it is clear that GloSea achieves high levels of skill despite this bias, understanding the origin of this bias may be important for explaining the lack of variability in the model, and for future improvements to forecasts for this region. To understand this, the bias evolution over time was studied over a stationary period of time (the 3 months of OND) for different forecast lead times. Figure 15a shows the evolution of the rainfall bias over East Africa as a function of lead time. At all lead times there is a wet bias. There is an approximately linear increasing trend in the wet bias as lead time increases; a model drift. To understand what may be causing this, the bias as a function of lead time was plotted for several other fields. Figure 15b shows the bias-lead time relation for the SST indices over the Pacific and Indian Oceans. A cold bias is present in both the Pacific and Indian Ocean; these biases remain approximately constant in the Pacific and western Indian Ocean, however the SETIO index displays a linear decrease in temperature with increasing lead time, this region was also highlighted as the most difficult to forecast in the previous section, as well as having an unrealistically large variance within GloSea [also seen in Lu et al. (2018)]. This increasing cold bias has an impact on the sea level pressure over the eastern Indian Ocean region, seen in Fig. 15c. The bias in pressure over the western Indian Ocean remains approximately constant, whilst the pressure over the eastern Indian Ocean increases
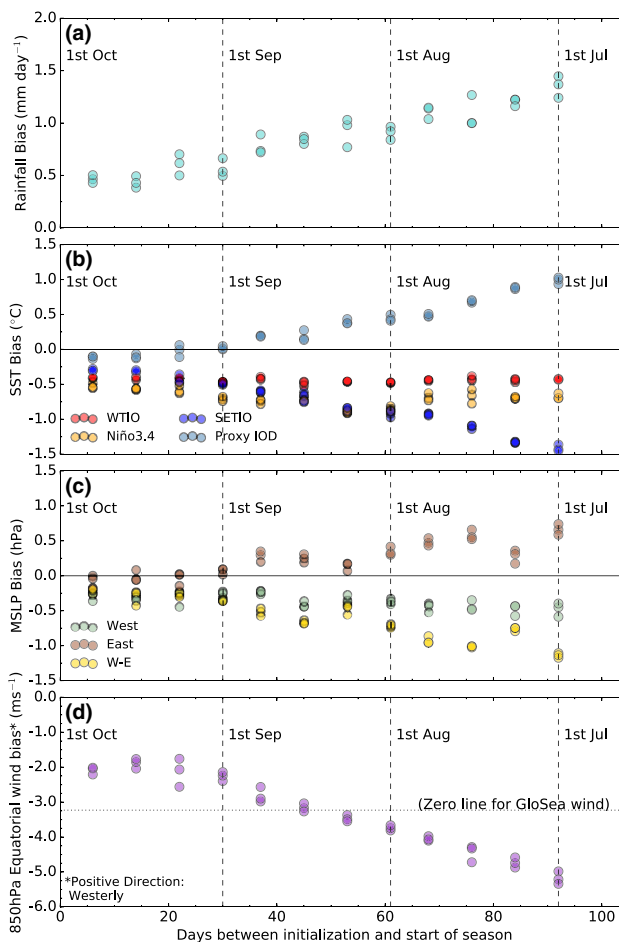

Fig. 15 GloSea lead time-bias relations over short rains season forecasts for **a** rainfall (against GPCP), **b** SST indices (against HadISST), **c** sea level pressure (against NCEP-NCAR Reanalysis), **d** 850 hPa equatorial zonal wind over Indian Ocean (against ERA-Interim Reanalysis). Dots on same day show ensemble members initialised at the same lead time. Vertical dashed lines mark the 1st September, August, July. Proxy IOD shows the index for model minus observations in the mean state. Mean sea level pressure west and east refer to same co-ordinates as west and east poles of IOD, whilst west minus east shows relative pressure gradient compared to observed. Zonal winds averaged over (5°N–5°S, 60°E–90°E). Dotted line on bottom panel shows point at which zonal average wind in box is zero

with increasing lead time, consistent with the cooler SSTs at longer lead times, generating a west to east pressure gradient.

Figure 15d shows the equatorial zonal wind bias over the Indian Ocean (5°N–5°S, 60°E–90°E) as a function of lead time. At all lead times there is an easterly wind bias of these zonal winds. Matching with the pressure biases, the zonal winds become more easterly (more negative in Fig. 15d) with increasing lead times, with the average wind direction within the model switching from the observed westerlies to become easterly between 40 and 50 days lead time. This wind anomaly is likely to draw more moisture

toward the African continent from the Indian Ocean, as well as having an effect on the Indian Ocean Walker circulation, reproducing a positive IOD-like response within the mean state. This is likely to reduce the impact of further increases in these winds in providing moisture. Whilst this is not necessarily the case for GloSea, it could explain part of the weakened coupling between the Indian Ocean and the short rains, as well as the lack of variability in rainfall with respect to the observations.

Capturing the direction of these winds is known to be difficult for coupled models, with Hirons and Turner (2018) recently showing that the majority of CMIP5 models incorrectly capture the mean state of these winds, and the models with incorrect easterly zonal winds in the mean state struggle to capture correctly the influence of the IOD on rainfall in the short rains.

4 Conclusions

Skilful seasonal forecasts of rainfall are vitally important for many sectors in East Africa. In this study, the most widely issued operational seasonal forecast within the region, the GHACOF consensus forecast, has been evaluated against observations and compared to the UK Met Office dynamical seasonal forecast system, GloSea. In addition, physical rainfall-producing processes within the dynamical model related to the short rains season were investigated and an analysis of the origin of the model's regional wet bias was performed.

The ability of Met Office GloSea system operational hindcasts were evaluated on their ability to predict seasonal rainfall anomalies over East Africa at 1 month lead time before the start of the two rainy seasons. GloSea demonstrates an ability to represent the climatology of the rainfall seasons well, but with a large wet bias of approximately 40% during the short rains, and a lack of interannual variability. GloSea performs much better at predicting interannual variability during the short rains than the long rains due to its ability to capture teleconnections between SST anomalies and rainfall in the short rains season, as documented by Batté and Déqué (2011), Shukla et al. (2016), Nicholson (2017). However, GloSea's short rains forecasts can be outperformed by a statistical forecast using persisted SST anomalies from August. A similar statistical model based on GloSea's SST forecasts can, however, outperform both GloSea's own rainfall prediction and the aforementioned statistical forecast using persistence. The ability to better predict rainfall using GloSea's SST field suggests that further improvements to predictions of the short rains could be made by improving the atmospheric response to the ocean state.

GloSea displayed little ability in forecasting rainfall during the long rains, with a correlation between GloSea and GPCP of 0.07, a result common to previous dynamical seasonal forecast models in this season (e.g. Batté and Déqué 2011; Shukla et al. 2016) with the potential for increases to approximately 0.25 in a larger ensemble than the ensemble of 9 members used. In both seasons it was demonstrated that an increase in ensemble size above the current operational size of 42 members would provide limited benefits, although could offer relatively larger improvements to the long rains than the short rains.

Probabilistic verification was performed on both GloSea and the GHACOF consensus forecasts. Both GloSea and GHACOF displayed positive skill in forecasting outer tercile categories of rainfall over East Africa, and promisingly, both demonstrated similar spatial patterns of skill, with a coherent region of high skill coinciding with the area most highly correlated with Indian Ocean SST anomalies during the short rains. However, in general GHACOF was outperformed by GloSea over the two seasons, with the exception of the below normal category within the long rains. The predictability here could be related to GHACOF utilising information not represented within dynamical models, and demonstrates the value of using both statistical and dynamical modelling techniques (Doblas-Reyes et al. 2013), as is done within the GHACOF forecasts.

Despite the positive skill, GHACOF demonstrated several features that are potentially harmful to the usefulness of the forecast. The stand out error is the tendency to over-forecast the near normal category of rainfall, common to RCOFs in other regions (Mason and Chidzambwa 2008; Bliefernicht et al. 2018). GHACOF regularly issue a probability of over 40% in the near normal category, and this category is issued as the highest probability category at over 70% of the forecast grid points over both seasons. Not only is it demonstrated that forecasting this category is less skilful than forecasting for the outer categories, but this tendency also undermines the use of tercile categories, as, over the period of the forecasts, the three tercile categories have not been forecast to occur equally often. This could confuse interpretation of the forecasts by user groups, who have regularly noted difficulties in understanding probabilistic forecasts. This lack of confidence also lowers the statistical resolution of the forecasts; forecasts predicting the most wet and most dry events often appear remarkably similar, with the probabilities in the outer categories often only shifting by 5 or 10%.

Another common behaviour was the tendency to avoid forecasting 30% probability, this is due to the method with which probabilities are assigned. In general a probability of 40% is used as an initial value for the near normal category, the 30% forecast is then avoided so as to ensure issuing a forecast with different probabilities for above and below normal years. In some cases however, a forecast for 30% may indeed be most appropriate. These tendencies identified

within the GHACOF forecast process are performed within a risk averse strategy, and this is reflected in the low number of times where the opposite outer category was forecast as the most probable, to what subsequently occurred. Whilst this strategy of reducing the number of complete misses may be a desirable property in building trust between forecasters and users, it also reduces the utility of the forecast.

A promising result from this study is the contrasting behaviour between the dynamical forecast, which often over-confidently forecasts a wet or dry year, and the comparatively risk averse consensus forecast. A way to reduce the under-confidence issues in the GHACOF forecasts would be to give an increased confidence weighting to the dynamical forecast in scenarios where the dynamical models are known to be skilful. These results demonstrate the benefit of using a consistent comparison method for forecast evaluation, something commonly produced for dynamical forecast verification, but rarely applied elsewhere.

It was shown that in years where a driver such as the IOD is forecast as active, prediction skill of both GloSea and GHACOF is increased, however GHACOF still show evidence of under-confidence within the forecasts. This suggests that in years when a strong driver is forecast, the probabilities of the relevant outer categories of the GHACOF forecast should be more confidently forecast to reflect the increased predictability. This can be aided by the fact that GloSea outperforms persistence SST forecasts even at a 1 month lead time.

The large rainfall bias during the short rains was shown to primarily originate from the evolution of a cold SST anomaly in the eastern Indian Ocean and easterly wind anomalies across the equatorial Indian Ocean, a situation reminiscent of a positive IOD state (Saji et al. 1999). At short lead times, there is little SST bias, however an easterly wind bias forms very quickly, suggesting that the mechanism for the generation of the IOD-like state is caused by the wind bias: an easterly wind bias across the Indian Ocean causes upwelling and cooling of the eastern side of the Indian Ocean basin, reducing SSTs. This causes a higher pressure to form over the eastern IO, generating a west to east pressure gradient, further increasing the easterly wind. This positive Bjerknes feedback (Bjerknes 1969) then causes the increase in bias with increased lead time.

Recent results from Hirons and Turner (2018) demonstrate that CMIP5 models with easterly zonal winds across the Indian Ocean in the mean state fail to capture the observed moisture advection in the short rains linked to Indian Ocean SSTs, and struggle to capture the observed teleconnection patterns. This bias should be further investigated to understand what impact it has on predictions on a seasonal timescale, and whether improvements to the Indian Ocean and the Walker circulation can reduce the rainfall bias and improve predictions of the short rains.

References

Adler RF, Huffman GJ, Chang A, Ferraro R, Xie PP, Janowiak J, Rudolf B, Schneider U, Curtis S, Bolvin D, Gruber A, Susskind J, Arkin P, Nelkin E (2003) The version-2 global precipitation climatology project (GPCP) monthly precipitation analysis (1979-Present). J Hydrometeorol 4(6):1147–1167

Anyah RO, Qiu W (2012) Characteristic 20th and 21st century precipitation and temperature patterns and changes over the Greater Horn of Africa. Int J Climatol 32(3):347–363. https://doi.org/10.1002/joc.2270

Arribas A, Glover M, Maidens A, Peterson K, Gordon M, MacLachlan C, Graham R, Fereday D, Camp J, Scaife AA, Xavier P, McLean P, Colman A, Cusack S (2011) The GloSea4 ensemble prediction system for seasonal forecasting. Mon Weather Rev 139(6):1891–1910. https://doi.org/10.1175/2010MWR3615.1

Bahaga TK, Mengistu Tsidu G, Kucharski F, Diro GT (2015) Potential predictability of the sea-surface temperature forced equatorial east african short rains interannual variability in the 20th century. Quart J R Meteorol Soc 141(686):16–26. https://doi.org/10.1002/qj.2338

Bahaga TK, Kucharski F, Tsidu GM, Yang H (2016) Assessment of prediction and predictability of short rains over equatorial East Africa using a multi-model ensemble. Theor Appl Climatol 123(3–4):637–649. https://doi.org/10.1007/s00704-014-1370-1

Bahaga TK, Fink AH, Knippertz P (2019) Revisiting interannual to decadal teleconnections influencing seasonal rainfall in the Greater Horn of Africa during the 20th century. Int J Climatol 39(5):2765–2785. https://doi.org/10.1002/joc.5986

Barnston AG, Chelliah M, Goldenberg SB (1997) Documentation of a highly ENSO-related SST region in the equatorial pacific: research

note. Atmos Ocean 35(3):367–383. https://doi.org/10.1080/07055900.1997.9649597

Batté L, Déqué M (2011) Seasonal predictions of precipitation over Africa using coupled ocean-atmosphere general circulation models: skill of the ENSEMBLES project multimodel ensemble forecasts. Tellus, Ser A: Dyn Meteorol Oceanogr 63A(2):283–299. https://doi.org/10.1111/j.1600-0870.2010.00493.x

Behera SK, Luo JJ, Masson S, Delecluse P, Gualdi S, Navarra A, Yamagata T (2005) Paramount impact of the Indian ocean dipole on the East African short rains: a CGCM study. J Clim 18(21):4514–4530. https://doi.org/10.1175/JCLI3541.1

Bjerknes J (1969) Atmospheric teleconnections from the equatorial Pacific. Mon Weather Rev 97(3):163–172. https://doi.org/10.1175/1520-0493(1969)097⟨0163:ATFTEP⟩2.3.CO;2

Black E, Slingo J, Sperber KR (2003) An observational study of the relationship between excessively strong short rains in coastal East Africa and Indian Ocean SST. Mon Weather Rev 131(1):74–94. https://doi.org/10.1175/1520-0493(2003)131⟨0074:AOSOTR⟩2.0.CO;2

Bliefernicht J, Waongo M, Salack S, Seidel J, Laux P, Kunstmann H (2018) Quality and value of seasonal precipitation forecasts issued by the West African regional climate outlook forum. J Appl Meteorol Climatol 2014:621–642. https://doi.org/10.1175/jamc-d-18-0066.1

Bowler NE, Arribas A, Beare SE, Mylne KR, Shutts GJ (2009) The local ETKF and SKEB: Upgrades to the MOGREPS short-range ensemble prediction system. Quart J R Meteorol Soc 135:767–776. https://doi.org/10.1002/qj.394

Camberlin P, Philippon N (2002) The East African March–May rainy season: associated atmospheric dynamics and predictability over the 1968–97 period. J Clim 15(9):1002–1019

Camberlin P, Wairoto JG (1997) Intraseasonal wind anomalies related to wet and dry spells during the "long" and "short" rainy seasons in Kenya. Theor Appl Climatol 58(1–2):57–69. https://doi.org/10.1007/BF00867432

Cattani E, Merino A, Levizzani V (2016) Evaluation of monthly satellite-derived precipitation products over East Africa. J Hydrometeorol 17(10):2555–2573. https://doi.org/10.1175/JHM-D-15-0042.1

Clark CO, Webster PJ, Cole JE (2003) Interdecadal variability of the relationship between the Indian Ocean zonal mode and East African coastal rainfall anomalies. J Clim 16(3):548–554

Dee DP, Uppala SM, Simmons AJ, Berrisford P, Poli P, Kobayashi S, Andrae U, Balmaseda MA, Balsamo G, Bauer P, Bechtold P, Beljaars AC, van de Berg L, Bidlot J, Bormann N, Delsol C, Dragani R, Fuentes M, Geer AJ, Haimberger L, Healy SB, Hersbach H, Hólm EV, Isaksen L, Kållberg P, Köhler M, Matricardi M, Mcnally AP, Monge-Sanz BM, Morcrette JJ, Park BK, Peubey C, de Rosnay P, Tavolato C, Thépaut JN, Vitart F (2011) The ERA-Interim reanalysis: configuration and performance of the data assimilation system. Q J R Meteorol Soc 137(656):553–597. https://doi.org/10.1002/qj.828

Delsole T, Shukla J (2010) Model fidelity versus skill in seasonal forecasting. J Clim 23(18):4794–4806. https://doi.org/10.1175/2010JCLI3164.1

Doblas-Reyes FJ, García-Serrano J, Lienert F, Biescas AP, Rodrigues LR (2013) Seasonal climate predictability and forecasting: status and prospects. Wiley Interdiscip Rev: Clim Change 4(4):245–268. https://doi.org/10.1002/wcc.217

Eade R, Smith D, Scaife A, Wallace E, Dunstone N, Hermanson L, Robinson N (2014) Do seasonal-to-decadal climate predictions underestimate the predictability of the real world? Geophys Res Lett 41(15):5620–5628. https://doi.org/10.1002/2014GL061146

Ebdon RA (1960) Notes on the wind flow at 50 mb in tropical and sub-tropical regions in January 1957 and January 1958. Q J

R Meteorol Soc 86(370):540–542. https://doi.org/10.1002/qj.49708637011

Farmer G (1988) Seasonal forecasting of the Kenya coast short rains, 1901–84. J Climatol 8(5):489–497. https://doi.org/10.1002/joc.3370080505

Frías MD, Herrera S, Cofiño AS, Gutiérrez JM (2010) Assessing the skill of precipitation and temperature seasonal forecasts in Spain: windows of opportunity related to ENSO events. J Clim 23(2):209–220. https://doi.org/10.1175/2009JCLI2824.1

Graham R, Colman A, Vellinga M, Wallace E (2012) Use of dynamical seasonal forecasts in the consensus outlooks of African Regional Climate Outlook Forums (RCOFs). ECMWF Seminar on Seasonal Prediction (September) 3–7

Graham RJ, Yun WT, Kim J, Kumar A, Jones D, Bettio L, Gagnon N, Kolli RK, Smith D (2011) Long-range forecasting and the global framework for climate services. Clim Res 47(1–2):47–55. https://doi.org/10.3354/cr00963

Hartmann HC, Pagano TC, Sorooshian S, Bales R (2002) Confidence builders: evaluating seasonal climate forecasts from user perspectives. Bull Am Meteorol Soc 83(5):683–698

Hastenrath S (2000) Zonal circulations over the equatorial Indian Ocean. J Clim 13(15):2746–2756

Hastenrath S (2007) Circulation mechanisms of climate anomalies in East Africa and the equatorial Indian Ocean. Dyn Atmos Oceans 43(1–2):25–35. https://doi.org/10.1016/j.dynatmoce.2006.06.002

Hastenrath S, Nicklis A, Greischar L (1993) Atmospheric-hydrospheric mechanisms of climate anomalies in the western equatorial Indian Ocean. J Geophys Res 98(C11):20,219–20,235. https://doi.org/10.1029/93JC02330

Hastenrath S, Polzin D, Mutai C (2011) Circulation mechanisms of Kenya rainfall anomalies. J Clim 24(2):404–412. https://doi.org/10.1175/2010JCLI3599.1

Heidke P (1926) Berechnung Des Erfolges Und Der Güte Der Windstärkevorhersagen Im Sturmwarnungsdienst. Geografiska Annaler 8(4):301–349. https://doi.org/10.1080/20014422.1926.11881138

Hellmuth M, Moorhead A, Thomson M, Williams J (2007) Climate Risk Management in Africa: Learning from Practice

Hewitt HT, Copsey D, Culverwell ID, Harris CM, Hill RS, Keen AB, McLaren AJ, Hunke EC (2011) Design and implementation of the infrastructure of HadGEM3: the next-generation Met Office climate modelling system. Geosci Model Dev 4(2):223–253. https://doi.org/10.5194/gmd-4-223-2011

Hirons L, Turner A (2018) The impact of Indian Ocean mean-state biases in climate models on the representation of the East African short rains. J Clim 31(16):6611–6631. https://doi.org/10.1175/JCLI-D-17-0804.1

Indeje M, Semazzi FH (2000) Relationships between QBO in the lower equatorial stratospheric zonal winds and East African seasonal rainfall. Meteorol Atmos Phys 73(3–4):227–244. https://doi.org/10.1007/s007030050075

Indeje M, Semazzi FH, Ogallo LJ (2000) ENSO signals in East African rainfall seasons. Int J Climatol 20(1):19–46

Kalnay E et al. (1996) The NCEP/NCAR 40-year reanalysis project. Bull Am Meteorol Soc 77(3):437–472

Kimani MW, Hoedjes JC, Su Z (2017) An assessment of satellite-derived rainfall products relative to ground observations over East Africa. Rem Sens 9(5). https://doi.org/10.3390/rs9050430

Kirtman BP, Min D, Infanti JM, Kinter JL, Paolino DA, Zhang Q, Van Den Dool H, Saha S, Mendez MP, Becker E, Peng P, Tripp P, Huang J, Dewitt DG, Tippett MK, Barnston AG, Li S, Rosati A, Schubert SD, Rienecker M, Suarez M, Li ZE, Marshak J, Lim YK, Tribbia J, Pegion K, Merryfield WJ, Denis B, Wood EF (2014) The North American multimodel ensemble: phase-1 seasonal-to-interannual prediction; phase-2 toward developing intraseasonal

prediction. Bull Am Meteorol Soc 95(4):585–601. https://doi.org/10.1175/BAMS-D-12-00050.1

Kumar A, Peng P, Chen M (2014) Is there a relationship between potential and actual skill? Mon Weather Rev 142(6):2220–2227. https://doi.org/10.1175/MWR-D-13-00287.1

Lawrence AJ (1976) On conditional and partial correlation. Am Stat 30(3):146–149. https://doi.org/10.2307/2683864

Li G, Xie SP (2014) Tropical biases in CMIP5 multimodel ensemble: the excessive equatorial pacific cold tongue and double ITCZ problems. J Clim 27(4):1765–1780. https://doi.org/10.1175/JCLI-D-13-00337.1

Liebmann B, Hoerling MP, Funk C, Bladé I, Dole RM, Allured D, Quan X, Pegion P, Eischeid JK (2014) Understanding recent eastern Horn of Africa rainfall variability and change. J Clim 27(23):8630–8645. https://doi.org/10.1175/JCLI-D-13-00714.1

Lu B, Ren HL, Scaife AA, Wu J, Dunstone N, Smith D, Wan J, Eade R, MacLachlan C, Gordon M (2018) An extreme negative Indian Ocean Dipole event in 2016: dynamics and predictability. Clim Dyn 51(1–2):89–100. https://doi.org/10.1007/s00382-017-3908-2

MacLachlan C, Arribas A, Peterson KA, Maidens A, Fereday D, Scaife AA, Gordon M, Vellinga M, Williams A, Comer RE, Camp J, Xavier P, Madec G (2015) Global seasonal forecast system version 5 (GloSea5): a high-resolution seasonal forecast system. Quart J R Meteorol Soc 141(689):1072–1084. https://doi.org/10.1002/qj.2396

Madden RA, Julian PR (1971) Detection of a 40–50 day oscillation in the zonal wind in the tropical Pacific. J Atmos Sci 28(5):702–708

Madden RA, Julian PR (1972) Description of global-scale circulation cells in the tropics with a 40–50 day period. Journal of the Atmospheric Sciences 29(6):1109–1123. https://doi.org/10.1175/1520-0469(1972)029<1109:DOGSCC>2.0.CO;2

Magadzire T, Harrison L, Galu G, Nsadisa F (2016) Seasonal forecasting using the GeoCOF software: GeoCOF version 2.1 manual. FEWS NET/Climate Hazards Group

Marchant R, Mumbi C, Behera S, Yamagata T (2007) The Indian Ocean dipole—the unsung driver of climatic variability in East Africa. African J Ecol 45(1):4–16. https://doi.org/10.1111/j.1365-2028.2006.00707.x

Mason I (1982) A model for assessment of weather forecasts 30

Mason S, Chidzambwa S (2008) Verification of African RCOF forecasts. https://doi.org/10.7916/D85T3SB0

Mason SJ (2013) Guidance on verification of operational seasonal climate forecasts. In: World Meteorological Organisation, Commision for Climatology XIV Technical Report

Mason SJ, Tippett MK (2016) Climate Predictability Tool version 15.3 https://doi.org/10.7916/D8NS0TQ6

Meehl GA, Covey C, Delworth T, Latif M, Mcavaney B, Mitchell JFB, Stouffer RJ, Karl ET (2007) The WCRP CMIP3 Multimodel: A new era in climate change research. Am Meteorol Soc (September) 1383–1394. https://doi.org/10.1175/BAMS-88-9-1383

Mutai CC, Ward MN (2000) East African rainfall and the tropical circulation/convection on intraseasonal to interannual timescales. Journal of Climate 13(22):3915–3939. https://doi.org/10.1175/1520-0442(2000)013<3915:EARATT>2.0.CO;2

Mutai CC, Ward MN, Colman AW (1998) Towards the prediction of the East Africa short rains based on sea-surface temperature-atmosphere coupling. Int J Climatol 18(9):975–997

Mwangi E, Wetterhall F, Dutra E, Di Giuseppe F, Pappenberger F (2014) Forecasting droughts in East Africa. Hydrol Earth Syst Sci 18(2):611–620. https://doi.org/10.5194/hess-18-611-2014

Nicholson S (1996) A review of climate dynamics and climate variability in Eastern Africa. In: The limnology, climatology and paleoclimatology of the East African lakes, CRC Press, pp 25–56

Nicholson SE (2014) The predictability of rainfall over the Greater Horn of Africa. Part I: prediction of seasonal rainfall. J

Hydrometeorol 15(3):1011–1027. https://doi.org/10.1175/JHM-D-13-062.1

Nicholson SE (2015) The predictability of rainfall over the Greater Horn of Africa. Part II: prediction of monthly rainfall during the long rains. J Hydrometeorol 16(5):2001–2012. https://doi.org/10.1175/JHM-D-14-0138.1

Nicholson SE (2017) Climate and climatic variability of rainfall over eastern Africa. Rev Geophys 55(3):590–635. https://doi.org/10.1002/2016RG000544

Nicholson SE, Entekhabi D (1986) The quasi-periodic behavior of rainfall variability in Africa and its relationship to the southern oscillation. Arch Meteorol, Geophys, Bioclimatol Ser A 34(3–4):311–348. https://doi.org/10.1007/BF02257765

Nicholson SE, Kim J (1997) The relationship of the El Niño Southern Oscillation to African rainfall. International Journal of Climatology 17(2):117–135. https://doi.org/10.1002/(SICI)1097-0088(199702)17:2<117::AID-JOC84>3.0.CO;2-O

Ogallo L, Bessemoulin P, Ceron JP, Mason S, Connor S (2008) Adapting to climate variability and change: the Climate Outlook Forum process. WMO Bull 57(2):93–102

Ogallo LJ (1988) Relationships between seasonal rainfall in East Africa and the Southern Oscillation. J Climatol 8(1):31–43. https://doi.org/10.1002/joc.3370080104

Okoola RE (1998) Spatial evolutions of the active convective patterns across the equatorial eastern Africa region during northern hemisphere spring season using outgoing longwave radiation records. Meteorol Atmos Phys 66(1–2):51–63. https://doi.org/10.1007/BF01030448

Okoola RE (1999) A diagnostic study of the eastern Africa monsoon circulation during the northern hemisphere spring season. Int J Climatol 19(2):143–168

Patt AG, Ogallo L, Hellmuth M (2007) Sustainability: learning from 10 years of climate outlook forums in Africa. Science 318(5847):49–50. https://doi.org/10.1126/science.1147909

Pegion K, Kumar A (2013) Does an ENSO-conditional skill mask improve seasonal predictions? Mon Weather Rev 141(12):4515–4533. https://doi.org/10.1175/mwr-d-12-00317.1

Philippon N, Camberlin P, Fauchereau N (2002) Empirical predictability study of October–December East African rainfall. Q J R Meteorol Soc 128(585 PART A):2239–2256. https://doi.org/10.1256/qj.01.190

Pohl B, Camberlin P (2006a) Influence of the Madden–Julian Oscillation on East African rainfall. I: intraseasonal variability and regional dependency. Q J R Meteorol Soc 132(621):2521–2539. https://doi.org/10.1256/qj.05.104

Pohl B, Camberlin P (2006b) Influence of the Madden–Julian Oscillation on East African rainfall. II. March–May season extremes and interannual variability. Q J R Meteorol Soc 132(621):2541–2558. https://doi.org/10.1256/qj.05.223

Rayner NA, Paker DE, Horton EB, Folland CK, Alexander LV, Rowell DP, Kent EC, Kaplan A (2003) Global analyses of sea surface temperature, sea ice, and night marine air temperature since the late nineteenth century. J Geophys Res 108(D14):4407. https://doi.org/10.1029/2002JD002670

Reed RJ, Campbell WJ, Rasmussen LA, Rogers DG (1961) Evidence of a downward-propagating, annual wind reversal in the equatorial stratosphere. J Geophys Res 66(3):813–818. https://doi.org/10.1029/JZ066i003p00813

Richter I, Chang P, Doi T, Kataoka T, Nagura M, Oettli P, de Szoeke S, Tozuka T, Xu Z (2016) An overview of coupled GCM biases in the tropics. In: Indo-Pacific Climate Variability and Predictability, pp 213–263

Rodhe H, Virji H (1976) Trends and periodicities in East African rainfall data. Monthly Weather Review 104(3):307–315. https://doi.org/10.1175/1520-0493(1976)104<0307:TAPIEA>2.0.CO;2

Saha S, Moorthi S, Wu X, Wang J, Nadiga S, Tripp P, Behringer D, Hou Y, Chuang H, Iredell M, Ek M, Meng J, Yang R, Mendez MP, van den Dool H, Zhang Q, Wang W, Chen M, Becker E (2014) The NCEP climate forecast system version 2. J Clim 27:2185–2208. https://doi.org/10.1175/JCLI-D-12-00823.1

Saji NH, Yamagata T (2003) Possible impacts of Indian Ocean Dipole mode events on global climate. Clim Res 25(2):151–169. https://doi.org/10.3354/cr025151

Saji NH, Goswami BN, Vinayachandran PN, Yamagata T (1999) A dipole mode in the tropical Indian ocean. Nature 401(6751):360–363. https://doi.org/10.1038/43854

Scaife AA, Smith D (2018) A signal-to-noise paradox in climate science. NPJ Clim Atmos Sci 1(1):28. https://doi.org/10.1038/s41612-018-0038-4

Scaife AA, Copsey D, Gordon C, Harris C, Hinton T, Keeley S, O'Neill A, Roberts M, Williams K (2011) Improved Atlantic winter blocking in a climate model. Geophys Res Lett 38(23):L23,703. https://doi.org/10.1029/2011GL049573

Scaife AA, Arribas A, Blockey E, Brookshaw A, Clark RT, Dunstone N, Eade R, Fereday D, Folland CK, Gordon M, Hermanson L, Knight JR, Lea DJ, MacLachlan C, Maidens A, Martin M, Peterson AK, Smith D, Vellinga M, Wallace E, Waters J, Williams A (2014) Skillful long range prediction of European and North American winters. Geophys Res Lett 5(7):2514–2519. https://doi.org/10.1002/2014GL059637

Scaife AA, Ferranti L, Alves O, Athanasiadis P, Baehr J, Déqué M, Dippe T, Dunstone N, Fereday D, Gudgel RG, Greatbatch RJ, Hermanson L, Imada Y, Jain S, Kumar A, MacLachlan C, , Merryfield W, Müller WA, Ren HL, Smith DM, Takaya Y, Vecchi G, Yang X (2018) Tropical rainfall predictions from multiple seasonal forecast systems. Int J Climatol pp 1–15. https://doi.org/10.1002/joc.5855

Shukla S, Roberts J, Hoell A, Funk CC, Robertson F, Kirtman B (2016) Assessing North American multimodel ensemble (NMME) seasonal forecast skill to assist in the early warning of anomalous hydrometeorological events over East Africa. Climate Dynamics pp 1–17, https://doi.org/10.1007/s00382-016-3296-z

Skamarock WC, Klemp, Joseph B, Dudhia J, Gill DO, Barker DM, Duda MG, Xiang-Yu H, Wang W, Powers JG (2008) A description of the advanced research WRF version 3. NCAR/TN-475+STR pp 1–113

Taylor KE, Stouffer RJ, Meehl GA (2012) An overview of CMIP5 and the experiment design. Bull Am Meteorol Soc 93(4):485–498. https://doi.org/10.1175/BAMS-D-11-00094.1

Torrence C, Webster PJ (1998) The annual cycle of persistence in the El Niño/Southern Oscillation. Q J R Meteorol Soc 124(550):1985–2004. https://doi.org/10.1002/qj.49712455010

Troccoli A (2010) Seasonal climate forecasting. Meteorol Appl 17(3):251–268. https://doi.org/10.1002/met.184

Ummenhofer CC, Gupta AS, England MH, Reason CJC (2009) Contributions of Indian Ocean sea surface temperatures to enhanced East African rainfall. J Clim 22(4):993–1013. https://doi.org/10.1175/2008JCLI2493.1

van den Dool HM, Toth Z (1991) Why do forecasts for near normal often fail? Weather and Forecasting 6(1):76–85. https://doi.org/10.1175/1520-0434(1991)006<0076:wdffno>2.0.co;2

Vellinga M, Milton S (2018) Drivers of interannual variability of the East African 'Long Rains'. Quarterly Journal of the Royal Meteorological Society. https://doi.org/10.1002/qj.3263

Webster PJ, Moore AM, Loschnigg JP, Leben RR (1999) Coupled ocean–atmosphere dynamics in the Indian Ocean during 1997–98. Nature 401(6751):356–360. https://doi.org/10.1038/43848

Wilks DS (2006) Statistical methods in the atmospheric sciences, 3rd edn. Elsevier, Oxford

Yamagata T, Behera SK, Luo JJ, Masson S, Jury MR, Rao SA (2004) Coupled ocean-atmosphere variability in the tropical Indian Ocean. In: Earth's Climate, pp 189–211. https://doi.org/10.1029/147GM12

Yang W, Seager R, Cane MA, Lyon B (2015) The rainfall annual cycle bias over East Africa in CMIP5 coupled climate models. J Clim 28(24):9789–9802. https://doi.org/10.1175/JCLI-D-15-0323.1

Yule GU (1907) On the theory of correlation for any number of variables, treated by a new system of notation. Proc R Soc Lond Ser A, Contain Papers Math Phys Char 79(529):182–193. https://doi.org/10.1098/rspa.1907.0028

Chapter 3.

Common mechanism for inter-annual and decadal variability in the East African long rains

Common Mechanism for Interannual and Decadal Variability in the East African Long Rains

Dean P. Walker[1] , **John H. Marsham[1,2]** , **Cathryn E. Birch[1]** , **Adam A. Scaife[3,4]** , and **Declan L. Finney[1]**

[1]School of Earth and Environment, University of Leeds, Leeds, UK, [2]National Centre for Atmospheric Science, Leeds, UK, [3]Met Office Hadley Centre, Exeter, UK, [4]College of Engineering, Mathematics and Physical Sciences, University of Exeter, Exeter, UK

Abstract The East African long rains constitute the main crop-growing season in the region. Interannual predictability of this season is low in comparison to the short rains, and recent decadal drying contrasts with climate projections of a wetter future (the "East African climate paradox"). Here, we show that long rains rainfall totals are strongly correlated with 700 hPa zonal winds across the Congo basin and Gulf of Guinea ($r = 0.73$). Westerly anomalies align with more rainfall, with the same mechanism controlling covariability on interannual and decadal time scales. On both time scales wind anomalies are linked to geopotential anomalies over the Sahel and Sahara, and warming there. Rainfall and wind are significantly correlated with the Madden-Julian Oscillation (MJO) amplitude, and around 18% of the decadal drying can be explained by MJO amplitude variability. This work shows that predictions of East African rainfall across time scales require robust prediction of both zonal winds and MJO activity.

Plain Language Summary East Africa has two rainfall seasons, the main season, the long rains, runs from March to May. There is currently little understanding of what controls the amount of rainfall during this season. Recent drying, causing many areas to suffer from droughts and food shortages, contrasts with climate projections of a wetter future (the "East African climate paradox"). Rainfall is found to be connected to the strength of easterly winds over the Congo basin and Gulf of Guinea, with the same mechanism controlling variability on both interannual and decadal time scales. From 1998 to 2011 the winds had been getting stronger, with reduced rainfall over East Africa. The cause of the stronger wind is investigated and is partly explained by relatively fast warming in the Sahel than over the Congo, while variation in Madden-Julian Oscillation (a large-scale tropical wave) activity, explains around 18% of the decadal drying.

1. Introduction

Equatorial East Africa has two rainfall seasons per year, the long rains, occurring March-May (MAM), and short rains, occurring October-December (OND). A large contrast in the predictability of the two seasons has been observed (Batté & Déqué, 2011; Camberlin & Philippon, 2002; Dutra et al., 2013; Nicholson, 2017; Walker et al., 2019). This has been attributed to the short rains being influenced by global-scale modes of variability such as El Niño–Southern Oscillation (Indeje et al., 2000; Nicholson & Entekhabi, 1986), and the Indian Ocean Dipole (Black et al., 2003; Saji et al., 1999), while such relationships are absent during the long rains (Ogallo, 1988).

In most areas of equatorial East Africa, the long rains is the main crop growing season, generally providing greater (Camberlin & Wairoto, 1997), and more reliable (Camberlin & Philippon, 2002), rainfall amounts. However, in recent decades there has been an observed drying trend in this season (Funk et al., 2005, 2008; Liebmann et al., 2014; Maidment et al., 2015), which sharply contrasts the wetting predicted by most climate projections (Otieno & Anyah, 2013; Shongwe et al., 2011), often referred to as the "East African Climate Paradox" (Rowell et al., 2015). Some authors have demonstrated that the long rains decline is linked with natural decadal variability in the Pacific Ocean (Bahaga et al., 2019; Lyon, 2014; Yang et al., 2014), while others suggest anthropogenic factors (Funk & Hoell, 2015; Rowell et al., 2015; Williams & Funk, 2011). Meanwhile, recent work by Wainwright et al. (2019) has shown that over the Horn of Africa the observed long rains drying trend is caused by a shortening of the rainfall season and that in more recent years,

the long rains have begun to recover. Therefore, the future of the long rains is still highly uncertain. Improved understanding and prediction of variability in this season on interannual and decadal time scales, leading to improved rainfall forecasts, would be of great benefit to the local population.

Finney et al. (2019) recently demonstrated that although the climatological wind is easterly (Figure S1a in the supporting information), days with westerly winds originating from over the Congo basin do occur during the long rains season, and throughout the year. These events import moist air from over the Congo basin, causing convergence within the Lake Victoria basin, thereby leading to enhanced rainfall, with the record breaking 2018 long rains serving as a prime example (Kilavi et al., 2018). During MAM 2018 several westerly days occurred, linked to tropical cyclones in the Indian Ocean. Finney et al. (2019) also highlighted the role of the Madden-Julian Oscillation (MJO; Madden & Julian, 1971, 1972) influencing the formation of these tropical cyclones.

A more direct effect of MJO influence on the long rains has been documented by Pohl and Camberlin (2006a, 2006b). Pohl and Camberlin (2006a), using phases of the MJO defined by Wheeler and Hendon (2004), identified that Phases 2 and 3 from the Wheeler-Hendon index, when the convective core is over Africa and the Indian Ocean, were linked to increased rainfall over the East African highlands. Meanwhile, Vellinga and Milton (2018) demonstrated that a greater seasonal mean amplitude of the MJO as defined by Wheeler and Hendon (2004), regardless of phase, contributed to more abundant rainfall, due to an asymmetric response of the rainfall to the ascent/descent caused by specific phases.

While anomalous westerly wind influence over East Africa has been regularly described qualitatively in past literature (Camberlin & Wairoto, 1997; Diem et al., 2019; Nkunzimana et al., 2019; Okoola, 1999a, 1999b), little quantitative evidence for this had been presented until the work by Finney et al. (2019). Finney et al. (2019) showed the role of absolute westerlies for East African rainfall; this work uses this understanding to demonstrate the connection between zonal wind anomalies and East African rainfall on both interannual and decadal time scales, demonstrating a link between long-term change in the zonal winds over the Congo basin and the long rains drying trend (section 3.1), and also investigating explanations for variability of the zonal winds (section 3.2).

2. Data and Methods

The rainfall data for this study are Global Precipitation Climatology Project Version 2.3 (GPCP; Adler et al., 2003), while wind, geopotential height, and temperature data were obtained from European Centre for Medium-Range Weather Forecasts (ECMWF) Interim Reanalysis (ERA-Interim; Dee et al., 2011). MJO phase and amplitude data were obtained from the Bureau of Meteorology, where phase and amplitude are calculated using the method outlined in Wheeler and Hendon (2004), using National Oceanic and Atmospheric Administration (NOAA) outgoing long-wave radiation satellite observations (Liebmann & Smith, 1996), and National Centers for Environmental Prediction-National Center for Atmospheric Research (NCEP-NCAR; Kalnay et al., 1996) reanalysis winds. National Aeronautics and Space Administration (NASA) Modern Era Retrospective Analysis for Research and Applications, Version 2 (MERRA-2; Gelaro et al., 2017) winds and geopotential height data were used to verify relations between ERA-Interim variables and other observations.

This study uses the period 1979–2018, matching the satellite era and earliest available data from ERA-Interim and GPCP. Results were tested with the outlying year 2018 removed, with similar conclusions. The region considered for rainfall is highlighted in blue in Figure 1a, and future references to East Africa will refer to this region, while the zonal wind index is calculated as the mean 700 hPa zonal wind within 5°N to 5°S, 10°W to 30°E (brown box on Figures 1d and 1e).

Wet, dry, and recovery periods of the long rains, similar to those in Wainwright et al. (2019), are defined from 1979–1997 (P1), 1998–2011 (P2), and 2012–2018 (P3), respectively. Composites of the drying trend are considered using P2-P1. The wettest and driest years are calculated by fitting a cubic polynomial to the raw time series data, and then removing this, to remove long-term trends. The wettest and driest years within the long rains are defined as years where the rainfall total after trend removal is more than 0.8 standard deviations above and below the 1979–2018 seasonal mean, respectively. When discussing these sets of years, DECADAL will refer to the altered Wainwright periods (P2-P1), and INTERANNUAL will refer to the
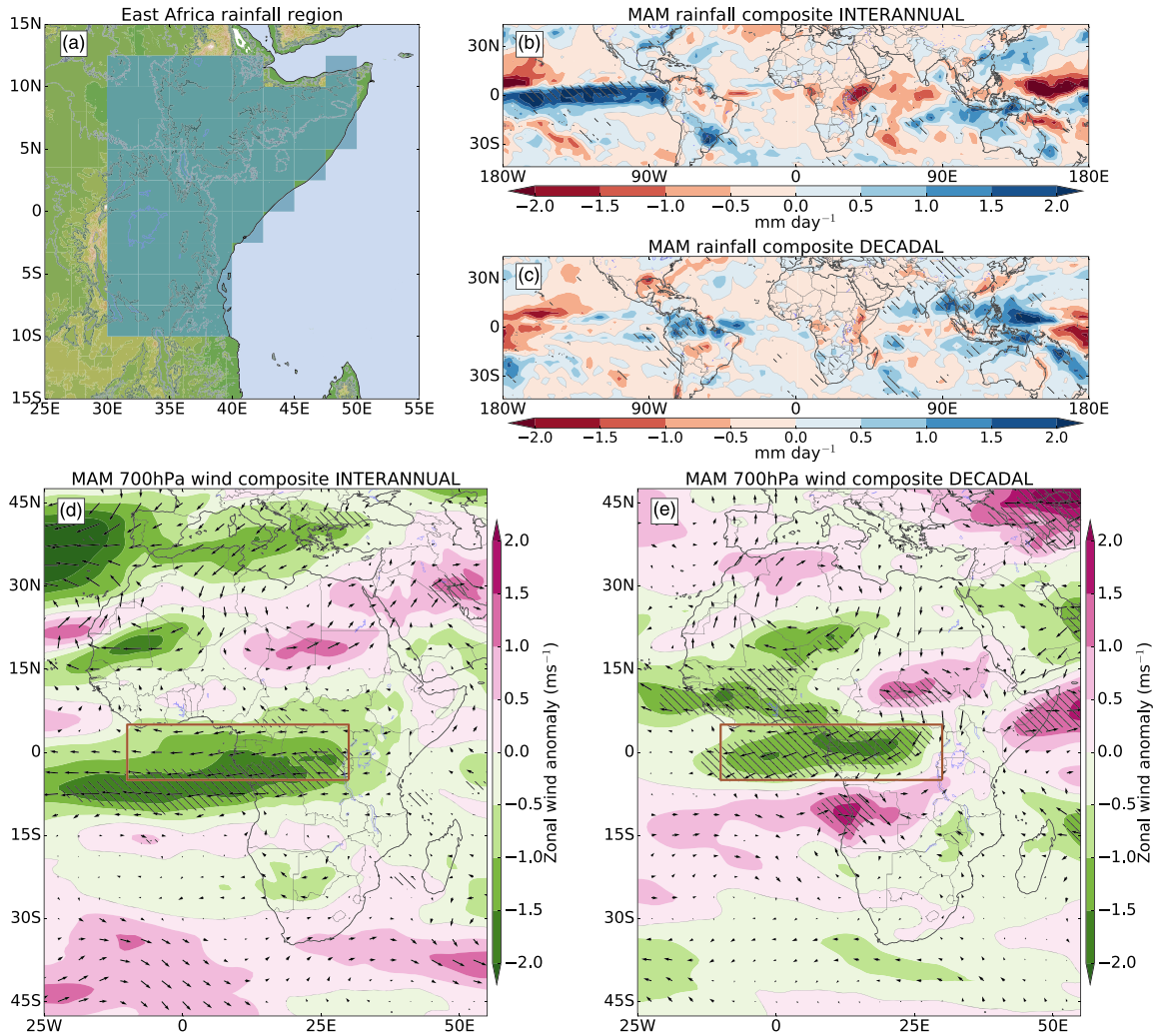
Figure 1. Interannual and decadal rainfall changes in East Africa. (a) East Africa rainfall region shaded blue (land within 12.5°N to 10°S, 30°E to 52.5°E), East Africa topography, colors, 500 and 1,000 m contours in light and dark gray. Composite of rainfall across the tropics during the long rains for (b) driest years minus wettest years, (c) dry period minus wet period (P2-P1). Composite of 700 hPa winds and zonal wind (colors) across Africa during the long rains for (d) driest years minus wettest years, (e) dry period minus wet period (P2-P1). Brown boxes show region used to calculate zonal wind index, hatching denotes areas where the composite values are significantly different from 0.

driest minus wettest years. Significance of trends were tested using the Mann-Kendall test, (Kendall, 1975; Mann, 1945), further details of which can be found in Wilks (2011).

The expected trend in mean rainfall between P1 and P2, $\Delta \bar{r}_{exp}$, due to the observed change in mean wind from P1 to P2, $\bar{u}_{P2} - \bar{u}_{P1}$, is given by

$$\Delta \bar{r}_{exp} = \frac{\mathrm{d}r}{\mathrm{d}u}(\bar{u}_{P2} - \bar{u}_{P1}) \qquad (1)$$

where $\frac{\mathrm{d}r}{\mathrm{d}u}$ is the gradient of the regression of rainfall against wind after removing the polynomial fit. Variables r and u can be replaced by other variables. If $\Delta \bar{r}_{exp} \approx \Delta \bar{r}_{obs}$, where $\Delta \bar{r}_{obs}$ is the observed change in rainfall, then this is evidence that the mechanism that links rainfall and winds on interannual time scales can also explain the decadal variability in the rainfall.

Figure 2. Temporal variations in East African rainfall and winds. (a) Time series of seasonal mean zonal wind anomaly (brown) a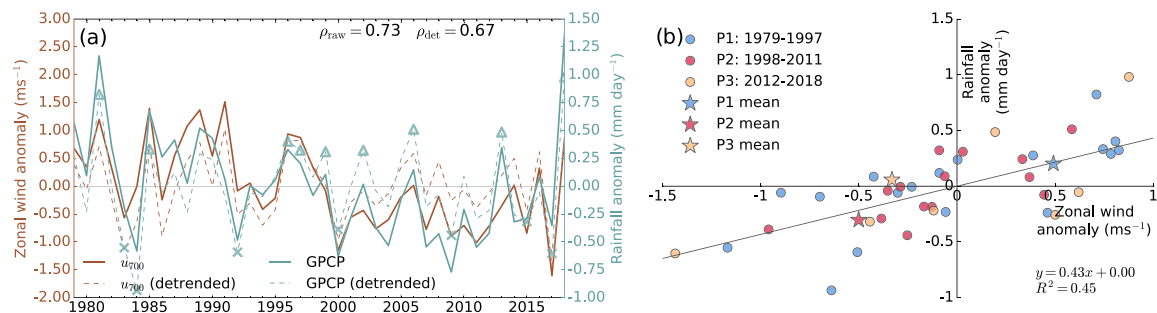nd rainfall anomaly (blue) for boxes defined in Figure 1, dashed lines show time series after removing polynomial fit. The wet and dry years used for the INTERANNUAL composites are highlighted as triangles and crosses, respectively. Correlation values of zonal winds against rainfall, before and after detrending given in top right. (b) Scatter of zonal wind anomaly against rainfall anomaly after detrending, colored by P1 (blue), P2 (red), and P3 (yellow) periods. Black line is regression line fitted against the scatter, with regression equation and R^2 value given. Colored stars show mean anomaly of each period, with respect to 1979–2018 mean, before trend is removed.

3. Results

3.1. Interannual and Decadal Variability of the Long Rains

Figure 1 shows rainfall anomalies over the tropics and 700 hPa wind anomaly composites over Africa for INTERANNUAL and DECADAL. The 700 hPa level was chosen as it is largely above the topography of East Africa and was found to have the largest single-level moisture flux, and moisture flux anomaly in the INTERANNUAL composite (Figure S1b). In Figures 1b and 1c a dry signal is apparent over East Africa as expected, with wet anomalies over the Maritime Continent, and dry anomalies over the western Pacific, in a pattern reminiscent of the Pacific "V" discussed in Funk and Hoell (2015), Funk et al. (2019), and Lyon and Dewitt (2012). In Figures 1d and 1e a large easterly anomaly is present over the equatorial Atlantic Ocean and Congo basin. In INTERANNUAL, this extends to the Horn of Africa where it meets a westerly anomaly from the Indian Ocean, while in DECADAL this easterly anomaly is also present, but only reaches as far as the orography separating the Congo basin from East Africa. In DECADAL, the easterly anomalies appear to be linked to an anticyclonic anomaly over the Sahara desert; this level exhibits a midtropospheric high pressure, over the location of the summertime Saharan Heat Low (SHL), suggesting a stronger SHL in drier years (Evan et al., 2015). Heating and ascent in the SHL causes a low pressure near the surface and high pressure aloft at 700 hPa (Lavaysse et al., 2009; Rácz & Smith, 1999) and the 925 to 700 hPa thickness is directly proportional to the air temperature in the column. The 700 hPa anticyclone is therefore a useful measure of the SHL. The zonal wind anomaly (outlined by the brown box) is largely consistent with the findings of Finney et al. (2019), as an easterly anomaly in the seasonal mean is likely to contain less westerly, or weak easterly days. These results are insensitive to the reanalysis used, with similar patterns observed in equivalent MERRA-2 composites (Figures S2a and S2b).

Figure 2 shows the time series of the zonal wind index and long rains seasonal rainfall anomalies. A correlation between the rainfall and zonal winds of 0.73 is found, 0.67 with polynomial fits removed (both significant at the 1% level). This demonstrates the very strong connection between interannual variability in zonal wind and rainfall. This is again consistent in MERRA-2, with correlations of 0.81 (0.71 when detrended; Figure S2c). It is apparent from Figure 2a that both the rainfall and zonal wind demonstrate a decreasing trend, both significant at the 5% level, when treated linearly, using the Mann-Kendall trend test. Both variables show some signs of a recovery in P3, consistent with Wainwright et al. (2019). This is more apparent in the rainfall than winds in Figure 2a, while for MERRA-2 (Figure S2c) a recovery in the zonal winds is more visible.

Figure 2b shows the scatter of rainfall against zonal wind after detrending. The linear regression equation between the two variables is $r = 0.43u - 0.00$. From this, and from the linear trend of each variable, an expected trend of rainfall due to the observed trend in the zonal winds can be calculated (Equation 1). The expected change in mean rainfall from observed change in mean zonal wind from P1 to P2 is -0.43 ± 0.14 mm day^{-1}, the observed change is -0.50 ± 0.16 mm day^{-1}. These are statistically
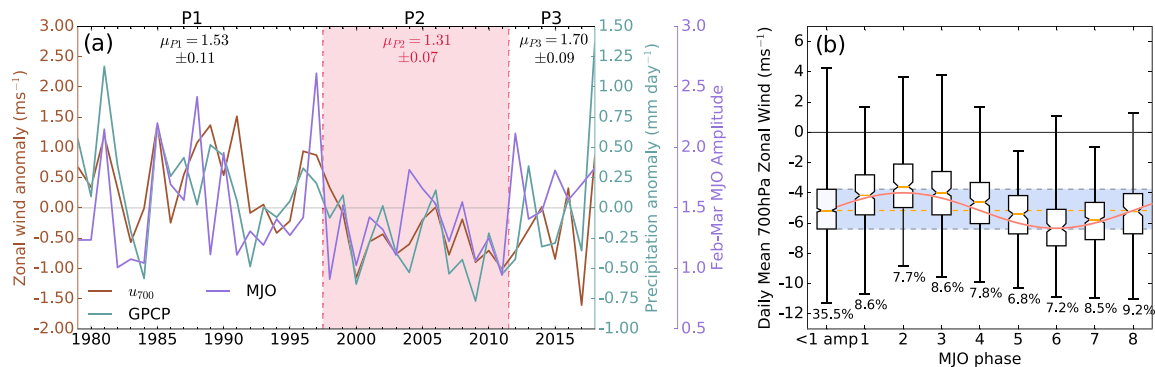
Figure 3. The MJO and East African rainfall. (a) Time series of zonal wind anomaly (brown) and rainfall anomaly (blue) as in Figure 2a, and February-March mean MJO amplitude (purple), means and standard errors of the MJO amplitudes during P1, P2, and P3 are given at the top, with periods separated by red dashed lines, and red shading over the dry period, P2. (b) Box plots of daily mean zonal wind separated by MJO phase, inactive days (MJO amplitude < 1) grouped in left box, notches on boxes show 95% confidence interval calculated from bootstrap resampling of 1,000 values, numbers below minimum of each box show percentage of days in that phase, blue shading shows interquartile range of inactive days, orange dashed line shows median of inactive days. Pink curve shows sine wave fitted to active days assuming a mean value equal to the median of the inactive days.

indistinguishable, so it is concluded that the observed decadal drying in the long rains can be largely explained by the same mechanism controlling the interannual relation between the zonal wind and rainfall.

While it is difficult to establish causality between the variability in the zonal winds and rainfall, and is likely the two operate in a coupled system, (Finney et al., 2019) provides a potential mechanism. By examining lagged relationships it is found that zonal winds early in the long rains (March) are more strongly correlated with rainfall later in the season (April-May), than the inverse (0.61 compared to 0.37). By also considering daily zonal winds against rainfall, it is found that the peak correlation occurs at 1 day lag (zonal wind of one day against rainfall of the next), and is found to be significantly higher than a 1 day lead correlation. Therefore, both monthly and daily analysis support wind anomalies leading to rainfall anomalies.

3.2. Drivers of Variability of the Zonal Winds

As the main conclusion of section 3.1 is that the zonal winds are strongly correlated with the long rains on the interannual time scale and can explain the decadal drying trend, an important question is to understand what is the controlling variability in these zonal winds on interannual and decadal time scales.

Recent work has shown the influence of the MJO amplitude on the long rains on interannual time scales (Pohl & Camberlin, 2006b; Vellinga & Milton, 2018). Figure 3a shows the time series of rainfall and zonal wind index alongside the February-March MJO amplitude used in Vellinga and Milton (2018). Correlation between MJO amplitude and zonal winds is 0.31, and between MJO and rainfall is 0.36 (0.34 and 0.35, respectively, when detrended). These fairly weak correlations are nevertheless significant at the 5% level, and correlations between MJO and zonal wind are stronger in MERRA-2 (0.48, 0.54 when detrended). In Figure 3a, there is significantly lower (at 5% level) mean MJO amplitude during P2 than P1 and P3. The mean MJO amplitude of P2 is 1.31 ± 0.07 while P1 and P3 are 1.53 ± 0.11 and 1.70 ± 0.09, respectively. The zonal wind index was regressed against the MJO amplitude (a), giving a regression equation of $u = 0.58a - 0.86$. The change in mean MJO amplitude from P1 to P2 is -0.21 ± 0.14, giving an expected change in mean zonal wind of -0.13 ± 0.07 m s^{-1} from Equation 1. The observed change in the zonal wind from P1 to P2 is -0.99 ± 0.26 m s^{-1}, meaning ~13% of the change in zonal wind can be attributed to the decrease in MJO amplitude. Similarly, regressing the rainfall against the MJO amplitude leads to an expected change of -0.09 ± 0.10 mm day^{-1}. The observed change in mean of the rainfall from P1 to P2 is -0.50 ± 0.14 mm day^{-1}, so ~18% of the change in rainfall can be attributed to the decrease in MJO amplitude.

Pohl and Camberlin (2006a) highlighted how different phases of the MJO influence winds around East Africa, some phases giving easterly anomalies, others westerly, so it is likely that by considering only amplitude these opposite influences mostly cancel out, accounting for the low correlations when amplitude alone is considered. However, if the wind response to phases is asymmetric, as for rainfall (Vellinga & Milton, 2018), this could explain the significant correlation, providing evidence that the MJO influences
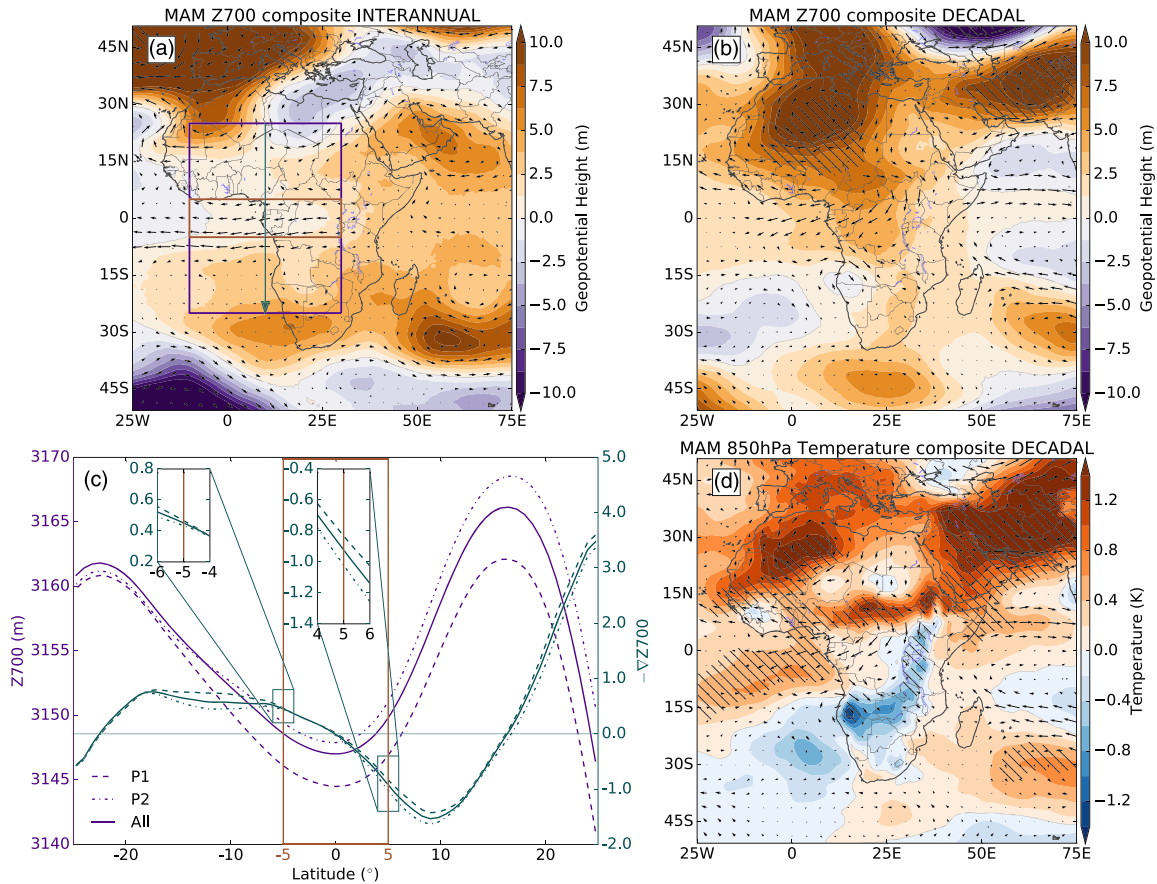
107

Figure 4. Interannual and decadal geopotential patterns over Africa. (a) Composites of 700 hPa geopotential height and winds for (a) INTERANNUAL, and (b), DECADAL. (c) Transect of mean geopotential height (purple) across each latitude for the purple box shown in (a), and gradient of the geopotential height (blue) multiplied by −1, following blue arrow shown in (a), for P1 (dashed), P2 (dotted), all years (solid). Inset boxes show geopotential gradients zoomed in to edges of zonal wind box (brown box). (d) 850 hPa temperature and 700 hPa winds for DECADAL, hatching denotes areas where the composite values are significantly different from 0.

interannual and decadal variability of the zonal winds. Alternatively, it may be that the mechanism driving variability in the zonal winds also impacts MJO amplitude. The effects of different phases of the MJO on the zonal winds and rainfall are considered. Figure 3b shows box and whisker diagrams of the daily mean of the zonal wind index, separated by MJO phase and separated into inactive days (amplitude < 1) and active days (amplitude > 1), in MAM. If the zonal winds of the inactive days are more strongly easterly than the active days, it can be concluded that the influence of the MJO on wind is asymmetric as discussed above. To determine this, it is assumed that the converse is true: the mean winds of active and inactive days are the same. A sinusoidal wave is fitted based on this assumption; however, the wind is overall less easterly than predicted by the curve, implying that the mean winds of active and inactive days are different. In particular, the phases reducing strength of easterlies (1–4) and also Phase 5, are less strongly easterly, while the phases increasing strength of easterlies lie roughly on the curve. To confirm this, taking the mean zonal wind of all active (-4.81 m s^{-1}), and inactive days (-5.02 m s^{-1}), and performing a one-sided t test, it is found that the mean zonal winds of active days are less easterly, significant at the 1% level (a similar but weaker result is found using MERRA-2, significant at the 5% level). Despite this asymmetry, it is still possible that rather than the MJO influencing the zonal winds (or vice versa), the correlation could result from a third process influencing both the MJO amplitude and zonal winds separately.

While the MJO can explain some of the interannual and decadal variability of the zonal winds, the fairly weak correlation and low percentage of explained change in mean suggests that other factors must be

involved. Figure 4 shows dry minus wet composites of geopotential height at 700 hPa (Z700), for INTER-ANNUAL and DECADAL. In both the INTERANNUAL and DECADAL the 700 hPa wind anomalies follow closely the gradients in anomaly in Z700, as expected. Figure 4c also shows the 850 hPa temperature for DECADAL. By the hypsometric equation, the geopotential thickness between two layers is directly proportional to the mean temperature within them, and this composite is therefore similar to the geopotential thickness between 700 and 925 hPa (not shown).

In the INTERANNUAL composite (Figure 4a), there is a geopotential anomaly over the eastern Sahel, extending over Arabia. This area is also where both geopotential thickness and Z700 are maximal in the climatology (Figures S1c and S1d). Therefore, in dry years, the maxima in geopotential thickness and Z700 are increased, causing a larger meridional geopotential gradient from the Sahel to the Congo, consistent with increased strength of easterly winds.

In the DECADAL composites (Figures 4c and 4d), there are large similarities between the composites of Z700 and 850 hPa temperature. An anomaly over the eastern Sahel, as in Figure 4a also stands out in both of these, with positive anomalies, reducing in magnitude from 15°N southward through the equator. This again gives an increased geopotential gradient at 700 hPa, consistent with increased strength of easterly winds. Two large anomalies stand out over the west Sahara and Arabian peninsula. These are the approximate locations of the summertime SHL and Arabian Heat Low (AHL). The 700–925 hPa geopotential thickness is a common measure of the strength of the SHL, as defined by Lavaysse et al. (2009), implying that both the SHL and AHL have increased in strength.

Figure 4c shows the latitudinally averaged Z700 across the purple box in Figure 4a, and latitudinal gradient of Z700 multiplied by −1 over this region, for P1, P2, and all years. An increase in Z700 across the region in P2 compared with P1 is evident. There is also a maximum (trough) in the gradient at roughly 10°N, with P2 displaying a stronger maximum. This causes a stronger gradient on the north side of the zonal wind box (5°N: right inset of Figure 4c) while at the southern edge of the box (5°S: left inset of Figure 4c) such a pattern is absent. This shows that the increased meridional geopotential gradient across the zonal wind box is related to the increased geopotential gradient to the north, from the increasingly strong maximum in the Z700 in the eastern Sahel. This is also apparent in MERRA-2 (Figure S2d). In Figure 4d, from P1 to P2, the increase in temperature (and geopotential thickness) is driven by a more rapidly warming eastern Sahel and west Sahara, than over the Congo basin, increasing the meridional geopotential gradient at 700 hPa, with increasingly strong easterly winds over the Congo region and drier East Africa.

Another possible mechanism could be analogous to equatorial superrotation (Dima et al., 2005; Kraucunas & Hartmann, 2005; Yang et al., 2013). Rainfall is associated with organized convection which can excite Rossby wave propagation and convergence of zonal momentum to the source of the disturbances. Further, any regional wind change influences divergence; an easterly anomaly to the west, reducing in magnitude eastward, produces a decrease in moisture flux convergence over East Africa. However this alone is not enough to imply that the zonal winds drive rainfall, as anomalous heating from rainfall can also feed back onto local convergence and circulation.

4. Discussion and Conclusions

This study has investigated the relationship between 700 hPa zonal winds across the Gulf of Guinea and Congo basin, and rainfall during the East African long rains. It was found that the seasonal mean 700 hPa zonal wind over this area is strongly correlated with long rains rainfall totals ($r = 0.73$). Considering periods similar to Wainwright et al. (2019), with a wet (P1: 1979–1997), dry (P2: 1998–2011), and recovery period (P3: 2012–2018), it was found that the same relationship is seen on decadal time scales (P2-P1), showing the importance of the zonal winds to East African climate paradox drying. Meanwhile, a recovery during P3, in agreement with Wainwright et al. (2019), is seen not only in rainfall but also in the zonal winds. The mechanism linking the zonal winds to rainfall on interannual time scales is found to quantitatively explain the long rains drying trend through the decreasing trend in the zonal winds.

The mechanism driving variability in the zonal winds was explored, with some contribution coming from the MJO amplitude, both on interannual and decadal time scales, with wind response to MJO by phase being subtly asymmetric, as seen for rainfall (Vellinga & Milton, 2018). There was a significantly weaker MJO amplitude during P2, accounting for 18% and 13% of the decline in rainfall and wind, respectively.

Meanwhile, another mechanism for the interannual and decadal variability was shown considering changes in geopotential gradients. For interannual variability, these lead to stronger easterlies in drier years due to higher geopotential height over the eastern Sahel, caused by increased warming here, strengthening the geopotential gradient. For decadal variability, a similar mechanism is present but is also aligned to increased heating around Arabia and Sahara regions.

What has not been explored is the source of differing rates of warming between the Sahel and the Congo basin. During the study period, a decadal decline in rainfall over Arabia has been reported (Almazroui et al., 2012), excess heating during this period could be linked to a decadal trend in dust activity over the Arabian Peninsula (Yu et al., 2015), that is also causing a strengthening AHL (Solmon et al., 2015). Wainwright et al. (2019) linked a deepening AHL to faster progression of the tropical rainband over East Africa during the long rains, shortening the season, and Dunning et al. (2018) links a deepening SHL under climate change to a delayed return of the rainband southward in boreal autumn. This motivates further investigation into variations in seasonal Hadley Cell migration, and the associated impacts on zonal flow. The eastern Sahel and Arabia region has experienced a rapid, almost step-like change in temperature around the end of P1 (Almazroui et al., 2012; Attada et al., 2018; Hu et al., 2019; Taylor et al., 2018). The amplified Saharan change in temperature is linked to the observed deepening of the SHL, also responsible for the partial recovery of the Sahelian drought (Evan et al., 2015). Thus the SHL plays two key roles: affecting monsoon onset/ retreat and the latitudinal progression of the rain band (Dunning et al., 2018; Lavaysse et al., 2009), and as shown here by affecting zonal winds across central Africa, which are important for water vapor transport and East African rainfall (Finney et al., 2019). Further strengthening of the SHL is expected under climate change (Biasutti et al., 2009; Dong & Sutton, 2015), which through the above mechanisms could lead to further drying of the long rains.

Based on these results, further understanding of how relative warming rates might change in the future could provide an alternative viewpoint into the future of the long rains through changes in regional dynamics (also supported by Kent et al., 2015). For example, Giannini et al. (2018) demonstrated that in the Coupled Model Intercomparison Project phase 5 (CMIP5; Taylor et al., 2012), a mechanism consistent with wetter years shown here is present during MAM, with moisture advected away from the Congo toward East Africa, linked to a slower overturning circulation under climate change.

While in the long rains, sea surface temperatures (SSTs) are less well connected to rainfall totals than in the short rains, weaker, but significant, relations do exist on both interannual (Ogallo, 1988; Vellinga & Milton, 2018), and longer-term (Bahaga et al., 2019; Liebmann et al., 2014; Williams & Funk, 2011) time scales. Understanding how the processes discussed here are influenced by SSTs could determine their predictability. Given that these zonal winds are of great importance to variability within the long rains, it should be a priority to investigate whether forecast models are able to capture this relationship. This could improve seasonal forecasting and provide useful information on the potential future of the long rains.

Data Availability Statement

All data used in this study can be freely downloaded from the following locations: GPCP data were provided by NOAA/ESRL PSD (www.esrl.noaa.gov/psd/data/gridded/data.gpcp.html) ERA-Interim Reanalysis data were provided by ECMWF (www.ecmwf.int/en/forecasts/datasets/reanalysis-datasets/era-interim). MERRA-2 was provided by the Global Modeling and Assimilation Office, NASA (gmao.gsfc.nasa.gov/reanalysis/MERRA-2/). Daily MJO Index data were provided by the Bureau of Meteorology, Melbourne, Australia (www.bom.gov.au/climate/mjo).

References

Adler, R. F., Huffman, G. J., Chang, A., Ferraro, R., Xie, P.-P., Janowiak, J., et al. (2003). The Version-2 Global Precipitation Climatology Project (GPCP) monthly precipitation analysis (1979-Present). *Journal of Hydrometeorology*, *4*(6), 1147–1167. https://doi.org/10.1175/1525-7541(2003)004<1147:TVGPCP>2.0.CO;2

Almazroui, M., Islam, M. N., Jones, P. D., Athar, H., & Rahman, M. A. (2012). Recent climate change in the Arabian Peninsula: Seasonal rainfall and temperature climatology of Saudi Arabia for 1979–2009. *Atmospheric Research*, *111*, 29–45. https://doi.org/10.1016/j.atmosres.2012.02.013

Attada, R., Dasari, H. P., Chowdary, J. S., Yadav, R. K., Knio, O., & Hoteit, I. (2018). Surface air temperature variability over the Arabian Peninsula and its links to circulation patterns. *International Journal of Climatology*, *39*(1), 445–464. https://doi.org/10.1002/joc.5821

Bahaga, T. K., Fink, A. H., & Knippertz, P. (2019). Revisiting interannual to decadal teleconnections influencing seasonal rainfall in the Greater Horn of Africa during the 20th century. *International Journal of Climatology*, *39*(5), 2765–2785. https://doi.org/10.1002/joc.5986

110

Batté, L., & Déqué, M. (2011). Seasonal predictions of precipitation over Africa using coupled ocean-atmosphere general circulation models: Skill of the ENSEMBLES project multimodel ensemble forecasts. *Tellus, Series A: Dynamic Meteorology and Oceanography*, *63A*(2), 283–299. https://doi.org/10.1111/j.1600-0870.2010.00493.x

Biasutti, M., Sobel, A. H., & Camargo, S. J. (2009). The role of the Sahara low in summertime Sahel rainfall variability and change in the CMIP3 models. *Journal of Climate*, *22*(21), 5755–5771. https://doi.org/10.1175/2009JCLI2969.1

Black, E., Slingo, J., & Sperber, K. R. (2003). An observational study of the relationship between excessively strong short rains in coastal East Africa and Indian Ocean SST. *Monthly Weather Review*, *131*(1), 74–94. https://doi.org/10.1175/1520-0493(2003)131<0074: AOSOTR>2.0.CO;2

Camberlin, P., & Philippon, N. (2002). The East African March-May rainy season: Associated atmospheric dynamics and predictability over the 1968–97 period. *Journal of Climate*, *15*(9), 1002–1019. https://doi.org/10.1175/1520-0442(2002)015<1002:TEAMMR>2.0.CO;2

Camberlin, P., & Wairoto, J. G. (1997). Intraseasonal wind anomalies related to wet and dry spells during the "long" and "short" rainy seasons in Kenya. *Theoretical and Applied Climatology*, *58*(1–2), 57–69. https://doi.org/10.1007/BF00867432

Dee, D. P., Uppala, S. M., Simmons, A. J., Berrisford, P., Poli, P., Kobayashi, S., et al. (2011). The ERA-Interim reanalysis: Configuration and performance of the data assimilation system. *Quarterly Journal of the Royal Meteorological Society*, *137*(656), 553–597. https://doi.org/10.1002/qj.828

Diem, J. E., Sung, H. S., Konecky, B. L., Palace, M. W., Salerno, J., & Hartter, J. (2019). Rainfall characteristics and trends and the role of Congo westerlies in the western Uganda transition zone of equatorial Africa from 1983 to 2017. *Journal of Geophysical Research: Atmospheres*, *124*, 10,712–10,729. https://doi.org/10.1029/2019JD031243

Dima, I. M., Wallace, J. M., & Kraucunas, I. (2005). Tropical zonal momentum balance in the NCEP reanalyses. *Journal of the Atmospheric Sciences*, *62*(7 II), 2499–2513. https://doi.org/10.1175/JAS3486.1

Dong, B., & Sutton, R. (2015). Dominant role of greenhouse-gas forcing in the recovery of Sahel rainfall. *Nature Climate Change*, *5*(8), 757–760. https://doi.org/10.1038/nclimate2664

Dunning, C. M., Black, E., & Allan, R. P. (2018). Later wet seasons with more intense rainfall over Africa under future climate change. *Journal of Climate*, *31*(23), 9719–9738. https://doi.org/10.1175/JCLI-D-18-0102.1

Dutra, E., Magnusson, L., Wetterhall, F., Cloke, H. L., Balsamo, G., Boussetta, S., & Pappenberger, F. (2013). The 2010–2011 drought in the Horn of Africa in ECMWF reanalysis and seasonal forecast products. *International Journal of Climatology*, *33*(7), 1720–1729. https://doi.org/10.1002/joc.3545

Evan, A. T., Flamant, C., Lavaysse, C., Kocha, C., & Saci, A. (2015). Water vapor-forced greenhouse warming over the Sahara desert and the recent recovery from the Sahelian drought. *Journal of Climate*, *28*(1), 108–123. https://doi.org/10.1175/JCLI-D-14-00039.1

Finney, D. L., Marsham, J. H., Walker, D. P., Birch, C. E., Woodhams, B. J., Jackson, L. S., & Hardy, S. (2019). The effect of westerlies on East African rainfall and the associated role of tropical cyclones and the Madden-Julian Oscillation. *Quarterly Journal of the Royal Meteorological Society*, *146*, 647–664. https://doi.org/10.1002/qj.3698

Funk, C. C., Dettinger, M. D., Michaelsen, J. C., Verdin, J. P., Brown, M. E., Barlow, M., & Hoell, A. (2008). Warming of the Indian Ocean threatens eastern and southern African food security but could be mitigated by agricultural development. *Proceedings of the National Academy of Sciences*, *105*(32), 11,081–11,086. https://doi.org/10.1073/pnas.0708196105

Funk, C. C., & Hoell, A. (2015). The leading mode of observed and CMIP5 ENSO-residual sea surface temperatures and associated changes in Indo-Pacific climate. *Journal of Climate*, *28*(11), 4309–4329. https://doi.org/10.1175/JCLI-D-14-00334.1

Funk, C. C., Pedreros, D., Nicholson, S., Hoell, A., Korecha, D., Galu, G., et al. (2019). Examining the potential contributions of extreme Western V sea surface temperatures to the 2017 March-June East African drought. *Bulletin of the American Meteorological Society*, *100*(1), S55–S60. https://doi.org/10.1175/BAMS-D-18-0108.1

Funk, C. C., Senay, G., Asfaw, A., & Verdin, J. (2005). Recent drought tendencies in Ethiopia and equatorial-subtropical eastern Africa. FEWS NET Special Report.

Gelaro, R., McCarty, W., Suárez, M. J., Todling, R., Molod, A., Takacs, L., et al. (2017). The Modern-Era Retrospective Analysis for research and applications, version 2 (MERRA-2). *Journal of Climate*, *30*(14), 5419–5454. https://doi.org/10.1175/JCLI-D-16-0758.1

Giannini, A., Lyon, B., Seager, R., & Vigaud, N. (2018). Dynamical and thermodynamic elements of modeled climate change at the East African margin of convection. *Geophysical Research Letters*, *45*, 992–1000. https://doi.org/10.1002/2017GL075486

Hu, L., Luo, J.-J., Huang, G., & Wheeler, M. C. (2019). Synoptic features responsible for heat waves in Central-Africa, a region with strong multi-decadal trend. *Journal of Climate*, *32*(22), 7951–7970. https://doi.org/10.1175/jcli-d-18-0807.1

Indeje, M., Semazzi, F. H. M., & Ogallo, L. J. (2000). ENSO signals in East African rainfall seasons. *International Journal of Climatology*, *20*(1), 19–46. https://doi.org/10.1002/(SICI)1097-0088(200001)20:1<19::AID-JOC449>3.0.CO;2-0

Kalnay, E., Kanamitsu, M., Kistler, R., Collins, W., Deaven, D., Gandin, L., et al. (1996). The NCEP/NCAR 40-year reanalysis project. *Bulletin of the American Meteorological Society*, *77*(3), 437–472. https://doi.org/10.1175/1520-0477(1996)077<0437:TNYRP>2.0.CO;2

Kendall, M. G. (1975). *Rank correlation methods* (4th ed.). London: Charles Griffin.

Kent, C., Chadwick, R., & Rowell, D. P. (2015). Understanding uncertainties in future projections of seasonal tropical precipitation. *Journal of Climate*, *28*(11), 4390–4413. https://doi.org/10.1175/JCLI-D-14-00613.1

Kilavi, M., MacLeod, D., Ambani, M., Robbins, J., Dankers, R., Graham, R., et al. (2018). Extreme rainfall and flooding over central Kenya including Nairobi city during the long-rains season 2018: Causes, predictability, and potential for early warning and actions. *Atmosphere*, *9*(12), 472. https://doi.org/10.3390/atmos9120472

Kraucunas, I., & Hartmann, D. L. (2005). Equatorial superrotation and the factors controlling the zonal-mean zonal winds in the tropical upper troposphere. *Journal of the Atmospheric Sciences*, *62*(2), 371–389. https://doi.org/10.1175/JAS-3365.1

Lavaysse, C., Flamant, C., Janicot, S., Parker, D. J., Lafore, J. P., Sultan, B., & Pelon, J. (2009). Seasonal evolution of the West African heat low: A climatological perspective. *Climate Dynamics*, *33*(2-3), 313–330. https://doi.org/10.1007/s00382-009-0553-4

Liebmann, B., Hoerling, M. P., Funk, C. C., Bladé, I., Dole, R. M., Allured, D., et al. (2014). Understanding recent eastern Horn of Africa rainfall variability and change. *Journal of Climate*, *27*(23), 8630–8645. https://doi.org/10.1175/JCLI-D-13-00714.1

Liebmann, B., & Smith, C. A. (1996). Description of a complete (interpolated) outgoing longwave radiation dataset. *Bulletin of the American Meteorological Society*, *77*(6), 1275–1277.

Lyon, B. (2014). Seasonal drought in the Greater Horn of Africa and its recent increase during the March-May long rains. *Journal of Climate*, *27*(21), 7953–7975. https://doi.org/10.1175/JCLI-D-13-00459.1

Lyon, B., & Dewitt, D. G. (2012). A recent and abrupt decline in the East African long rains. *Geophysical Research Letters*, *39*, L02702. https://doi.org/10.1029/2011GL050337

Madden, R. A., & Julian, P. R. (1971). Detection of a 40–50 day oscillation in the zonal wind in the tropical Pacific. *Journal of the Atmospheric Sciences*, *28*(5), 702–708. https://doi.org/10.1175/1520-0469(1971)028<0702:DOADOI>2.0.CO;2

111

Madden, R. A., & Julian, P. R. (1972). Description of global-scale circulation cells in the tropics with a 40–50 day period. *Journal of the Atmospheric Sciences*, *29*(6), 1109–1123. https://doi.org/10.1175/1520-0469(1972)029<1109:DOGSCC>2.0.CO;2

Maidment, R. I., Allan, R. P., & Black, E. (2015). Recent observed and simulated changes in precipitation over Africa. *Geophysical Research Letters*, *42*, 8155–8164. https://doi.org/10.1002/2015GL065765

Mann, H. B. (1945). Nonparametric tests against trend. *Econometrica*, *13*(3), 245–259.

Nicholson, S. E. (2017). Climate and climatic variability of rainfall over eastern Africa. *Reviews of Geophysics*, *55*, 590–635. https://doi.org/10.1002/2016RG000544

Nicholson, S. E., & Entekhabi, D. (1986). The quasi-periodic behavior of rainfall variability in Africa and its relationship to the southern oscillation. *Archives for Meteorology, Geophysics, and Bioclimatology Series A*, *34*(3–4), 311–348. https://doi.org/10.1007/BF02257765

Nkunzimana, A., Bi, S., Jiang, T., Wu, W., & Abro, M. I. (2019). Spatiotemporal variation of rainfall and occurrence of extreme events over Burundi during 1960 to 2010. *Arabian Journal of Geosciences*, *12*, 176. https://doi.org/10.1007/s12517-019-4335-y

Ogallo, L. J. (1988). Relationships between seasonal rainfall in East Africa and the Southern Oscillation. *Journal of Climatology*, *8*(1), 31–43. https://doi.org/10.1002/joc.3370080104

Okoola, R. E. (1999a). A diagnostic study of the eastern Africa monsoon circulation during the northern hemisphere spring season. *International Journal of Climatology*, *19*(2), 143–168. https://doi.org/10.1002/(SICI)1097-0088(199902)19:2<143::AID-JOC342>3.0.CO;2-U

Okoola, R. E. (1999b). Midtropospheric circulation patterns associated with extreme dry and wet episodes over equatorial Eastern Africa during the Northern Hemisphere spring. *Journal of Applied Meteorology*, *38*(8), 1161–1169. https://doi.org/10.1175/1520-0450(1999)038<1161:MCPAWE>2.0.CO;2

Otieno, V. O., & Anyah, R. O. (2013). CMIP5 simulated climate conditions of the Greater Horn of Africa (GHA). Part II: Projected climate. *Climate Dynamics*, *41*(7–8), 2099–2113. https://doi.org/10.1007/s00382-013-1694-z

Pohl, B., & Camberlin, P. (2006a). Influence of the Madden-Julian Oscillation on East African rainfall. I: Intraseasonal variability and regional dependency. *Quarterly Journal of the Royal Meteorological Society*, *132*(621), 2521–2539. https://doi.org/10.1256/qj.05.223

Pohl, B., & Camberlin, P. (2006b). Influence of the Madden-Julian Oscillation on East African rainfall. II: March-May season extremes and interannual variability. *Quarterly Journal of the Royal Meteorological Society*, *132*(621), 2541–2558. https://doi.org/10.1256/qj.05.104

Rácz, Z., & Smith, R. K. (1999). The dynamics of heat lows. *Quarterly Journal of the Royal Meteorological Society*, *125*(533), 225–252. https://doi.org/10.1002/qj.49712555313

Rowell, D. P., Booth, B. B. B., Nicholson, S. E., & Good, P. (2015). Reconciling past and future rainfall trends over East Africa. *Journal of Climate*, *28*(24), 9768–9788. https://doi.org/10.1175/JCLI-D-15-0140.1

Saji, N. H., Goswami, B. N., Vinayachandran, P. N., & Yamagata, T. (1999). A dipole mode in the tropical Indian Ocean. *Nature*, *401*(6751), 360–363. https://doi.org/10.1038/43854

Shongwe, M. E., van Oldenborgh, G. J., van den Hurk, B., & van Aalst, M. (2011). Projected changes in mean and extreme precipitation in Africa under global warming. Part II: East Africa. *Journal of Climate*, *24*(14), 3718–3733. https://doi.org/10.1175/2010JCLI2883.1

Solmon, F., Nair, V. S., & Mallet, M. (2015). Increasing Arabian dust activity and the Indian summer monsoon. *Atmospheric Chemistry and Physics*, *15*(14), 8051–8064. https://doi.org/10.5194/acp-15-8051-2015

Taylor, C. M., Fink, A. H., Klein, C., Parker, D. J., Guichard, F., Harris, P. P., & Knapp, K. R. (2018). Earlier seasonal onset of intense mesoscale convective systems in the Congo basin since 1999. *Geophysical Research Letters*, *45*, 13,458–13,467. https://doi.org/10.1029/2018GL080516

Taylor, K. E., Stouffer, R. J., & Meehl, G. A. (2012). An overview of CMIP5 and the experiment design. *Bulletin of the American Meteorological Society*, *93*(4), 485–498. https://doi.org/10.1175/BAMS-D-11-00094.1

Vellinga, M., & Milton, S. F. (2018). Drivers of interannual variability of the East African 'Long Rains'. *Quarterly Journal of the Royal Meteorological Society*, *144*, 861–876. https://doi.org/10.1002/qj.3263

Wainwright, C. M., Marsham, J. H., Keane, R. J., Rowell, D. P., Finney, D. L., Black, E., & Allan, R. P. (2019). 'Eastern African Paradox' rainfall decline due to shorter not less intense Long Rains. *npj Climate and Atmospheric Science*, *2*(1), 1–9. https://doi.org/10.1038/s41612-019-0091-7

Walker, D. P., Birch, C. E., Marsham, J. H., Scaife, A. A., Graham, R. J., & Segele, Z. T. (2019). Skill of dynamical and GHACOF consensus seasonal forecasts of East African rainfall. *Climate Dynamics*, *53*(7), 4911–4935. https://doi.org/10.1007/s00382-019-04835-9

Wheeler, M. C., & Hendon, H. H. (2004). An all-season real-time multivariate MJO Index: Development of an index for monitoring and prediction. *Monthly Weather Review*, *132*(8), 1917–1932. https://doi.org/10.1175/1520-0493(2004)132<1917:AARMMI>2.0.CO;2

Wilks, D. S. (2011). *Statistical methods in the atmospheric sciences* (3rd ed.). Oxford: Elsevier.

Williams, A. P., & Funk, C. C. (2011). A westward extension of the warm pool leads to a westward extension of the Walker circulation, drying eastern Africa. *Climate Dynamics*, *37*(11–12), 2417–2435. https://doi.org/10.1007/s00382-010-0984-y

Yang, W., Seager, R., & Cane, M. A. (2013). Zonal momentum balance in the tropical atmospheric circulation during the global monsoon mature months. *Journal of the Atmospheric Sciences*, *70*(2), 583–599. https://doi.org/10.1175/JAS-D-12-0140.1

Yang, W., Seager, R., Cane, M. A., & Lyon, B. (2014). The East African long rains in observations and models. *Journal of Climate*, *27*(19), 7185–7202. https://doi.org/10.1175/JCLI-D-13-00447.1

Yu, Y., Notaro, M., Liu, Z., Wang, F., Alkolibi, F., Fadda, E., & Bakhrjy, F. (2015). Climatic controls on the interannual to decadal variability in Saudi Arabian dust activity: Toward the development of a seasonal dust prediction model. *Journal of Geophysical Research: Atmospheres*, *120*, 1739–1758. https://doi.org/10.1002/2014JD022611

112

Supporting Information for "Common mechanism for interannual and decadal variability in the East African long rains"

Dean P. Walker[1], Cathryn E. Birch[1], John H. Marsham[1,2], Adam A. Scaife[3,4], Declan L. Finney[1]

[1]School of Earth and Environment, University of Leeds, Leeds, UK

[2]National Centre for Atmospheric Science, Leeds, UK

[3]Met Office Hadley Centre, Exeter, UK

[4]College of Engineering, Mathematics and Physical Sciences, University of Exeter, Exeter, UK

Contents of this file

1. Figures S1 to S2

Introduction

The following supporting information provides climatologies for relevant physical variables over Africa during the long rains referred to in the main text, as well as repeats of some of the key figures within the main text using a different reanalysis dataset, MERRA-2, instead of ERA-Interim. This is to demonstrate robustness of the results between reanalysis datasets. It should be noted that the period of data for MERRA-2 is 1980-2018, rather than 1979-2018 as in ERA-Interim. These figures are not necessary for understanding of results, however, provide useful information for readers.

1
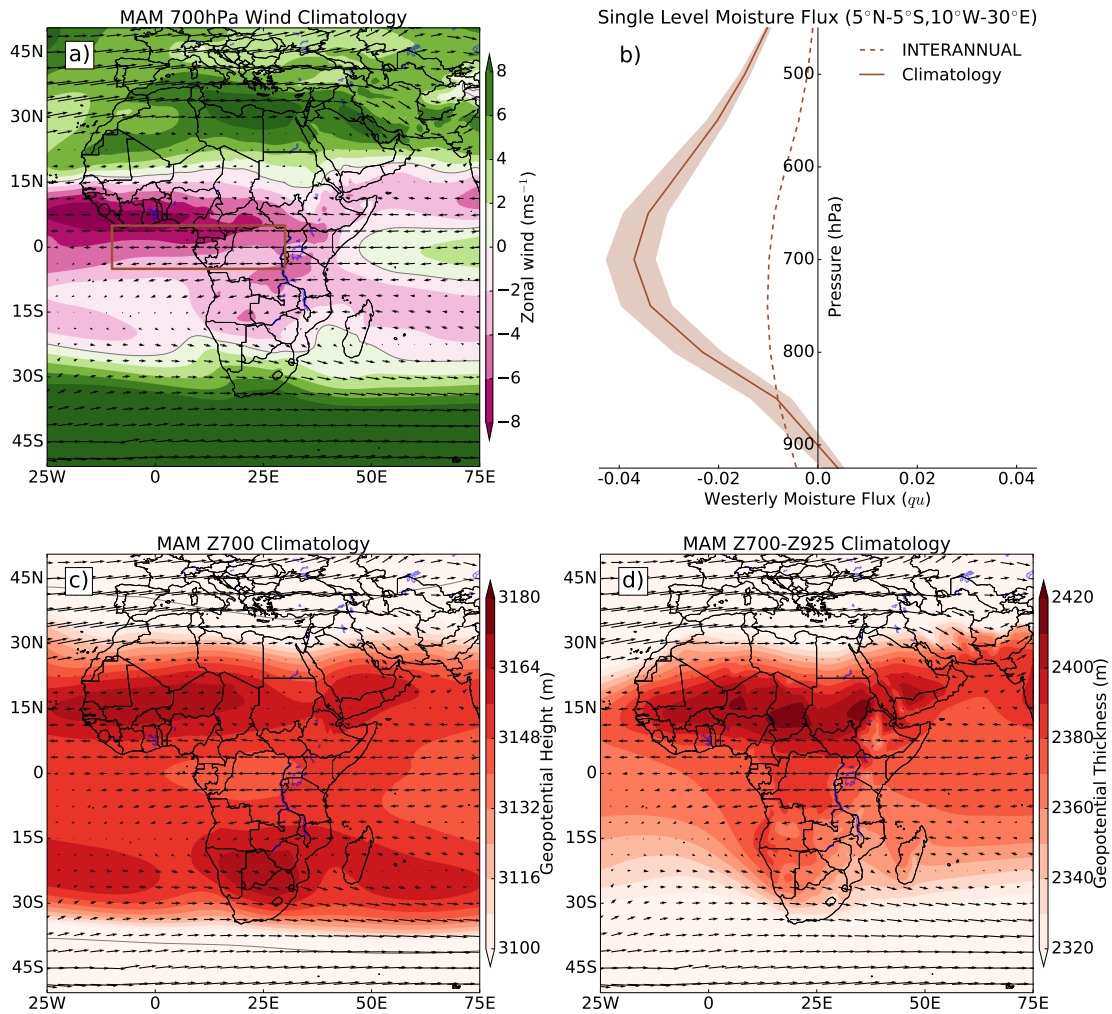
Figure S1. Long rains climatologies. (a) Climatology of 700hPa winds and zonal winds (colours) during MAM. (b) Climatology of single level moisture flux over the brown box in a, during MAM, calculated as monthly mean zonal wind, u, multiplied by monthly mean specific humidity, q, solid line. Shading bounds the moisture flux of the mean of the INTERANNUAL wet years and dry years. Dashed line shows the moisture flux anomaly at each level for INTERANNUAL driest years minus wettest years. (c) Climatology of 700hPa winds and geopotential height (colours) during MAM. (d) Climatology of 700hPa winds and geopotential thickness between 700hPa and 925hPa (colours) during MAM.
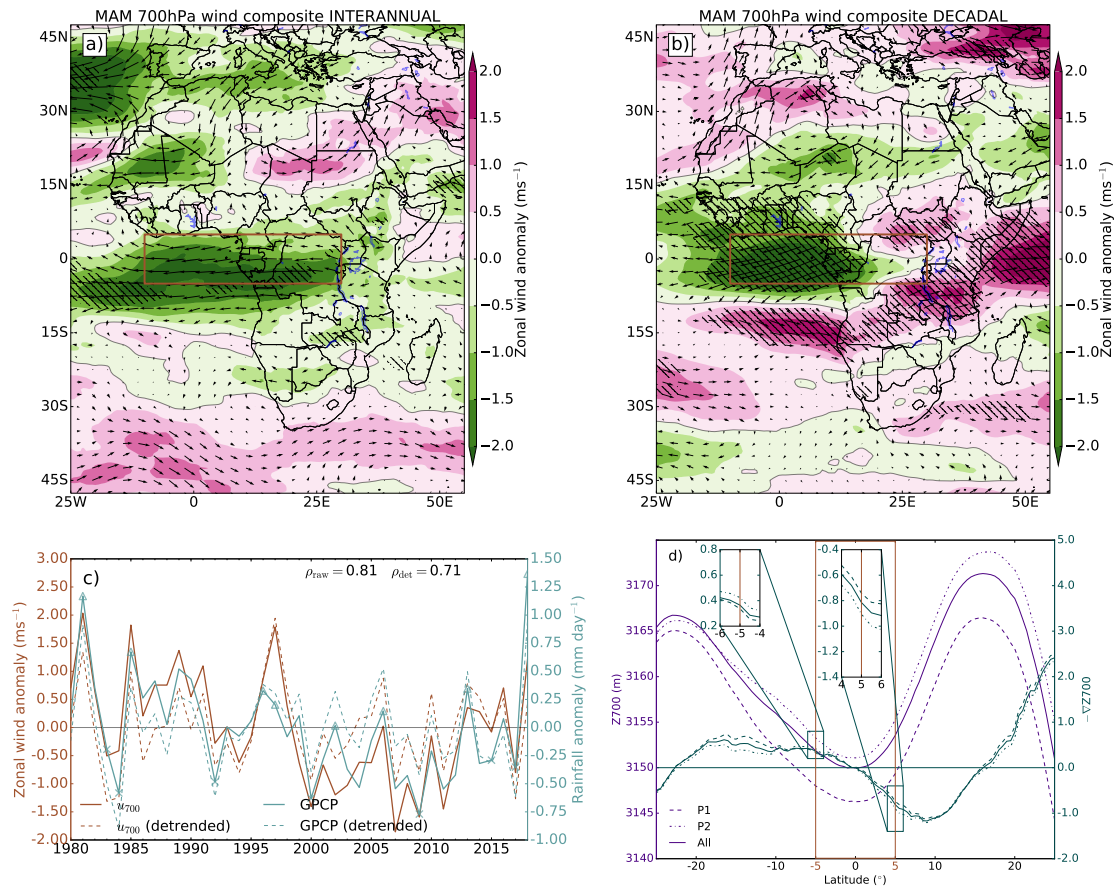
Figure S2. MERRA-2 Reanalysis results. Repeated plots of Figure 1d,e, 2a, 4c, using MERRA-2 instead of ERA-Interim. Composite of 700hPa winds and zonal wind (colours) across Africa during the long rains for (a) driest years minus wettest years, (b) dry period minus wet period (P2−P1). Brown boxes show region used to calculate zonal wind index, hatching shows regions significantly different from 0. (c) Time series of zonal wind anomaly (brown) and rainfall anomaly (blue) for boxes defined in Figure 1, dashed lines show time series after removing linear trends. (d) transect of mean geopotential height (purple) across each latitude for the purple box in Figure 4a, for P1 (dashed), P2 (dash-dotted) and all years (solid). Inset boxes show geopotential gradients zoomed in to edges of zonal wind box (brown box).

Chapter 4.

Skilful dynamical seasonal predictions of the East African long rains with a mid-latitude driver

Prepared for submission to *Geophysical Research Letters.*

Contributions from: John H. Marsham, Adam A. Scaife, Cathryn E. Birch

Abstract

The East African March-May long rains season is poorly forecast by dynamical models in comparison to the short rains. Recent studies have demonstrated that the strength of zonal winds over the Congo basin are tied to long rains rainfall totals. Here this relationship is shown to be reproduced in the UK Met Office dynamical seasonal forecast model, GloSea5. Seasonal predictability of these zonal winds is investigated, with significant negative skill found (r=-0.41), meaning the sign of anomalies are generally inverted. Forecasts correctly predicting the zonal winds produce skilful forecasts of the long rains. The Congo zonal winds are connected to the North Atlantic Oscillation (NAO) by an equatorward propagating Rossby wave, linking the NAO to the long rains (r=0.50). GloSea5 is able to capture this relationship in its ensemble members but not its mean due to a low signal-to-noise ratio. However GloSea5 skilfully forecasts the NAO, offering hope for skilful dynamical predictions of the long rains.

Plan Language Summary

The East African long rains season, from March to May is poorly forecast by dynamical models, used to predict weather and climate. However, winds over the Congo basin have been found to control rainfall over East Africa during this season, with winds moving eastwards towards East Africa producing more rainfall. Here, a dynamical model for seasonal forecasts is used. It is found that the model correctly captures the relationship between eastward winds over the Congo and the East African long rains. However, when the model tries to predict the strength of these winds, it consistently gets the forecast in the opposite direction to the observations. It is found that the winds over the Congo are partly controlled by conditions over the North Atlantic, in particular the pressure gradient between the Azores Islands and Iceland, known as the North Atlantic Oscillation (NAO). The model also reproduces this link, and also can predict changes in the spring NAO, however it underestimates the size of these changes. If the model can further get the size of the changes correct, then it may be able to produce useful forecasts for the East African long rains.

4.1. Introduction

The East Africa region is highly vulnerable to the impacts of weather and climate extremes. In particular, due to the aridity of much of East Africa, droughts are a regular occurrence, for example a year long drought over 2010-11 caused by the failure of two successive rainfall seasons led to widespread famine costing approximately 250,000 lives (FAO and FEWS NET 2013). From approximately the 1980s, rainfall totals during the main rainfall season, the long rains occurring from March to May (MAM), have been declining (Funk et al. 2005, 2008; Lyon and Dewitt 2012; Viste et al. 2013; Liebmann et al. 2014; Hoell and Funk 2014; Rowell et al. 2015). Rainfall totals have somewhat recovered in very recent years (Wainwright et al. 2019). Record breaking rainfall during the 2018 long rains led to flooding and damage to infrastructure, and caused the displacement of approximately 300,000 people (Kilavi et al. 2018). Meanwhile the wet 2020 long rains, following a wet end of 2019, led to record breaking Lake Victoria lake levels, and extensive flooding (Wainwright et al. 2020).

Due to the seasonal nature of rainfall in this region, and the timescales of occurrence of these events, seasonal forecasts can be an invaluable tool in preparing for, mitigating, or even preventing, humanitarian disasters. Over the short rains season occurring from October to December (OND), skilful seasonal forecasts have long been produced, both using statistical (Farmer 1988; Mutai et al. 1998), and dynamical (Batté and Déqué 2011; Bahaga et al. 2016; Walker et al. 2019) models. These largely rely on the teleconnections between the short rains and large-scale modes of variability in sea surface temperatures (SSTs), with links to El Niño-Southern Oscillation (ENSO) in the Pacific Ocean (Ogallo 1988, 1989; Hutchinson 1992; Nicholson and Kim 1997; Indeje et al. 2000; Camberlin et al. 2001) and the Indian Ocean Dipole (IOD), in the Indian Ocean (Saji et al. 1999; Webster et al. 1999; Black et al. 2003; Yamagata et al. 2004; Behera et al. 2005). Such correlations with large-scale modes of variability in SSTs are, however, absent in the long rains (Ogallo 1988; Camberlin and Wairoto 1997; Pohl and Camberlin 2006), and dynamical forecasts have demonstrated little forecast skill (Batté and Déqué 2011; Dutra et al. 2013; Mwangi et al. 2014; Walker et al. 2019). Statistical models of rainfall totals during this season have had slightly more success. Funk et al. (2014) demonstrated that an emerging connection between the long rains and a developing gradient in SSTs in the west Pacific, linked to recent droughts (Williams and Funk 2011), can be used to generate an empirical forecast.

Most other statistical predictions of the long rains have involved the use of atmospheric variables as predictors, finding increased skill compared to using just SSTs (Nicholson

2014, 2015, 2017; Vellinga and Milton 2018). Meanwhile, the technique of using dynamical models to forecast predictable large-scale factors, followed by statistical downscaling using observed or modelled relationships with rainfall, has also been used with some success (Shukla et al. 2014; Colman et al. 2020).

Previous work has highlighted that westerly winds into East Africa originating from over the Congo basin are particularly relevant to the long rains (Nakamura 1968; Okoola 1999a,b; Kilavi et al. 2018; Finney et al. 2019; Walker et al. 2020). Finney et al. (2019) demonstrated that on westerly days during the long rains, there is above average rainfall due to advection of moist air from the Congo. Meanwhile Walker et al. (2020) showed that a strong relationship between 700hPa zonal winds over the Congo basin, and long rains rainfall totals, occurs on both an inter-annual and decadal timescale, offering an explanation for recent East African decadal drying trends.

Motivated by the previous results of statistical forecasts of the long rains using atmospheric variables, the dire need for seasonal forecasts for the long rains season, and the observed relation between westerly winds and the long rains, this work investigates the potential for improved dynamical model predictions of the long rains. Section 4.2 introduces the data used for this study. Section 4.3.1 looks at the observed relationship between westerly winds and East African rainfall in a dynamical seasonal forecast model. Section 4.3.2 further examines the observed relation, and identifies a potential source of predictability in the mid-latitudes, the spring North Atlantic Oscillation (NAO). Section 4.3.3 demonstrates that the NAO is responsible for some of the variability in the long rains, and that this is captured in the dynamical model. Finally Section 4.4 provides a discussion and summary of the results.

4.2. Data and Methods

The dynamical seasonal forecast model used in this study is the UK Met Office Global Seasonal Forecast System version 5 (GloSea5; MacLachlan et al. 2015). GloSea5 is a coupled atmosphere-ocean forecast system. The core of GloSea5 is the Hadley Centre Global Environmental Model version 3 (HadGEM3; Hewitt et al. 2011). It has an horizontal atmospheric resolution of $0.833° \times 0.556°$, with 85 vertical levels. The oceanic component consists of the Nucleus for European Modelling of the Ocean (NEMO; Madec 2016) version 3, with an ocean resolution of $0.25° \times 0.25°$ and 75 vertical levels.

For this study, operational hindcasts are used. These are run alongside the forecast for

the purposes of bias correction and skill estimation. They cover the period 1993-2016. For each initialisation month, 28 members are initialised, with 7 members initialised on 4 fixed dates per month (1st, 9th, 17th, 25th). Members initialised on the same date have their initial conditions perturbed using a stochastic physics scheme (Bowler et al. 2009). Hindcasts run for 210 days from the initialisation date, meaning they cover the 6 full months after the initialisation month. For this study, hindcasts initialised in February are used.

The observational rainfall data for this study are Global Precipitation Climatology Project Version 2.3 (GPCP; Adler et al. 2003), whilst wind and pressure data were obtained from European Centre for Medium-Range Weather Forecasts (ECMWF) Interim Reanalysis (ERA-Interim; Dee et al. 2011). The region of East Africa used here is defined as land areas between 12.5°N to 10°S, 30°E to 52.5°E. The Congo zonal winds were calculated as the mean zonal wind at 700hPa over the region 5°N to 5°S, 10°E to 30°E. In the climatology the zonal winds over the Congo at 700hPa are easterlies, strong enough that on the seasonal timescale they always appear easterly, although they can be westerly on individual days. Positive anomalies from the mean in the zonal winds are westerly anomalies. Composites based upon the zonal winds take the years with the largest westerly anomalies (referred to as weakest easterlies), and subtract them from the years with the largest easterly anomalies (referred to as strongest easterlies).

The North Atlantic Oscillation (NAO) index is defined as the pressure difference between the Azores islands and Iceland. In this study this is defined as the mean sea level pressure difference between boxes located over 45°N to 35°N, 30°W to 10°W for the Azores, and 67.5°N to 57.5°N, 30°W to 10°W for Iceland. In GloSea5, these are shifted 5° northwards, although results are insensitive to slight shifts in the exact definitions of these locations. The pressure difference is then converted to a standardised anomaly, with the mean pressure difference subtracted from the data, then divided by the standard deviation.

All indices in this study are calculated as the seasonal mean over March to May. The period considered for all results is 1993-2016, matching with the years of the GloSea5 hindcasts.

4.3. Results

4.3.1. Seasonal forecasting of the long rains and Congo westerlies in GloSea5

Walker et al. (2020) demonstrated an interannual correlation of approximately 0.7 between the East African long rains (MAM) rainfall totals and zonal wind anomalies at 700hPa over the Congo basin (5°N to 5°S, 10°W to 30°E) during MAM. Figure 4.1a shows a scatter of seasonal mean East African rainfall against seasonal mean zonal winds in a similar, smaller box located at 5°N to 5°S, 10°E to 30°E for both observations and individual ensemble members of GloSea5, over the period 1993-2016. The correlation in observations over this smaller region and shorter period is consistent with the findings of Walker et al. (2020), at 0.72, and is statistically indistinguishable from that of GloSea5 over all ensemble members at 0.68. Considering individual ensemble members separately, a box and whisker diagram of the range of correlations (Figure 4.1a inset) shows that this relationship is captured across all members, with a spread from approximately 0.52 to 0.83, with the observed correlation lying within this range. This all suggests that the ensemble members realistically capture the processes linking the zonal winds and East African rainfall. This is physically reasonable due to the zonal wind box being adjacent to East Africa. Additionally, due to the topography, the air at 700hPa is still relatively moist, and so the strengths of the zonal winds over the Congo are likely tied to the moisture flux into the East Africa region, and through atmospheric water budget constraints, also tied to the rainfall total. Note that the ensemble mean correlation between the zonal winds and rainfall, however, is much weaker (although still significant at the 5% level), at 0.48.

A previous study of the forecasting ability of GloSea5 by Walker et al. (2019) identified that the model performs well at predicting rainfall totals during the short rains, with a correlation of approximately 0.7 with the observations, and generally skilful relative operating characteristic (ROC) scores, whilst forecast skill is lower for the long rains. It is plausible that, due to the strength of connection between the zonal winds over the Congo, and the rainfall, that a lack of skill in forecasting the winds may account for a lack of skill in predicting rainfall. Figure 4.1b shows the correlation coefficient of GloSea5 forecasts of the Congo zonal winds over MAM against observations as a function of ensemble size, where ensembles of each size are repeatedly randomly generated from the available members to obtain a mean correlation. This process is repeated to examine the ability of the model to predict itself, by replacing the observations with
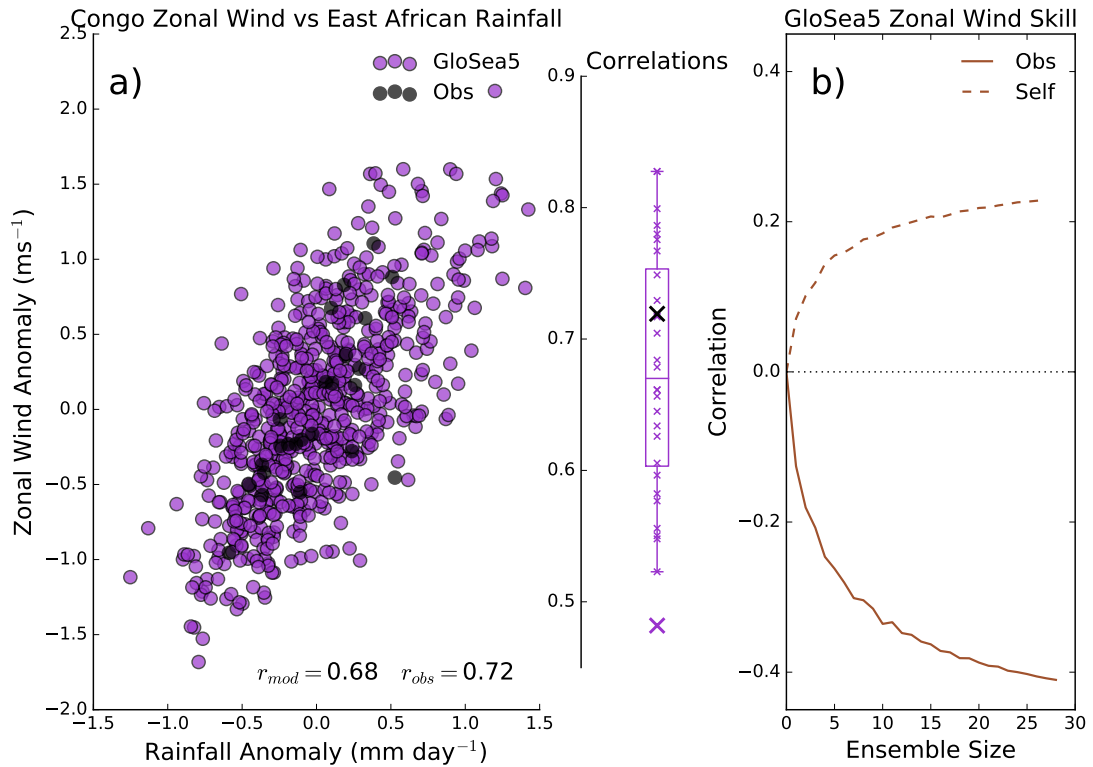
Figure 4.1.: East African rainfall and Congo winds. a) Scatter of March-May (MAM) seasonal mean 700hPa zonal wind over the Congo against rainfall over East Africa, for observations (black) and individual ensemble members of GloSea5 (purple) for 1993-2016. The r-value at the bottom is the correlation of all model points. Inset box and whisker plot of correlation coefficients of zonal wind against rainfall for individual GloSea5 ensemble members. Small purple crosses show individual ensemble member samples of equal size to the observed record, large purple cross shows ensemble mean correlation, the black cross shows observed correlation. b) Correlation coefficient of GloSea5 forecast Congo zonal wind against observations, as a function of ensemble size (solid). Ensembles of each size are generated through selecting random members of the ensemble, and repeating 1000 times. The dashed line is the correlation when replacing observations with one member of the ensemble.

a single random ensemble member each time. This can be considered as a measure to estimate how well the forecast may be able to predict the observations, however, recent studies have found a signal-to-noise paradox in seasonal forecasts, whereby the forecasts are more capable of predicting the observations than themselves (Scaife et al. 2014; Eade et al. 2014; Scaife and Smith 2018). In Figure 4.1b the comparison against observations demonstrates a striking negative correlation, that consistently increases in magnitude with increased ensemble size, giving a significant negative correlation value of -0.41 between the observations and model when the full ensemble is considered, which indicates that the model tends to forecast variations in the wind to be in the opposite direction to those observed. In contrast, comparing the model against itself leads to a weakly positive correlation.

This significant negative correlation leads to the conclusion that there may indeed be predictability for the long rains within dynamical models through correct prediction of these zonal winds. As the model is capable of predicting the observed variability in the zonal winds (albeit with a reversed sign), then, given the correct physics in the model linking the zonal winds and the rainfall, forecasting of the rainfall is theoretically possible.

To demonstrate the potential for predictability, for each year of the hindcast period, only ensemble members who correctly forecast the sign of the anomaly of the zonal winds relative to the mean were taken, and their rainfall predictions used to calculate an adjusted ensemble mean. A time series of these predictions is shown in Figure 4.2. Corrected zonal winds in an adjusted ensemble are shown in Figure 4.2a, with circles marking ensemble members that forecast the correct sign of the anomaly of the zonal wind. Doing this unsurprisingly leads to a very high correlation between the observed and predicted zonal wind, and this smaller ensemble now represents an ensemble that correctly forecasts the zonal winds. By looking at the rainfall predictions in this smaller ensemble, shown in 4.2b, the correlation between the adjusted ensemble mean and observed rainfall is found to be 0.71, compared to the original ensemble correlation of 0.16. This sensitivity test confirms that correct forecasts of the zonal winds would vastly improve dynamical model forecasts of long rains rainfall.

4.3.2. Predictability of zonal wind variability

Practically, it is impossible to determine in advance which ensemble members will correctly forecast the sign of the zonal wind anomaly. However, given the results of the
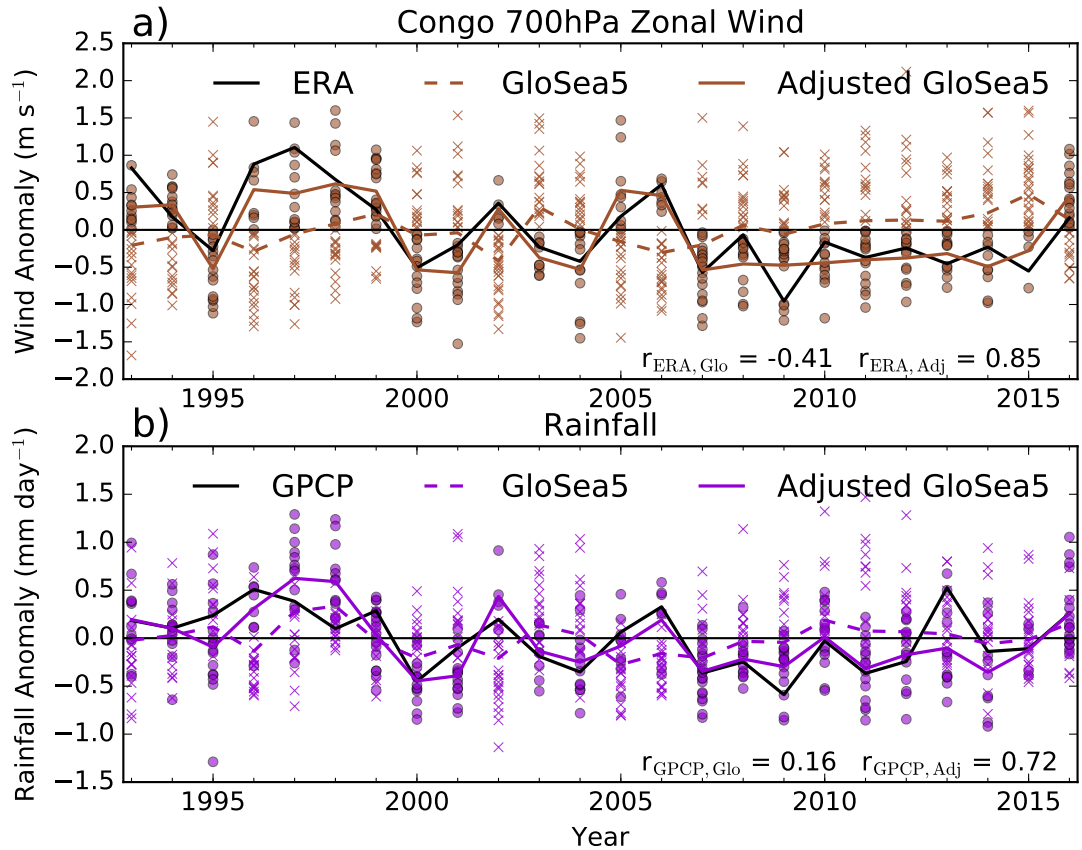
Figure 4.2.: Time series of a) Congo 700hPa zonal wind, and b) East African rainfall, for observations (GPCP/ERA-Interim; solid black lines), GloSea5 ensemble mean (dashed coloured lines), and adjusted GloSea5 ensemble mean (solid coloured lines). Scatter points show GloSea5 ensemble members for each year. The adjusted ensemble uses only the ensemble members that correctly predicted the sign of the zonal wind anomaly (shown with circles), whilst crosses show those members that incorrectly predicted the sign of the zonal wind and so are excluded from the adjusted ensemble. Correlations of the original and adjusted ensembles with observations are given in the bottom right corner.

previous section, if there exists potential for skilful prediction of the zonal winds over the Congo, then it follows that dynamical model skill in predicting the long rains would also improve. To understand the context of the zonal wind anomalies over the Congo within the larger-scale atmospheric circulation, composites are created containing years of the largest anomalies of the zonal winds, to investigate potential sources of the anomalies. Figure 4.3 shows composites of the weakest easterly minus strongest easterly years of mean zonal wind within the Congo box, for observations, and ensemble members of GloSea5. In addition to the expected (due to the design of the composite) westerly anomaly over the Congo, a pattern of alternating anomalous easterly and westerly winds, oriented with a diagonal tilt from southwest to northeast, are apparent from the Congo up to the north Atlantic. In particular, these zonal winds appear connected to the northern hemisphere extratropical jet, with opposing wind anomalies over the north Atlantic near Iceland, and the Azores islands, in a pattern reminiscent of the North Atlantic Oscillation (NAO). This pattern is also present in the GloSea5 composite, and stands out as the only one of any magnitude here. There are however some notable biases between the two composites; in particular over northern Africa, extending over the tropical Atlantic Ocean, where the sign of the anomaly in GloSea5 is reversed in comparison to ERA-Interim. This may be related to previously observed biases over the Atlantic Ocean, common in many dynamical models (e.g. Richter et al. 2012).

It has previously been shown that GloSea5 can skilfully predict the NAO during boreal winter (Scaife et al. 2014). If skill extends into spring this leads to the possibility that the long rains may in fact be predictable via the equatorward propagating Rossby wave train in Figure 4.3.

4.3.3. The North Atlantic Oscillation and the long rains

Figure 4.4a-c show composites of zonal winds, similar to those seen in Figure 4.3 but for negative NAO years minus positive NAO years, for observations, GloSea5 ensemble members, and ensemble mean respectively. In Figure 4.4a,b, the previously observed patterns of zonal wind anomalies starting over the North Atlantic and extending equatorward are still present. The correlations within observations between the MAM NAO index and the MAM Congo zonal winds, and between the MAM NAO index and long rains rainfall are -0.39 and -0.49 respectively, both significant at 5% level. This relationship is also well captured within the ensemble members, with mean correlations of -0.37 and -0.42 respectively. The negative sign here means that the Congo winds are more easterly during a positive NAO. However, in Figure 4.4c, the ensemble mean
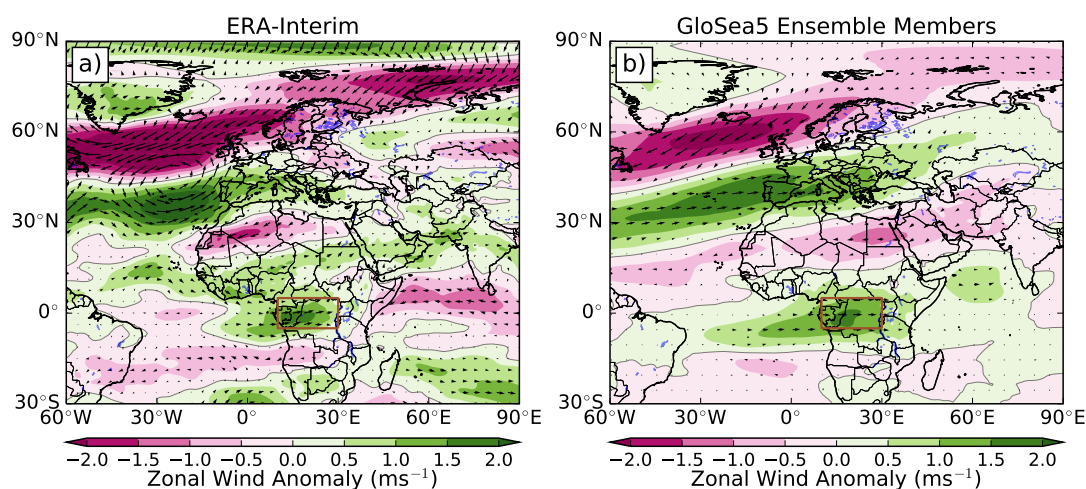
Figure 4.3.: Composite of 700hPa winds (arrows) and zonal winds (colours) over MAM, using years of weakest easterlies over the Congo (brown box) minus years of strongest easterlies over the Congo, for a) ERA-Interim, and b) GloSea5 ensemble members. Years used in the composites are determined within their own datasets.

fails to capture this relationship. The amplitude of the zonal wind anomalies is much smaller over the North Atlantic, and so the teleconnection fails to reach the zonal winds over the Congo. This is reflected in the fact that the ensemble members capture the correlation between the NAO and zonal winds seen in the observations, meanwhile the ensemble mean does not (correlations of the ensemble mean NAO against rainfall and zonal wind are found to not be significantly different from zero). As the ensemble mean measures the predictable component of the variability, this lack of teleconnection could mean the relationship is unpredictable, or that there is an error related to the amplitude of the NAO signal.

The ability of the ensemble mean to predict the NAO during MAM is investigated. It is found that the correlation skill between the ensemble mean NAO and the observed NAO index is 0.51, significant at the 5% level. Figure 4.4d shows a repeat of Figure 4.1b for the NAO, with correlation of GloSea5 against observations, as a function of ensemble size. The dashed line also shows the correlation against a single randomly chosen ensemble member. From this, several things are apparent. Firstly, that GloSea5 is capable of predicting the spring NAO. Secondly, given the shape of the curve, a larger ensemble could still add a reasonable improvement to the skill. Thirdly, the model's ability to predict itself is low. This is in agreement with Scaife et al. (2014), who found good forecast skill in winter in predicting the NAO, but showed a similar error in winter forecasts.
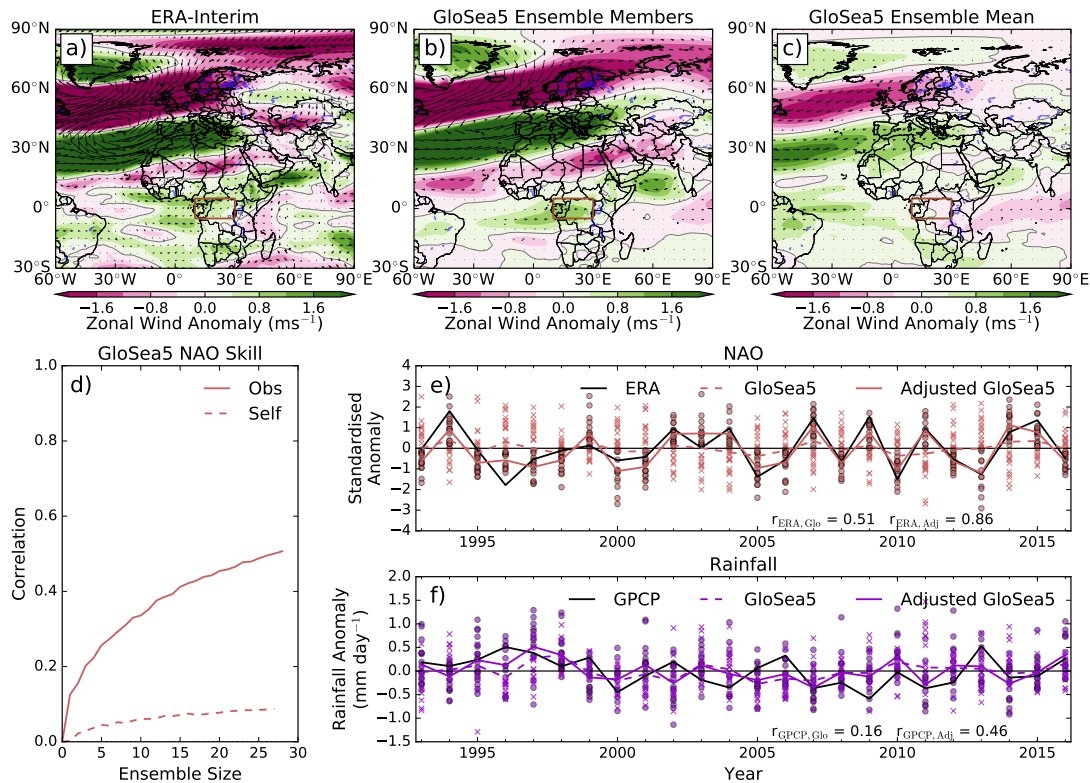
Figure 4.4.: Composite of 700hPa winds (arrows) and zonal winds (colours) over MAM, using years of negative NAO index minus years of positive NAO index, for a) ERA-Interim, b) GloSea5 ensemble members, and c) GloSea5 ensemble mean. Years used in the composites are determined within their own datasets. d) Correlation coefficient of GloSea5 forecast MAM seasonal mean NAO index against observations, as a function of ensemble size (solid). Ensembles of each size are generated through selecting random members of the ensemble, and repeated 1000 times. Dashed line is correlation when replacing observations with one member of the ensemble. Time series of e) NAO, and f) East African rainfall, for observations (GPCP/ERA-Interim; solid black lines), GloSea5 ensemble mean (dashed coloured lines), and adjusted GloSea5 ensemble mean (solid coloured lines). Scatter points show GloSea5 ensemble members for each year. The adjusted ensemble uses only the ensemble members that correctly predicted the sign of the NAO index (shown with circles), whilst crosses show those members that incorrectly predicted the sign of the NAO index and so are excluded from the adjusted ensemble. Correlations of the original and adjusted ensembles with observations are given in the bottom right corner.

The NAO in the ensemble mean, although well predicted, is too small, and so the teleconnections relating it to East Africa are hidden by noise. However, if the technique applied to the ensemble using zonal winds in Figure 4.2, is applied to the NAO, the impact of better NAO forecasts can be measured. Selecting only the ensemble members correctly forecasting the sign of the NAO, generates an ensemble with a larger amplitude NAO (Figure 4.4e). Considering East African rainfall in this case (shown in Figure 4.4f), a correlation of 0.46 with the observations is found. This is statistically significant at 5% level, and further demonstrates that the long rains are indeed predictable.

4.4. Discussion and Conclusions

There has long been a contrast in the seasonal forecasting skill of the long rains and short rains over East Africa (Walker et al. 2019). Meanwhile recent work has demonstrated the potential importance of westerly winds originating from over the Congo basin in controlling inter-annual variability in the long rains (Finney et al. 2019; Walker et al. 2020). This study has investigated whether such a relationship between the zonal winds over the Congo and East African rainfall during the long rains exists in a dynamical seasonal forecast model, GloSea5. It was found that not only did the dynamical model capture this relationship, but that there was the potential for predictability of the zonal winds within the model. However, the sign of the correlation of the forecast zonal winds and the observed was negative. It was demonstrated that correct predictions of the zonal winds would allow skilful seasonal forecasts for the long rains.

The study then investigated potential sources of predictability of the Congo zonal winds. Considering composites of weak and strong zonal winds years, a Rossby wavetrain was observed in both the model and the observations connecting the Congo winds to the mid-latitudes, in particular, over the Atlantic Ocean. This suggested the possible role of the North Atlantic Oscillation (NAO), which has previously been shown to be predictable in GloSea5 in boreal winter.

Further investigation into the NAO using composites of zonal winds demonstrated that the NAO does indeed contribute to zonal wind variability over the Congo basin. This was seen in both the observations, and captured in GloSea5 ensemble members. Significant correlations between the NAO and Congo zonal winds and East African rainfall were found. The teleconnection was found to be absent in the ensemble mean however, which also displayed a much reduced amplitude of the NAO. It was found that, in agreement with previous studies looking at boreal winter NAO there is a weak signal-

to-noise ratio in the spring NAO forecasts (Scaife et al. 2014; Eade et al. 2014; Scaife and Smith 2018; Smith et al. 2020); the NAO is predictable, however it's amplitude is small given the high correlation, and so its teleconnections are overwhelmed by noise. Considering an ensemble with an increased NAO amplitude demonstrates that a skilful forecast of the East African long rains can be produced.

The question still remains over why GloSea5 demonstrates negative skill in forecasting the Congo zonal winds in the ensemble mean: the forecast predicts stronger easterlies when weaker easterlies are observed and vice versa. Given the signal linking the NAO to the Congo zonal winds disappears in the ensemble mean, other factors must be controlling them. It is likely that biases within the model are partly responsible. Previous studies have identified several SST biases, particularly over the Atlantic which are likely to be relevant here, common to many dynamical models (Richter et al. 2012). These biases are likely to have effects on the mean state of the circulation in this region, that could affect predictability. The presence of such biases should be checked within GloSea5, and sensitivity experiments (such as nudging experiments pushing found biases towards observations) could be performed to examine whether this improves the zonal wind predictions. Further analysis could also be performed to investigate the Rossby wave mechanism, such as using ray-tracing. Differences in the mean state circulation between observations and the model could alter the Rossby wavetrain, leading to a misplaced teleconnection which may also help explain the negative predictability within GloSea5.

Acknowledgements

GloSea5 seasonal forecasts were generated by the UK Met Office and provided by the Copernicus Climate Change Service (C3S) Climate Data Store (`https://cds.climate.copernicus.eu/`).

References

Adler, R. F., Huffman, G. J., Chang, A., Ferraro, R., Xie, P.-P., Janowiak, J., Rudolf, B., Schneider, U., Curtis, S., Bolvin, D., Gruber, A., Susskind, J., Arkin, P., and Nelkin, E. (2003). The Version-2 Global Precipitation Climatology Project (GPCP) monthly precipitation analysis (1979-Present). *Journal of Hydrometeorology*, 4(6):1147–1167.

Bahaga, T. K., Kucharski, F., Tsidu, G. M., and Yang, H. (2016). Assessment of prediction and predictability of short rains over equatorial East Africa using a multi-model ensemble. *Theoretical and Applied Climatology*, 123(3-4):637–649.

Batté, L. and Déqué, M. (2011). Seasonal predictions of precipitation over Africa using coupled ocean-atmosphere general circulation models: Skill of the ENSEMBLES project multimodel ensemble forecasts. *Tellus, Series A: Dynamic Meteorology and Oceanography*, 63A(2):283–299.

Behera, S. K., Luo, J. J., Masson, S., Delecluse, P., Gualdi, S., Navarra, A., and Yamagata, T. (2005). Paramount impact of the Indian ocean dipole on the East African short rains: A CGCM study. *Journal of Climate*, 18(21):4514–4530.

Black, E., Slingo, J., and Sperber, K. R. (2003). An observational study of the relationship between excessively strong short rains in coastal East Africa and Indian Ocean SST. *Monthly Weather Review*, 131(1):74–94.

Bowler, N. E., Arribas, A., Beare, S. E., Mylne, K. R., and Shutts, G. J. (2009). The local ETKF and SKEB: Upgrades to the MOGREPS short-range ensemble prediction system. *Quarterly Journal of the Royal Meteorological Society*, 135:767–776.

Camberlin, P., Janicot, S., and Poccard, I. (2001). Seasonality and atmospheric dynamics of the teleconnection between African rainfall and tropical sea-surface temperature: Atlantic vs. ENSO. *International Journal of Climatology*, 21(8):973–1005.

Camberlin, P. and Wairoto, J. G. (1997). Intraseasonal wind anomalies related to wet and dry spells during the "long" and "short" rainy seasons in Kenya. *Theoretical and Applied Climatology*, 58(1-2):57–69.

Colman, A. W., Graham, R. J., and Davey, M. K. (2020). Direct and indirect seasonal rainfall forecasts for East Africa using global dynamical models. *International Journal of Climatology*, 40(2):1132–1148.

Dee, D. P., Uppala, S. M., Simmons, A. J., Berrisford, P., Poli, P., Kobayashi, S., Andrae, U., Balmaseda, M. A., Balsamo, G., Bauer, P., Bechtold, P., Beljaars, A. C., van de Berg, L., Bidlot, J., Bormann, N., Delsol, C., Dragani, R., Fuentes, M., Geer, A. J., Haimberger, L., Healy, S. B., Hersbach, H., Hólm, E. V., Isaksen, L., Kållberg, P., Köhler, M., Matricardi, M., Mcnally, A. P., Monge-Sanz, B. M., Morcrette, J. J., Park, B. K., Peubey, C., de Rosnay, P., Tavolato, C., Thépaut, J. N., and Vitart, F. (2011). The ERA-Interim reanalysis: configuration and performance of the data assimilation system. *Quarterly Journal of the Royal Meteorological Society*, 137(656):553–597.

Dutra, E., Magnusson, L., Wetterhall, F., Cloke, H. L., Balsamo, G., Boussetta, S., and Pappenberger, F. (2013). The 2010-2011 drought in the Horn of Africa in ECMWF reanalysis and seasonal forecast products. *International Journal of Climatology*, 33(7):1720–1729.

Eade, R., Smith, D., Scaife, A., Wallace, E., Dunstone, N., Hermanson, L., and Robinson, N. (2014). Do seasonal-to-decadal climate predictions underestimate the predictability of the real world? *Geophysical Research Letters*, 41(15):5620–5628.

FAO and FEWS NET (2013). Mortality among populations of southern and central Somalia affected by severe food insecurity and famine during 2010-2012. Available at: `https://reliefweb.int/report/somalia/mortality-among-populations-southern-and-central-somalia-affected-severe-food`. Last accessed: 22 September 2020.

Farmer, G. (1988). Seasonal forecasting of the Kenya coast short rains, 1901-84. *Journal of Climatology*, 8(5):489–497.

Finney, D. L., Marsham, J. H., Walker, D. P., Birch, C. E., Woodhams, B. J., Jackson, L. S., and Hardy, S. (2019). The effect of westerlies on East African rainfall and the associated role of tropical cyclones and the Madden-Julian Oscillation. *Quarterly Journal of the Royal Meteorological Society*.

Funk, C. C., Dettinger, M. D., Michaelsen, J. C., Verdin, J. P., Brown, M. E., Barlow, M., and Hoell, A. (2008). Warming of the Indian Ocean threatens eastern and southern African food security but could be mitigated by agricultural development. *Proceedings of the National Academy of Sciences*, 105(32):11081–11086.

Funk, C. C., Hoell, A., Shukla, S., Bladé, I., Liebmann, B., Roberts, J. B., Robertson, F. R., and Husak, G. (2014). Predicting East African spring droughts using Pacific

and Indian Ocean sea surface temperature indices. *Hydrology and Earth System Sciences*, 18(12):4965–4978.

Funk, C. C., Senay, G., Asfaw, A., and Verdin, J. (2005). Recent drought tendencies in Ethiopia and equatorial-subtropical eastern Africa. *FEWS NET Special Report*.

Hewitt, H. T., Copsey, D., Culverwell, I. D., Harris, C. M., Hill, R. S., Keen, A. B., McLaren, A. J., and Hunke, E. C. (2011). Design and implementation of the infrastructure of HadGEM3: The next-generation Met Office climate modelling system. *Geoscientific Model Development*, 4(2):223–253.

Hoell, A. and Funk, C. C. (2014). Indo-Pacific sea surface temperature influences on failed consecutive rainy seasons over eastern Africa. *Climate Dynamics*, 43(5-6):1645–1660.

Hutchinson, P. (1992). The Southern Oscillation and prediction of "Der" season rainfall in Somalia. *Journal of Climate*, 5(5):525–531.

Indeje, M., Semazzi, F. H., and Ogallo, L. J. (2000). ENSO signals in East African rainfall seasons. *International Journal of Climatology*, 20(1):19–46.

Kilavi, M., MacLeod, D., Ambani, M., Robbins, J., Dankers, R., Graham, R., Helen, T., Salih, A. A., and Todd, M. C. (2018). Extreme rainfall and flooding over central Kenya including Nairobi city during the long-rains season 2018: Causes, predictability, and potential for early warning and actions. *Atmosphere*, 9(12).

Liebmann, B., Hoerling, M. P., Funk, C. C., Bladé, I., Dole, R. M., Allured, D., Quan, X., Pegion, P., and Eischeid, J. K. (2014). Understanding recent eastern Horn of Africa rainfall variability and change. *Journal of Climate*, 27(23):8630–8645.

Lyon, B. and Dewitt, D. G. (2012). A recent and abrupt decline in the East African long rains. *Geophysical Research Letters*, 39(2):L02702.

MacLachlan, C., Arribas, A., Peterson, K. A., Maidens, A., Fereday, D., Scaife, A. A., Gordon, M., Vellinga, M., Williams, A., Comer, R. E., Camp, J., Xavier, P., and Madec, G. (2015). Global Seasonal forecast system version 5 (GloSea5): a high-resolution seasonal forecast system. *Quarterly Journal of the Royal Meteorological Society*, 141(689):1072–1084.

Madec, G. (2016). NEMO ocean engine, Note du Pôle de modélisation. Technical report.

Mutai, C. C., Ward, M. N., and Colman, A. W. (1998). Towards the prediction of the East Africa short rains based on sea-surface temperature-atmosphere coupling. *International Journal of Climatology*, 18(9):975–997.

Mwangi, E., Wetterhall, F., Dutra, E., Di Giuseppe, F., and Pappenberger, F. (2014). Forecasting droughts in East Africa. *Hydrology and Earth System Sciences*, 18(2):611–620.

Nakamura, K. (1968). Equatorial westerlies over East Africa and their climatological significance. *Geographical Review of Japan*, 41(6):359–373.

Nicholson, S. E. (2014). The predictability of rainfall over the Greater Horn of Africa. Part I: Prediction of seasonal rainfall. *Journal of Hydrometeorology*, 15(3):1011–1027.

Nicholson, S. E. (2015). The predictability of rainfall over the Greater Horn of Africa. Part II: Prediction of monthly rainfall during the long rains. *Journal of Hydrometeorology*, 16(5):2001–2012.

Nicholson, S. E. (2017). Climate and climatic variability of rainfall over eastern Africa. *Reviews of Geophysics*, 55(3):590–635.

Nicholson, S. E. and Kim, J. (1997). The relationship of the El Niño Southern Oscillation to African rainfall. *International Journal of Climatology*, 17(2):117–135.

Ogallo, L. J. (1988). Relationships between seasonal rainfall in East Africa and the Southern Oscillation. *Journal of Climatology*, 8(1):31–43.

Ogallo, L. J. (1989). The spatial and temporal patterns of the East African seasonal rainfall derived from principal component analysis. *International Journal of Climatology*, 9(2):145–167.

Okoola, R. E. (1999a). A diagnostic study of the eastern Africa monsoon circulation during the northern hemisphere spring season. *International Journal of Climatology*, 19(2):143–168.

Okoola, R. E. (1999b). Midtropospheric Circulation Patterns Associated with Extreme Dry and Wet Episodes over Equatorial Eastern Africa during the Northern Hemisphere Spring. *Journal of Applied Meteorology*, 38(8):1161–1169.

Pohl, B. and Camberlin, P. (2006). Influence of the Madden-Julian Oscillation on East African rainfall. II: March-May season extremes and interannual variability.

Quarterly Journal of the Royal Meteorological Society, 132(621):2541–2558.

Richter, I., Xie, S. P., Wittenberg, A. T., and Masumoto, Y. (2012). Tropical Atlantic biases and their relation to surface wind stress and terrestrial precipitation. *Climate Dynamics*, 38(5-6):985–1001.

Rowell, D. P., Booth, B. B., Nicholson, S. E., and Good, P. (2015). Reconciling past and future rainfall trends over East Africa. *Journal of Climate*, 28(24):9768–9788.

Saji, N. H., Goswami, B. N., Vinayachandran, P. N., and Yamagata, T. (1999). A dipole mode in the tropical Indian ocean. *Nature*, 401(6751):360–363.

Scaife, A. A., Arribas, A., Blockey, E., Brookshaw, A., Clark, R. T., Dunstone, N., Eade, R., Fereday, D., Folland, C. K., Gordon, M., Hermanson, L., Knight, J. R., Lea, D. J., MacLachlan, C., Maidens, A., Martin, M., Peterson, A. K., Smith, D., Vellinga, M., Wallace, E., Waters, J., and Williams, A. (2014). Skillful long range prediction of European and North American winters. *Geophysical Research Letters*, 5(7):2514–2519.

Scaife, A. A. and Smith, D. (2018). A signal-to-noise paradox in climate science. *npj Climate and Atmospheric Science*, 1(1):28.

Shukla, S., Funk, C. C., and Hoell, A. (2014). Using constructed analogs to improve the skill of National Multi-Model Ensemble March-April-May precipitation forecasts in equatorial East Africa. *Environmental Research Letters*, 9(9):094009.

Smith, D. M., Scaife, A. A., Eade, R., Athanasiadis, P., Bellucci, A., Bethke, I., Bilbao, R., Borchert, L. F., Caron, L. P., Counillon, F., Danabasoglu, G., Delworth, T., Doblas-Reyes, F. J., Dunstone, N. J., Estella-Perez, V., Flavoni, S., Hermanson, L., Keenlyside, N., Kharin, V., Kimoto, M., Merryfield, W. J., Mignot, J., Mochizuki, T., Modali, K., Monerie, P. A., Müller, W. A., Nicolí, D., Ortega, P., Pankatz, K., Pohlmann, H., Robson, J., Ruggieri, P., Sospedra-Alfonso, R., Swingedouw, D., Wang, Y., Wild, S., Yeager, S., Yang, X., and Zhang, L. (2020). North Atlantic climate far more predictable than models imply. *Nature*, 583(7818):796–800.

Vellinga, M. and Milton, S. (2018). Drivers of interannual variability of the East African 'Long Rains'. *Quarterly Journal of the Royal Meteorological Society*.

Viste, E., Korecha, D., and Sorteberg, A. (2013). Recent drought and precipitation tendencies in Ethiopia. *Theoretical and Applied Climatology*, 112(3-4):535–551.

Wainwright, C. M., Finney, D. L., Kilavi, M., Black, E., and Marsham, J. H. (2020). Extreme rainfall in East Africa, October 2019–January 2020 and context under future climate change. *Weather*.

Wainwright, C. M., Marsham, J. H., Keane, R. J., Rowell, D. P., Finney, D. L., Black, E., and Allan, R. P. (2019). 'Eastern African Paradox' rainfall decline due to shorter not less intense Long Rains. *npj Climate and Atmospheric Science*, 2(1):1–9.

Walker, D. P., Birch, C. E., Marsham, J. H., Scaife, A. A., Graham, R. J., and Segele, Z. T. (2019). Skill of dynamical and GHACOF consensus seasonal forecasts of East African rainfall. *Climate Dynamics*, 53(7):4911–4935.

Walker, D. P., Marsham, J. H., Birch, C. E., Scaife, A. A., and Finney, D. L. (2020). Common mechanism for inter-annual and decadal variability in the East African long rains. *Geophysical Research Letters*.

Webster, P. J., Moore, A. M., Loschnigg, J. P., and Leben, R. R. (1999). Coupled ocean-atmosphere dynamics in the Indian Ocean during 1997-98. *Nature*, 401(6751):356–360.

Williams, A. P. and Funk, C. C. (2011). A westward extension of the warm pool leads to a westward extension of the Walker circulation, drying eastern Africa. *Climate Dynamics*, 37(11-12):2417–2435.

Yamagata, T., Behera, S. K., Luo, J.-J., Masson, S., Jury, M. R., and Rao, S. A. (2004). Coupled ocean-atmosphere variability in the tropical Indian Ocean. In *Earth's Climate*, pages 189–211.

Chapter 5.

Conclusions

5.1. Overview

The aim of this thesis was to improve the current state of understanding of the predictability and variability of the rainfall seasons in East Africa, in particular considering seasonal forecasts. It aimed to do this through evaluating seasonal forecasts to identify weaknesses before investigating physical processes controlling rainfall variability. This work is important for improvements to seasonal forecasting, in order to develop early warning systems for high impact events such as widespread droughts. A recent example is the 2010-11 drought that cost as many as a quarter of a million lives through failed harvests leading to famine (FAO and FEWS NET 2013). Additionally, due to the high percentage contribution of agriculture to gross domestic product (GDP) in the region, improvements to seasonal forecasts would allow increased productivity of crop growth, boosting economic development.

In Chapter 2, the thesis evaluated the current status of the ability of seasonal forecasts to predict East Africa's rainfall seasons. The ability of the UK Met Office operational dynamical seasonal forecasting model, GloSea5, was evaluated, and compared to the most widely used forecasts within the region, the Greater Horn of Africa Climate Outlook Forum (GHACOF) consensus forecasts. Previous work has performed evaluation of other dynamical models predictions of East African rainfall (e.g. Batté and Déqué 2011; Bahaga et al. 2016), and an evaluation of Regional Climate Outlook Forums (RCOFs) across Africa, including GHACOF, was performed by Mason and Chidzambwa (2008) after 10 years of forecasts had been produced. However, no study has previously provided a side-by-side comparison of these two types of forecasts to identify the relative merits and drawbacks of each. Additionally, regular evaluation of GHACOF forecasts

was previously only performed on a single forecast basis, rather than updating the performance of the forecasts as a whole. Improved understanding of the ability of the consensus forecasts allows for improvements and better usage and communication to users of the potential uncertainties involved, which can aid in decision making.

It was found that in both GloSea5 and GHACOF, the ability to forecast the October-December (OND) short rains was high. In particular, forecasting seasons with above or below normal rainfall showed high skill, with these being important to forecast due to their adverse impacts of flooding or droughts respectively. Skilful forecasts of above normal rainfall could also offer economic benefits by taking advantage of increased crop growth, such as in the case of the 2009 short rains, where additional seeds were distributed to farmers in Kenya following an above normal rainfall forecast, with many farmers producing an increased yield (Graham et al. 2012). The skill of forecasts for near normal rainfall was found to be low, a common result of probabilistic forecasts split into tercile categories (van den Dool and Toth 1991). Meanwhile in both forecasts, skill for the long rains was low. In general GloSea5 outperformed GHACOF, with higher relative operating characteristic (ROC) scores, and Heidke skill score (HSS) values across both seasons, the exception to this being below normal forecasts of the long rains, in which GHACOF performed better.

Spatial maps of the ROC score of the two forecasts highlighted similar regions in both where the forecast was most skilful. In the short rains season it was found that this coincided with the regions most strongly influenced by the Indian Ocean Dipole (IOD) and El Niño-Southern Oscillation (ENSO). Limiting the forecasts to years where an IOD event was forecast (positive or negative) in GloSea led to widespread increase in skill in both the GHACOF and dynamical forecasts.

Several potential areas for improvement were identified within the GHACOF forecasts. These were related to the method and strategy with which the forecasts are put together. Forecasts are made to be risk averse, and large numbers of the forecasts were found to frequently over-estimate the probability of near normal rainfall, which has been shown to have low skill, and is considered of less importance than prediction of the extremes. This led to the knock on effect that forecast probabilities of the above and below normal categories were often too low, and changed little between wet and dry years, leading to under-confident forecasts of low resolution. This is in agreement with the earlier findings of Mason and Chidzambwa (2008). Increasing the confidence of these forecasts would likely produce benefits, especially in the short rains season, when an IOD or ENSO event is forecast to take place. GloSea5 meanwhile displayed

over-confidence, where it forecast too strongly in one direction or another. It was also noted that the contrasting over-confidence in GloSea5, and the under-confidence in GHACOF could mean that increased use of the dynamical model forecast probabilities in the GHACOF forecast could generate a more balanced forecast.

Further investigation into the GloSea5 system revealed that during the short rains there was a large wet bias in the model. This increased approximately linearly with lead time, and was accompanied by biases over the Indian Ocean. In the eastern Indian Ocean a cold sea surface temperature (SST) bias that increased with lead time was observed. With the cold bias was an accompanying high surface pressure bias over the eastern Indian Ocean, and a resulting easterly wind bias over the Indian Ocean in the lower troposphere. This setup is similar to a positive IOD event as outlined by (Saji et al. 1999). A similar bias has previously been found to exist in many of the Coupled Model Intercomparison Project version 5 (CMIP5) models (Hirons and Turner 2018), and those with this bias struggle to fully capture the influence that year-to-year variations in the IOD have on the short rains. This was also the case in GloSea5, where it was found that coupling between the Indian Ocean and the short rains was too weak, suggesting that improvements to this bias could further improve short rains forecasts.

The result from Chapter 2 highlighting the low skill of forecasts of the long rains narrowed the focus of Chapters 3 and 4 towards improving the understanding of the long rains, to ultimately provide information that may improve seasonal forecasts for this season. A recent study by Finney et al. (2019) demonstrated that days where zonal winds over East Africa, in particular over Lake Victoria, were westerly, more abundant rainfall was observed, as moist air from over the Congo was imported into the region.

In Chapter 3, the study by Finney et al. (2019) was extended, and the influence of winds over the Congo basin on the East African long rains was investigated. A strong relationship was found between the zonal winds at 700hPa over the Congo basin, and rainfall during the long rains on an inter-annual timescale. Wetter long rains seasons were accompanied by zonal winds that had a westerly anomaly, agreeing with previous studies (Nakamura 1968; Okoola 1999; Finney et al. 2019). It was also observed that the decadal trends of the zonal winds matched that of the long rains. The widely observed and documented drying of the long rains in recent decades (Funk et al. 2005, 2008; Lyon and Dewitt 2012; Liebmann et al. 2014; Hoell and Funk 2014; Rowell et al. 2015) coincided with generally more strongly easterly zonal winds over the Congo. Additionally, Wainwright et al. (2019) suggested there is a possibility of a recovery in the long rains is emerging, and there appeared to be a recovery in the zonal winds in

agreement with this. It was further found that based on the inter-annual relationship between the zonal winds and the rainfall, the decadal change observed in the zonal winds would give a sufficient change in the rainfall to explain the observed drying trend.

The study also demonstrated some possible sources of variations in the zonal winds. It was found that the amplitude of the Madden-Julian Oscillation (MJO), known to link to the East African long rains (Pohl and Camberlin 2006a,b; Vellinga and Milton 2018) contained decadal variability, with a lower mean amplitude during the driest period of the long rains.

A proposed mechanism for the decadal variability in the zonal winds was that in recent years heating of low-level air over the eastern Sahel has occurred more quickly than further south over the Congo region, which by the hypsometric equation is directly proportional to the geopotential thickness of the layer of air. This has increased the geopotential gradient between the Sahel and Congo, leading to stronger easterly winds.

Chapter 4 built on the results of Chapter 3, by investigating the Congo zonal winds in GloSea5, and further determining whether the Congo zonal winds are predictable. GloSea5 was found to correctly reproduce the observed link between the Congo zonal winds and the rainfall in its ensemble members, and also in the ensemble mean, however this relationship was found to be weaker in the ensemble mean. Predictions of variability of the Congo zonal wind were investigated in GloSea5, and it was found that the correlation coefficient between GloSea5 and the observations was significant but negative (i.e. forecasts for stronger easterly winds coincided with observations of weaker easterly winds), suggesting that its possible that the zonal winds are predictable. By selecting only ensemble members that correctly forecast the sign of the zonal wind anomaly, skilful forecasts of the rainfall can be obtained. This cannot be performed on a real-time operational forecast, as it requires prior knowledge of the observed state of zonal winds during the season being forecast. However, it is an indication that if the zonal winds could be forecast skilfully, then the resulting long rains rainfall forecasts would also be skilful.

Composites of the large-scale circulation of years with the strongest and weakest easterlies across the Congo were considered. It was found that the anomalies over the Congo were accompanied by anomalies of alternating sign northwards up towards the northern Atlantic Ocean. It was proposed that these anomalies originate here, and are linked to the North Atlantic Oscillation (NAO), propagating equatorward via a Rossby wave. Composites of the circulation during the NAO were produced to verify

the relationship, with anomalies of similar structure observed. This was also captured in ensemble members of GloSea5, however, the NAO in the ensemble mean was found to have a much smaller amplitude, and the magnitude of the zonal wind anomalies was thus much smaller over the North Atlantic region, and therefore the propagation of these anomalies down to the equator does not occur, or is simply overwhelmed by noise.

The ability of GloSea5 to forecast the NAO in boreal winter was previously studied by Scaife et al. (2014), who found high correlations of the model NAO with the observed when using a sufficiently large ensemble. However, Scaife et al. (2014) also identified a similar problem whereby the amplitude of the NAO is too small. Here, it was found that predictions of the NAO in MAM also achieved high skill with larger ensemble sizes. By comparing the ensemble to individual ensemble members, a lower correlation is found; the model is better at predicting the observations than itself. This is part of the signal-to-noise paradox recently discovered in seasonal forecast and climate models (Eade et al. 2014; Scaife and Smith 2018; Smith et al. 2020). An ensemble of GloSea5 with a corrected NAO was built, by selecting members that forecast the same sign of anomaly as the observations, and this was shown to produce skilful forecasts of the long rains. In the future, if the signal-to-noise ratio of the NAO can be improved, along with improved skill for forecasting the NAO, then skilful operational dynamical forecasts of the long rains may be possible.

5.2. Wider impact of the work

An updated evaluation of the GHACOF forecasts will aid the Intergovernmental Authority on Development (IGAD) Climate Prediction and Applications Centre (ICPAC) both on producing their forecasts, and communicating them with the stakeholders. ICPAC have since updated the format of their forecasts, working alongside the UK Department for International Development (DFID) Weather and Climate Information Services for Africa (WISER) Support to ICPAC Project (W2-SIP), as well as through the Global Challenges Research Fund (GCRF) African Science for Weather Information and Forecasting Techniques (SWIFT) and Science for Humanitarian Emergencies and Resilience (SHEAR) Towards Forecast-based Preparedness Action (ForPAc) projects. The forecasts have moved from the semi-objective, consensus approach discussed and evaluated in Chapter 2, to an objective forecast directly utilising the outputs of the different forecasting tools also described in Chapter 2 (WISER 2019). The outputs
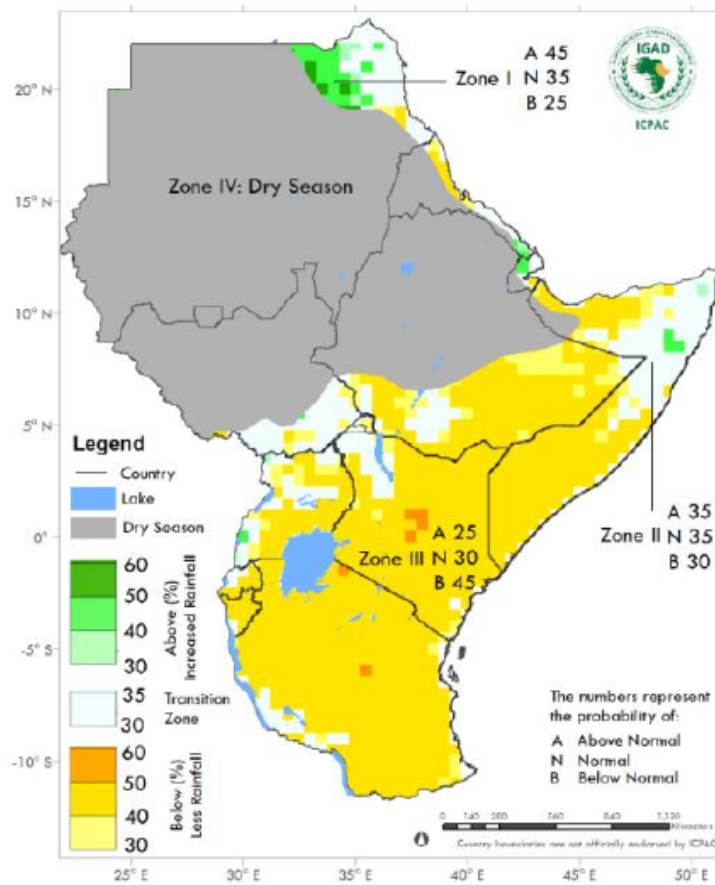
Figure 5.1.: Example of the new format of the GHACOF forecasts, in this case for OND 2020. Figure taken from ICPAC (2020).

are now also digitised and provided in a gridded format. An example of which is seen in Figure 5.1. This approach means that future, more comprehensive evaluations of the GHACOF forecasts can be performed. Several other issues highlighted within the forecasts have also since been addressed, such as the tendency to avoid forecasting with a probability of 30%. The forecasts are now also presented slightly differently; zones are used as before, but now they label individually regions where each category is most probable. Each zone has a scale providing different probabilities for the most probable category. This enhanced detail should make it easier to differentiate between more and less confident forecasts, and improve the under-confidence and resolution issues highlighted in Chapter 2. Further, work on performing evaluation of another RCOF has since taken place for Western Africa (Pirret et al. 2020).

Meanwhile, the evaluation of GloSea5 in Chapter 2, and presentation of the origin of biases could provide useful for model developers, especially due to the result that

these biases appear consistent between GloSea5 and many other dynamical models such as those in CMIP5 (Hirons and Turner 2018). Many dynamical models with similar biases to those found in GloSea here also incorrectly capture the annual cycle of rainfall, with more rainfall in the short rains than the long rains (Anyah and Qiu 2012; Yang et al. 2014). Improvements reducing these biases could strengthen the models ability to capture the link between the Indian Ocean and the short rains, which may further improve the skill of forecasts for the short rains, with some work already in place to investigate this further (MacLeod et al. 2020).

It has long been questioned whether the long rains are predictable, or whether a large proportion of the variability within this season is down to unpredictable noise and internal factors. Recent studies, such as those by Funk et al. (2014); Vellinga and Milton (2018) have suggested that predictability may be possible, and that the long rains do have links to predictable, large-scale modes of variability such as the MJO and Pacific and Indian Ocean SSTs and the results of Chapters 3 and 4 further demonstrate this. Although dynamical forecasts of the long rains may not reach the current capabilities of their short rains forecasts, any improvement of the understanding of variability, especially the possibility to correctly forecast extreme dry years leading to droughts, could have large impacts on the region, by helping to prepare for such events, humanitarian disasters seen in previous events such as the 2010-11 drought (FAO and FEWS NET 2013) could be reduced.

5.3. Limitations of the work

In Chapter 2, difficulties in evaluating the GHACOF consensus forecasts were discussed. The first identified difficulty in performing an evaluation on the GHACOF forecasts was the format of forecasts themselves. The regions containing different forecasts were split with hand-drawn lines. To tackle this, the forecasts were converted into gridded format using rasterization. This, combined with the coarse resolution of the observations used, meant that many grid boxes of the GHACOF forecast could have been assigned to two or even more than two, different probabilities. Further to this, it was noted that due to the consensus nature of the forecasts, the issued probabilities were not strictly the anticipated probability of each category, but more a representation of the confidence of the forecasters based on the available information. Therefore, comparison with the dynamical model, which the evaluation metrics have been designed for, could be considered a little unfair. The evaluation was also performed on a relatively small

dataset of 18 years, meaning there was likely a reasonable uncertainty in the skill score estimates.

Meanwhile, the limited number of years and relatively small ensemble size of the GloSea5 operational hindcasts was also an issue within Chapter 2. This lowered the robustness of results. It should be noted that the ensemble size of the hindcasts has since been increased from 12 per month to 28 per month. This was a particular problem for results where active ENSO and IOD years were selected out from the data, as this dataset then only contained a small number of years for the analysis.

Similarly, in Chapter 3 and 4, the relatively smaller number of years available (40 in Chapter 3, and 24 in Chapter 4) means that the composite analysis technique only utilises a small number of years in each case. This lowers the significance of results, and raises the noise within the composites, making it more difficult to draw conclusions about the relevant features.

A limitation across all results was the availability and quality of observational data. The work mostly made use of observations from satellite products for rainfall, due to sparsity of available rain gauge data, whilst for other fields, reanalyses were the primary source of a comparison dataset, treated as observations. Satellite observations are known to have biases due to often measuring rainfall indirectly through other fields, this is particularly problematic over mountainous regions such as much of East Africa (Dinku et al. 2007; Cattani et al. 2016). As mentioned above, using observations from only the satellite era onwards also limits the length of available data, which may impact on the robustness of results.

5.4. Recommendations for future work

5.4.1. Evaluation of GHACOF and other RCOFs

Several limitations have been highlighted within the evaluation of GHACOF performed in Chapter 2. One method to improve the evaluation would be to repeat with a higher resolution observational dataset. A low resolution observation dataset was used to correspond to the World Meteorological Organisation guidelines for evaluating dynamical seasonal forecasts, however, the evaluation of GHACOF would be more accurate with a higher resolution, due to the method of their construction. Further, it is recommended that regular evaluation of these forecasts should now take place. This should

be made more straightforward with recent progress in digitising the forecasts. Eventually, the new, objective forecasts should be evaluated separately from the original semi-subjective forecasts to give an idea of any added value from this new method. Alternatively, for a faster result, a hindcast set of these objective forecasts could be generated for the purposes of verification. This would, however, be computationally expensive. Similar evaluation should also be considered across other RCOF forecasts, as many other regions use these as their primary operational forecast, with little to no regular evaluation. Additionally, GHACOF also issues temperature forecasts alongside the rainfall forecasts, these should also be evaluated in a similar manner.

Other, more user centred metrics could also be considered for performing evaluation. For example, the extended ROC score presented by Semazzi and Mera (2006), which combines the original ROC score with the economic value method to evaluate the forecasts based on a cost-loss ratio that can be defined by the user. This would be a useful tool for explaining the potential value of taking actions based on the forecasts to users, by putting for example the relative costs and losses of taking actions or not, in different outcomes for forecasts. This would also provide another method to further demonstrate the usage of probabilistic forecasts to users, which still remains a challenge (Hansen et al. 2011).

With regards to the comparison of GHACOF with dynamical models, the new version of the GHACOF forecast should also allow a fairer comparison. Additionally, fairer comparison would be against a multimodel ensemble rather than against a single dynamical model, due to the variety of sources utilised within the GHACOF forecast. A multimodel ensemble would simulate the GHACOF forecast process, as contrasting results from models would likely lead to a forecast with more forecasts producing less confident predictions. Previous evaluation of a multimodel ensemble over the short rains (Bahaga et al. 2016) has also shown that many models may possess less forecast skill for the short rains than GloSea5.

5.4.2. Congo zonal wind and East African rainfall

Chapter 3 identified the decadal variability of the Congo zonal winds and its influence on the East African long rains. This relationship could be tested in climate models such as within the CMIP models to first verify whether these models capture the relationship, and secondly, examine how it is projected to change under climate change. Giannini et al. (2018) suggested that weakening moisture convergence over the Congo basin takes

place in the future climate projections, resulting in the weakening of near-surface winds and increasing the moisture advected towards East Africa. Given this, it is likely that the CMIP models do indeed capture the relationship, however, this should be verified. Understanding the uncertainty on this could aid in understanding projections of the long rains.

Results of Chapter 4 demonstrated that GloSea5 could capture the observed relationship between zonal winds over the Congo basin and the East African long rains, as well as being able to produce a skilful forecast of the zonal winds, with incorrect sign. It should be investigated whether these features are unique to GloSea5, or common amongst dynamical models. If this result is robust amongst dynamical models, it offers further evidence that skilful dynamical model forecasts of the long rains are plausible in the future with model improvements. The potential causes of the negative forecast skill should be investigated, by investigating whether biases within the model, such as SST biases in the Atlantic Ocean, are impacting the circulation. This could be performed by using nudging experiments to alleviate any found biases that may be responsible, and determining whether this alters the negative skill in forecasting the zonal winds.

The link between the NAO and the long rains should be investigated in more detail in observations. Currently only a short time period of 24 years is being used. The proposed Rossby wave response has also not yet been verified, and this is necessary to truly confirm the result. Performing this would likely involve studying higher temporal resolution data to identify the occurrence of the Rossby wave. Alternatively, if the proposed Rossby wave mechanism is not correct, then understanding of how the NAO might otherwise connect to East Africa needs to be determined before confident usage of this new information can take place.

Additionally, if the above is verified, the possibility of utilising this new knowledge to produce a statistical forecast of the long rains should be investigated, as applying improvements to dynamical models is incredibly complex and can be time consuming. Statistical forecasts meanwhile, are relatively cheap and fast to produce and make use of new knowledge (Doblas-Reyes et al. 2013). Although statistical models have drawbacks such as the potential for over-fitting, when using a well understood mechanism linking the predictors to the predictand, with careful model construction and verification, increased confidence can be placed in the forecast.

5.4.3. Directions for model development

Two key areas for potential future investigation by model developers have been high-lighted in the results of Chapters 2 and 4. Firstly, in Chapter 2, a large wet bias during the short rains in GloSea5 was identified. Whilst GloSea5 still displayed good skill in predicting the short rains, the coupling between the short rains and the IOD appeared too weak, whilst Hirons and Turner (2018) identified that CMIP5 models with a similar bias struggled to capture the moisture advection into East Africa during positive IOD events. Given the results of Hirons and Turner (2018), it is likely that this bias is not unique to GloSea5 within seasonal forecast models, so it should be investigated in other seasonal models. For example, do models with smaller Indian Ocean biases better forecast the IOD, and if so do they better forecast the short rains? Alternatively is there a link between the bias and the coupling of the IOD and short rains?

The results of Chapter 4 further highlight the problem of the signal-to-noise paradox in seasonal forecasts, previously found by Scaife et al. (2014); Eade et al. (2014); Scaife and Smith (2018). It is also present in climate models (Smith et al. 2020). The ratio of the standard deviation of the ensemble mean and the ensemble members is expected to be greater than the correlation between the ensemble mean and observations. Alternatively, the ratio of the correlation between an ensemble mean and observations, and the average correlation between an ensemble mean and a single ensemble member, is expected to be less than 1; the model is expected to be better at predicting itself than the observations (Eade et al. 2014; Scaife and Smith 2018), although a perfect system should be equally good at predicting both. However, it has been found that in certain regions, such as the North Atlantic, this is not the case, and the model is better at predicting the real word than itself. This generally means that each ensemble member contains a large amount of noise. Fixing this issue would strengthen model responses to phenomena such as the NAO, which could unveil new predictability, and improve the skill of seasonal forecasts.

5.5. Summary

The results presented in this thesis advance understanding of the predictability and variability of the rainfall seasons of East Africa, particularly the long and short rains seasons experienced in much of the region. This was achieved by first performing an evaluation of the current state of seasonal forecasts, before building new understand-

ing of some of the physical processes connecting large-scale atmospheric conditions to seasonal rainfall. Finally, these relationships were investigated in the dynamical model used within the initial evaluation to identify whether this new understanding could lead to improved forecasts, and make recommendations for future improvements.

In the evaluation of seasonal forecasts, the UK Met Office dynamical model, GloSea5, as well as the GHACOF forecasts both demonstrated good skill at forecasting the short rains season, but generally did little better than guesswork at forecasting the long rains season. This is due to the differing relationships between rainfall and large-scale modes of variability in the two seasons; the short rains are strongly tied to SSTs, whereas the long rains are not.

Studies then investigated the relationship between winds over the Congo basin and the East African long rains, finding a strong connection between the long rains and zonal winds at 700hPa on both inter-annual and decadal timescales. Finally, this relationship was studied in the dynamical model, and it was found to be well captured, however, the model incorrectly predicts the zonal winds. These zonal winds were found to be partially controlled by the NAO, which is a known source of variability and predictability, particularly for the extra-tropics, and is reasonably well forecast by GloSea5. It was demonstrated that improvements to the model in capturing a more realistic amplitude of NAO could then produce skilful seasonal rainfall forecasts for the long rains.

Taken together, the results of Chapters 2-4 provide an evaluation of the current state of seasonal forecasting, provide new information on controls of the variability, in particular for the poorly forecast long rains season, and demonstrate the potential for future forecasting capability for the long rains based upon this new understanding. However, it is also clear that more work needs to be done in addressing model issues, particularly relating to the signal-to-noise paradox, in order for this potential to be fulfilled.

References

Anyah, R. O. and Qiu, W. (2012). Characteristic 20th and 21st century precipitation and temperature patterns and changes over the Greater Horn of Africa. *International Journal of Climatology*, 32(3):347–363.

Bahaga, T. K., Kucharski, F., Tsidu, G. M., and Yang, H. (2016). Assessment of prediction and predictability of short rains over equatorial East Africa using a multi-model ensemble. *Theoretical and Applied Climatology*, 123(3-4):637–649.

Batté, L. and Déqué, M. (2011). Seasonal predictions of precipitation over Africa using coupled ocean-atmosphere general circulation models: Skill of the ENSEMBLES project multimodel ensemble forecasts. *Tellus, Series A: Dynamic Meteorology and Oceanography*, 63A(2):283–299.

Cattani, E., Merino, A., and Levizzani, V. (2016). Evaluation of monthly satellite-derived precipitation products over East Africa. *Journal of Hydrometeorology*, 17(10):2555–2573.

Dinku, T., Ceccato, P., Grover-Kopec, E., Lemma, M., Connor, S. J., and Ropelewski, C. F. (2007). Validation of satellite rainfall products over East Africa's complex topography. *International Journal of Remote Sensing*, 28(7):1503–1526.

Doblas-Reyes, F. J., García-Serrano, J., Lienert, F., Biescas, A. P., and Rodrigues, L. R. (2013). Seasonal climate predictability and forecasting: status and prospects. *Wiley Interdisciplinary Reviews: Climate Change*, 4(4):245–268.

Eade, R., Smith, D., Scaife, A., Wallace, E., Dunstone, N., Hermanson, L., and Robinson, N. (2014). Do seasonal-to-decadal climate predictions underestimate the predictability of the real world? *Geophysical Research Letters*, 41(15):5620–5628.

FAO and FEWS NET (2013). Mortality among populations of southern and central Somalia affected by severe food insecurity and famine during 2010-2012. Available at: https://reliefweb.int/report/somalia/mortality-among-populations-southern-and-central-somalia-affected-severe-food. Last accessed: 22 September 2020.

Finney, D. L., Marsham, J. H., Walker, D. P., Birch, C. E., Woodhams, B. J., Jackson, L. S., and Hardy, S. (2019). The effect of westerlies on East African rainfall and the associated role of tropical cyclones and the Madden-Julian Oscillation. *Quarterly*

Journal of the Royal Meteorological Society.

Funk, C. C., Dettinger, M. D., Michaelsen, J. C., Verdin, J. P., Brown, M. E., Barlow, M., and Hoell, A. (2008). Warming of the Indian Ocean threatens eastern and southern African food security but could be mitigated by agricultural development. *Proceedings of the National Academy of Sciences*, 105(32):11081–11086.

Funk, C. C., Hoell, A., Shukla, S., Bladé, I., Liebmann, B., Roberts, J. B., Robertson, F. R., and Husak, G. (2014). Predicting East African spring droughts using Pacific and Indian Ocean sea surface temperature indices. *Hydrology and Earth System Sciences*, 18(12):4965–4978.

Funk, C. C., Senay, G., Asfaw, A., and Verdin, J. (2005). Recent drought tendencies in Ethiopia and equatorial-subtropical eastern Africa. *FEWS NET Special Report*.

Giannini, A., Lyon, B., Seager, R., and Vigaud, N. (2018). Dynamical and thermodynamic elements of modeled climate change at the East African margin of convection. *Geophysical Research Letters*, 45(2):992–1000.

Graham, R., Colman, A., Vellinga, M., and Wallace, E. (2012). Use of dynamical seasonal forecasts in the consensus outlooks of African Regional Climate Outlook Forums (RCOFs). *ECMWF Seminar on Seasonal Prediction*, (September):3–7.

Hansen, J. W., Mason, S. J., Sun, L., and Tall, A. (2011). Review of seasonal climate forecasting for agriculture in sub-Saharan Africa. *Experimental Agriculture*, 47(2):205–240.

Hirons, L. and Turner, A. (2018). The impact of Indian Ocean mean-state biases in climate models on the representation of the East African short rains. *Journal of Climate*, 31(16):6611–6631.

Hoell, A. and Funk, C. C. (2014). Indo-Pacific sea surface temperature influences on failed consecutive rainy seasons over eastern Africa. *Climate Dynamics*, 43(5-6):1645–1660.

ICPAC (2020). GHACOF 56 Forecast. Available at: `https://icpac.net/ghacof56/`. Last accessed: 18 November 2020.

Liebmann, B., Hoerling, M. P., Funk, C. C., Bladé, I., Dole, R. M., Allured, D., Quan, X., Pegion, P., and Eischeid, J. K. (2014). Understanding recent eastern Horn of Africa rainfall variability and change. *Journal of Climate*, 27(23):8630–8645.

Lyon, B. and Dewitt, D. G. (2012). A recent and abrupt decline in the East African long rains. *Geophysical Research Letters*, 39(2):L02702.

MacLeod, D., Graham, R., O'Reilly, C., Otieno, G., and Todd, M. (2020). Causal pathways linking different flavours of ENSO with the Greater Horn of Africa short rains. *Atmospheric Science Letters*, pages 1–11.

Mason, S. and Chidzambwa, S. (2008). *Verification of African RCOF forecasts.*

Nakamura, K. (1968). Equatorial westerlies over East Africa and their climatological significance. *Geographical Review of Japan*, 41(6):359–373.

Okoola, R. E. (1999). Midtropospheric Circulation Patterns Associated with Extreme Dry and Wet Episodes over Equatorial Eastern Africa during the Northern Hemisphere Spring. *Journal of Applied Meteorology*, 38(8):1161–1169.

Pirret, J. S., Daron, J. D., Bett, P. E., Fournier, N., and Foamouhoue, A. K. (2020). Assessing the skill and reliability of seasonal climate forecasts in Sahelian West Africa. *Weather and Forecasting*, 35(3):1035–1050.

Pohl, B. and Camberlin, P. (2006a). Influence of the Madden-Julian Oscillation on East African rainfall. I: Intraseasonal variability and regional dependency. *Quarterly Journal of the Royal Meteorological Society*, 132(621):2521–2539.

Pohl, B. and Camberlin, P. (2006b). Influence of the Madden-Julian Oscillation on East African rainfall. II: March-May season extremes and interannual variability. *Quarterly Journal of the Royal Meteorological Society*, 132(621):2541–2558.

Rowell, D. P., Booth, B. B., Nicholson, S. E., and Good, P. (2015). Reconciling past and future rainfall trends over East Africa. *Journal of Climate*, 28(24):9768–9788.

Saji, N. H., Goswami, B. N., Vinayachandran, P. N., and Yamagata, T. (1999). A dipole mode in the tropical Indian ocean. *Nature*, 401(6751):360–363.

Scaife, A. A., Arribas, A., Blockey, E., Brookshaw, A., Clark, R. T., Dunstone, N., Eade, R., Fereday, D., Folland, C. K., Gordon, M., Hermanson, L., Knight, J. R., Lea, D. J., MacLachlan, C., Maidens, A., Martin, M., Peterson, A. K., Smith, D., Vellinga, M., Wallace, E., Waters, J., and Williams, A. (2014). Skillful long range prediction of European and North American winters. *Geophysical Research Letters*, 5(7):2514–2519.

Scaife, A. A. and Smith, D. (2018). A signal-to-noise paradox in climate science. *npj Climate and Atmospheric Science*, 1(1):28.

Semazzi, F. H. M. and Mera, R. J. (2006). An extended procedure for implementing the relative operating characteristic graphical method. *Journal of Applied Meteorology and Climatology*, 45(9):1215–1223.

Smith, D. M., Scaife, A. A., Eade, R., Athanasiadis, P., Bellucci, A., Bethke, I., Bilbao, R., Borchert, L. F., Caron, L. P., Counillon, F., Danabasoglu, G., Delworth, T., Doblas-Reyes, F. J., Dunstone, N. J., Estella-Perez, V., Flavoni, S., Hermanson, L., Keenlyside, N., Kharin, V., Kimoto, M., Merryfield, W. J., Mignot, J., Mochizuki, T., Modali, K., Monerie, P. A., Müller, W. A., Nicolí, D., Ortega, P., Pankatz, K., Pohlmann, H., Robson, J., Ruggieri, P., Sospedra-Alfonso, R., Swingedouw, D., Wang, Y., Wild, S., Yeager, S., Yang, X., and Zhang, L. (2020). North Atlantic climate far more predictable than models imply. *Nature*, 583(7818):796–800.

van den Dool, H. M. and Toth, Z. (1991). Why do forecasts for "near normal" often fail? *Weather and Forecasting*, 6(1):76–85.

Vellinga, M. and Milton, S. (2018). Drivers of interannual variability of the East African 'Long Rains'. *Quarterly Journal of the Royal Meteorological Society*.

Wainwright, C. M., Marsham, J. H., Keane, R. J., Rowell, D. P., Finney, D. L., Black, E., and Allan, R. P. (2019). 'Eastern African Paradox' rainfall decline due to shorter not less intense Long Rains. *npj Climate and Atmospheric Science*, 2(1):1–9.

WISER (2019). Improved seasonal forecast for Eastern Africa. Technical report.

Yang, W., Seager, R., Cane, M. A., and Lyon, B. (2014). The East African long rains in observations and models. *Journal of Climate*, 27(19):7185–7202.